

NEW CHALLENGES IN Rh(I)-CATALYSED [2+2+2] CYCLOADDITION REACTION

Martí Fernández Wang

Per citar o enllaçar aquest document:

Para citar o enlazar este documento:

Use this url to cite or link to this publication:

<http://hdl.handle.net/10803/663661>

ADVERTIMENT. L'accés als continguts d'aquesta tesi doctoral i la seva utilització ha de respectar els drets de la persona autora. Pot ser utilitzada per a consulta o estudi personal, així com en activitats o materials d'investigació i docència en els termes establerts a l'art. 32 del Text Refós de la Llei de Propietat Intel·lectual (RDL 1/1996). Per altres utilitzacions es requereix l'autorització prèvia i expressa de la persona autora. En qualsevol cas, en la utilització dels seus continguts caldrà indicar de forma clara el nom i cognoms de la persona autora i el títol de la tesi doctoral. No s'autoritza la seva reproducció o altres formes d'explotació efectuades amb finalitats de lucre ni la seva comunicació pública des d'un lloc aliè al servei TDX. Tampoc s'autoritza la presentació del seu contingut en una finestra o marc aliè a TDX (framing). Aquesta reserva de drets afecta tant als continguts de la tesi com als seus resums i índexs.

ADVERTENCIA. El acceso a los contenidos de esta tesis doctoral y su utilización debe respetar los derechos de la persona autora. Puede ser utilizada para consulta o estudio personal, así como en actividades o materiales de investigación y docencia en los términos establecidos en el art. 32 del Texto Refundido de la Ley de Propiedad Intelectual (RDL 1/1996). Para otros usos se requiere la autorización previa y expresa de la persona autora. En cualquier caso, en la utilización de sus contenidos se deberá indicar de forma clara el nombre y apellidos de la persona autora y el título de la tesis doctoral. No se autoriza su reproducción u otras formas de explotación efectuadas con fines lucrativos ni su comunicación pública desde un sitio ajeno al servicio TDR. Tampoco se autoriza la presentación de su contenido en una ventana o marco ajeno a TDR (framing). Esta reserva de derechos afecta tanto al contenido de la tesis como a sus resúmenes e índices.

WARNING. Access to the contents of this doctoral thesis and its use must respect the rights of the author. It can be used for reference or private study, as well as research and learning activities or materials in the terms established by the 32nd article of the Spanish Consolidated Copyright Act (RDL 1/1996). Express and previous authorization of the author is required for any other uses. In any case, when using its content, full name of the author and title of the thesis must be clearly indicated. Reproduction or other forms of for profit use or public communication from outside TDX service is not allowed. Presentation of its content in a window or frame external to TDX (framing) is not authorized either. These rights affect both the content of the thesis and its abstracts and indexes.



Doctoral Thesis

**New challenges in Rh(I)-catalysed
[2+2+2] cycloaddition reactions**

Martí Fernández Wang

2017

Doctoral Programme in Chemistry

Supervised by: Prof. Anna Roglans Ribas and Dr. Anna Pla Quintana

Tutor: Prof. Anna Roglans Ribas

Presented in partial fulfilment of the requirements for a **doctoral degree**
from the **University of Girona**



Prof. Anna Roglans Ribas and Dr. Anna Pla Quintana, from the University of Girona

WE DECLARE:

That the thesis entitled “New challenges in Rh(I)-catalysed [2+2+2] cycloaddition reactions” presented by **Martí Fernández Wang** to obtain a doctoral degree has been completed under our supervision and meets the requirements to opt for an International Doctorate.

For all intents and purposes, we hereby sign this document.

Prof. Anna Roglans Ribas

Dr. Anna Pla Quintana

Girona, 8th of June, 2017

ACKNOWLEDGMENTS

Quan vaig començar la carrera de química l'any 2008 mai m'hauria imaginat que acabaria el 2017 amb una tesi doctoral sota el braç. És molt difícil resumir tota la gent que ha format part d'aquest projecte que ha durat quatre anys, però faré el millor que pugui.

Per començar, vull agrair a l'Anna Roglans i l'Anna Pla tots aquests anys de guiatge sota la seva tutela: tots els seus consells i tot el temps que m'han dedicat, sempre perquè donés el millor de mi i poder culminar en el que es presenta en aquesta tesi. Sempre hi han alts i baixos, però el seu optimisme i la seva insistència sempre m'han empès en la bona direcció.

I also would like to thank Anne-Marie Caminade for her suport during my visit in her lab in Toulouse, where I worked for three months and from which a chapter of this thesis arises. *A la Dra. Roser Pleixats pel temps que també em va acollir al seu laboratori quan feia el màster a la Universitat Autònoma de Barcelona, feina de la qual va sorgir un article i un capítol d'aquesta tesi. I finalment, també vull agrair a la Mònica Iglesias per la seva ajuda en la determinació del rodi en els materials híbrids.*

El laboratori s'ha convertit en la meva segona residència al llarg d'aquests anys i, com a tal, els habitants d'aquesta han estat companys i amics a la vegada. L'Òscar va començar abans que jo al grup tot i que som de la mateixa promoció de la carrera, i sempre l'he tingut com un referent com a persona treballadora i que s'entrega a la investigació, i estic segur que tindrà molt d'èxit en el postdoc que ara començarà. La Magda va ser la meva primera supervisora dins el laboratori i a ella li agraeixo tot el que em va ensenyar al principi i la paciència que va tenir, sense ella no hauria pogut arribar on sóc ara. A en Dani, que va començar un any més tard, l'animo en aquest any que li queda, el tram final és dur, però també el més satisfactori al veure tota la feina que has fet durant aquests anys. A l'Ewelina li desitjo que tingui molta sort en la seva vida a Polònia, que tot i que estiguem lluny me'n recordo sovint d'ella i de la seva alegria. Finalment, a l'Albert, el més recent doctorand, també li desitjo molta sort en aquests anys de recerca que li queden.

Què hauria fet jo sense la companyia de les meves princeses del passadís? Amb l'Ester hem compartit carrera, pis, màster, passadís, amics, llibres, jocs, sèries, confidències, viatges... una resumida llista plena d'anècdotes que estic segur que recordarem durant molts anys. Amb la Cristina he establert amistat durant el doctorat i hi he compartit menys anys, no obstant amb les dues m'emporto una amistat amb noies alegres, simpàtiques (quan volen), i que, per molt que no sabem on estarem d'aquí uns anys, estic segur que les tindrè al meu costat en tot el que necessiti (i elles a mi). No oblidarem els minions, els enanitos, les comandes, els moments punkis, els piropos espontanis, els dinars organitzats, el calendari del compte enrere allargat fins el 2020... i per suposat els esmorzars amb en Pep Duran i la Montse Rodríguez que ens han servit a tots per desfogar-nos quan ho necessitaven i de pas riure una estona amb anècdotes verdes que mai sabíem qui les començava... La Carlota també ha estat molt present durant aquests anys i ens ha acompanyat en moltes ocasions. Estic segur que a totes elles els hi espera un futur exitós allà on vagin i sigui el que sigui que es dediquin.

Evidentment no em puc oblidar d'en Jonathan, un gran amic que vaig fer durant el màster a la UAB i que a dia d'avui encara ens veiem quan podem coincidir. Ell ha estat fent el doctorat a la UAB i no ens hem pogut veure tan com voldríem, però sempre que he necessitat la seva ajuda ha

estat al meu costat i sé que, tot i que ens veiem poc, sempre puc comptar amb ell. La seva naturalesa entregada i sincera fa que sigui una persona agradable de tenir al costat i li desitjo molta sort i ànims en aquest tram final del doctorat en el que ell també es troba.

A en Ruben, la Laura i la Gemma, la colla analítica que sempre enredem en els nostres plans descabellats, els hi desitjo molta sort en el que els queda de doctorat i en les estades que en breu començaran.

Als amics de la carrera amb els que ens hem seguit veient també els hi vull agrair les tardes de grannys, cine i jocs que hem passat junts: en Ming, l'Adrià, l'Ismael i en Juan. També gràcies a en Toni pel temps que va estar al meu costat.

En Xavi és una amistat que conservo dels meus dies de la carrera tot i que ell sigui biòleg... Sé que encara que estiguem separats per la distància és un amic amb el que sempre puc comptar, sobretot si és per compartir xafarderies.

Hi ha una persona amb qui recentment he establert amistat, però que s'ha convertit en algú indispensable en el meu dia a dia. Amb ell he viscut moments que no canviaria per res del món i m'ha ajudat en molts aspectes. Pels esmorzars a la fàbrica, per les nostres tardes voltant botigues, al gimnàs, prenent sucs, per les nostres converses que a vegades sembla que no tinguin fi... Per tot, gràcies Dani, espero poder seguir comptant sempre amb tu.

Des que vaig començar a desenvolupar la tesi em vaig traslladar de casa els meus pares situada a Sant Feliu de Guíxols a un pis al Carrer Santa Clara a Girona. Durant aquests anys he compartit pis amb gent diversa, però sempre m'he emportat quelcom positiu de tots i totes. Vaig començar vivint amb l'Anna, la Gemma i l'Alba i he acabat vivint amb en Joel, l'Anna, l'Ale i el gat Goku. Gràcies a tots i totes per haver aguantat la convivència amb mi amb les meves diverses manies.

Un cop em vaig establir a Girona vaig veure que a prop de casa tenia un gimnàs petit, anomenat Fuji, situat a un pis del Carrer Nord i vaig decidir apuntar-me per tal de millorar el meu estil de vida. Tres anys després haig d'agrair a en Xevi Soler per tot el temps que m'ha dedicat, gràcies a ell he aconseguit fer un canvi físic molt important i tot ha estat gràcies al seus consells i la seva capacitat de motivar-me.

Un dia que mirava despistat els cursos que es fan als centres cívics de Girona n'hi va haver un que em va cridar l'atenció i que porto practicant durant dos anys i mig. La capoeira ha estat també una part fonamental en aquests anys de tesi que m'ha ajudat a desconnectar quan tot ho veia negre. Vull agrair al grup ABADÁ Capoeira de Girona per tot el que m'ha ensenyat i els valors que m'ha impartit, gràcies a Graduado Nei per les seves classes i la seva dedicació amb tots els seus alumnes. Evidentment no em puc oblidar dels meus companys més fidels que sempre estan presents a cada classe i amb els que he anat a varis esdeveniments: la Sonia i en Xevi. Amb ells he compartit viatges i moments de motivació mútua quan algú de nosaltres estava en hores baixes.

També vull mencionar a en Jordi i l'Arnau per les vegades que m'han fet voltar per Catalunya i les petites escapades a les que em conviden, i a en Pau i en Pau que, tot i que ara estiguem més desconnectats sé que sempre que els necessito estan allà.

A la meva família vull agrair tot el suport que m'han donat durant aquests anys i que segur que em seguiran donant.

Finally, I would like to thank the support from the following agencies:

- AGAUR of Generalitat de Catalunya for financial support through the project 2014-SGR-931 and for the Ph.D Grant FI-DGR 2014.
- MINECO of Spain for financial support through projects CTQ2011-2312-P and CTQ2014-54306-P.
- Serveis Tècnics de Recerca from University of Girona and Dr. Teodor Parella from the Universitat Autònoma de Barcelona for technical support.

PUBLICATIONS

This doctoral thesis has resulted in the following publications:

- Rhodium-NHC hybrid silica materials as recyclable catalysts for [2+2+2] cycloaddition reaction of alkynes. Fernández, M.; Ferré, M.; Pla-Quintana, A.; Parella, T.; Pleixats, R.; Roglans, A. *Eur. J. Org. Chem.* **2014**, 6242.
- Rhodium-catalysed [2+2+2] cycloaddition of diynes with Morita-Baylis-Hillman adducts: a stereoselective entry to densely functionalized cyclohexadiene scaffolds. Fernández, M.; Parera, M.; Parella, T.; Lledó, A.; Le Bras, J.; Muzart, J.; Pla-Quintana, A.; Roglans, A. *Adv. Synth. Catal.* **2016**, 358, 1848.
- Chiral induction in intramolecular rhodium-catalysed [2+2+2] cycloadditions of optically active allene-ene/yne-allene substrates. Haraburda, E.; Fernández, M.; Gifreu, A.; Garcia, J.; Parella, T.; Pla-Quintana, A.; Roglans, A. *Adv. Synth. Catal.* **2017**, 359, 506.

Contributions in other publications not included in this thesis:

- A simple catalytic system based on PdCl₂(CH₃CN)₂ in water for cross-coupling reactions using diazonium salts. El Bakouri, O.; Fernández, M.; Brun, S.; Pla-Quintana, A.; Roglans, A. *Tetrahedron* **2013**, 69, 9761.

ABBREVIATIONS

°C	Celsius degrees
μW	microwave
ν (in IR)	frequency (units: cm ⁻¹)
Ac	acetyl
AcOEt	ethyl acetate
anh.	anhydrous
aq.	aqueous
Ar	aryl
ATR	Attenuated Total Reflectance
BET	Brunauer-Emmett-Teller
BINOL	1,1'-bi-2-naphthol
BJH	Barrett-Joyner-Halenda
Bn	benzyl
Boc	<i>tert</i> -butyloxycarbonyl
Bu	butyl
CID	Collision-Induced Dissociation
COD	1,5-cyclooctadiene
Cp	cyclopentadienyl
Cp*	pentamethyl-η ⁵ -cyclopentadienyl
CP-MAS	Cross-Polarization Magic Angle Spinning
Cy	cyclohexyl
DAB	diaminobutane
DABCO	1,4-diazabicyclo[2.2.2]octane
DCE	1,2-dichloroethane
DFT	Density Functional Theory
DIAD	diisopropyl azodicarboxylate
DMAP	4-dimethylaminopyridine
DMF	dimethylformamide
DMSO	dimethyl sulfoxide
EA	elemental analysis
ee	enantiomeric excess
eq.	equivalent
ESI	Electrospray Ionization
Et	ethyl
Et ₂ O	diethyl ether
EtO	ethoxy
EtOH	ethanol
EWG	Electron Withdrawing group
g	grams
GC	Gas Chromatography
h.	hours
Hex	hexyl
HMPA	hexamethylphosphoramide

HOMO	Highest Occupied Molecular Orbital
HPLC	High Performance Liquid Chromatography
HRMS	High Resolution Mass Spectrometry
HWE	Horner-Wadsworth-Emmons
ICP	Inductively Coupled Plasma
IMes	1,3-bis(2,4,6-trimethylphenyl)imidazol-2-ylidene
Ind	indenyl
IPr	1,3-bis(2,6-diisopropylphenyl)imidazol-2-ylidene
<i>i</i>Pr	isopropyl
<i>i</i>PrOH	isopropanol
IR	infrared spectroscopy
K	Kelvin
L	ligand
lit.	literature
<i>m</i>	meta
M	molar
m.p.	melting point
<i>m/z</i>	mass to charge ratio
MBH	Morita-Baylis-Hillman
Me	methyl
MeO	methoxy
MeOH	methanol
Mes	2,4,6-trimethylphenyl
min.	minutes
mL	milliliter
mol%	mol percentage
MS	Mass Spectrometry
Ms	mesyl
MS/MS	tandem mass spectrometry
MW	Molecular Weight
NBD	norbornadiene
NHC	<i>N</i> -heterocyclic carbene
Ns	nosyl
<i>o</i>	<i>ortho</i>
<i>p</i>	<i>para</i>
PAMAM	polyamidoamine
PEG	poly(ethylene glycol)
Ph	phenyl
PNSO	<i>N</i> -phosphino- <i>tert</i> -butylsulfonamide
PPI	poly(propyleneimine)
PTA	1,3,5-triaza-7-phosphaadamantane
r.t.	room temperature
rac	racemic
S_{BET}	surface area measured by BET
SIP	secondary iminophosphorane

SIPr	1,3-bis(2,6-diisopropylphenyl)-4,5-dihydroimidazol-2-ylidene
SSNMR	Solid State Nuclear Magnetic Resonance
T	temperature
TADDOL	$\alpha,\alpha,\alpha',\alpha'$ -tetraaryl-1,3-dioxolane-4,5-dimethanol
TBAF	tetrabutylammonium fluoride
^tBu	<i>tert</i> -butyl
TEOS	tetraethoxysilane
Tf	triflate, trifluoromethanesulfonyl
TFA	trifluoroacetic acid
TGA	thermogravimetric analysis
THF	tetrahydrofuran
TLC	Thin Layer Chromatography
TMS	trimethylsilyl group
Tol	tolyl
Tripp	2,4,6-triisopropylphenyl
Ts	tosyl, 4-methylphenylsulfonyl
UV/Vis	ultraviolet/visible
w/v	mass/volume percentage

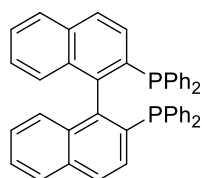
Abbreviations used in Nuclear Magnetic Resonance (NMR)

δ	chemical shift (units: ppm)
¹³C-NMR	¹³ -Carbon Nuclear Magnetic Resonance
¹H-NMR	Proton Nuclear Magnetic Resonance
³¹P{¹H}-NMR	Proton decoupled ³¹ -Phosphorus Nuclear Magnetic Resonance
br s	broad signal
d	doublet
dd	double doublet
dq	double quartet
ddt	double double triplet
ddq	double double quartet
J	coupling constant
m	multiplet
NOE	Nuclear Overhauser Effect
NOESY	Nuclear Overhauser Effect Spectroscopy
q	quartet
qd	quadruple doublet
s	singlet
t	triplet
TMS	tetramethylsilane

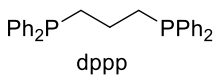
Biphosphines

BINAP	2,2'-bis(diphenylphosphino)-1,1'-binaphthalene
dppp	1,3-Bis(diphenylphosphino)propane

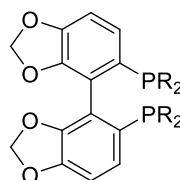
DTBM-SEGPPOS	5,5'-bis[di(3,5-di- <i>tert</i> -butyl-4-methoxyphenyl)phosphino]-4,4'-bi-1,3-benzodioxole
H₈-BINAP	2,2'-bis(diphenylphosphino)-5,5',6,6',7,7',8,8'-octahydro-1,1'-binaphthyl
SEGPPOS	5,5'-bis(diphenylphosphine)-4,4'-bi-1,3-benzodioxole
Tol-BINAP	2,2'-Bis(di- <i>p</i> -tolylphosphino)-1,1'-binaphthyl
Xyl-BINAP	2,2'-bis(di(3,5-xyl)phosphino)-1,1'-binaphthyl
Xyl-P-PHOS	4,4'-bis[di(3,5-xyl)phosphino]-2,2',6,6'-tetramethoxy-3,3'-bipyridine



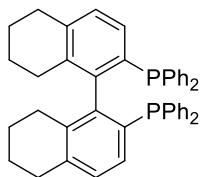
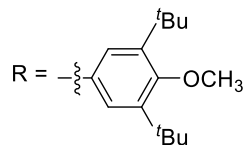
BINAP



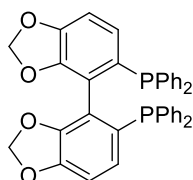
dppp



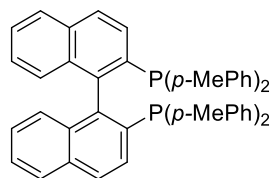
DTBM-SEGPPOS



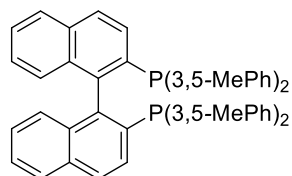
H₈-BINAP



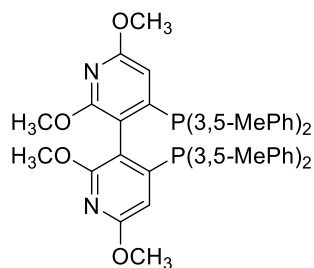
SEGPPOS



Tol-BINAP



Xyl-BINAP



Xyl-P-PHOS

GRAPHICAL SUMMARY

Summary (Page 1)

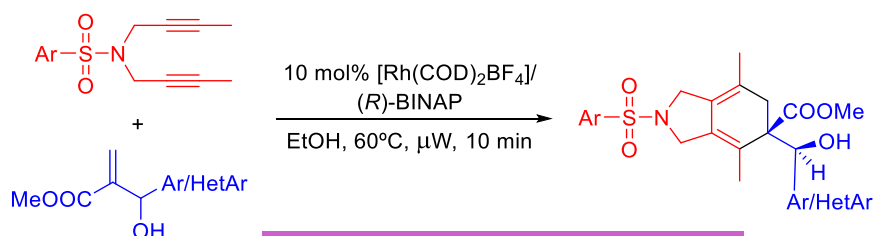
Resumen (Page 2)

Resum (Page 3)

Chapter 1. General introduction (Page 4)

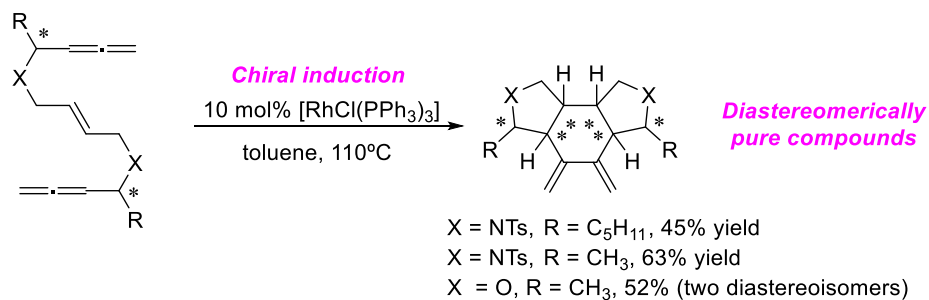
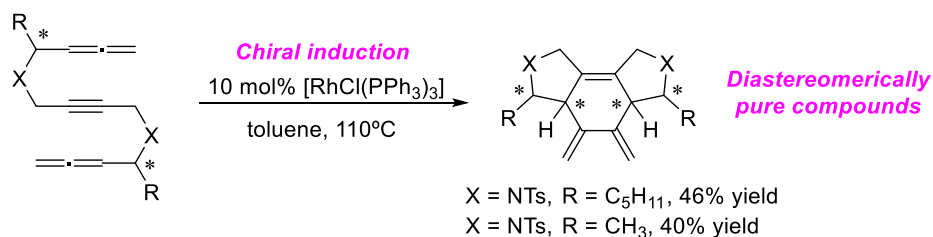
Chapter 2. Objectives (Page 37)

Chapter 3. Rhodium-catalysed [2+2+2] cycloadditions of diynes with Morita-Baylis-Hillman adducts (Page 39)

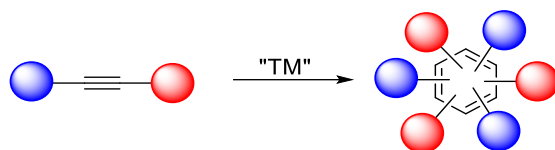


- ✓ diastereoselective process
- ✓ kinetic resolution of the Morita-Baylis-Hillman adduct
- ✓ products with a tertiary/quaternary stereocenter in a 84-97% ee

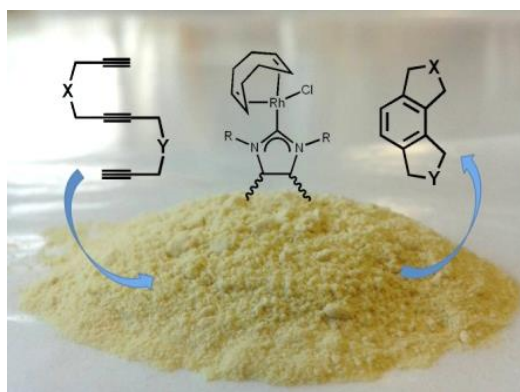
Chapter 4. Chiral induction in intramolecular rhodium-catalysed [2+2+2] cycloadditions of optically active allene-yne/ene-allene substrates (Page 54)



Chapter 5. [2+2+2] cycloaddition reaction for the synthesis of non-symmetric dendrimers (Page 71)



Chapter 6. Rhodium-NHC hybrid silica materials as recyclable catalysts for [2+2+2] cycloaddition reactions (Page 96)



Chapter 7. General conclusions (Page 132)

Chapter 8. Methods (Page 134)

Bibliography (Page 169)

SUPPLEMENTARY DATA

The material listed below is attached as supplementary data on the CD included in the thesis:

- **tesi1de5.pdf:** Memory of the thesis
- **tesi2de5.pdf:** Selection of the ^1H -NMR, ^{13}C -NMR, IR and MS spectra, and HPLC chromatograms and X-ray of the products synthesized in Chapter 3.
- **tesi3de5.pdf:** Selection of the ^1H -NMR, ^{13}C -NMR, IR and MS spectra and HPLC chromatograms of the products synthesized in Chapter 4.
- **tesi4de5.pdf:** Selection of the ^1H -NMR, ^{13}C -NMR, $^{31}\text{P}\{^1\text{H}\}$ -NMR and MS spectra of the products synthesized in Chapter 5.
- **tesi5de5.pdf:** Selection of the ^1H -NMR, ^{13}C -NMR, ^{13}C -SSNMR, ^{29}Si -SSNMR, IR and MS spectra, and BET, pore size distribution and powder X-ray diffraction graphs of the products synthesized in Chapter 6.

List of figures

Figure 1.1. Phosphoramidite modular architecture.	24
Figure 1.2. Structures of dendrimers G1, G2 and G3.....	28
Figure 1.3. Possible coordination modes of the <i>N</i> -phosphino sulfinamide ligands with mono- and bimetallic complexes.....	28
Figure 1.4. Hemilabile S-stereogenic and P-stereogenic ligands.....	30
Figure 1.5. NH/PH tautomeric equilibrium.....	30
Figure 1.6. Proposed catalytic cycle of the [Ni(IPr) ₂]-catalysed [2+2+2] cycloaddition of diynes and nitriles.....	33
Figure 3.1. Morita-Baylis-Hillman adducts: different perspectives.....	39
Figure 3.2. Synthesized diynes.....	43
Figure 3.3. ¹ H-NMR spectrum of 4a	46
Figure 3.4. ORTEP diagram of cycloadduct (<i>R,S</i>)- 4a	48
Figure 3.5. Formation of cycloadduct 4a over time (hours).....	49
Figure 3.6. Key 2D NOESY contacts for 9c	52
Figure 4.1. Bisallene substrates used.....	57
Figure 4.2. Stereoisomers of 13 when the synthesis is performed starting from <i>rac</i> - 18	59
Figure 4.3. HPLC chromatogram of <i>rac</i> - 13	60
Figure 4.4. HPLC chromatogram of (<i>R,R</i>)- 13	60
Figure 4.5. Three possible stereoisomers that could be formed upon cycloaddition of (<i>S,S</i>)- 10	62
Figure 4.6. Main observed NOESY correlations in good agreement with the proposed structure of 25	62
Figure 4.7. Possible stereoisomers of 24	63
Figure 4.8. Main observed NOESY correlations of cycloadduct 24 supporting the proposed structure.....	63
Figure 4.9. a) ¹ H-NMR chemical shifts (black) and ¹³ C-NMR chemical shifts (blue) of (3 <i>R</i> , 4 <i>R</i> , 9 <i>R</i> , 10 <i>S</i>)- 26 . b) Main observed NOESY correlations of cycloadduct 26 supporting the proposed structure.....	64
Figure 4.10. a) ¹ H-NMR chemical shifts (black) and ¹³ C-NMR chemical shifts (blue) of <i>rac</i> - 27 . b) Main NOESY correlations observed for <i>rac</i> - 27	66
Figure 4.11. a) ¹ H-NMR chemical shifts (black) and ¹³ C-NMR chemical shifts (blue) of <i>rac</i> - 28 . b) Main NOESY correlations observed for <i>rac</i> - 28	66
Figure 4.12. HPLC chromatogram of <i>rac</i> - 27	67
Figure 4.13. HPLC chromatogram of <i>rac</i> - 28	67
Figure 4.14. Six possible stereoisomers that could be formed upon cycloaddition of (<i>S,S</i>)- 14	69

Figure 4.15. ^1H -NMR spectrum of the olefinic part of the cycloadduct mixture from (<i>S,S</i>)- 14 .	69
Figure 4.16. ^1H -NMR chemical shifts (black) and ^{13}C -NMR chemical shifts (blue) of (<i>3R, 4S, 6R, 7R, 9S, 10S</i>)- 30 and (<i>3R, 4S, 6S, 7S, 9S, 10S</i>)- 31 .	70
Figure 5.1. Schematic representation of a dendrimer. C: core, B: branching units, S: surface groups.	72
Figure 5.2. Fréchet's poly(aryl ether) dendrimer.	74
Figure 5.3. Moore's poly(phenylacetylene) dendrimer.	74
Figure 5.4. Dendrimers synthesized with the divergent method.	75
Figure 5.5. Third generation fullerodendrimer.	77
Figure 5.6. Graphic depiction of layer, surface and segment-block dendrimers.	77
Figure 5.7. First layer-block dendrimer described. The core is represented in blue, aryl ester groups are in red, and aryl ether groups in black.	78
Figure 5.8. Layer-block dendrimer containing units derived from D- and L-tartaric acid.	78
Figure 5.9. First surface-block dendrimer described.	80
Figure 5.10. Amphiphilic surface-block dendrimer.	80
Figure 5.11. First segment-block dendrimer described. The core is represented in blue, arylester groups are in red and arylether groups in black.	82
Figure 5.12. Dendrimer containing polyester and polyaryl ether dendrons synthesized with a Diels-Alder reaction.	84
Figure 5.13. Product obtained from the Glaser coupling of 37 .	88
Figure 5.14. $^{31}\text{P}\{^1\text{H}\}$ -NMR of 42 .	90
Figure 5.15. Segment-block dendrimer containing PTA ligands and poly(ethylene glycol) chains.	91
Figure 5.16. ESI-MS spectrum of 52 .	94
Figure 5.17. $^{31}\text{P}\{^1\text{H}\}$ -NMR spectrum of 52 .	95
Figure 6.1. Hybrid silica material classification.	98
Figure 6.2. Thermogravimetric curve for M1 .	102
Figure 6.3. Example of ^{29}Si -SSNMR of material M1 .	103
Figure 6.4. Silicon environments and their corresponding label in the ^{29}Si -SSNMR.	104
Figure 6.5. Comparison of ^{13}C -NMR of compound 60 in CDCl_3 solution (red) and ^{13}C -CP-MAS of material M1 (blue).	104
Figure 6.6. Types of isotherm according to the IUPAC rules.	106
Figure 6.7. Types of hysteresis loops according to the IUPAC rules.	107
Figure 6.8. Schematic representation of Bragg's law.	108
Figure 6.9. Examples of powder X-ray diffraction patterns.	108
Figure 6.10. Imidazolium salts 54 and 55 containing triethoxysilyl groups.	113

Figure 6.11. ^1H -NMR of complex 60	116
Figure 6.12. ^{13}C -NMR of complex 60	117
Figure 6.13. Representation of the two isomers of 60 -allyl showing the major NOESY correlations observed.....	117
Figure 6.14. ^1H -NMR spectrum of complex 61	118
Figure 6.15. ^{13}C -NMR spectrum of complex 61	119
Figure 6.16. Gel formed with complex 60 and TEOS (molar ratio 1:30).....	120
Figure 6.17. ^{29}Si -NMR in solid state of M1	121
Figure 6.18. ^{13}C -NMR in solid state of M1	122
Figure 6.19. TGA curve of M1	122
Figure 6.20. Pore size distribution of M4	123
Figure 6.21. N_2 adsorption-desorption isotherm of M4	123
Figure 6.22. N_2 adsorption-desorption isotherm of M1	124
Figure 6.23. Pore size distribution of M1	124
Figure 6.24. N_2 adsorption-desorption isotherm of M2	125
Figure 6.25. Pore size distribution of M2	125
Figure 6.26. N_2 adsorption-desorption isotherm of M3	125
Figure 6.27. Pore size distribution of M3	126

List of schemes

Scheme 1.1. Transition metal-catalysed [2+2+2] cycloaddition reaction of alkynes (M = transition metal catalyst).....	5
Scheme 1.2. Postulated general mechanism of alkyne [2+2+2] cycloaddition reaction, where M = transition metal catalyst.....	6
Scheme 1.3. [2+2+2] Cycloaddition of 20- and 25-membered azamacrocycles.....	8
Scheme 1.4. Reaction studied by cyclic voltammetry, conductivity measurements, ³¹ P-NMR and ESI-MS.	8
Scheme 1.5. Rh-catalysed [2+2+2] cycloaddition of diynes and monoalkynes studied by ESI-MS.	9
Scheme 1.6. Transition metal-catalysed [2+2+2] cycloadditions between two alkynes and different unsaturations.	10
Scheme 1.7. [2+2+2] Cycloaddition of enediyne azamacrocycles.	11
Scheme 1.8. Rh(I)-catalysed enantioselective synthesis of 1,3-cyclohexadienes.	12
Scheme 1.9. Possible explanation proposed by Shibata for the different enantioselectivities obtained in the [2+2+2] cycloadditions of (<i>E</i>)-enediynes.	12
Scheme 1.10. [2+2+2] Cycloaddition of linear yne-ene-yne and yne-yne-ene substrates.	14
Scheme 1.11. Proposed mechanism for the [2+2+2] cycloaddition of yne-yne-ene substrates based on DFT studies.	14
Scheme 1.12. Mechanism proposed by Saá for the partial intramolecular [2+2+2] cycloaddition catalysed by ruthenium of diynes and linear or cyclic alkenes.....	15
Scheme 1.13. Partial intramolecular [2+2+2] cycloaddition of enynes and alkynes.	15
Scheme 1.14. [2+2+2] Cycloaddition between 1,6-enynes and asymmetric alkynes for the synthesis of 1,3-cyclohexadienes.....	16
Scheme 1.15. [2+2+2] Cycloaddition between enynes and vinyl enamides, and vinyl carboxylates.	16
Scheme 1.16. Partially intramolecular [2+2+2] cycloaddition between diynes and 1,2-disubstituted alkenes.....	17
Scheme 1.17. [2+2+2] Cycloaddition of diynes and 1,1-disubstituted alkenes.....	17
Scheme 1.18. [2+2+2] Cycloaddition between 1,6-diynes and non-symmetric alkenes.....	17
Scheme 1.19. Enantioselective [2+2+2] cycloaddition of diyne with styrene derivatives.	18
Scheme 1.20. Rh(I)-catalysed enantioselective [2+2+2] cycloaddition of diynes with dehydroamino acid.	18
Scheme 1.21. Enantioselective cycloaddition cascade of 1,6-diynes with 1,5-dienes.	19
Scheme 1.22. First [2+2+2] cycloaddition of allenes reported by Benson and Lyndsey.	19
Scheme 1.23. Yne-allene-yne and yne-yne-allene intramolecular [2+2+2] cycloaddition.	20

Scheme 1.24. Axial to central chirality transfer by a [2+2+2] cycloaddition of an allene-diyne substrate.	20
Scheme 1.25. Steroid analogue synthesized by a [2+2+2] cycloaddition of an yne-allene-yne substrate.	21
Scheme 1.26. Ruthenium(II)-catalysed [2+2+2] cycloaddition of allene-yne-ene substrates.	21
Scheme 1.27. Polycyclic scaffolds synthesized by a rhodium(I)-catalysed [2+2+2] cycloaddition of yne-allene-ene substrates.	21
Scheme 1.28. Rhodium(I)-catalysed [2+2+2] cycloaddition of allene-yne/ene-allene substrates.	22
Scheme 1.29. Key intermediates proposed by DFT calculations in the Rh(I)-catalysed [2+2+2] cycloaddition of allene-ene-allene substrates.	22
Scheme 1.30. Rhodium(I)-catalysed [2+2+2] cycloadditions of acyclic allene-yne-cyano derivatives.	23
Scheme 1.31. [2+2+2] Cycloaddition of yne-allene-imine substrates.	23
Scheme 1.32. Mechanistic proposal for the different cycloadducts formed.	24
Scheme 1.33. Partially intermolecular [2+2+2] cycloaddition between alkynes and alkene isocyanates.	25
Scheme 1.34. Proposed pathways in the [2+2+2] cycloaddition between alkynes and alkene isocyanates.	25
Scheme 1.35. Synthesis of an analogue of the FR901483 alkaloid.	26
Scheme 1.36. Rh(I)-catalysed [2+2+2] cycloaddition of carbodiimides with aryl- and heteroarylacetylenes.	26
Scheme 1.37. [2+2+2] Cycloaddition of monoalkynes and benzyl isocyanates.	27
Scheme 1.38. Synthesis of chiral polysubstituted piperidines by cleavage on the oxygen tether.	27
Scheme 1.39. [2+2+2] Cycloaddition reaction between <i>N</i> -tosyl 1,6-diyne and 2-methoxynaphthalene alkynyl derivatives.	28
Scheme 1.40. Pauson-Khand reaction of the PNSO-dicobalt complexes with norbornadiene. ..	29
Scheme 1.41. Preparation of cationic rhodium complexes [Rh(L*)(COD)]OTf and [Rh(L*) ₂]OTf.	29
Scheme 1.42. Rh(I)-catalysed [2+2+2]cycloaddition with PNSO ligands.	30
Scheme 1.43. Preparation of cationic Rh(I) complexes with secondary iminophosphorane (SIP) ligands.	31
Scheme 1.44. Asymmetric SIP-Rh(I) catalysed [2+2+2] cycloaddition of enediynes.	31
Scheme 1.45. Ni-catalysed [2+2+2] cycloadditions with IPr or SIPr ligands.	32
Scheme 1.46. Hoveyda-Grubbs's complex-catalysed [2+2+2] cycloaddition reaction involving heterounsaturations.	33

Scheme 1.47. Hoveyda-Grubbs's complex-catalysed [2+2+2] cycloaddition reaction involving alkenes.	34
Scheme 1.48. [2+2+2] Cycloaddition catalysed by Rh(I)-NHC complexes.	35
Scheme 3.1. Synthesis of Morita-Baylis-Hillman adducts.....	39
Scheme 3.2. Generally accepted mechanism of the Baylis-Hillman reaction.	40
Scheme 3.3. Reaction strategies employed with the Morita-Baylis-Hillman derivatives for the generation of cyclic compounds.	40
Scheme 3.4. Cu(I)-catalysed asymmetric 1,3-dipolar cycloaddition of various azomethine ylides with a Morita-Baylis-Hillman adduct.....	41
Scheme 3.5. [2+2+2] Cycloaddition of diynes and 1,1-disubstituted alkenes.....	41
Scheme 3.6. [2+2+2] cycloaddition between diynes and MBH adducts.....	41
Scheme 3.7. Synthesis of MBH adducts.....	42
Scheme 3.8. Synthesis of MBH adducts 2f and 2g	43
Scheme 3.9. Synthesis of diynes 1h and 1i	44
Scheme 3.10. Homocoupling reaction of diyne 1a	46
Scheme 3.11. Isomerization of MBH adduct 2a	46
Scheme 3.12. Kinetic resolution of allylic alcohols by selective isomerization to the ketone reported by Zhang.....	47
Scheme 3.13. Kinetic resolution of MBH adduct 2a	48
Scheme 3.14. Cycloaddition reactions with enantioenriched (<i>R</i>)- 2a	49
Scheme 3.15. Scope of the process	50
Scheme 3.16. [2+2+2] Cycloaddition reactions between diyne 1b and Morita-Baylis-Hillman adducts 3	51
Scheme 3.17. Diels-Alder cycloaddition between 1,3-cyclohexadienes 4b and 4c and dienophile 8	52
Scheme 4.1. Central to axial chirality induction in the cobalt-catalysed formation of pyridines.	54
Scheme 4.2. [2+2+2] Cycloaddition of chiral tetraynes with monoynes to achieve axially chiral biaryls	55
Scheme 4.3. [2+2+2] Cycloaddition of optically pure aromatic triynes to obtain helicene-like scaffolds.	55
Scheme 4.4. Synthesis of helicenoidal-DMAP compound by the Wilkinson-catalysed [2+2+2] cycloaddition of an optically pure triyne.	56
Scheme 4.5. Rhodium(I)-catalysed [2+2+2] cycloaddition of allene-yne/ene-allene substrates.	56
Scheme 4.6. Mechanism of the Crabbé homologation for the synthesis of allenes.	57
Scheme 4.7. Synthesis of (<i>S,S</i>)- 10 and (<i>S,S</i>)- 11	58

Scheme 4.8. Synthesis of (<i>R,R</i>)- 12 and (<i>R,R</i>)- 13	59
Scheme 4.9. Synthesis of (<i>S,S</i>)- 14	60
Scheme 4.10. Wilkinson-catalysed [2+2+2] cycloaddition reaction of allene-yne-allene 10 . a) ¹ H-NMR spectra of the olefinic part of the cycloadduct mixture from 10 and b) from optically pure (<i>S,S</i>)- 10	61
Scheme 4.11. Stereochemical correlations in the cycloaddition of 10	63
Scheme 4.12. Wilkinson-catalysed [2+2+2] cycloaddition reaction of allene-yne-allene (<i>R,R</i>)- 12	64
Scheme 4.13. [RhCl(PPh ₃) ₃]-catalysed [2+2+2] cycloaddition reaction of 13	65
Scheme 4.14. Wilkinson-catalysed [2+2+2] cycloaddition reaction of allene-ene-allene (<i>R,R</i>)- 13	67
Scheme 4.15. Wilkinson-catalysed [2+2+2] cycloaddition reaction of allene-ene-allene (<i>S,S</i>)- 11	68
Scheme 4.16. Wilkinson-catalysed [2+2+2] cycloaddition reaction of the oxygen-tethered allene-ene-allene (<i>S,S</i>)- 14	68
Scheme 5.1. Simplified model of the convergent synthesis.	73
Scheme 5.2. Divergent synthesis strategy.	75
Scheme 5.3. Synthetic strategy followed by Caminade, Majoral et al.	76
Scheme 5.4. Poly(aryl ether) dendrimer synthesized by a Co(I)-catalysed [2+2+2] cycloaddition reaction.	76
Scheme 5.5. Synthesis of the first generation layer-block π -conjugated dendrimer with alternating thienylenevinylene and phenylenevinylene units by a HWE reaction.	79
Scheme 5.6. Multi-charged phosphorus-containing surface-block dendrimer.	81
Scheme 5.7. Yamamoto's third generation segment-block dendrimer.	82
Scheme 5.8. Segment-block dendrimer containing a carbosilane dendron and a phosphorhydrazone dendron.	83
Scheme 5.9. Segment-block dendrimer synthesized by a copper-catalysed 1,3-dipolar cycloaddition between an alkyne and an azide.	83
Scheme 5.10. Retrosynthetic analysis of the surface-block dendrimer.	85
Scheme 5.11. Synthesis of <i>p</i> -ethynylbenzaldehyde (equation a) and <i>p</i> -iodobenzaldehyde (equation b).....	86
Scheme 5.12. Mechanism of the Bouveault aldehyde synthesis.....	86
Scheme 5.13. Synthesis of <i>N</i> -methyl-dichlorophosphorhydrazine.	86
Scheme 5.14. Synthesis of the poly(ethylene glycol) derivative 35	87
Scheme 5.15. Synthesis of the phosphorus-containing moieties 37 and 38	87
Scheme 5.16. Sonogashira reaction between fragments 37 and 38	88
Scheme 5.17. Sonogashira reaction between <i>p</i> -ethynylbenzaldehyde and 38	88

Scheme 5.18. Preparation of the Co complex of 40 .	89
Scheme 5.19. Synthesis of the model substrate 41 .	89
Scheme 5.20. Co-catalysed [2+2+2] cycloaddition reaction of 41 .	90
Scheme 5.21. Possible isomers formed in the [2+2+2] cycloaddition reaction.	91
Scheme 5.22. Retrosynthetic analysis for dendrimer 48 .	92
Scheme 5.23. Synthesis of 50 .	93
Scheme 5.24. Co-catalysed [2+2+2] cycloaddition of 50 .	93
Scheme 5.25. Synthesis of the cobalt complex of 50 .	93
Scheme 5.26. Alkylation of 51 with PTA.	94
Scheme 6.1. a) Physics and b) chemistry of the sol-gel process.	98
Scheme 6.2. Hydrolysis of tetraalkoxysilane promoted by acidic catalysis.	99
Scheme 6.3. Hydrolysis of tetraalkoxysilane promoted by basic catalysis.	99
Scheme 6.4. Hydrolysis of tetraalkoxysilane promoted by nucleophilic catalysis.	99
Scheme 6.5. a) Cogelification and b) Synthesis of bridged silsesquioxanes.	100
Scheme 6.6. Surfactant-assisted formation of a mesoporous material.	101
Scheme 6.7. Schematic pathway of the grafting method.	101
Scheme 6.8. Rh-catalysed [2+2+2] cycloaddition reaction in aqueous media.	109
Scheme 6.9. Air-stable [CpCoL(fumarate)] complexes for [2+2+2] cycloaddition reactions.	110
Scheme 6.10. Synthesis of a polystyrene immobilized [CpRh(C ₂ H ₄) ₂] complex.	111
Scheme 6.11. Pd(II) complexes tethered to a polysiloxane skeleton for [2+2+2] cycloadditions.	111
Scheme 6.12. Ni-complexes immobilised on silica.	112
Scheme 6.13. Silica-immobilized Co-catalyst for the [2+2+2] cycloaddition between diynes and nitriles.	112
Scheme 6.14. Synthetic pathway for imidazolium salt 54 .	114
Scheme 6.15. Synthetic pathway for imidazolium salt 55 .	114
Scheme 6.16. Synthesis of Rh-NHC complex described by Esteruelas et al.	115
Scheme 6.17. Synthesis of [Rh(μ -OEt)(COD)] ₂ .	115
Scheme 6.18. Synthesis of NHC-rhodium complex 60 .	115
Scheme 6.19. Synthesis of NHC-rhodium complex 61 .	115
Scheme 6.20. Preparation of hybrid silica materials M1 and M2 .	119
Scheme 6.21. Preparation of hybrid silica materials M3 and M4 .	120

List of tables

Table 3.1. Synthesis of diyne derivatives.....	44
Table 3.2. Optimization of the [2+2+2] cycloaddition between 1a and 2a	45
Table 6.1. Analytical data of materials M1-M4	121
Table 6.2. Textural data of materials M1-M4	123
Table 6.3. Catalytic performance of hybrid silica materials in the [2+2+2] cycloaddition of triyne 62	127
Table 6.4. Catalytic performance of hybrid silica materials in the [2+2+2] cycloaddition of triyne 64	128
Table 6.5. Catalytic performance of hybrid silica materials in the [2+2+2] cycloaddition of triyne 66	129
Table 6.6. Catalytic performance of hybrid silica material M4 under microwave irradiation..	129
Table 6.7. Catalytic performance of hybrid silica material M4 in the [2+2+2] cycloaddition between diynes 68 and monoalkynes 69	130

TABLE OF CONTENTS

Summary	1
Resumen.....	2
Resum.....	3
Chapter 1. General introduction	4
1.1 Transition metal-catalysed [2+2+2] cycloaddition reactions	5
1.1.1. The mechanism	5
1.1.2. Participating unsaturated substrates	10
1.1.2.1. Alkenes in rhodium-catalysed [2+2+2] cycloaddition reactions	11
1.1.2.1.1. <i>Totally intramolecular reaction</i>	11
1.1.2.1.2. <i>Partial intramolecular reaction</i>	15
1.1.2.2. Allenes in transition-metal catalysed [2+2+2] cycloaddition reactions	19
1.1.3. Rh-based catalysts for the [2+2+2] cycloaddition reaction.....	24
1.1.3.1. Phosphoramidite ligands in the Rh-catalysed [2+2+2] cycloaddition reaction.....	24
1.1.3.2. <i>N</i> -phosphino- <i>tert</i> -butylsulfonamide and secondary iminophosphorane ligands in the Rh-catalysed [2+2+2] cycloaddition reaction.....	28
1.1.3.3. <i>N</i> -heterocyclic carbene ligands in transition-metal catalysed [2+2+2] cycloaddition reactions.....	32
Chapter 2. Objectives	36
Chapter 3. Rhodium-catalysed [2+2+2] cycloadditions of diynes with Morita-Baylis-Hillman adducts	38
3.1 Precedents.....	39
3.1.1. Morita-Baylis-Hillman adducts.....	39
3.2 Results and discussion.....	41
3.2.1. Synthesis of Morita-Baylis-Hillman substrates.....	42
3.2.2. Synthesis of diyne substrates.....	43
3.2.3. [2+2+2] Cycloaddition of diynes and Morita-Baylis-Hillman adducts.....	45
Chapter 4. Chiral induction in intramolecular rhodium-catalysed [2+2+2] cycloadditions of optically active allene-yne/ene-allene substrates	53
4.1 Precedents.....	54
4.1.1. Chirality induction	54
4.2 Results and discussion.....	56
4.2.1. Synthesis of chiral allene-ene-allene and allene-yne-allene substrates	56
4.2.2. [2+2+2] Cycloaddition of allene-yne-allene substrates	60
4.2.3. [2+2+2] Cycloaddition of allene-ene-allene substrates	65

Chapter 5. [2+2+2] Cycloaddition reaction for the synthesis of non-symmetric dendrimers .	71
5.1 Precedents.....	72
5.1.1. Dendrimers.....	72
5.1.1.1. Synthetic strategies.....	73
5.1.1.2. Layer-block dendrimers.....	78
5.1.1.3. Surface-block dendrimers	79
5.1.1.4. Segment-block dendrimers	81
5.2 Results and discussion.....	84
5.2.1. Synthesis of a surface-block dendrimer.....	84
5.2.2. Synthesis of a segment-block dendrimer.....	91
Chapter 6. Rhodium-NHC hybrid silica materials as recyclable catalysts for [2+2+2] cycloaddition reactions	96
6.1 Precedents.....	97
6.1.1. Organic-inorganic hybrid silica materials.....	97
6.1.1.1. Preparation of organic-inorganic hybrid silica materials.	98
6.1.1.2. Characterization of hybrid silica materials.....	102
6.1.1.2.1. Thermogravimetric analysis (TGA).....	102
6.1.1.2.2. Elemental analysis.....	103
6.1.1.2.3. ²⁹ Si and ¹³ C Solid State Nuclear Magnetic Resonance (SSNMR).....	103
6.1.1.2.4. Surface area analysis.....	105
6.1.1.2.5. Powder X-ray diffraction	108
6.1.2. Recyclable catalysts in [2+2+2] cycloadditions	109
6.2 Results and discussion.....	113
6.2.1. Preparation of the hybrid silica materials.....	113
6.2.1.1. Synthesis of the N-heterocyclic carbene (NHC) ligand precursors	113
6.2.1.2. Synthesis of Rh-carbene complexes 60 and 61	114
6.2.1.3. Spectroscopic characterization of Rh-NHC complexes 60 and 61	116
6.2.1.4. Preparation of organic-inorganic hybrid silica materials	119
6.2.1.5. Characterization of hybrid silica materials.....	120
6.2.2. Catalytic tests of the rhodium-containing hybrid silica materials in [2+2+2] cycloaddition reactions	126
Chapter 7. General conclusions	132
Chapter 8. Methods.....	134
8.1 General materials and instrumentation.....	135
8.2. Experimental procedure for the products synthesised in Chapter 3.....	136

8.2.1. Synthesis of Morita-Baylis-Hillman substrates.....	136
8.2.2. Synthesis of diyne substrates.....	139
8.2.2.1. Synthesis of sulfonamide diynes	139
8.2.2.2. Synthesis of diyne 1h	140
8.2.2.3. Synthesis of diyne 1i	141
8.2.3. Rh-catalysed [2+2+2] cycloaddition between diynes and MBH adducts.....	141
8.2.4. Diels-Alder cycloaddition between 1,3-cyclohexadienes 4 and 4-phenyl-1,2,4-triazoline-3,5-dione.....	147
8.3. Experimental procedure for the products synthesised in Chapter 4.....	148
8.3.1. Synthesis of allene-yne-allene (<i>R,R</i>)- 12	148
8.3.2. Synthesis of allene-ene-allene (<i>R,R</i>)- 13	150
8.3.3. Synthesis of allene-ene-allene (<i>S,S</i>)- 14	151
8.3.4. Cycloaddition reaction of (<i>R,R</i>)- 12	151
8.3.5. Cycloaddition reaction of 13	152
8.3.6. Cycloaddition reaction of (<i>R,R</i>)- 13	153
8.3.7. Cycloaddition reaction of (<i>S,S</i>)- 14	153
8.4. Experimental procedure for the products synthesised in Chapter 5.....	154
8.4.1. Synthesis of poly(ethylene glycol) derivative 35	154
8.4.2. Synthesis of compound 37	155
8.4.2. Synthesis of compound 38	157
8.4.3. Synthesis of compound 40	158
8.4.4. Synthesis of compound 42	158
8.4.5. Synthesis of compound 52	159
8.5. Experimental procedure for the products synthesised in Chapter 6.....	160
8.5.1. Synthesis of 1,3-dimesityl-4,5-bis[3-(triethoxysilyl)propyl]-4,5-dihydroimidazolium chloride, 54	160
8.5.2. Synthesis of 1-mesityl-3-(3-(triethoxysilyl)propyl)-1H-3-imidazolium chloride, 59	162
8.5.3. Synthesis of Rh(I)-NHC complexes.	163
8.5.3.1. Synthesis of ethoxy(1,5-cyclooctadiene)rhodium(I) dimer.....	163
8.5.3.2. Synthesis of 60 , 60 -allyl and 61	163
8.5.4. Preparation of hybrid silica materials.	165
8.5.4.1. Synthesis of M1-M3	165
8.5.4.2. Synthesis of M4	166
8.5.5. Synthesis of triyne 62	166
8.5.6. Synthesis of triyne 64	167

8.5.7. Synthesis of triyne 66	168
8.5.6. [2+2+2] Cycloaddition of alkynes using materials M	169
Bibliography	171

Summary

One of the most important topics in organic chemistry is the development of new efficient processes for the formation of carbon-carbon bonds. The transition-metal catalysed [2+2+2] cycloaddition reaction is an efficient method to obtain six-membered polysubstituted carbo- and heterocyclic derivatives in a single synthetic step in an atom economy process.

This doctoral thesis is divided into eight different chapters and studies the involvement of challenging unsaturated substrates in the transition-metal catalysed [2+2+2] cycloaddition reaction, as well as new catalytic systems for the reaction. Chapter 1 contains a general introduction to this process and key examples found in the literature are used to establish a basis from which the other chapters are developed. Chapter 2 sets out the general objectives of the thesis. In Chapter 3, Morita-Baylis-Hillman adducts are involved in the partial intramolecular rhodium(I)-catalysed [2+2+2] cycloaddition reaction. This reaction affords an enantiopure cycloadduct featuring vicinal quaternary and tertiary carbon atoms through a kinetic resolution of the Morita-Baylis-Hillman adduct. Moreover, the cycloadducts undergo Diels-Alder reaction in a highly diastereoselective fashion. In Chapter 4, linear chiral allene-yne/ene-allene substrates are synthesized and submitted to [2+2+2] cycloaddition reaction conditions. The process works with effective chirality induction of the chiral centres of the linear compounds to the cycloadducts, which are obtained as a single enantiomer in most cases. The chirality of the cycloadduct obtained is studied by NMR techniques. In Chapter 5, the synthesis of a dendrimer by means of a Co-catalysed [2+2+2] cycloaddition reaction to form the core is described. The dendrimer contains a poly(ethylene glycol) moiety to provide it with solubility in water, as well as a ligand that can coordinate to a metal. In Chapter 6, hybrid silica materials containing rhodium(I) complexes are prepared and fully characterized. These materials are used for the [2+2+2] cycloaddition of alkynes (triyne and diyne with monoalkynes) and can be recovered by simple filtration and reused in further reactions. Chapter 7 draws general conclusions from the results of these studies. Finally, Chapter 8 contains the experimental procedure and the characterisation data for the compounds synthesised in this thesis.

Resumen

Uno de los temas más importantes en química orgánica es el desarrollo de nuevos procesos eficientes para la formación de enlaces carbono-carbono. La reacción de cicloadición [2+2+2] catalizada por metales de transición es un método eficiente para obtener derivados hetero- o carbocíclicos de seis miembros en un solo paso sintético en un proceso de economía atómica.

Esta tesis doctoral se divide en ocho capítulos y estudia la participación de sustratos insaturados complejos en la reacción de cicloadición [2+2+2] catalizada por metales de transición, así como nuevos sistemas catalíticos para la reacción. El Capítulo 1 contiene una introducción general de esta reacción, en el que se explican ejemplos clave de la bibliografía para establecer una base sobre la que se desarrollaran los otros capítulos. En el Capítulo 2 se marcan los objetivos de la tesis. En el Capítulo 3, se involucran los aductos de Morita-Baylis-Hillman en la reacción de cicloadición [2+2+2] catalizada por rodio en su versión parcialmente intramolecular. La reacción lleva a la obtención de un cicloaducto enantiopuro que contiene átomos de carbono cuaternarios y terciarios mediante la resolución cinética del aducto de Morita-Baylis-Hillman. Además, se demuestra que los cicloaductos dan reacción de Diels-Alder de forma diastereoselectiva. En el Capítulo 4, se sintetizan sustratos lineales quirales, que siguen la secuencia aleno-ino/eno-aleno, y se someten a las condiciones de reacción de cicloadición [2+2+2]. Los centros quirales del compuesto lineal inducen la quiralidad de los centros quirales generados en el cicloaducto, los cuales se obtienen como un solo enantiómero en la mayoría de casos. La quiralidad del cicloaducto se estudia a través de técnicas de RMN. En el Capítulo 5, se describe la síntesis de un dendrímero a través de una reacción de cicloadición [2+2+2] catalizada por cobalto. El dendrímero contiene un residuo de polietilenglicol que le da solubilidad en agua, así como un ligando que puede coordinar a un metal. En el Capítulo 6, se preparan y se caracterizan materiales híbridos de sílice que contienen complejos de rodio(I). Estos materiales se usan en la cicloadición [2+2+2] de alquinos (triinos y diinos con monoalquinos) y se pueden recuperar por simple filtración y ser posteriormente reutilizados. En el Capítulo 7 se exponen las conclusiones generales que se pueden extraer de los resultados obtenidos en estos estudios. Finalmente, el Capítulo 8 contiene los procedimientos experimentales y los datos de caracterización de los compuestos sintetizados en esta tesis.

Resum

Un dels temes més importants en química orgànica és el desenvolupament de nous processos eficients per la formació d'enllaços carboni-carboni. La reacció de cicloadició [2+2+2] catalitzada per metalls de transició és un mètode eficient per a l'obtenció d'hetero- o carbocicles de sis membres en un sol pas sintètic en un procés d'economia d'àtom.

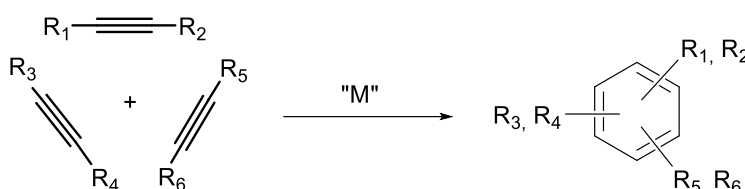
Aquesta tesi doctoral es divideix en vuit capítols i estudia la participació de substrats insaturats complexes en la reacció de cicloadició [2+2+2] catalitzada per metalls de transició, així com nous sistemes catalítics per la reacció. El Capítol 1 conté una introducció general a aquest procés i s'expliquen exemples clau trobats a la bibliografia per tal d'establir una base sobre la qual es desenvoluparan els altres capítols. Al Capítol 2 es marquen els objectius per a la tesi. Al Capítol 3 s'involucren adductes de Morita-Baylis-Hillman en la reacció de cicloadició [2+2+2] catalitzada per rodi en la seva versió parcialment intramolecular. En aquesta reacció s'obté un cicloadducte enantiopur, que conté un carboni quaternari i un de terciari veïnals, a través d'una resolució cinètica de l'adducte de Morita-Baylis-Hillman. A més a més, els cicloadductes poden participar en la reacció de Diels-Alder de manera diastereoselectiva. Al Capítol 4 es preparen substrats lineals quirals amb la seqüència al·lè-í/è-al·lè i es sotmeten a condicions de reacció de cicloadició [2+2+2]. Els centres quirals del compost lineal indueixen la quiralitat dels centres quirals generats en el cicloadducte, els quals s'obtenen com a un sol enantiòmer en la majoria de casos. La quiralitat del cicloadducte s'estudia a través de tècniques de RMN. Al Capítol 5 es descriu la síntesi d'un dendrímer a través d'una reacció de cicloadició [2+2+2] catalitzada per cobalt. El dendrímer conté un residu de polietilenglicol que li proporciona solubilitat en aigua, així com un lligand que pot coordinar a un metall. Al Capítol 6 es preparen i caracteritzen materials híbrids de sílice que contenen complexos de rodi(I). Aquests materials s'utilitzen en la cicloadició [2+2+2] d'alquins (triins i diins amb monoalquins) i es poden recuperar per simple filtració i reutilitzar-los en següents reaccions. Al Capítol 7 s'exposen les conclusions generals que es poden extreure dels resultats obtinguts en aquests estudis. Finalment, el Capítol 8 conté els procediments experimentals i les dades de caracterització dels compostos sintetitzats en aquesta tesi.

Chapter 1. General introduction

1.1 Transition metal-catalysed [2+2+2] cycloaddition reactions

The development of new chemical processes and efficient catalysts to enable the formation of carbon-carbon bonds is an important topic in organic chemistry. In particular, reactions where cyclic systems with high structural complexity are formed from simple precursors are of great importance. One of these processes is the metal-catalysed [2+2+2] cycloaddition reaction where a wide range of six-membered carbo- and heterocyclic compounds with different functionalities can be obtained.

The first substrates involved in this reaction were the alkynes and their transition metal-catalysed [2+2+2] cycloaddition represents one of the most elegant methods for the construction of polysubstituted benzene rings, as three carbon-carbon bonds are formed in an atom economy process (Scheme 1.1). In 1948, Reppe et al.¹ described the first transition metal-catalysed version of this transformation under nickel catalysis to obtain substituted benzene derivatives.



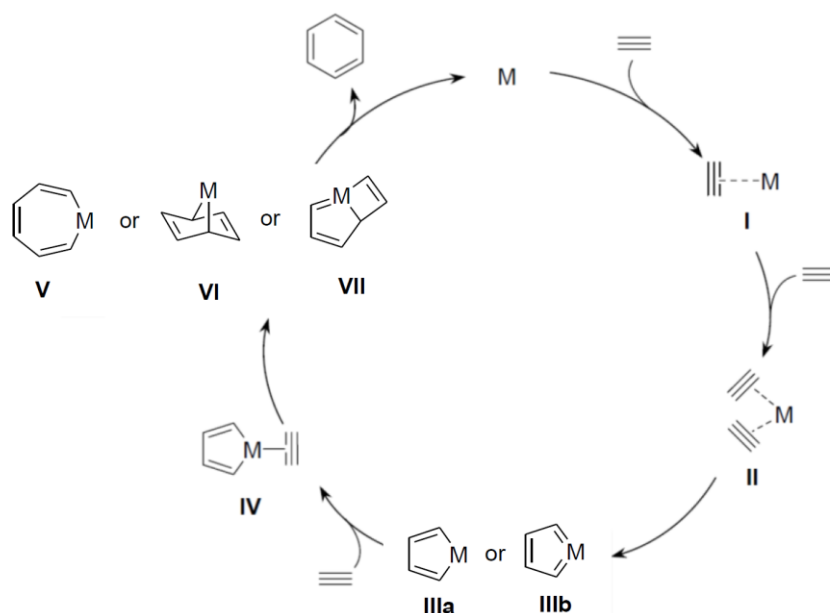
Scheme 1.1. Transition metal-catalysed [2+2+2] cycloaddition reaction of alkynes (M = transition metal catalyst).

Since this first study, many examples of alkyne cycloaddition catalysed by different transition metals have been described.² The most commonly used metals have been Ni, Co, Pd, Rh, Ru, Zr, and Ir. This reaction, which originally required stoichiometric amounts of the transition metal and extreme reaction conditions, has become a highly efficient catalytic process which can be performed in mild conditions and with low catalyst loads.

There are many aspects of this kind of reactions which are worthy of study. These include the mechanistic aspects that govern these processes, the type of unsaturated substrates that can participate in the cycloaddition (in which the chemo- and regioselectivity will have to be analysed, also the enantioselectivity when necessary) and the study of catalysts with high levels of activity. All of these aspects will be discussed here. Given that this thesis is based on Rh-catalysed [2+2+2] cycloaddition reactions, the examples described will be mainly focused on this kind of catalytic systems.

1.1.1. The mechanism

Progress in computational chemistry has allowed a breakthrough in the knowledge of the mechanistic rationale of the transition metal-catalysed [2+2+2] cycloaddition reaction. The specific reaction mechanism depends on the nature of the metal (Rh³, Ru⁴, Co⁵, Ir⁶, Cr⁶), ligands and substrate partners, but an overview of the most generally accepted pathway is shown in Scheme 1.2.



Scheme 1.2. Postulated general mechanism of alkyne [2+2+2] cycloaddition reaction, where M = transition metal catalyst.

In a first step, the coordination of one alkyne partner to the metal takes place leading to species **I**, followed by a second alkyne coordination to form species **II**. There is then an oxidative addition of the metal to afford the metallacyclopentadiene **IIIa** or the metallacyclopentatriene **IIIb** with a biscarbene type structure (when M = Ru) in which the metal adopts an oxidation state two units greater than in its precursor **II**. This has been found to be the rate-determining step in most cases.^{3e-i,n} It should be noted that a myriad of rhodacyclopentadiene⁷ complexes of type **IIIa** and ruthenacyclopentatriene⁸ complexes of type **IIIb** have been isolated and characterized to date, experimentally supporting the structure of these intermediates. The subsequent coordination of the third alkyne to intermediates **IIIa** or **IIIb** results in the formation of species **IV** and proceeds to either an alkyne insertion to form the metallacycloheptatriene **V** (the so-called Schore mechanism⁹), or by a metal-mediated [4+2] cycloaddition to afford the bicyclic complex **VI**,¹⁰ or by a formal [2+2] cycloaddition giving rise to metallabicyclo[3.2.0]heptatriene **VII**. Finally, reductive elimination of the metal results in the benzene ring formation and catalyst (M) being recovered.

The whole process is highly exothermic as the thermodynamic driving force is provided by the new σ -bonds formed and the aromaticity that is gained. Unlike the uncatalysed [2+2+2] cycloaddition of acetylenes, which presents a prohibitive energy barrier,¹¹ the barriers for the transition-metal-catalysed [2+2+2] cycloaddition are relatively low. This agrees with the fact that this reaction typically occurs under quite mild conditions.

Focusing on the Rh-catalysed [2+2+2] cycloaddition, the first theoretical study based on Density Functional Theory (DFT) of the mechanism involving this metal was in 2007, by Bickelhaupt et al.^{3e} In their study, the model catalyst was $[\text{CpRh}(\text{C}_2\text{H}_2)_2]$ and they studied the acetylene cyclotrimerization to form benzene and the co-cyclization of two acetylene molecules with acetonitrile to generate 2-methylpyridine. Experimental studies of the reaction of two alkynes with a nitrile have demonstrated that nitriles are less reactive than alkynes,¹² the results obtained in this study confirmed what was already known experimentally: the formation of

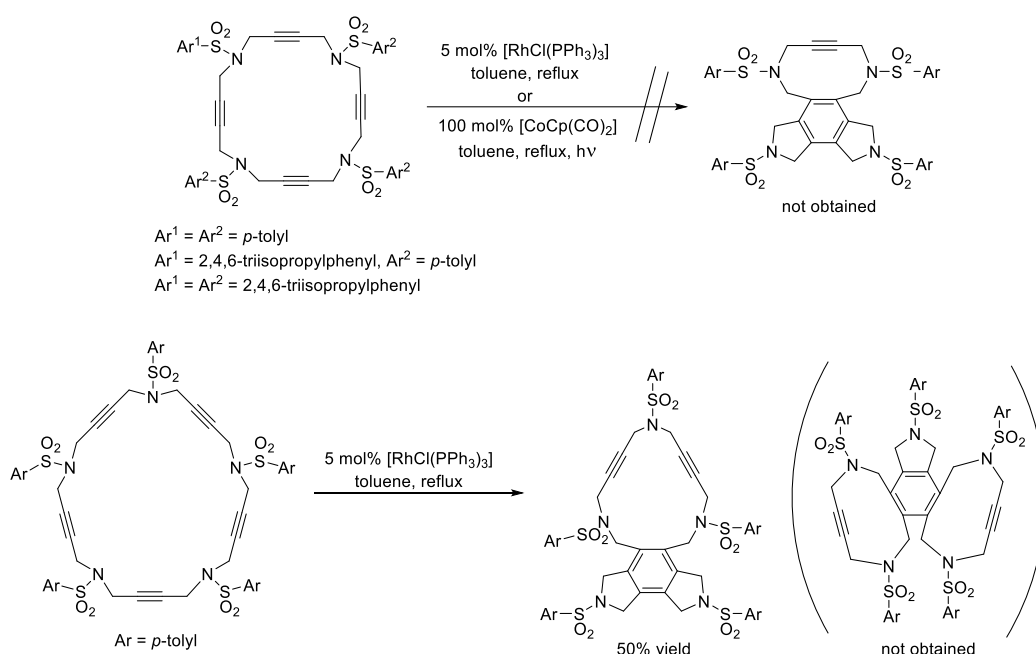
benzene is thermodynamically favoured in 39.5 kcal/mol, thus explaining why an excess of nitrile is required to obtain good yields of pyridine. Another feature studied was the substitution of the Cp ligand in the catalyst for an indenyl group. Booth et al.¹³ reported that when the cyclopentadienyl ligand is changed for an indenyl an enhancement of reactivity is observed for the cyclotrimerisation of alkynes (the so called indenyl effect, discovered by Basolo et al.¹⁴). However, in this case they found that the catalytic path of acetylene cyclotrimerization with the IndRh fragment is similar to that described with the CpRh fragment. In a more recent study in 2014 by Bickelhaupt in collaboration with Swart's group,^{3a} they studied the [2+2+2] cyclotrimerization of acetylene with both [CpRh(CO)₂] and [IndRh(CO)₂] complexes. Unlike the previous study, they hypothesize that an ancillary ligand of the precatalyst (CO) remains bonded to the metal centre through the whole catalytic cycle. This assumption is based on the experimental findings of Booth et al.,¹³ who found that this ancillary ligand has an effect on the yield and selectivity of the reaction. The conclusions drawn from Bickelhaupt's study were that, from a theoretical point of view, the mechanism in which an ancillary ligand remains through all the catalytic cycle is plausible, leading to the occurrence of the indenyl effect. Moreover, the highest activation energy is not for the formation of the five-membered rhodacycle, but rather for the coordination of the third acetylene molecule. In this last step, a change in the coordination mode of the metal in the corresponding Cp or Ind ligand concurs with a decrease in the energy barrier predicted for the coordination of the third acetylene molecule. The energy barrier for the IndRh complex (28.5 kcal mol⁻¹) is significantly lower than that predicted for CpRh (43.2 kcal mol⁻¹), thus explaining Booth's experimental results.

In our group we have also made several contributions to the field of DFT studies in Rh-catalysed [2+2+2] cycloaddition, using Wilkinson's complex as the catalyst. The most relevant of these studies will be outlined below.

As Bickelhaupt et al., our group has also studied the cyclotrimerization of acetylene by means of DFT but using [RhCl(PPh₃)₃] as the catalyst.³ⁱ In many theoretical organometallic chemistry studies involving Wilkinson's catalyst or similar catalysts, the PPh₃ ligands are substituted by PH₃ molecules. The replacement of PPh₃ by PH₃ in DFT studies is appealing because it significantly reduces the computational cost. In this work the study was made with both catalysts in order to compare the influence of the substitution of the phosphines. It was found that modeling PPh₃ by PH₃ in the catalyst results in minor changes in the thermodynamics and kinetics at 0 K. Both the reaction energies and the barriers in the rate determining step differ by less than 1 kcal·mol⁻¹. However, some differences have to be taken into account between the two reaction mechanisms. The initial step of the reaction is not the same, as for the case of Wilkinson's catalyst the lowest energy barrier is found when only one phosphine is present in the catalyst, whereas when PPh₃ is changed for PH₃ the lowest energy barriers are found when two phosphines are present. An alternative pathway for the attack of the third acetylene molecule on the rhodacyclopentadiene that is formed is also found to be operative for the Wilkinson's catalyst but not in the modeled [RhCl(PH₃)₃]. In addition, the Gibbs free energy barrier of the rate-determining step at 298 K is somewhat higher (about 5 kcal·mol⁻¹) for the model catalyst, [RhCl(PH₃)₃].

Our group has also developed rhodium(I)-catalysed cycloadditions of polyunsaturated azamacrocycles.¹⁵ DFT studies were carried out in order to understand the particular reactivity

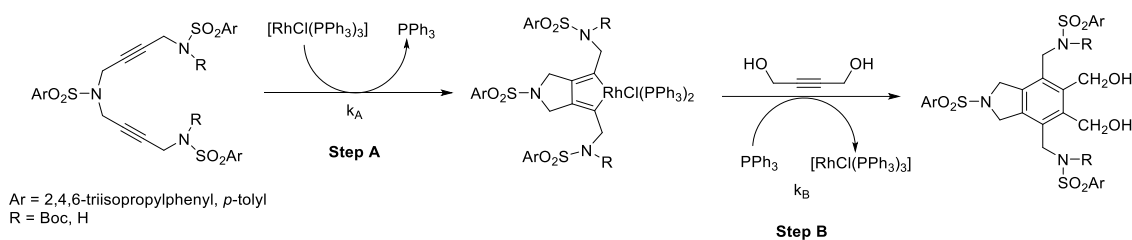
of two cases: 20-membered tetracetylenic azamacrocycles and 25-membered pentacetylenic azamacrocycles.^{3m} Experimentally, it was observed that the 20-membered azamacrocycle was unreactive under cycloaddition conditions. On the other hand, two different isomers could have been obtained for the 25-membered azamacrocycle, but only one was isolated (Scheme 1.3). DFT studies helped us to understand this reactivity. Calculations revealed two main factors that contribute to the lack of reactivity of the 20-membered azamacrocycle: first, the HOMO orbital is more stable and delocalised than in other azamacrocycles and, second, the presence of a strained 10-member ring in the cycloadduct. The same reason can be applied to the 25-membered azamacrocycle as the cycloadduct that was not obtained also contains two 10-membered rings.



Scheme 1.3. [2+2+2] Cycloaddition of 20- and 25-membered azamacrocycles.

As has been said earlier, a myriad of rhocyclopentadiene intermediates have been isolated experimentally, however structural information regarding the intermediate that is formed for the insertion of the third alkyne is hard to obtain. Our group has contributed to try to discern the structure of this intermediate.

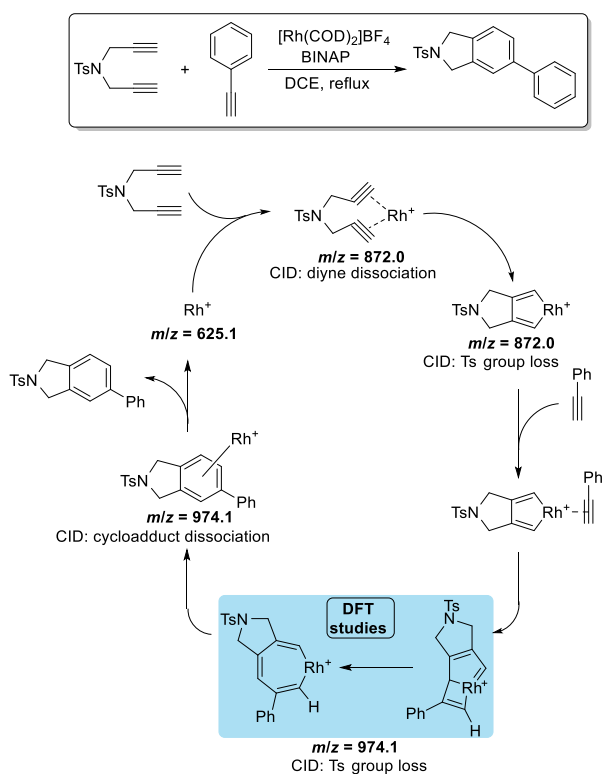
In 2009 we studied the Wilkinson's complex-catalysed [2+2+2] cycloaddition between a diyne and a monoalkyne by cyclic voltammetry, conductivity measurements, ³¹P-NMR and Electro Spray Ionisation Mass Spectrometry (ESI-MS) (Scheme 1.4).^{7d}



Scheme 1.4. Reaction studied by cyclic voltammetry, conductivity measurements, ³¹P-NMR and ESI-MS.

In this study, kinetic data for the two main steps of the catalytic cycle of the Wilkinson's complex-catalysed [2+2+2] cycloaddition of alkynes was presented for the first time. From the values of the half reaction times of the two main steps, it could be concluded that the rate-determining step varies depending on the structure of the starting reagents. When bulkier reagents are used ($R = \text{Boc}$ in Scheme 1.4), the oxidative addition of the rhodium to the diyne (Step A) is the rate-determining step, whereas when a less bulky diyne is used ($R = \text{H}$ in Scheme 1.4.), the reaction of the rhodacyclopentadiene with the monoalkynes (Step B), was rate-determining.

To deepen our understanding of the intermediate species formed during the reaction, ESI-MS was used to monitor the Rh-catalysed [2+2+2] cycloaddition of diynes and monoalkynes.^{7b} In this case a cationic rhodium complex was used given that when a neutral complex such as the Wilkinson's catalyst was employed, the intermediates were undetectable by ESI-MS. In a first step, the oxidative addition intermediate was detected and further characterized by conducting tandem mass spectrometry analysis (MS/MS). The most interesting finding of this study was the detection of a more advanced intermediate in the catalytic cycle arising from the insertion of the third alkyne into the rhodacyclopentadiene species. MS/MS analysis allowed the characterisation of this intermediate. For the first time, all of the intermediate species in the catalytic cycle were detected (Scheme 1.5).



Scheme 1.5. Rh-catalysed [2+2+2] cycloaddition of diynes and monoalkynes studied by ESI-MS.

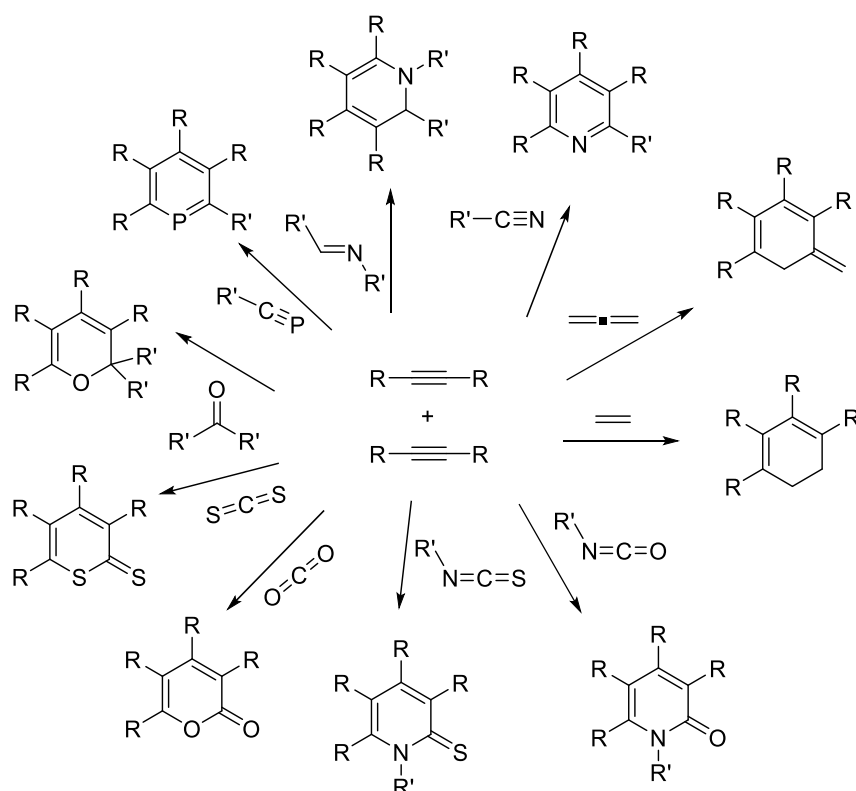
Although the structure of the intermediates was supported by MS/MS analysis, the structure of the third alkyne insertion intermediates (type **V**, **VI** and **VII** in Scheme 1.2) could not be determined by this methodology. Computer model studies based on DFT to elucidate the structure of the aforementioned intermediates concluded that that the cycloheptatriene intermediate was the most likely structure for the monoalkyne insertion intermediate. However,

the small differences in energy barriers did not allow us to rule out the possibility that the insertion intermediate was the rhodabicyclo-[3.2.0]heptatriene complex.

In a more recent study, Paneque et al.^{7a} managed to isolate and crystallize intermediates of the rhodium-catalysed [2+2+2] cycloaddition reaction of three alkynes by using an air stable [TpRh(C₂H₄)₂] complex (Tp = hydrotris(pyrazolyl)borate). Its reaction with dimethyl acetylenedicarboxylate afforded a myriad of complexes whose structure is consistent with intermediates in the [2+2+2] cycloaddition. These complexes could be crystallised and studied from a spectroscopic point of view and their stability towards reactivity was evaluated.

1.1.2. Participating unsaturated substrates

As was mentioned in section 1.1.1, alkynes are not the only unsaturations that can participate in this reaction. The transition-metal catalysed [2+2+2] cycloaddition has been modified to incorporate other unsaturated substrates such as nitriles, allenes, olefins, isocyanates, isothiocyanates, carbon dioxide, carbon disulphide, aldehydes, ketones and, more recently in a few reports, phosphalkynes¹⁶ and imines¹⁷. The reaction of these unsaturations with two alkynes to afford the corresponding six-membered ring compounds is shown in Scheme 1.6.^{2i-m,p-s}



Scheme 1.6. Transition metal-catalysed [2+2+2] cycloadditions between two alkynes and different unsaturations.

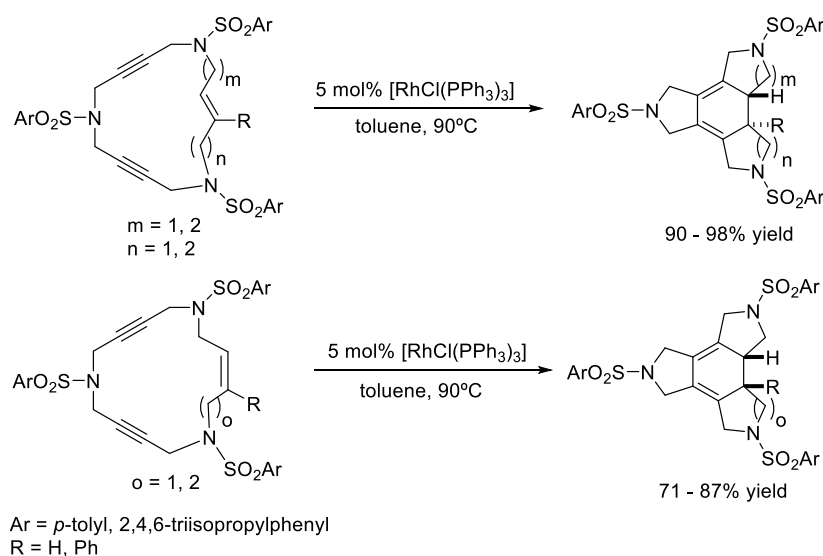
In this thesis, we aimed to study the [2+2+2] cycloaddition reaction of alkynes with both alkenes and allenes. The replacement of *sp* hybridised substrates by *sp*² hybridised ones generally concurs with a decrease in reactivity, but has the advantage of allowing for the eventual introduction of stereogenic centres in the newly formed six-membered ring. For example, a

cycloaddition employing three alkynes affords a product containing no stereocentres, whereas a cycloaddition involving three alkenes could generate a cyclohexane possessing up to six stereocentres in a single step, nevertheless this particular case has not been reported to date. The reaction of two alkynes with a properly substituted alkene allows chiral 1,3-cyclohexadienes to be synthesized. The synthesis of 1,3-cyclohexadienes by other means is not so easy¹⁸ as their preparation is usually based on the dehydrobromination of 1,2-dibromocyclohexane¹⁹ at high temperatures or by thermal electrocycloaddition of hexatrienes.²⁰ However, alkenes are more reluctant to react and, therefore, it is generally difficult to control the chemoselectivity given the high reactivity of the alkyne substrates. An excellent alternative to react sp^2 -hybridised unsaturations, thus generating stereocomplexity, while maintaining the reactivity is to use allenes.

1.1.2.1. Alkenes in rhodium-catalysed [2+2+2] cycloaddition reactions

1.1.2.1.1. Totally intramolecular reaction

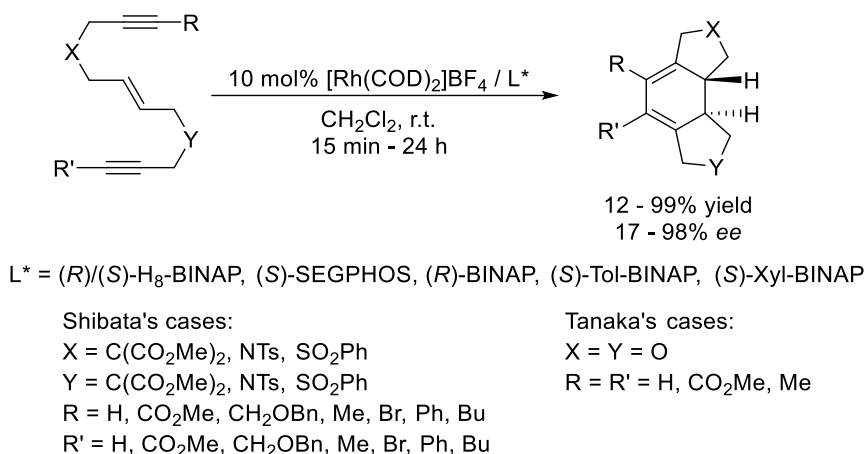
In line with the interest of the METSO group in the [2+2+2] cycloaddition of macrocyclic rings,^{15, 21} we tested the reactivity of macrocyclic enediynes bearing *E* and *Z* alkene moieties in the Wilkinson's complex-catalysed [2+2+2] cycloaddition.^{21a,b} The corresponding cycloadducts were obtained in good yields (Scheme 1.7). Through NMR analysis it could be seen that when the macrocycle bearing an *E* configuration was used, the corresponding protons in the cycloadduct were displayed in an *anti*-position, whereas when the *Z* isomer was used, the protons showed a *syn* relative position, proving that a stereoselective process was taking place.



Scheme 1.7. [2+2+2] Cycloaddition of enediynes azamacrocycles.

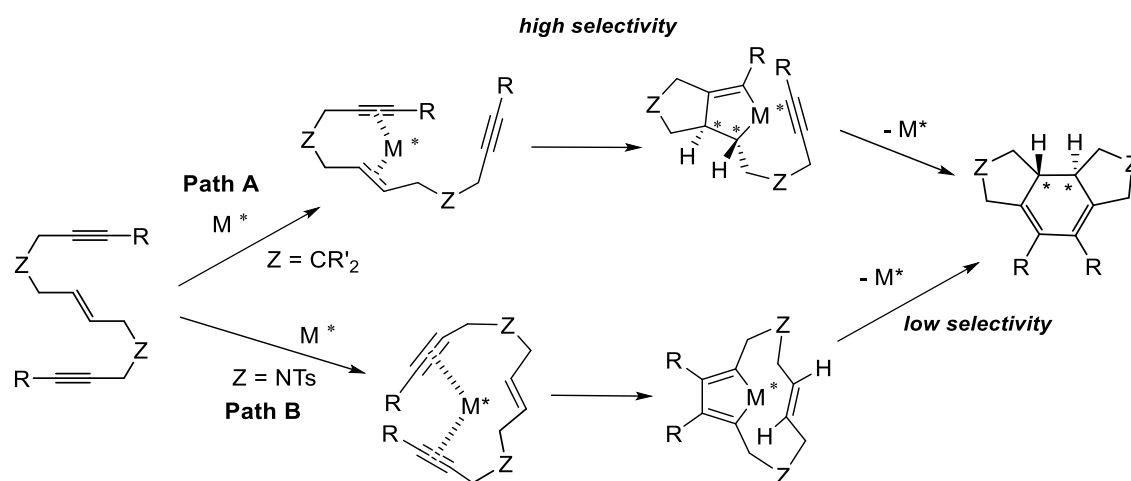
Inspired by these results, the groups of Shibata²² and Tanaka²³ reported at the same time, the asymmetric version of the totally intramolecular reaction of open-chain enediynes. They reported the enantioselective intramolecular [2+2+2] cycloaddition of different-substituted (*E*)-enediynes catalysed by $[\text{Rh}(\text{COD})_2]\text{BF}_4$ complex and chiral BINAP-type phosphines for the synthesis of chiral 1,3-cyclohexadienes (Scheme 1.8). These studies involved internal and terminal alkynes as well as different linkers between the unsaturations. Although different cyclohexadienes were obtained with moderate to good yields and enantioselectivities, Shibata's study proved that the process was highly sensitive to the nature of the substrate as well as the

phosphine used with (*R*)/(*S*)-H₈-BINAP and (*S*)-Tol-BINAP being found to give the highest enantiomeric excesses.



Scheme 1.8. Rh(I)-catalysed enantioselective synthesis of 1,3-cyclohexadienes.

Depending on the substrate structure, Shibata rationalized the different enantioselectivities obtained by the possible reaction pathways that they followed (Scheme 1.9). When the metal first coordinates with an alkyne and an alkene following path A in the scheme, high selectivity is expected since the two chiral centres are generated in a first step. However, when the metal coordinates to the two alkynes, as in path B, the enantioselectivity of the subsequent intramolecular alkene insertion is expected to be very low.



Scheme 1.9. Possible explanation proposed by Shibata for the different enantioselectivities obtained in the [2+2+2] cycloadditions of (*E*)-enediynes.

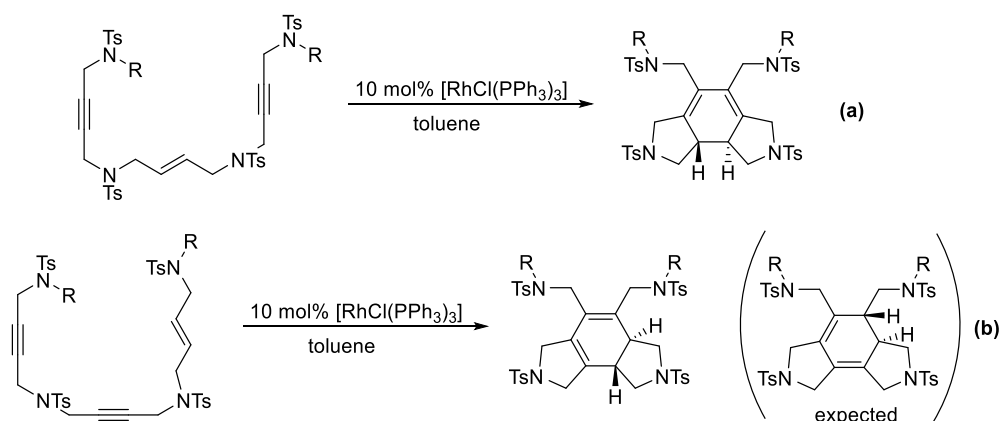
The process is influenced by two features: whether the alkynes are terminal or non-terminal and the nature of the tether. First of all, introduction of appropriate substituents on the alkyne termini of the enediyne was crucial for the suppression of the oxidative coupling of two alkyne moieties, which would decrease their reactivity and selectivity. In the case of enediynes with unsubstituted alkyne termini, the enantioselectivity was low, probably as a result of the high reactivity of the terminal alkynes that favour the oxidative coupling of two alkyne moieties over that of an eneyne moiety (path B in Scheme 1.9). The tether also has an influence on the pathway that is followed. In the case of carbon-tethered enediyne (path A in Scheme 1.9), the oxidative coupling is hypothesised as proceeding with high enantioselectivity to give the bicyclic

metallacyclopentene, where two chiral carbon centres are generated. The subsequent intramolecular alkyne insertion along with reductive elimination gives the tricyclic cyclohexadiene scaffold. In contrast, in the case of nitrogen-tethered enediyne (path B in Scheme 1.9), the oxidative coupling of two distant alkyne moieties is represented as proceeding before that of the enyne moiety to give a bicyclic metallacyclopentadiene given that the nitrogen tether activates the alkynes more than the carbon tether. The enantioselectivity of the subsequent intramolecular alkene insertion is expected to be very low and so the corresponding cycloadduct would be obtained in poor enantiomeric excesses. Only in the case of nitrogen-tethered enediynes (path B in Scheme 1.9), the choice of substituents on the alkyne termini was important to achieve high enantioselectivity and prevent alkyne-alkyne oxidative coupling of enediynes prior to alkyne-alkene coupling. The correct choice of chiral ligands was also essential as only H₈-BINAP achieved both a good yield and enantiomeric excess. Other BINAP derivatives, such as Tol-BINAP and BINAP, gave both poor yields and enantiomeric excesses.

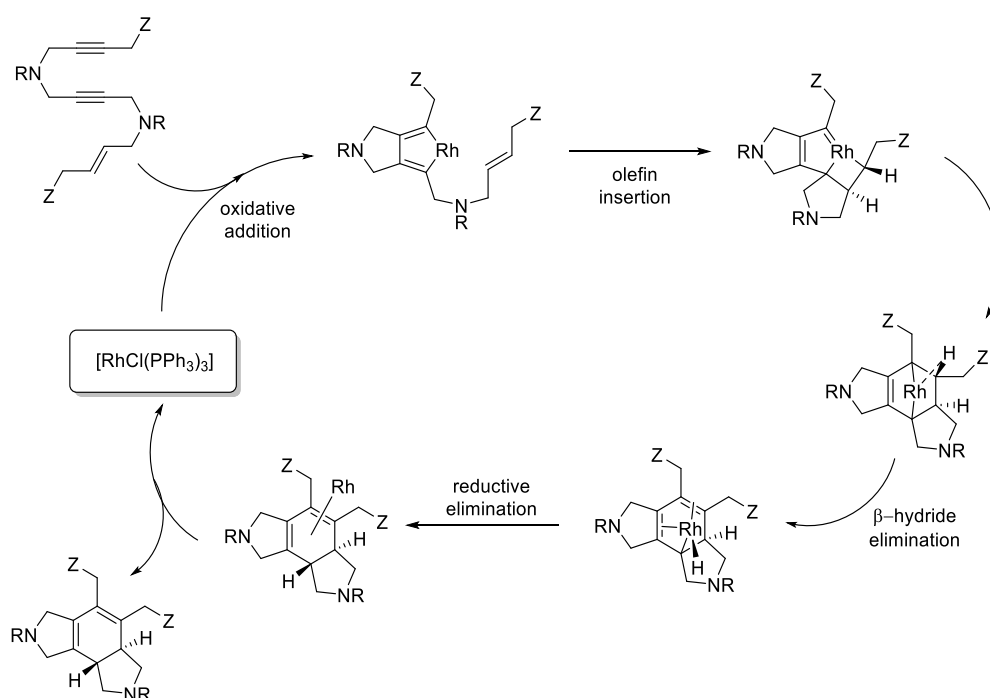
Our group also tested this catalytic system in the asymmetric [2+2+2] cycloaddition of the (*E*)-enediyne azamacrocycles shown in Scheme 1.7.^{21a} Using the [Rh(COD)₂]BF₄ cationic rhodium complex in combination with chiral phosphines ((*S*)-BINAP, (*S*)-(+)-neomenthyl diphenylphosphane and (2*S*,3*S*)-(-)-2,3-bis(diphenylphosphino)butane), the products were obtained in moderate enantiomeric excesses (10 - 44%).

To fully understand the mechanism of the [2+2+2] cycloaddition of two alkynes with one alkene, our group has studied the intramolecular reaction of enediynes both experimentally and theoretically. In a first work we reported a computational study of the Wilkinson's complex-catalysed [2+2+2] cycloaddition of enediynes.^{3k} It was observed that the preferred oxidative addition of the metal to the enediyne (the oxidative addition involving either two alkynes or one alkyne and one alkene) varies depending on the substituents and tethers in the substrate. This finding was in line with the experimental work of Shibata et al.²² using the [Rh((*S*)-H₈-BINAP)]BF₄ complex that postulated that different oxidative additions were possible, and those had consequences in the enantiomeric excess of the final cycloadduct (Scheme 1.9). In this study different factors that can have an influence on the preferred reaction pathway were analysed. It was found that when the tether was bulkier, alkyne-alkyne coupling was the preferred pathway. With regards to the alkyne moiety substituent, it can be seen that enyne coupling is preferred when there are bulky substituents, due to steric repulsion of the alkyne-alkyne coupling. While in some cases enyne coupling is preferred for acyclic enediynes, cyclic enediynes always prefer alkyne-alkyne coupling due to the high deformation energy required by the macrocycle to achieve the required geometry in order to undergo enyne oxidative addition.

In another study, enediynes with both yne-ene-yne and yne-yne-ene sequences were tested in the Wilkinson's complex-catalysed reaction (Scheme 1.10).^{3j} When yne-ene-yne derivatives were tested, the expected [2+2+2] cycloadduct was obtained (equation a in Scheme 1.10), but when yne-yne-ene compounds were submitted to reaction conditions an isomer of the expected cycloadduct was obtained (equation b in Scheme 1.10).

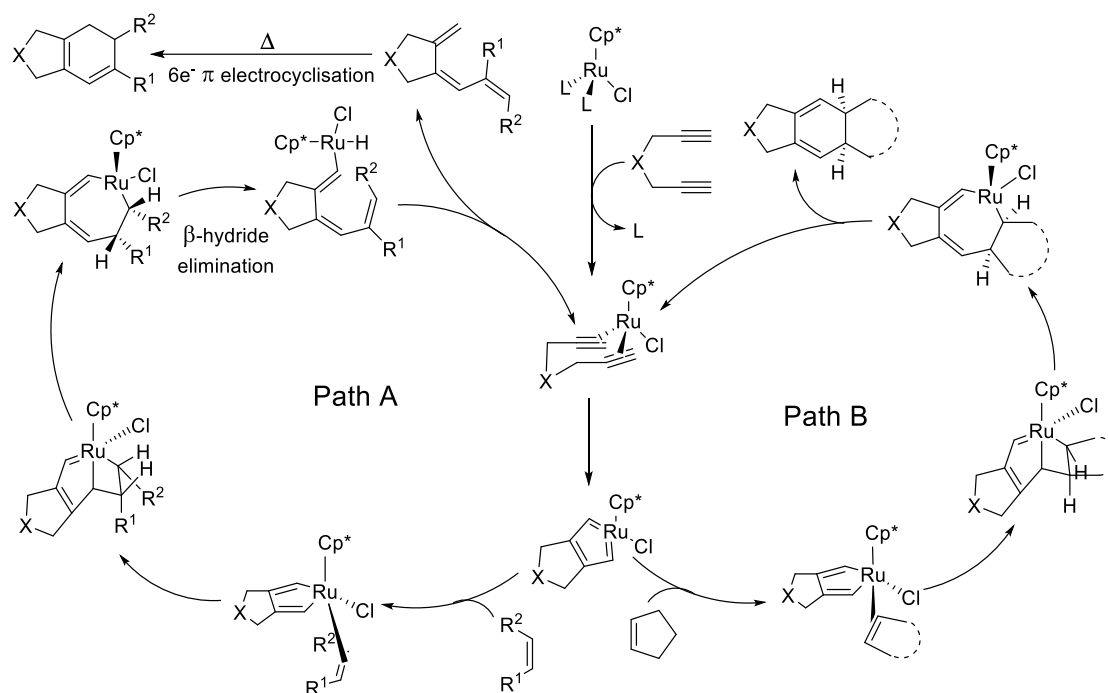


To understand the mechanistic rationale behind this phenomenon, DFT calculations were carried out. Yne-ene-yne enediynes followed the classical [2+2+2] cycloaddition mechanism: a first oxidative addition of the two alkynes, after which insertion of the alkene and reductive elimination afforded the expected cycloadduct. In the case of yne-yne-ene enediynes, the mechanism also starts with an oxidative addition of the alkynes, but, prior to the reductive elimination step, they suffer a β -hydride elimination, giving rise to an isomer of the expected cycloadduct (Scheme 1.11).



Saá et al.²⁴ described a similar reactivity in the partial intramolecular ruthenium-catalysed [2+2+2] cycloaddition between diynes and alkenes. The course of the [2+2+2] cycloaddition varies with the nature of the starting alkene. With cyclic alkenes as partners, standard 1,3-cyclohexadienes are obtained (path B in Scheme 1.12), but when acyclic alkenes are used, a tandem process is observed: by means of a β -elimination followed by a reductive elimination, a

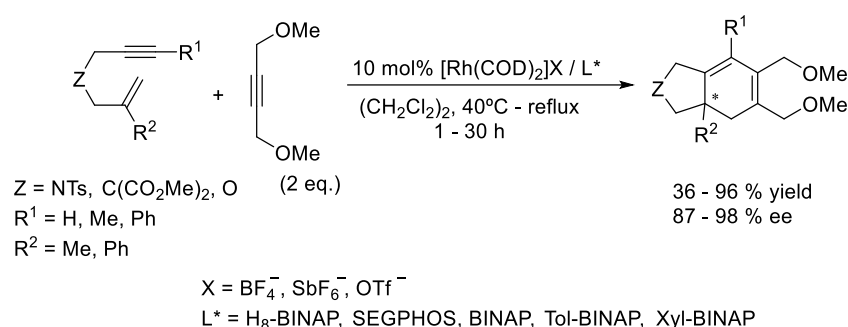
1,3,5-hexatriene intermediate is formed. Finally, a pure thermal $6e^- \pi$ electrocyclicization gives the resulting 1,3-cyclohexadiene derivative (path A in Scheme 1.12).



Scheme 1.12. Mechanism proposed by Saá for the partial intramolecular [2+2+2] cycloaddition catalysed by ruthenium of diynes and linear or cyclic alkenes.

1.1.2.1.2. Partial intramolecular reaction

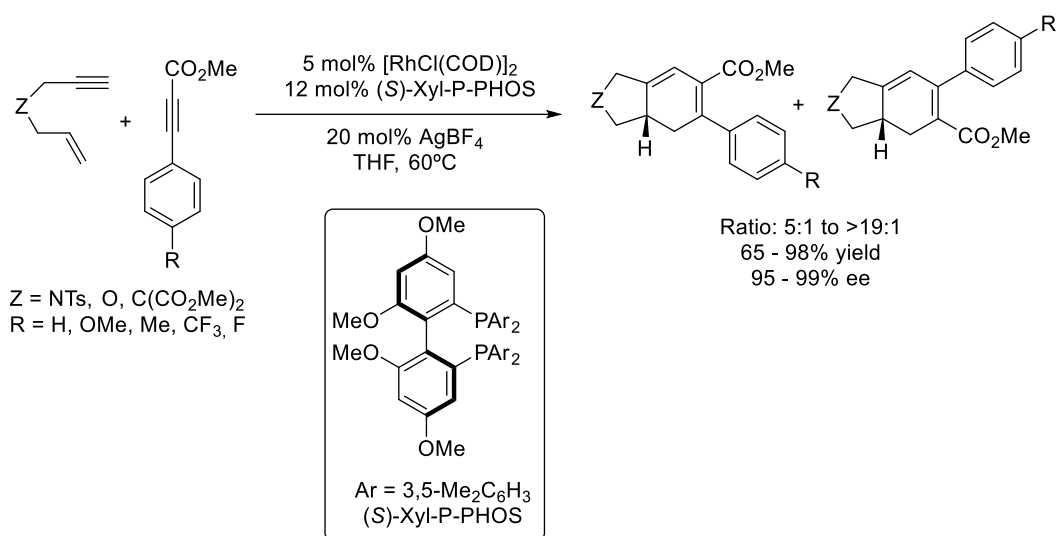
In 2005, Shibata et al.²⁵ reported the partial intramolecular Rh(I)-catalysed [2+2+2] cycloaddition between enynes and alkynes. Using the combination of a cationic rhodium complex and BINAP-type phosphines they successfully synthesized 1,3-cyclohexadienes containing a quaternary stereogenic carbon in good to excellent yields and with excellent enantiomeric excesses (Scheme 1.13). For this particular case, the best enantiomeric excesses and yields were obtained using a catalytic system combining $[\text{Rh}(\text{COD})_2]\text{BF}_4$ and Tol-BINAP.



Scheme 1.13. Partial intramolecular [2+2+2] cycloaddition of enynes and alkynes.

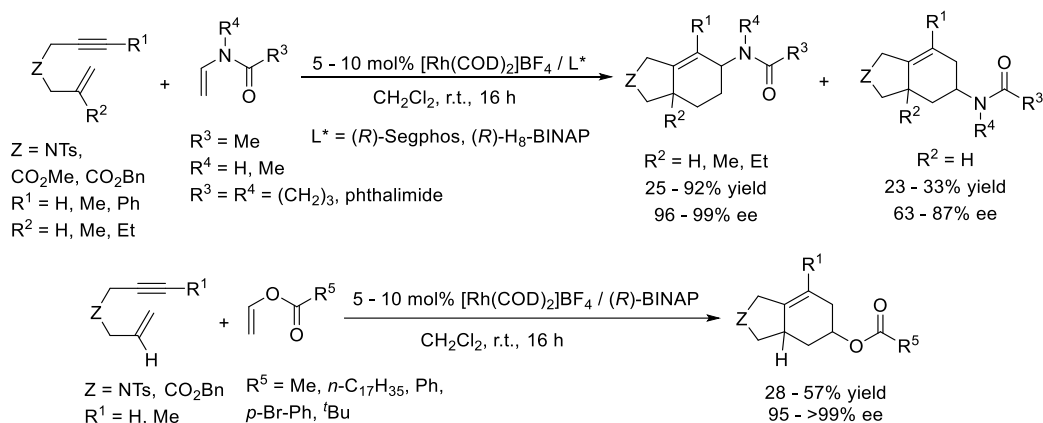
In the same year, Evans et al.²⁶ published the enantioselective Rh-catalysed [2+2+2] cycloaddition of 1,6-enynes and asymmetrically substituted alkynes. Using (*S*)-Xyl-P-PHOS as a chiral phosphine and AgBF₄ as the activating agent of rhodium catalyst $[\text{RhCl}(\text{COD})]_2$, a highly enantioselective and regioselective process was achieved (Scheme 1.14). As asymmetric alkynes are used, the regioselectivity of the reaction has to be taken into account. The nature of the tether has a profound influence on the level of regiocontrol (the oxygen tether gives greater

regiocontrol than NTs and $C(CO_2Me)_2$ was found to give the least regiocontrol). Similarly, the overall efficiency and regioselectivity can be directly related to the electronic nature of the aryl substituents.



Scheme 1.14. [2+2+2] Cycloaddition between 1,6-enynes and asymmetric alkynes for the synthesis of 1,3-cyclohexadienes.

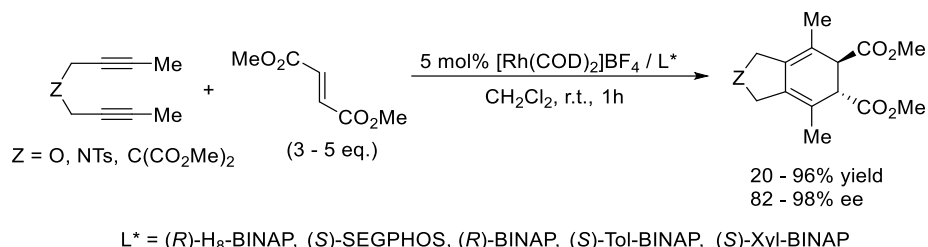
Systems in which enynes react with alkenes have also been reported. This case allows the synthesis of cyclohexenes that can contain more chiral centres than in the previously described cases. One recent example reported by Tanaka et al.²⁷ describes the asymmetric rhodium(I)-catalysed [2+2+2] cycloaddition between enynes and vinyl enamides and vinyl carboxylates (Scheme 1.15). It was observed that the regioselectivity of the reaction depended on the structure of the substrates used: when $R^2 = H$, the reaction was not regioselective as a mixture of regioisomers was obtained; whereas if R^2 contained an alkyl chain, only one regioisomer was formed.



Scheme 1.15. [2+2+2] Cycloaddition between enynes and vinyl enamides, and vinyl carboxylates.

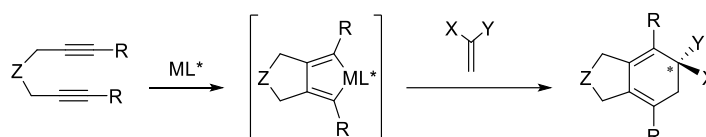
Returning to the synthesis of cyclohexadienes, the most challenging approach in terms of chemoselectivity (due to the low reactivity of the alkene) and enantioselectivity is the partially intramolecular [2+2+2] cycloaddition between diynes and alkenes. In a pioneering work by Singleton,²⁸ the first [2+2+2] cycloaddition of diynes and monosubstituted or 1,2-disubstituted alkenes was reported. Years later, Tanaka et al.²³ reported the partially intramolecular [2+2+2]

cycloaddition between diynes and 1,2-disubstituted alkenes (Scheme 1.16). The yield of the reaction significantly improved when three to five equivalents of the alkene were used together with slow addition of the corresponding diyne over the alkene. In this particular case, cyclohexadienes containing vicinal tertiary carbons were obtained with high enantioselectivity.



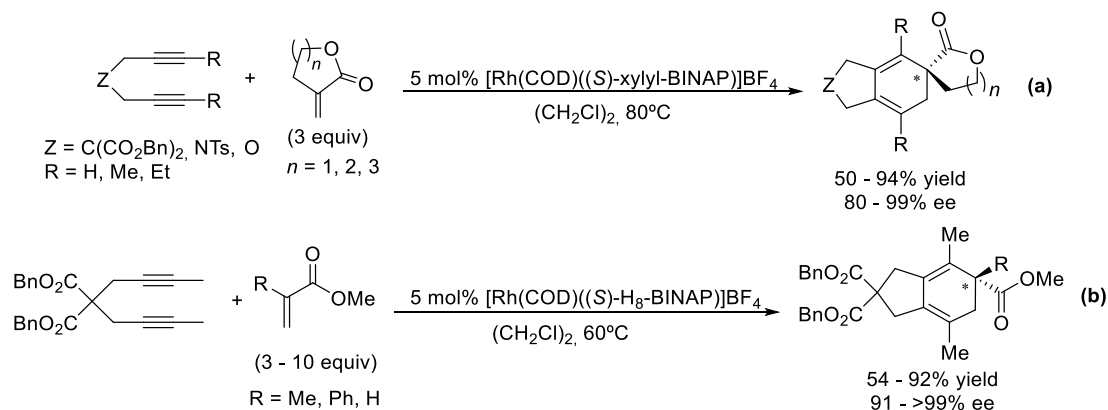
Scheme 1.16. Partially intramolecular [2+2+2] cycloaddition between diynes and 1,2-disubstituted alkenes.

In the case of non-symmetric 1,1-disubstituted alkenes, a quaternary carbon is generated (Scheme 1.17). The asymmetric synthesis of quaternary carbons is one of the most challenging problems in organic synthesis due to the steric repulsion between the carbon substituents, which complicates the stereoselective control of the reaction.



Scheme 1.17. [2+2+2] Cycloaddition of diynes and 1,1-disubstituted alkenes.

There are few examples of [2+2+2] cycloaddition reactions between alkynes and 1,1-disubstituted alkenes.

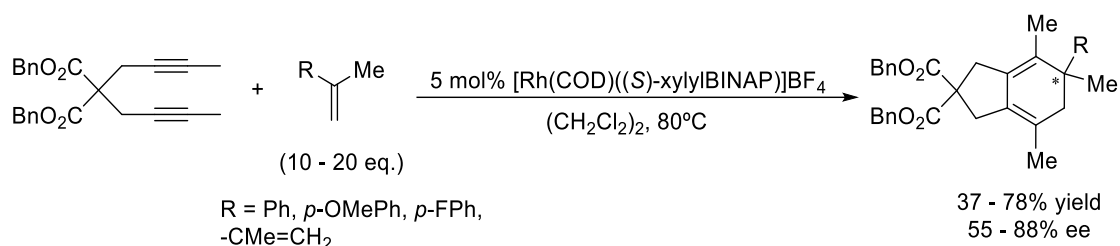


Scheme 1.18. [2+2+2] Cycloaddition between 1,6-diynes and non-symmetric alkenes.

Shibata et al.²⁹ in 2006 reported the construction of 1,3-cyclohexadiene compounds bearing a quaternary carbon by means of a [2+2+2] cycloaddition. *Exo*-methylenic lactones (equation a in Scheme 1.18) and acrylates (equation b in Scheme 1.18) were used as alkene moieties. Chiral spirocyclic structures were obtained in good to excellent yields and excellent enantiomeric excesses when an excess of *exo*-methylenic lactones was used and a cationic rhodium complex with (*S*)-xylyl-BINAP as phosphine was employed (equation a in Scheme 1.18). In the same study, the authors described three examples of [2+2+2] cycloaddition reactions of a diyne with

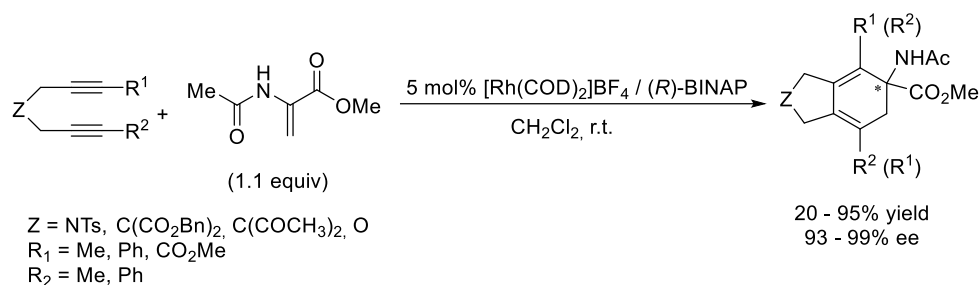
acrylates: by using a high excess of alkene the authors were able to obtain chiral cyclohexadienes in good to excellent yields and excellent enantiomeric excesses. However, the phosphine employed had to be changed to (*S*)-H₈-BINAP to obtain satisfactory results (equation b in Scheme 1.18).

The same authors³⁰ also described four cases involving unfunctionalized 1,1-disubstituted alkenes in partially intramolecular Rh-catalysed [2+2+2] cycloaddition (Scheme 1.19). Good yields and enantioselectivities of bicyclic cyclohexa-1,3-dienes were obtained by using a large excess of the corresponding alkenes.



Scheme 1.19. Enantioselective [2+2+2] cycloaddition of diene with styrene derivatives.

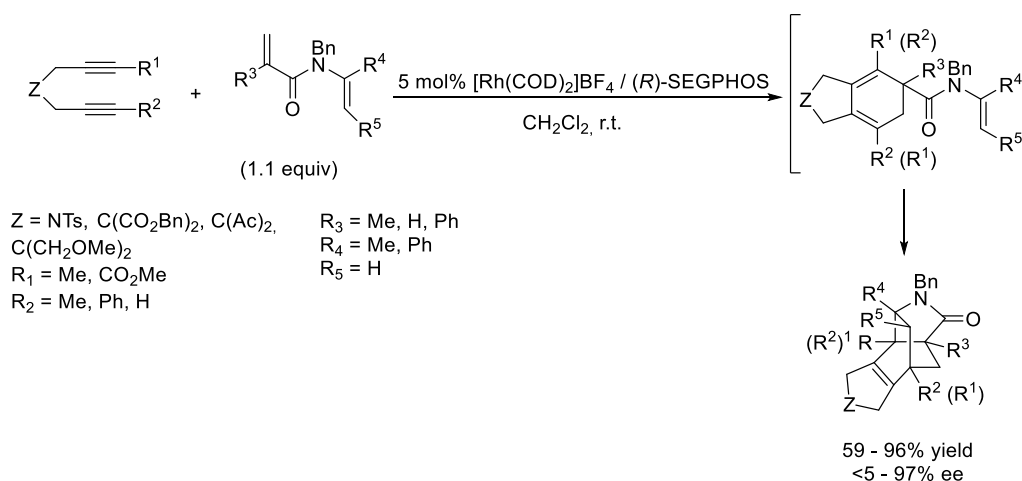
In 2008, Tanaka et al.³¹ described the enantioselective synthesis of α,α -disubstituted α -amino acids by Rh-catalysed [2+2+2] cycloaddition of 1,6-diynes with protected dehydroamino acids (Scheme 1.20).



Scheme 1.20. Rh(I)-catalysed enantioselective [2+2+2] cycloaddition of diynes with dehydroamino acid.

It is noteworthy that in this case only a slight excess of dehydroamino acid was necessary without the slow addition of diyne. The phosphine was observed to have an influence on the outcome of the reaction. For instance, (*R*)-BINAP gave the best results but the use of the sterically demanding phosphine xyl-BINAP significantly decreased the yield whilst not affecting the enantiomeric excess.

Finally, the same group³² published the enantioselective construction of bridged polycyclic skeletons through a partially intramolecular [2+2+2] cycloaddition/intramolecular Diels-Alder reaction cascade. Amide-linked 1,5-dienes were used as the alkene partners (Scheme 1.21).

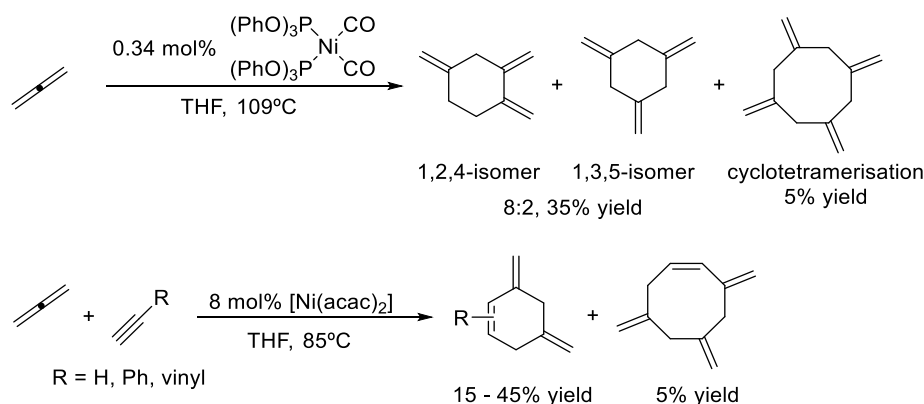


Scheme 1.21. Enantioselective cycloaddition cascade of 1,6-diynes with 1,5-dienes.

1.1.2.2. Allenes in transition-metal catalysed [2+2+2] cycloaddition reactions

Allenenes, cumulated systems with two contiguous carbon-carbon double bonds, are of increasing interest as partners for the [2+2+2] cycloaddition reaction due to their particularities: they are more reactive than alkenes and, when properly substituted, have inherent axial chirality and, furthermore, their substitution pattern has a direct effect on both the electronic density and the reactivity of each carbon atom. On the other hand, selectivity is more difficult to control with allenenes than with either alkynes or alkenes since it is necessary to control which of the two double bonds reacts as well as the chemoselectivity towards other unsaturations and the issues of regio- and stereoselectivity. Our group has recently published a review summarising the participation of allenenes in [2+2+2] cycloaddition reactions.^{2a}

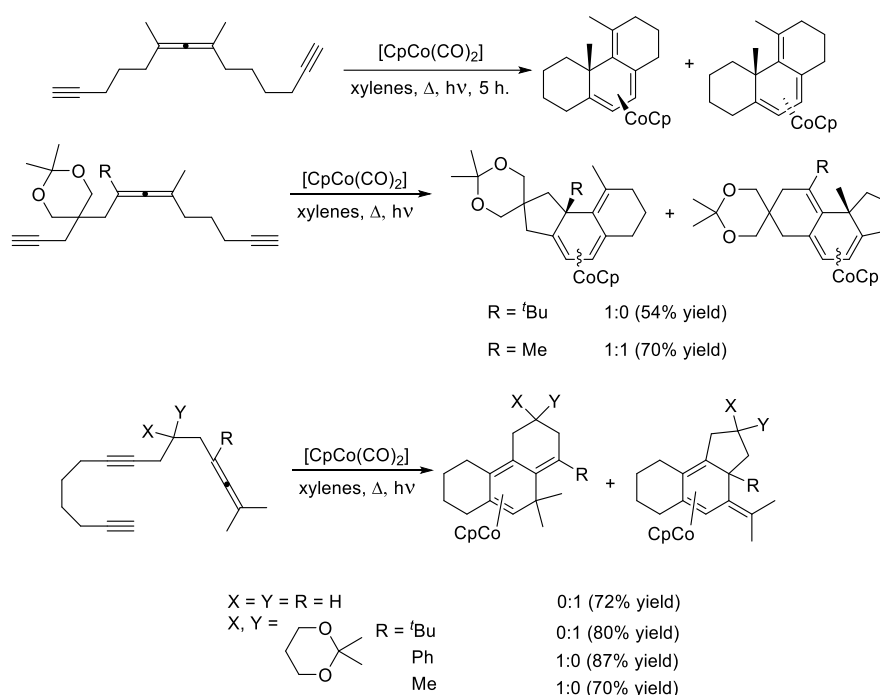
Benson and Lyndsey,³³ working for DuPont in 1958, published pioneering studies into the use of allenenes in nickel-catalysed cyclisations. They found that propadiene cyclotrimerised in the presence of nickel(0) catalysts in a moderate yield but with good selectivity versus cyclotetramerisation. The corresponding trimethylenecyclohexanes were obtained as a mixture of 1,2,4 and 1,3,5 isomers. Moreover, the introduction of an alkyne in the mixture and the use of nickel(II) acetylacetonate as the catalyst gave dimethylenecyclohexenes in good yields with good chemoselectivity (Scheme 1.22).



Scheme 1.22. First [2+2+2] cycloaddition of allenenes reported by Benson and Lyndsey.

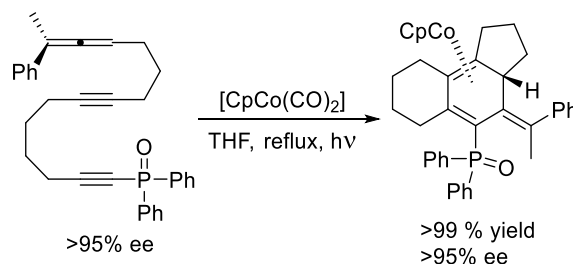
Although these reports proved the potential of allenes in cyclotrimerisation reactions, it was not until 35 years later that Malacria et al. reported new examples of [2+2+2] cycloadditions involving allenes.

Focusing on totally intramolecular cases, the group of Malacria³⁴ in 1994 began a series of studies employing allenes as substrates in [2+2+2] cycloadditions. Linear allene-diyne substrates in which the allene was placed either as the central unsaturation or at the terminus of the chain were tested in the Co(I)-mediated intramolecular cycloaddition (Scheme 1.23). When these substrates were reacted with stoichiometric amounts of $[\text{CpCo}(\text{CO})_2]$ under heating and ultraviolet light, tricyclic conjugated trienes were obtained as η^4 -Co complexes. However, the reaction did not take place when it was attempted to run with catalytical amounts of cobalt. In the particular case of when the allene was in the terminal position, two regioisomers could be obtained, depending on which of the two unsaturations of the allene reacted. When the molecule had sterically demanding substituents ($\text{R} = \text{}^t\text{Bu}$) or no substituents at all ($\text{X} = \text{Y} = \text{R} = \text{H}$), it was the internal double bond that reacted. However, in the case of $\text{R} = \text{Ph}$ or Me , the external double bond reacted.



Scheme 1.23. Yne-allene-yne and yne-yne-allene intramolecular [2+2+2] cycloaddition.

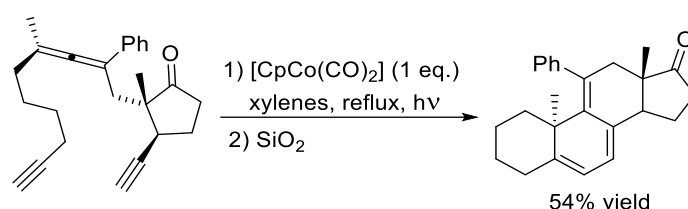
In a separate study, these same authors demonstrated that these cyclisations occur with effective axial to central chirality transfer.³⁵



Scheme 1.24. Axial to central chirality transfer by a [2+2+2] cycloaddition of an allene-diyne substrate.

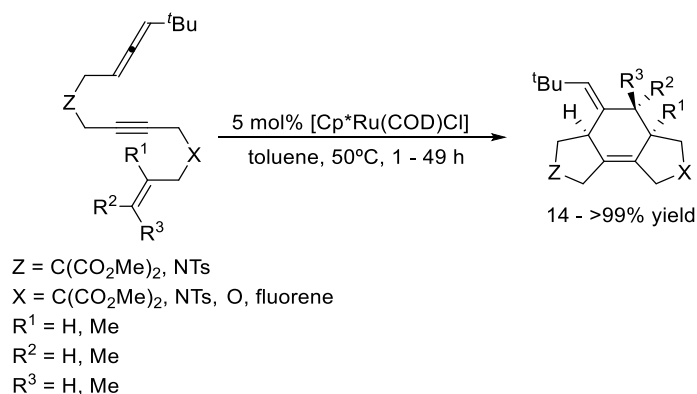
When a linear yne-yne-allene with chirality on the allene moiety was subjected to the Co(I)-mediated cyclisation, the corresponding triene- η^4 -cobalt complex was obtained as a single diastereoisomer with no decrease in the enantiomeric excess (Scheme 1.24).

Later they also used the high chemo- and diastereoselectivity observed in these processes to synthesize steroidal scaffolds. Upon cyclisation of a diastereomerically pure yne-allene-yne substrate, a steroid analogue in moderate yield but with complete diastereoselectivity was obtained (Scheme 1.25).³⁶



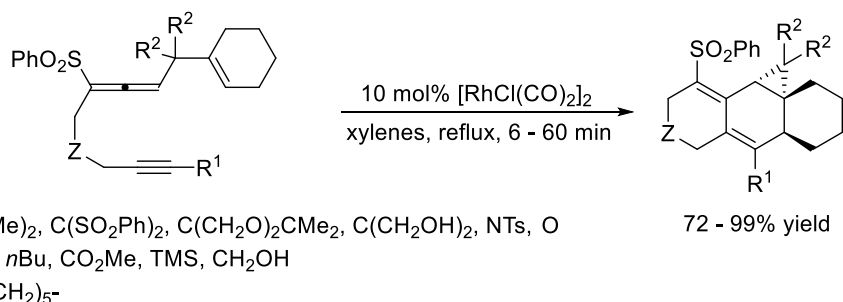
Scheme 1.25. Steroid analogue synthesized by a [2+2+2] cycloaddition of an yne-allene-yne substrate.

Saito, Sato et al.³⁷ reported the ruthenium(II)-catalysed [2+2+2] cycloaddition of allene-yne-ene substrates. Skipped diene products were obtained with complete diastereoselectivity by selective reaction of the internal double bond of the allene (Scheme 1.26).



Scheme 1.26. Ruthenium(II)-catalysed [2+2+2] cycloaddition of allene-yne-ene substrates.

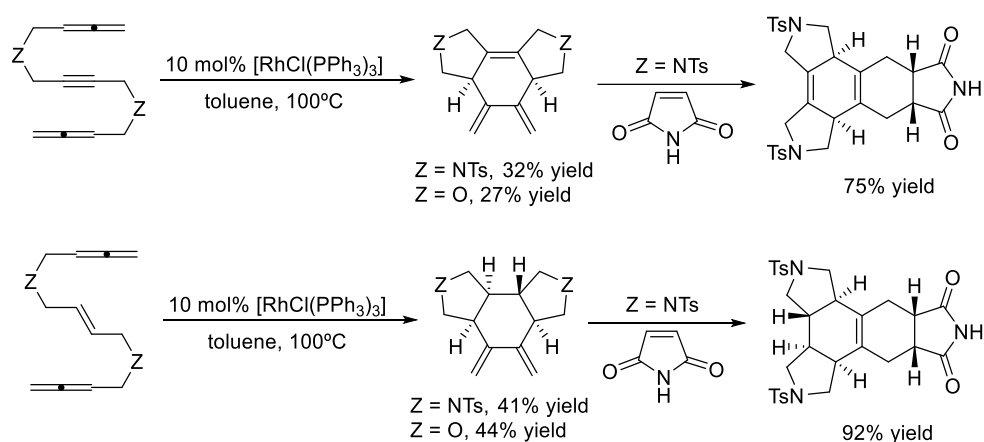
A similar study by Mukai et al.³⁸ inverted the order of the unsaturations in the starting material, placing the allene moiety in the middle of the chain. With this arrangement great structural variability was obtained, thus allowing the formation of complex tri- and tetracyclic scaffolds in a totally diastereoselective fashion (Scheme 1.27).



Scheme 1.27. Polycyclic scaffolds synthesized by a rhodium(I)-catalysed [2+2+2] cycloaddition of yne-allene-ene substrates.

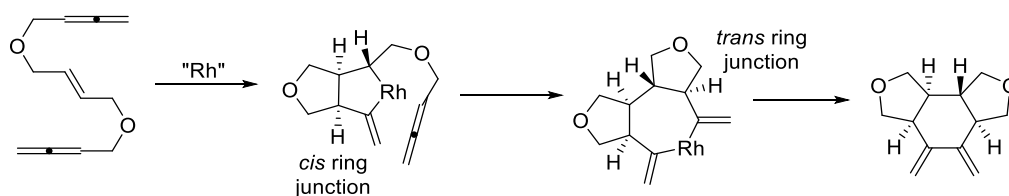
The authors employed a Rh(I) catalyst and obtained the corresponding products in good to excellent yields. With this approach it was possible to form cyclopropane-fused polycyclic structures. Besides the structures shown in Scheme 1.27, the flexibility of this methodology is such that the introduction of tethers of different lengths in the precursor structure, as well as changing the alkene partner or the phenylsulfonyl group, is possible, so enabling the synthesis of different sized polycyclic structures.

Our group has also contributed to this field. Polycyclic 1,3-diene products were synthesized starting from linear allene-yne/ene-allene substrates.^{3h} The Wilkinson's complex-catalysed cyclisation of these substrates delivered dienes with complete chemo- and diastereoselectivity (Scheme 1.28). The products obtained could also undergo Diels–Alder reactions with maleimide, affording complex pentacyclic products in excellent yields and with total stereoselectivity.



Scheme 1.28. Rhodium(I)-catalysed [2+2+2] cycloaddition of allene-yne/ene-allene substrates.

Additionally, detailed DFT calculations were carried out to rationalise the observed diastereoselectivity and to propose a mechanistic cycle. After a detailed analysis of the many possibilities for the key reaction intermediates, oxidative addition was postulated as taking place between the central alkene and the internal double bond of one of the allenes to give a *cis*-fused ring junction. The remaining allene is then inserted into the Rh–Csp³ bond of the rhodacyclopentane to give a *trans*-fused ring junction (Scheme 1.29), so determining the diastereoselectivity of the process.

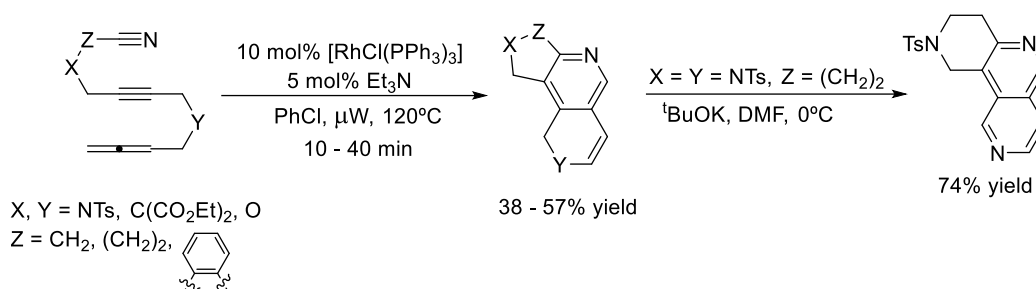


Scheme 1.29. Key intermediates proposed by DFT calculations in the Rh(I)-catalysed [2+2+2] cycloaddition of allene-ene-allene substrates.

The preference for cyclisation at the internal double bond of the allene was also analysed. This concurred with a higher energy of the occupied π molecular orbital localised at this double bond.

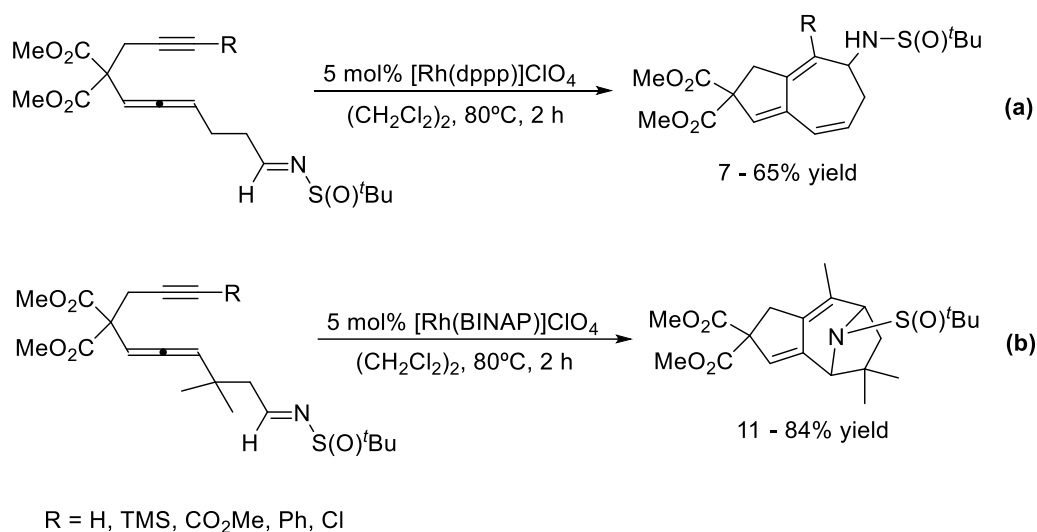
In our group, we have also introduced nitriles in this kind of systems, generating 2,6-naphthyridine scaffolds.³⁹ The use of Wilkinson's catalyst and catalytic amounts of triethylamine, allowed the chemoselective reaction of allenes through their external double bond to give

unsaturated pyridine-containing scaffolds after a dehydrogenative step (Scheme 1.30). Removal of the tosyl group allowed entry into 2,6-naphthyridine nuclei. Derivatives containing this scaffold have been found to have promising medicinal properties in HIV⁴⁰ and cancer research.⁴¹



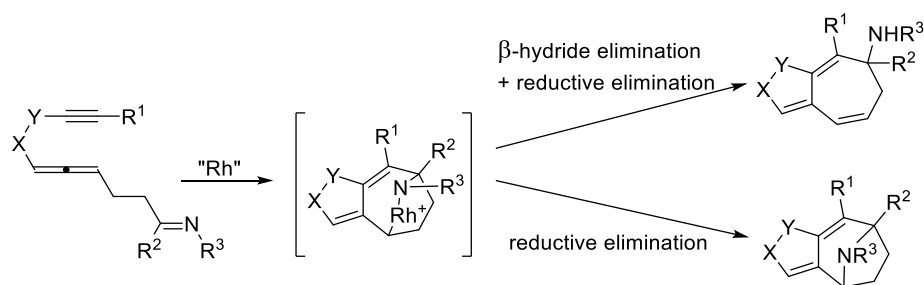
Scheme 1.30. Rhodium(I)-catalysed [2+2+2] cycloadditions of acyclic allene–yne–cyano derivatives.

Finally, in a recent work, Sato et al.⁴² reported the rhodium(I)-catalysed [2+2+2] cycloaddition of yne-allene-imine substrates. The authors synthesized linear substrates bearing *tert*-butylsulfinyl imine groups and submitted them to rhodium catalysis to afford 5,7-fused cyclic amine derivatives (equation a in Scheme 1.31). They then investigated the [2+2+2] cyclisation of substrates without hydrogen atoms at the β -position of the sulfinylimine moiety, in this case 8-azabicyclo[3.2.1]octane derivatives were obtained. However, a different ligand in the rhodium catalyst had to be used to achieve good yields of the cycloadducts (equation b in Scheme 1.31).



Scheme 1.31. [2+2+2] Cycloaddition of yne-allene-imine substrates.

The authors proposed a mechanistic rationale for the observed reactivity. The cyclization proceeds via a strained azarhodacycle intermediate. β -hydride elimination followed by reductive elimination gives rise to a 5,7-fused cyclic amide, while direct reductive elimination of the azarhodacycle intermediate affords a tricyclic product containing an 8-azabicyclo[3.2.1]octane skeleton (Scheme 1.32).



Scheme 1.32. Mechanistic proposal for the different cycloadducts formed.

1.1.3. Rh-based catalysts for the [2+2+2] cycloaddition reaction

As seen in the previous sections, Wilkinson's catalyst $[\text{RhCl}(\text{PPh}_3)_3]$, together with many catalytic systems consisting of a combination of a cationic rhodium species and phosphine ligands, are the most widely used catalytic systems in rhodium-catalysed [2+2+2] cycloaddition.²

Since the pioneering work of Grigg et al.⁴³ describing the Wilkinson's complex-catalysed [2+2+2] cycloaddition reaction of diynes with monoacetylenes for the first time, many examples involving this catalyst with substrates containing huge variety of unsaturations have been reported.

Tanaka et al.^{2t} in 2003 described, for the first time, the use of the cationic complex $[\text{Rh}(\text{COD})_2]\text{BF}_4$ in combination with BINAP-type ligands as an efficient catalyst for [2+2+2] cycloaddition. Many further examples of the use of this catalytic system have since been reported given that it is highly versatile, allowing the preparation in situ of many different rhodium complexes with different ligands, thus facilitating the tuning of reaction conditions. Moreover, this catalytic system has proven to be especially suitable for enantioselective processes due to the availability of chiral phosphines.

Besides these well-established catalytic systems, many groups have reported other ligands that can coordinate to the rhodium centre, some of which will be discussed below.

1.1.3.1. Phosphoramidite ligands in the Rh-catalysed [2+2+2] cycloaddition reaction

Phosphoramidite-type compounds arise from the union of two different synthons – one from a diol-type synthetic equivalent (in general, BINOL, biphenol or TADDOL) and the other from an amine (Figure 1.1) – through a trivalent phosphorous.

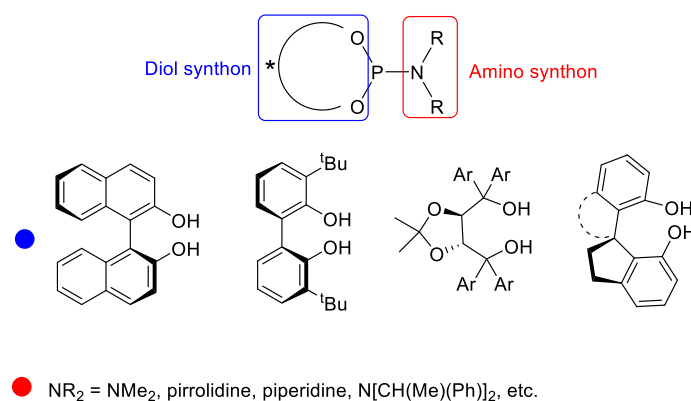
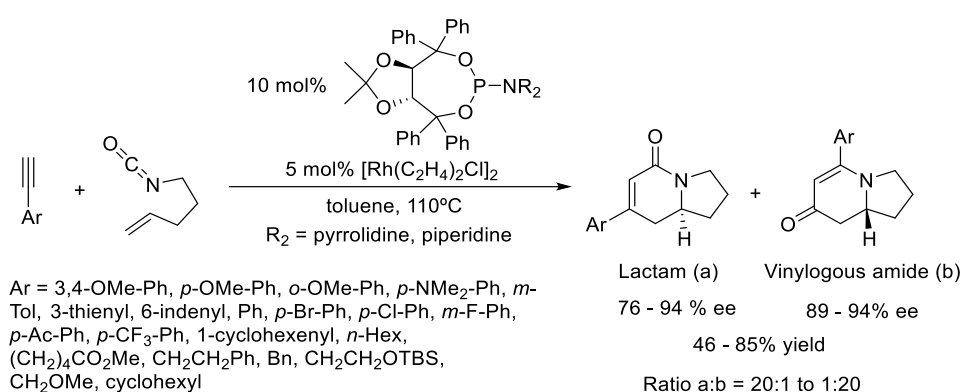


Figure 1.1. Phosphoramidite modular architecture.

The modification of the substituents of the two oxygen atoms and the substituents in the nitrogen atom allow the adjustment of the donor properties of the ligand (and thus the electronic properties of the metal centre) for a specific catalytic application. The chirality of these molecules is usually introduced by means of a chiral diol, although in some cases it can also be introduced with a chiral amino residue.

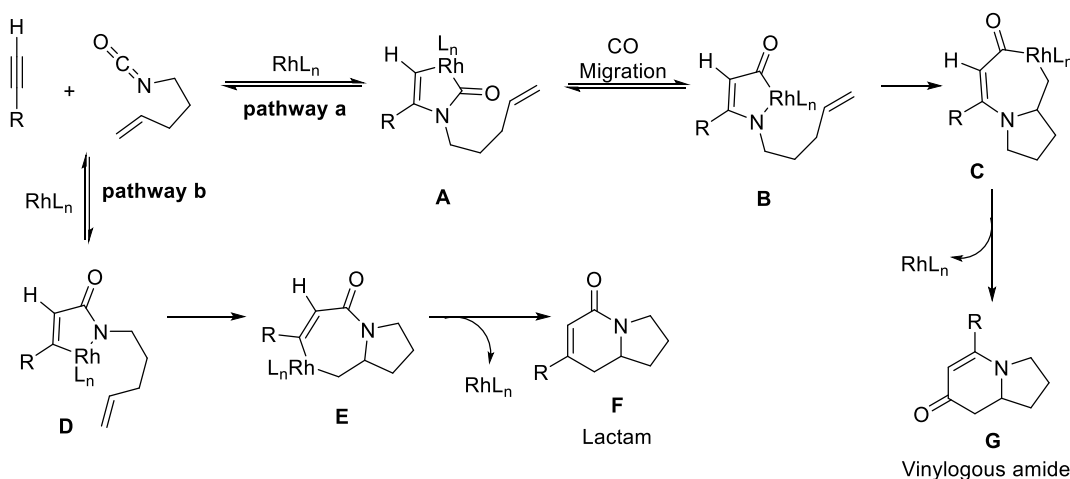
These compounds were first used as ligands in rhodium catalysis for hydrogenation reactions.⁴⁴ In 2000 Feringa et al.⁴⁵ described the asymmetric hydrogenation of olefins using a BINOL-based phosphoramidite ligand and $[\text{Rh}(\text{COD})_2]\text{BF}_4$ as the rhodium source.

In the particular case of the [2+2+2] cycloaddition reaction, the group of Rovis et al.⁴⁶ have made most of the contributions in the field of phosphoramidite ligands for the [2+2+2] cycloaddition reaction. In a first report they described the rhodium-catalysed [2+2+2] cycloaddition of alkynes and alkenyl isocyanates to afford bicyclic lactams and/or the corresponding vinylogous amides using chiral phosphoramidites as ligands (Scheme 1.33).⁴⁶ⁱ



Scheme 1.33. Partially intermolecular [2+2+2] cycloaddition between alkynes and alkene isocyanates.

The proposed mechanism for the formation of these two regioisomers is shown in Scheme 1.34.



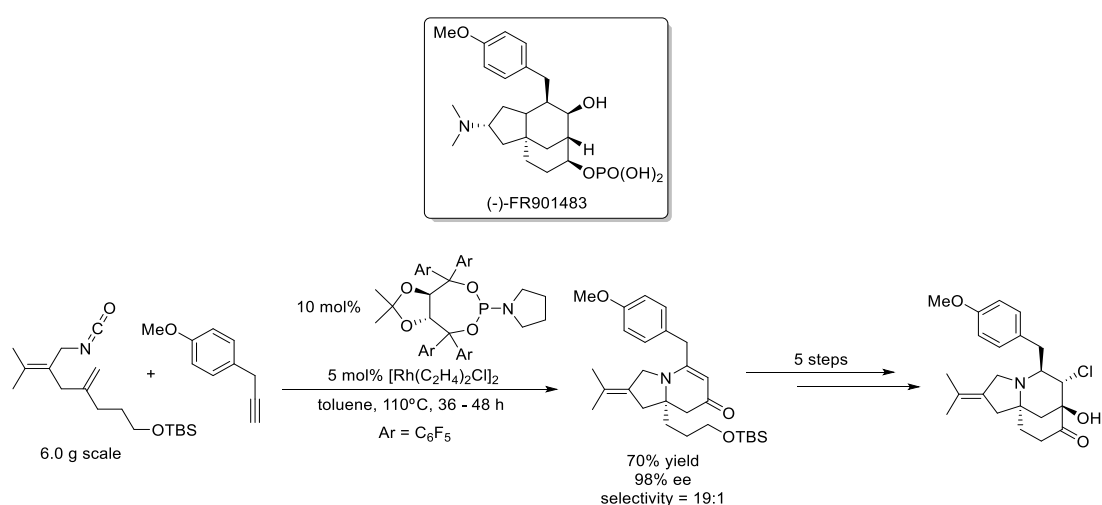
Scheme 1.34. Proposed pathways in the [2+2+2] cycloaddition between alkynes and alkene isocyanates.

An initial oxidative cyclization between the isocyanate and alkyne in an orientation where a C-N bond is formed provides the rhodacycle intermediate **A**. A CO migration to **B** followed by olefin insertion and reductive elimination furnishes the vinylogous amide compound (pathway a in Scheme 1.34). In a different orientation of the oxidative addition, metallacycle **D** is formed with

a C-C bond formation (pathway b in Scheme 1.34). Subsequent olefin insertion and reductive elimination provides the lactam derivative.

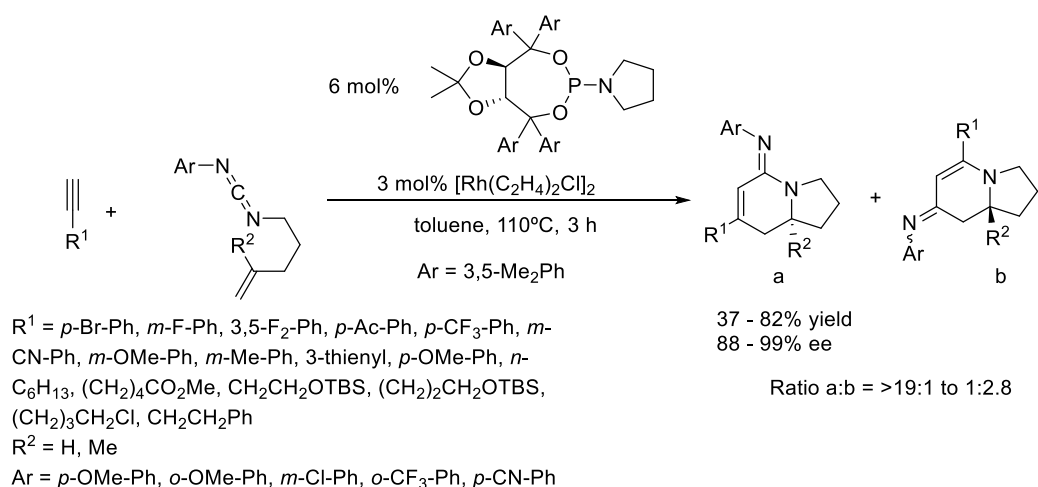
The regioselectivity of this process is controlled by steric and electronic factors.^{46e,g} Alkynes containing bulky or electron donating groups (aryl-like) favour the vinylogous amide. On the other hand, the lactam is favoured by alkynes with smaller substituents as well as less electron-donating substituents (alkyl-like).

In a more recent work they used this methodology to synthesize an analogue of the tricyclic framework of the alkaloid FR901483, which has immunosuppressive activity.^{46a} By means of a [2+2+2] cycloaddition between the appropriate alkenyl isocyanate and 4-methoxybenzylacetylene, they manage to obtain the indolizidine core of the alkaloid. After five more synthetic steps the desired tricyclic compound was obtained (Scheme 1.35).



Scheme 1.35. Synthesis of an analogue of the FR901483 alkaloid.

In an attempt to develop a methodology to selectively access compounds of type F in Scheme 1.34, the same authors involved carbodiimides in the process. They described the asymmetric synthesis of bicyclic amidines (Scheme 1.36) by means of a partially intramolecular [2+2+2] cycloaddition between alkenyl carbodiimides and terminal alkynes.^{46j}



Scheme 1.36. Rh(I)-catalysed [2+2+2] cycloaddition of carbodiimides with aryl- and heteroarylacetylenes.

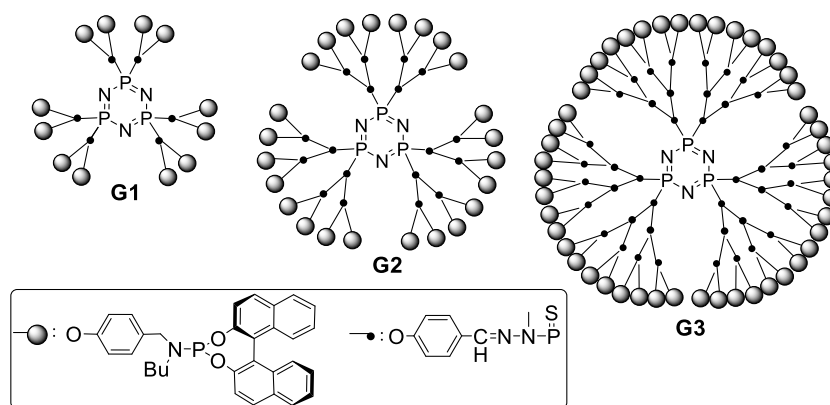
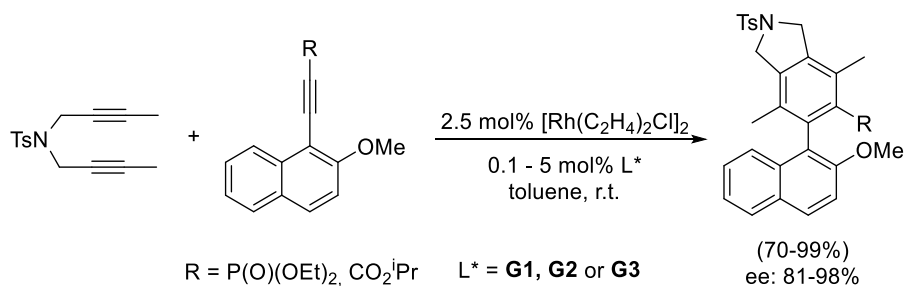


Figure 1.2. Structures of dendrimers G1, G2 and G3.



Scheme 1.39. [2+2+2] Cycloaddition reaction between *N*-tosyl 1,6-diyne and 2-methoxynaphthalene alkynyl derivatives.

More examples of recyclable catalysts for [2+2+2] cycloadditions will be discussed in Chapter 6.

1.1.3.2. *N*-phosphino-*tert*-butylsulfonamide and secondary iminophosphorane ligands in the Rh-catalysed [2+2+2] cycloaddition reaction

N-phosphino-*tert*-butylsulfonamide (PNSO) ligands are hemilabile ligands in which the sulfoxide moiety binds the metal through either sulfur or oxygen to provide either P,S or P,O chelation, depending on the electronic environment around the metal centre (Figure 1.3).

These PNSO ligands represent an efficient way of combining the easily accessible chirality of sulfur with the capacity for coordination of the phosphorous atom.⁴⁸

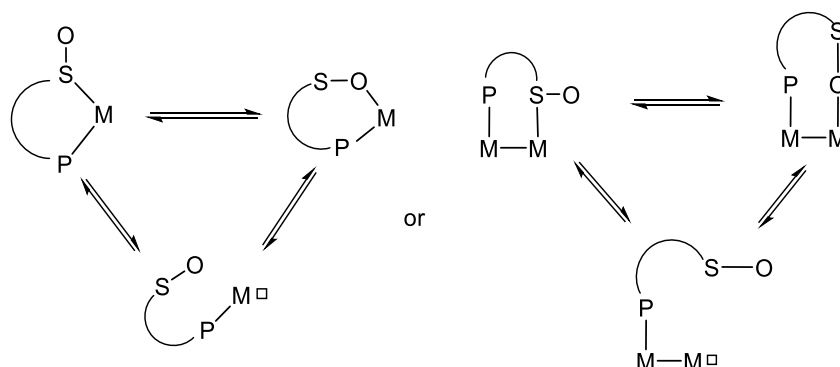
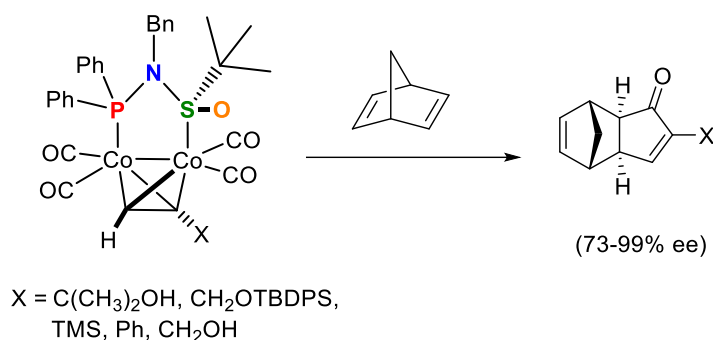


Figure 1.3. Possible coordination modes of the *N*-phosphino sulfonamide ligands with mono- and bimetallic complexes.

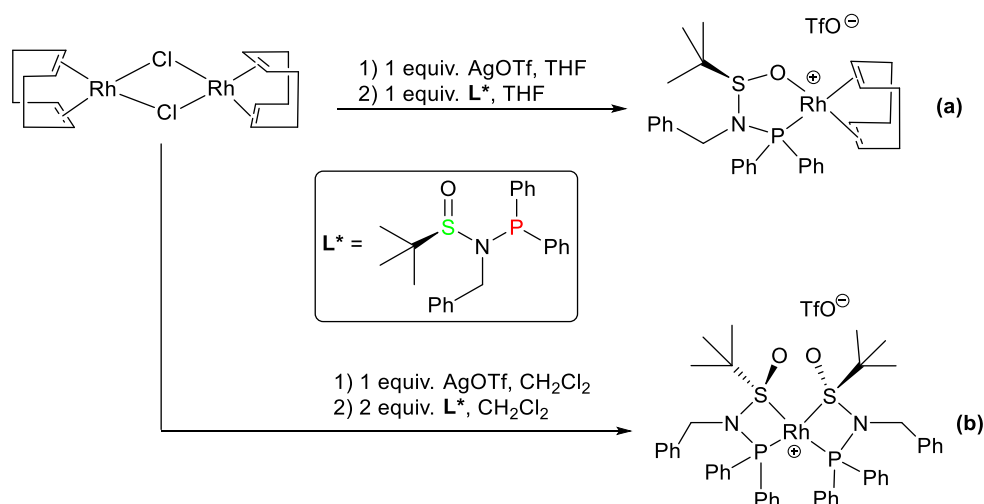
Prof. Riera et al. from the University of Barcelona proved that these ligands are useful in the intermolecular asymmetric Pauson-Khand reaction acting as bidentate P,S ligands. This study

was the first example of a chiral sulfur atom coordinated to a cobalt centre. The intermolecular Pauson–Khand reaction of the corresponding PNSO-Co complexes with norbornadiene occurred with unprecedented stereoselectivity (Scheme 1.40).



Scheme 1.40. Pauson-Khand reaction of the PNSO-dicobalt complexes with norbornadiene.

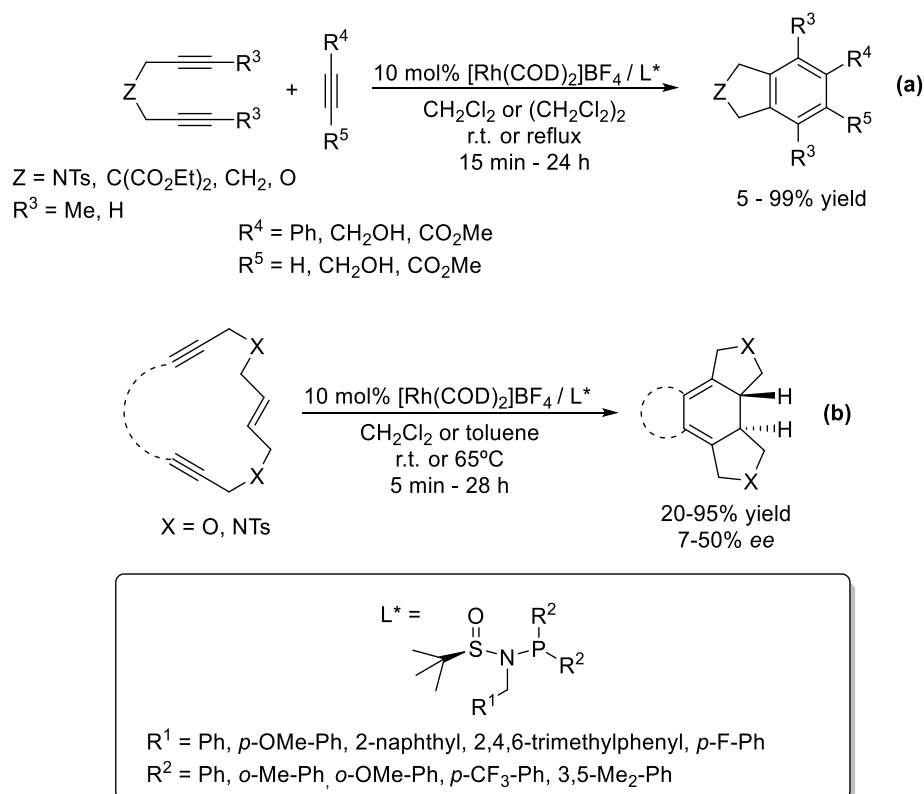
The same authors later published the synthesis and characterization of the first rhodium(I) complexes with the same ligand.⁴⁹ The reaction of [RhCl(COD)]₂ with one equivalent of PNSO ligand in the presence of AgOTf afforded complex [Rh(PNSO)(COD)]OTf (equation a in Scheme 1.41). When two equivalents of the ligand were used the corresponding disubstituted complex was also obtained (equation b in Scheme 1.41). It should be noted that when olefinic ligands such as COD were attached to the metal centre, the ligand presents a P,O coordination. On the other hand, rhodium complex with two PNSO ligands provided P,S coordination.



Scheme 1.41. Preparation of cationic rhodium complexes [Rh(L*)(COD)]OTf and [Rh(L*)₂]OTf.

In collaboration with Prof. Riera's group, we applied these ligands in the Rh-catalysed [2+2+2] cycloaddition.⁵⁰ The catalytic system was prepared in situ by mixing the corresponding ligand with [Rh(COD)₂]BF₄. When the activity of the mono-ligated catalyst (equation a in Scheme 1.41) was evaluated in the partially intermolecular version of the reaction, good to excellent yields of the cycloadducts were obtained (equation a in Scheme 1.42). The catalytic system was found to be robust and applicable to a broad range of substrates independently of the nature of the linker between unsaturations and the substitution at the termini of the alkynes. In addition, the enantioselectivity of the reaction was also evaluated in the intramolecular reaction of linear and macrocyclic enedynes, but only moderate enantioselectivities could be achieved (equation b in

Scheme 1.42). In this study it was observed that the complex with two ligands (equation b in Scheme 1.41) was not active for this reaction.



Scheme 1.42. Rh(I)-catalysed [2+2+2]cycloaddition with PNSO ligands.

The low enantioselectivity observed for these ligands may be explained by the distance of the chiral motif on the ligand from the metal centre, as PNSO ligands have the chirality on the hemilabile sulphur atom. Another family of this kind of compounds are secondary iminophosphorane (SIP) ligands, which contain their chirality on the phosphorous atom (Figure 1.4).



Figure 1.4. Hemilabile S-stereogenic and P-stereogenic ligands.

By placing the chirality on the phosphorous atom it is expected that it will have a greater influence on the enantioselectivity of the process. Moreover, these ligands present an NH/PH tautomeric equilibrium which render them stable to oxidation (Figure 1.5).

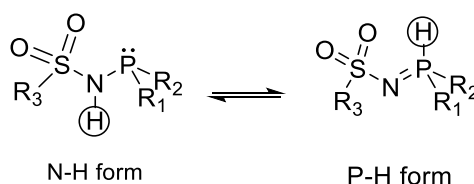
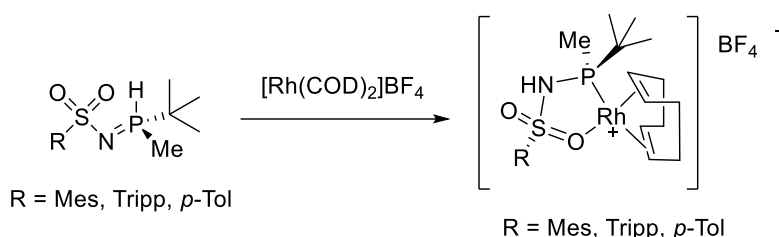


Figure 1.5. NH/PH tautomeric equilibrium.

The equilibrium usually shifts towards the P-H form, which prevents the oxidation of the phosphorous atom, although it can shift to the aminophosphine form (N-H) by the coordination of phosphorus to a metal. Furthermore, P-stereogenic secondary iminophosphoranes are configurationally stable and thus chiral information is preserved through the PH/NH equilibrium. This equilibrium is presumably governed by the electronic properties of the phosphine atom rather than the nature of the substituents of the sulfone.

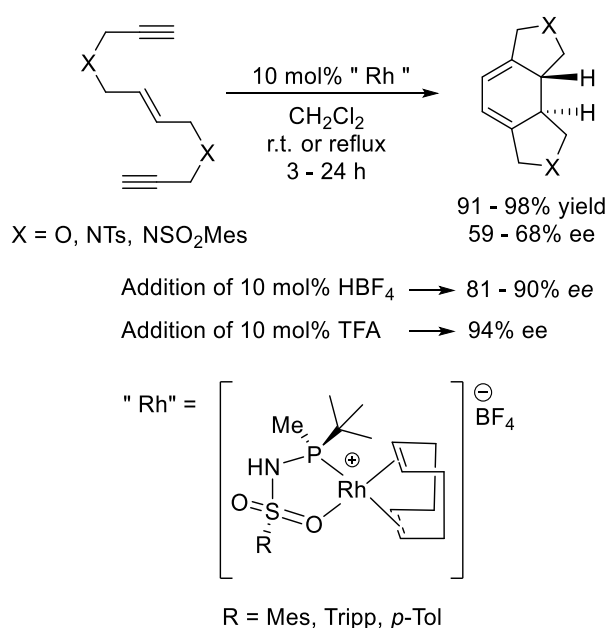
These ligands were also able to coordinate rhodium and their use in asymmetric catalysis was then studied. The reaction of bulky iminophosphoranes with $[\text{Rh}(\text{COD})_2]\text{BF}_4$ resulted in the exchange of a single COD unit (Scheme 1.43). The addition of an excess of secondary iminophosphoranes did not lead to a dimeric species, suggesting that the steric bulk of the ligand may be responsible for this behaviour.



Scheme 1.43. Preparation of cationic Rh(I) complexes with secondary iminophosphorane (SIP) ligands.

Upon coordination to rhodium, the tautomeric equilibrium is effectively displaced towards the phosphinosulfonamide form. This leaves a relatively acidic NH group in place.

These ligands were also evaluated in the rhodium-catalysed [2+2+2] cycloaddition.⁵¹ The catalytic system SIP-Rh(I) efficiently catalysed the [2+2+2] cycloaddition of enediynes with terminal alkynes, excellent conversions were observed and good to excellent enantioselectivities of the cycloadduct were achieved (Scheme 1.44). It is important to note that in the rhodium complexes used, the chirality remains in the *tert*-butylmethylphosphino moiety, which is strongly attached to the rhodium centre.



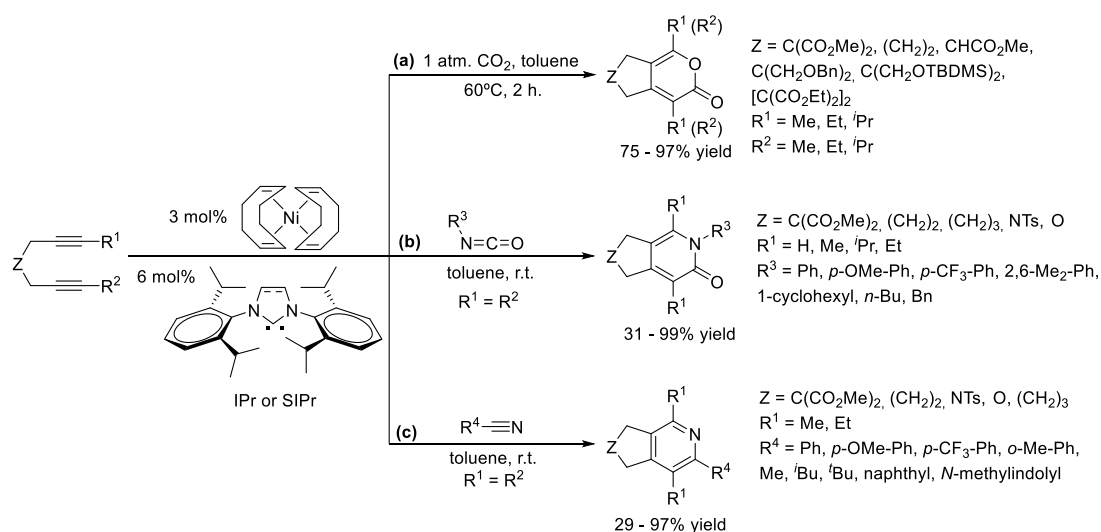
Scheme 1.44. Asymmetric SIP-Rh(I) catalysed [2+2+2] cycloaddition of enediynes.

In order to compare this catalytic system with the broadly used combination of a cationic rhodium complex with chiral biphosphine ligands, enediyne containing NSO₂Me_s tethers was submitted to cycloaddition conditions with the complex [Rh(COD)₂]BF₄ and (*R*)-BINAP. The cycloadduct was obtained in only a 45% yield and with 54% enantiomeric excess, whereas with the SIP-Rh complexes the product could be obtained with up to a 99% yield and 94% enantiomeric excess.

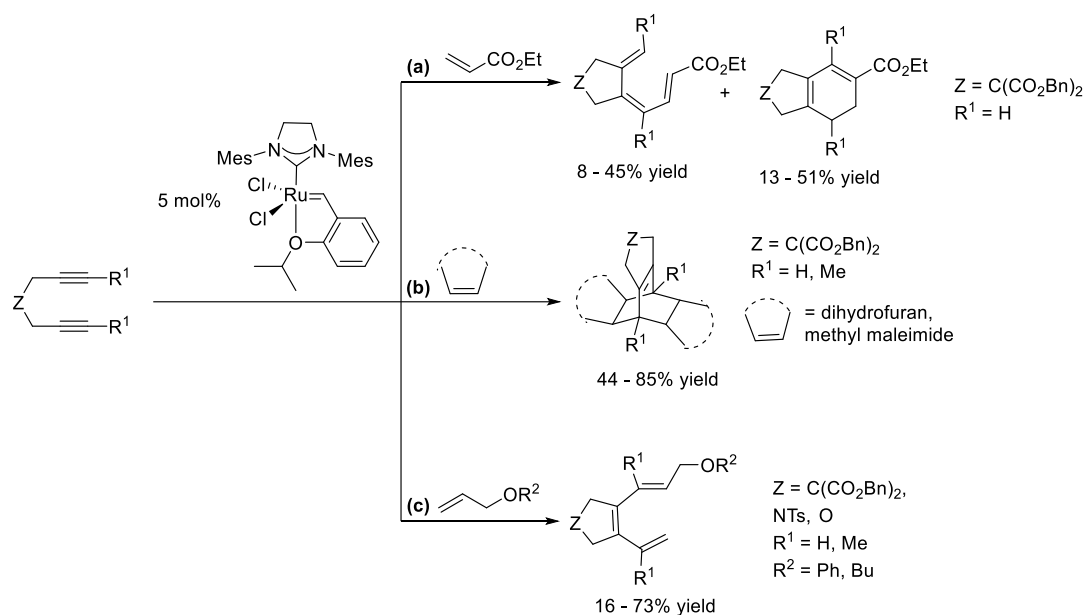
1.1.3.3. *N*-heterocyclic carbene ligands in transition-metal catalysed [2+2+2] cycloaddition reactions

Defined as neutral compounds containing a divalent carbon atom with a six-electron valence shell, carbenes are a class of carbon-containing compounds. However, free carbenes were considered as unstable due to their incomplete electron octet and coordinative unsaturation until Arduengo et al.⁵² reported an isolable carbene incorporated into a nitrogen heterocycle in 1991. The synthesis of the first *N*-heterocyclic carbene (NHC) led to an explosion of experimental and theoretical studies of this kind of molecules.⁵³ Ligands based on *N*-heterocyclic carbenes comprise a great variety of compounds derived from heterocyclic rings, although the most used ones are synthesized from imidazolium or 4,5-dihydroimidazolium salts.

In the particular case of the transition-metal catalysed [2+2+2] cycloaddition, there are few examples in which this reaction is catalysed by a transition metal with an NHC ligand. Louie et al. have made the greatest contribution to this field with nickel catalysts. They have reported Ni(0)-NHC complexes that catalyse the [2+2+2] cycloaddition between diynes and carbon dioxide,⁵⁴ isocyanates⁵⁵ or nitriles⁵⁶ (Scheme 1.45). In the case of carbon dioxide (equation a in Scheme 1.45), the authors report that when asymmetric diynes are used, the regioselectivity of the reaction is highly dependent on the ligand employed and the size of the terminal groups on the diyne, with the 3-position on the pyrone ring being the one that is preferred for the larger substituent. Moreover, pyrone derivatives were obtained in good to excellent yields. For the cases of isocyanates (equation b in Scheme 1.45) and nitriles^{56b} (equation c in Scheme 1.45) symmetric diynes were used, so no regioselectivity was studied. In these cases the heterocycloadducts were obtained in good to moderate yields.



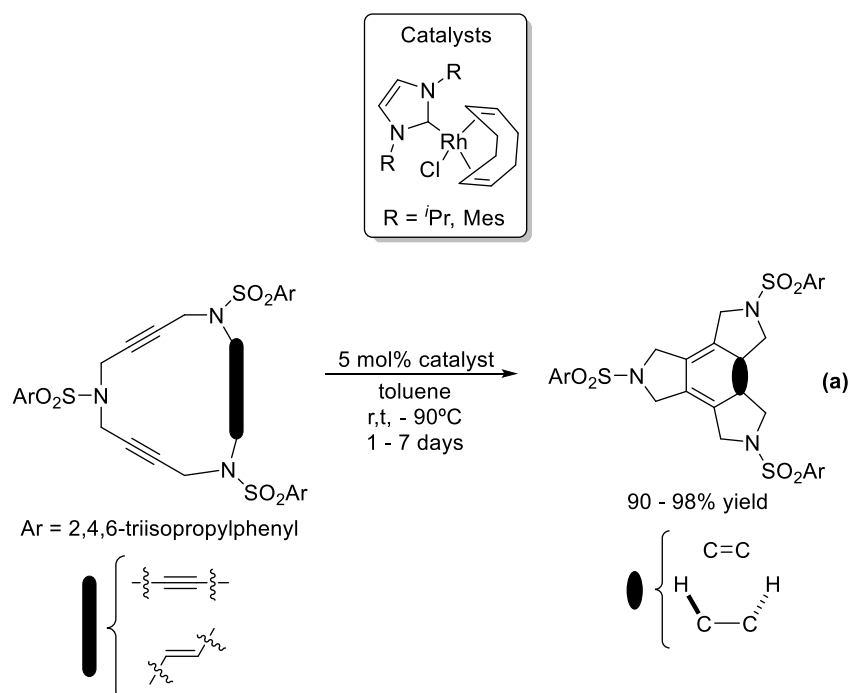
Scheme 1.45. Ni-catalysed [2+2+2] cycloadditions with IPr or SIPr ligands.

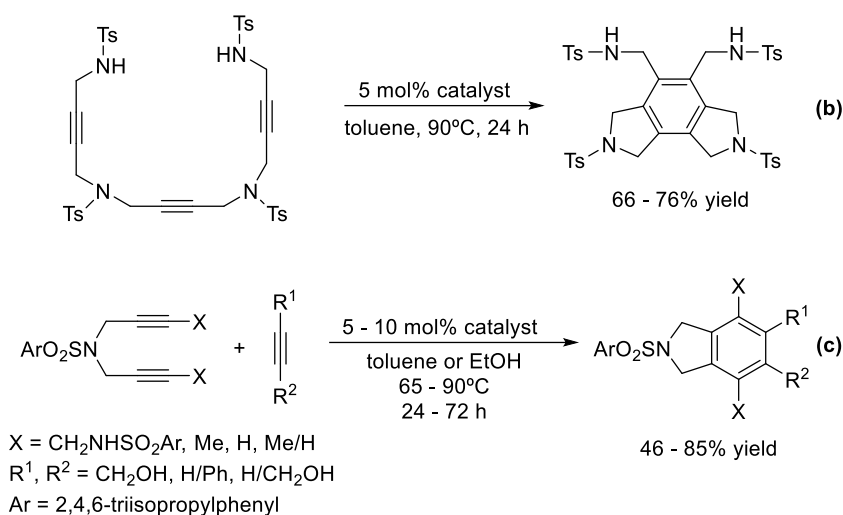


Scheme 1.47. Hoveyda-Grubbs's complex-catalysed [2+2+2] cycloaddition reaction involving alkenes.

For ethyl acrylate the reaction starts as a formal [2+2+2] cycloaddition reaction, but β -hydride elimination takes place before reductive elimination, giving rise to the products obtained (equation a). For cyclic alkenes, β -hydride elimination is not possible, thus giving the expected [2+2+2] cycloadduct, however the diene obtained further reacts with another equivalent of alkene through a Diels-Alder reaction to give the obtained pentacyclic scaffold (equation b). Finally, allyl ethers follow a metathetic cascade pathway: successive metatheses reactions of the diyne followed by reaction with the alkene gives rise to the obtained triene (equation c).

Rhodium complexes with NHC ligands show great electronic versatility, are easy to handle and are readily synthesized. In our group we have applied rhodium(I) complexes stabilized with NHC ligands in the [2+2+2] cycloaddition reaction (Scheme 1.48).⁶⁰





Scheme 1.48. [2+2+2] Cycloaddition catalysed by Rh(I)-NHC complexes.

Two already described Rh-carbene complexes ($[\text{RhCl}(\text{IPr})(\text{COD})]$ and $[\text{RhCl}(\text{IMes})(\text{COD})]$)⁶¹ were prepared and tested as catalysts for the [2+2+2] cycloaddition. The complexes were able to promote the cycloaddition of triunsaturated macrocycles (equation a in Scheme 1.48), triynes (equation b in Scheme 1.48) and, furthermore, the cycloaddition between diynes and monoalkynes (equation c in Scheme 1.48). Remarkably, the two rhodium complexes were efficient catalysts under aerobic conditions without the need to dry the solvent. When asymmetric diynes and alkynes were used, poor regioselectivity was observed (1.27:1 and 1.84:1) and the main compound was the one in which the bulkier substituents were in a relative *meta* position. The study demonstrated that the readily available Rh-NHC complexes were robust and highly efficient homogeneous catalysts for [2+2+2] cycloaddition reaction of three alkynes.

Finally, there are also a couple of reports in which, iron and cobalt with NHC ligands catalyse the [2+2+2] cycloaddition of triynes and enediynes. Malacria et al.⁶² reported a catalytic system based on one equivalent of copper iodide, one equivalent of manganese and catalytic amounts of IPr carbene. This catalytic system proved to be effective in the intramolecular cycloaddition of enediynes, tolerating the presence of heteroatoms, substituents on the alkyne terminus and substituents on both carbons of the alkene. Okamoto et al.⁶³ used a catalytic system based on iron(III) chloride, zinc and IPr carbene, all in catalytical amounts for the totally intramolecular [2+2+2] cycloaddition of triynes. This catalytic system was also tested in the total intramolecular [2+2+2] cycloaddition of pentaynes and triyne-diene compounds. The internal alkyne moieties of the substrates reacted selectively to provide benzene derivatives containing the corresponding terminal alkyne and allyl substituents.

Chapter 2. Objectives

Taking into account the precedents exposed, we set the objectives of the present thesis, aiming to give further insight into two main features of the transition-metal catalysed [2+2+2] cycloaddition: the reactivity of challenging unsaturated substrates and new catalysts for the reaction.

In the first part of the thesis we will aim to study the rhodium-catalysed [2+2+2] cycloaddition reaction involving different unsaturated substrates (Chapters 3 and 4). The synthesis of cyclic scaffolds containing chiral carbons when C-sp² saturations are involved is one of the most attractive features of the [2+2+2] cycloaddition. First, we will investigate the involvement of Morita-Baylis-Hillman adducts in the partial intramolecular version of the reaction. These adducts contain a 1,1-disubstituted alkene moiety which can potentially generate cyclohexadiene scaffolds containing a chiral quaternary carbon. Some features will have to be studied in order to optimise the process, such as the catalytic system used, which will be fundamental in studying the enantioselectivity of the process. The chemoselectivity of the reaction will also be of importance as alkenes are less prone to react than alkynes. In a final step, the scope of the reaction, as well as the reactivity of the cyclohexadiene scaffolds formed, will be studied.

Following our interest in C-sp² saturations and the formation of chiral centres, substrates containing allenes and chiral carbons will also be involved in the rhodium-catalysed [2+2+2] cycloaddition reaction. In a previous work from our group, allene/yne-ene/allene substrates underwent Rh-catalysed [2+2+2] cycloaddition in a diastereoselective manner. Based on that result, we plan to investigate whether the presence of a chiral carbon at the α -position of the allenes induces the chirality of the chiral carbons of the cycloadduct formed (Chapter 4). Both the racemic and enantiopure substrates bearing groups with different steric hindrance and different tethers will be prepared and their [2+2+2] cycloaddition studied. The configuration of the chiral scaffolds formed will be determined by NMR spectroscopy.

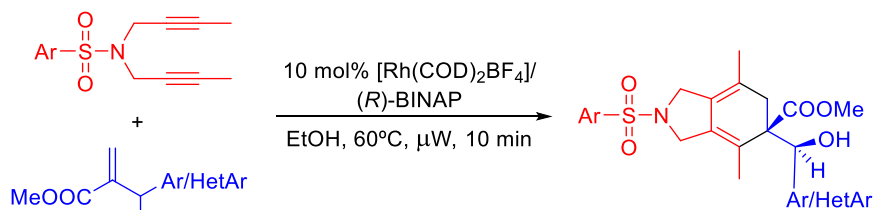
In the second part of the thesis, the synthesis of new catalysts for [2+2+2] cycloadditions will be presented (Chapters 5 and 6). Taking into account the high level of activity observed when phosphoramidite-containing dendrimers are used in rhodium-catalysed [2+2+2] cycloaddition, we aim to synthesize water soluble dendrimers to perform the reaction with water as the solvent. In collaboration with Prof. Anne-Marie Caminade's group at the *Laboratoire de Chimie de Coordination* in Toulouse, we wanted to synthesize water-soluble phosphoramidite-containing dendrimers. As an added value, the core will be formed by a [2+2+2] cycloaddition of an internal alkyne moiety.

As one of the most important issues in catalysis is the avoidance of wastage, we also aim to synthesize organometallic rhodium catalysts in such a way as to enable their recovery and reuse. In collaboration with Prof. Roser Pleixats' group at the *Universitat Autònoma de Barcelona* we planned to synthesize rhodium catalysts that could be immobilised on silica by the sol-gel process or the grafting method. After their characterisation, the activity of these heterogeneous catalysts would then be tested in the rhodium-catalysed [2+2+2] cycloaddition reaction of three alkynes.

Chapter 3. Rhodium-catalysed [2+2+2] cycloadditions of diynes with Morita-Baylis-Hillman adducts

This chapter has been published as:

Fernández, M.; Parera, M.; Parella, T.; Lledó, A.; Le Bras, J.; Muzart, J.; Pla-Quintana, A.; Roglans, A. *Adv. Synth. Catal.* **2016**, *358*, 1848.



- ✓ diastereoselective process
- ✓ kinetic resolution of the Morita-Baylis-Hillman adduct
- ✓ products with a tertiary/quaternary stereodiad in a 84-97% ee

3.1 Precedents

3.1.1. Morita-Baylis-Hillman adducts

Morita-Baylis-Hillman (MBH) adducts are densely functionalized molecules containing at least three functional groups (alcohol, alkene and electron- withdrawing group) in proximity which can participate in a wide range of organic transformations. Different perspectives of these compounds are shown in Figure 3.1.

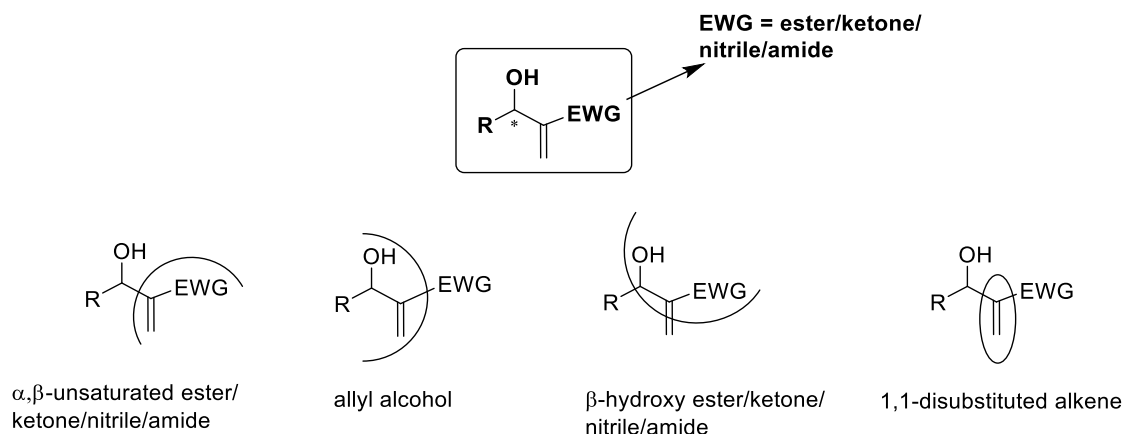
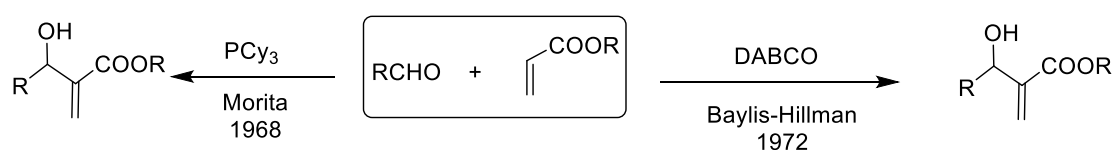


Figure 3.1. Morita-Baylis-Hillman adducts: different perspectives.

The synthesis of Morita-Baylis-Hillman adducts consists of a carbon-carbon bond-forming reaction, which involves an aldehyde and an activated alkene in the presence of a base. It is a three-step one-pot reaction involving successive Michael, aldol and elimination processes.⁶⁴ The reaction was discovered in 1968 when Morita⁶⁵ reported that the reaction of an aldehyde with an activated alkene in the presence of tricyclohexylphosphine afforded a densely functionalized product (Scheme 3.1). In 1972, Anthony Baylis and Melville Hillman⁶⁶ were granted a German patent for performing the same reaction using a tertiary amine instead of a phosphine catalyst (Scheme 3.1). Their greatest success was in the use of DABCO.

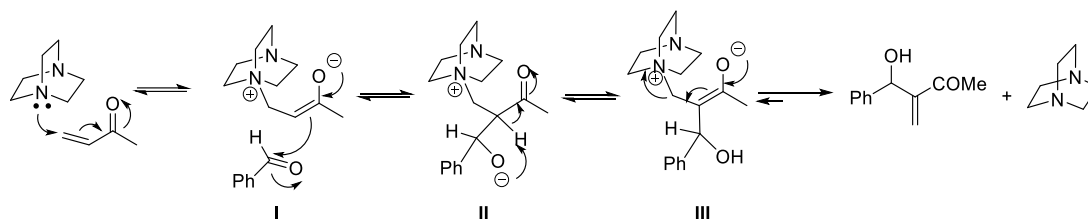


Scheme 3.1. Synthesis of Morita-Baylis-Hillman adducts.

In the 1980s, the reaction was taken up again and its scope was explored by Drewes⁶⁷, Hoffmann⁶⁸ and Basavaiah⁶⁹. Since then, the scope of the reaction has broadened beyond the use of just aldehydes and acrylates to include a wide range of activated unsaturated substrates.⁷⁰

The most generally accepted mechanism⁷¹ of the amine-catalysed reaction is illustrated in Scheme 3.2, taking as a model the reaction between methyl vinyl ketone (as the activated alkene) and benzaldehyde (as the electrophile) under the catalytic influence of DABCO. The first step in this catalytic cycle involves the Michael-type nucleophilic addition of the tertiary amine to the activated alkene to produce a zwitterionic enolate I, which makes a nucleophilic attack

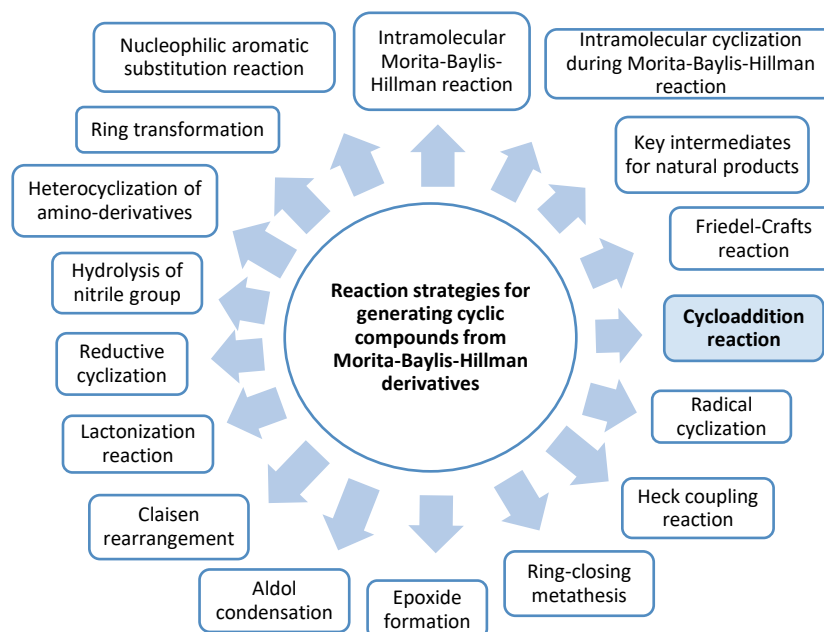
on the aldehyde in an aldol fashion to generate zwitterion **II**. Subsequent proton migration to afford **III** and the release of the catalyst provide the desired multifunctional molecules.



Scheme 3.2. Generally accepted mechanism of the Baylis-Hillman reaction.

The main drawback of the original Baylis-Hillman reaction is the extremely slow reaction rate and so alternative catalysts have been tested in an attempt to resolve this issue. Imidazole derivatives, tertiary amines/diamines and phosphines have been used as alternative catalysts, as well as Lewis acids⁷⁰ such as TiCl_4 , Et_2AlI and BX_3 in some few cases.

Having established the background of MBH adducts, now some of their reactivity will be explained. Of the multiple transformations in which MBH adducts can be involved,⁷² their use in the synthesis of cyclic compounds is particularly noteworthy (Scheme 3.3).

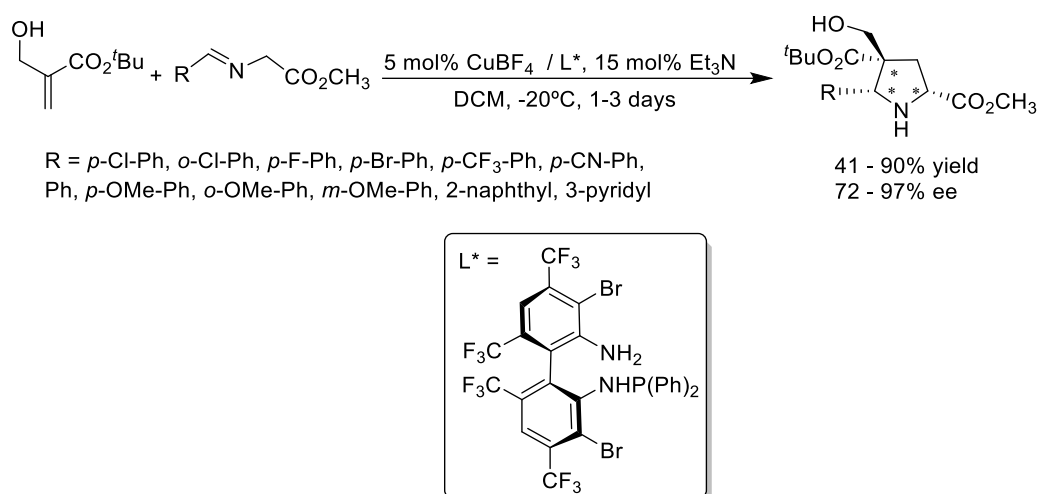


Scheme 3.3. Reaction strategies employed with the Morita-Baylis-Hillman derivatives for the generation of cyclic compounds.

Of the different strategies that are available for generating cyclic compounds from MBH adducts, cycloaddition reactions are particularly attractive due to their atom economy nature and the possibility of constructing multiple bonds in a single synthetic operation.

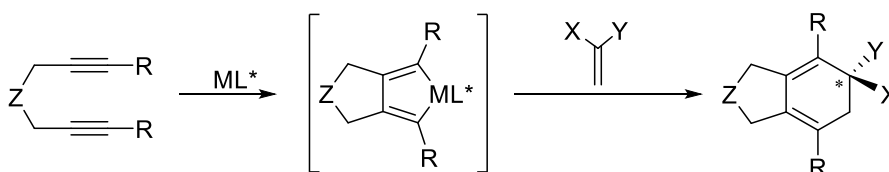
MBH adducts have been involved in thermally induced cycloaddition reactions such as Diels-Alder, [3+2] cycloaddition and 1,3-dipolar cycloaddition. To the best of our knowledge, there is only one study, by Wang et al.⁷³, in which they reported the use of a transition metal catalyst for a cycloaddition reaction in which MBH adducts were used. MBH adducts participated as

dipolarophiles in the copper(I)-catalysed 1,3-dipolar cycloaddition with azomethine ylides to construct pyrrolidine derivatives, containing one quaternary and two tertiary stereogenic centres (Scheme 3.4).



Scheme 3.4. Cu(I)-catalysed asymmetric 1,3-dipolar cycloaddition of various azomethine ylides with a Morita-Baylis-Hillman adduct.

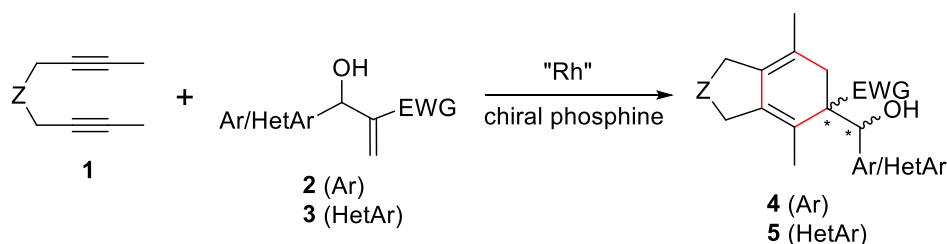
At the start of work on this thesis, the participation of Baylis-Hillman adducts as alkene substrates in transition metal-catalysed [2+2+2] cycloaddition reactions had not been reported. These substrates are attractive as alkene partners for the [2+2+2] cycloaddition reaction due to their 1,1-disubstituted pattern, which can lead to quaternary stereogenic centres (Scheme 3.5). This is an important feature of the reaction, as the formation of all-carbon quaternary stereocentres represents one of the most difficult contemporary challenges in synthetic organic chemistry.



Scheme 3.5. [2+2+2] Cycloaddition of diynes and 1,1-disubstituted alkenes.

3.2 Results and discussion

In this chapter, the participation of Morita-Baylis-Hillman adducts in the partial intramolecular [2+2+2] cycloaddition reaction (Scheme 3.6) will be investigated.



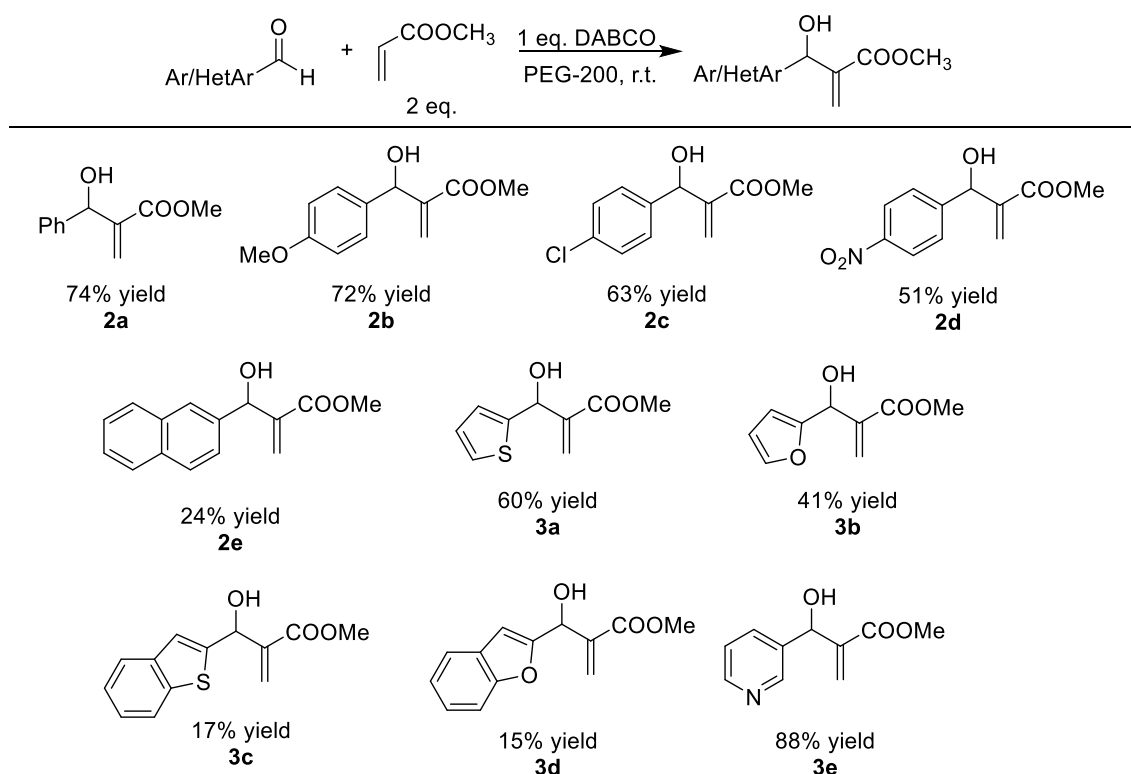
Scheme 3.6. [2+2+2] cycloaddition between diynes and MBH adducts.

The first aspect to be tackled was the optimization of the chemoselectivity of the reaction since alkenes are less prone to react than alkynes, so it was expected that homocoupling of the diyne would be an important undesired reaction. The control of the diastereo- and enantioselectivity of the process was the next step to be taken into account as the product expected contains a highly substituted 1,3-cyclohexadiene motif with chiral quaternary and tertiary carbon atoms. Finally, the study of the scope of the process was planned by placing different tethers on the diyne and changing the aryl and electron- withdrawing groups on the MBH adduct.

In order to study the aforementioned reaction, starting materials were previously synthesized.

3.2.1. Synthesis of Morita-Baylis-Hillman substrates

The synthetic procedure from which MBH adducts were synthesized was optimized by a previous member of our group during a predoctoral visit to the group of Prof. Jacques Muzart and Dr. Jean Le-Bras at the *Institut de Chimie Moléculaire* in Reims.



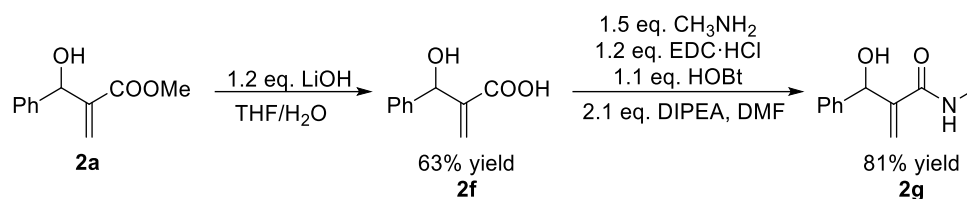
Scheme 3.7. Synthesis of MBH adducts.

The reaction between aryl aldehydes and methyl acrylate was run in polyethylene glycol with an average molecular weight of 200 g/mol (PEG-200) and one equivalent of 1,4-diazabicyclo[2.2.2]octane (DABCO) at room temperature. Solvents such as dioxane, acetonitrile and a mixture of poly(ethylene glycol) and water were also tested, but no reaction was observed in those cases. Nevertheless, poly(ethylene glycol) has been reported to be a good solvent for the MBH reaction between phenyl and heteroaromatic derivatives with acrylates,⁷⁴ and could also be applied to our case. Following this procedure, a wide range of MBH adducts were prepared (Scheme 3.7). We were interested in evaluating the electronic effect of the aryl group (**2b**, **2c** and **2d**), as well as changing the ester function for an acid or an amide (**2f** and **2g**, see Scheme 3.8). A naphthalene-containing adduct **2e** was also prepared. The influence of a

heteroatom in the aryl group was also of interest to us, therefore adducts containing thiophene (**3a** and **3c**), furan (**3b** and **3d**) and pyridine (**3e**) rings were synthesized.

The synthesis of MBH adduct **3e** was performed following a procedure in which the reaction was carried out with no solvent and at 0°C.⁷⁵

By derivatisation of MBH adduct **2a**, adducts **2f** and **2g** could be prepared (Scheme 3.8). Treating **2a** with a base the ester was hydrolysed affording the carboxylic acid derivative **2f**. Adduct **2g** bearing an amide group was synthesized from **2f**. Using a carbodiimide to activate the carboxylic acid functionality and methylamine as a nucleophile, adduct **2g** was obtained with an 81% yield.



Scheme 3.8. Synthesis of MBH adducts **2f** and **2g**.

3.2.2. Synthesis of diyne substrates

1,6-diyne prepared in this section are represented in Figure 3.2. We sought to evaluate the reactivity of *N*-tosyl-linked diynes with different substitution patterns (**1a-1g**) and compare it with the reactivity of carbon- and oxygen- tethered diynes such as **1h** and **1i**. To test substituents with different electronic properties, diynes bearing nitro (**1b**), fluorine (**1c**), bromine (**1d**) and morpholine (**1e**) groups on the *para* position of the aryl were synthesized. In order to introduce bulkier substituents, a triisopropyl-benzenesulfonamide diyne was prepared (**1g**). Finally, as a more challenging diyne, the 5-methyl-2-pyridinesulfonamide derivative **1f** was also synthesized in order to test whether the coordination ability of pyridine had a detrimental effect on this reaction.

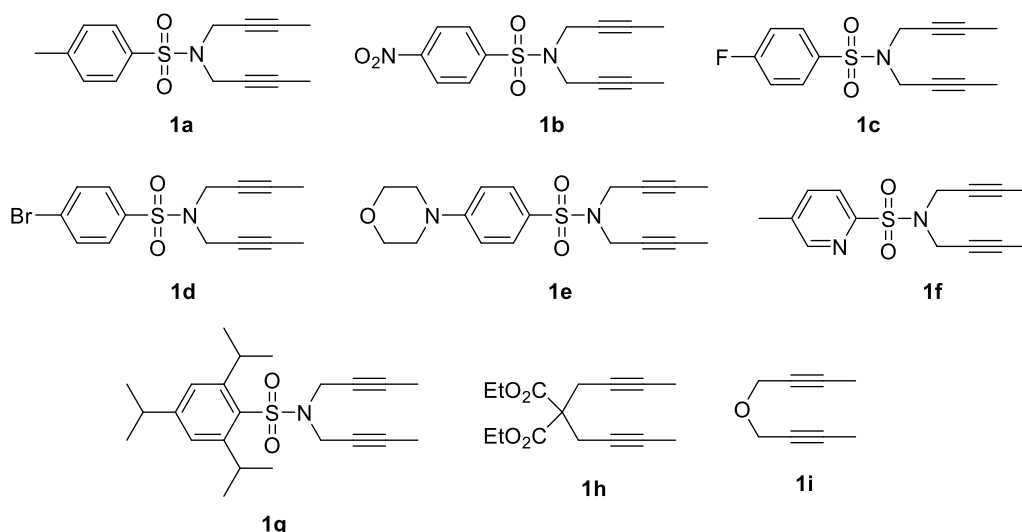
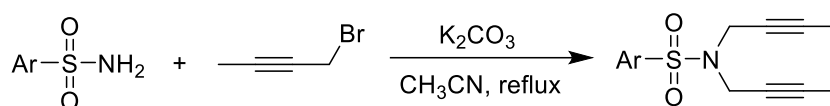


Figure 3.2. Synthesized diynes.

All sulfonamide-based diynes were synthesized as depicted in Table 3.1, starting from commercially available arylsulfonamides. Their reaction with 1-bromo-2-butyne in the presence

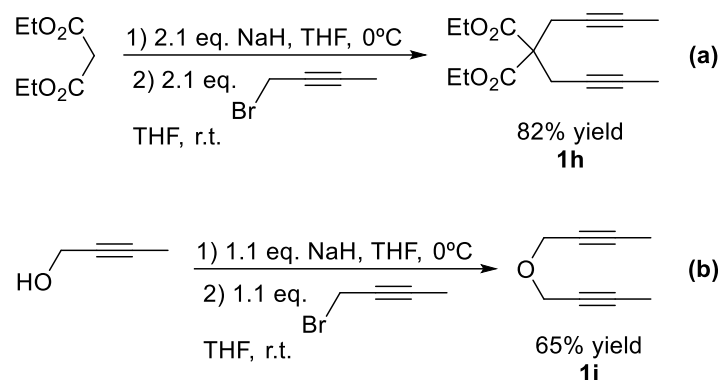
of potassium carbonate as a base successfully afforded the desired diynes when the reaction was heated to the reflux of acetonitrile.

Table 3.1. Synthesis of diyne derivatives.



Diyne	Yield (%)
1a	93
1b	79
1c	90
1d	84
1e	72
1f	79
1g	90

Diyne **1h** and **1i** were synthesized following methods described in the literature.^{17e} For diyne **1h** diethyl malonate was deprotonated with sodium hydride and upon addition of 1-bromo-2-butyne, the product was obtained with an 82% yield (equation a in Scheme 3.9). Diyne **1i** was obtained by means of a deprotonation with sodium hydride of 2-butyn-1-ol and further reaction with 1-bromo-2-butyne (equation b in Scheme 3.9).



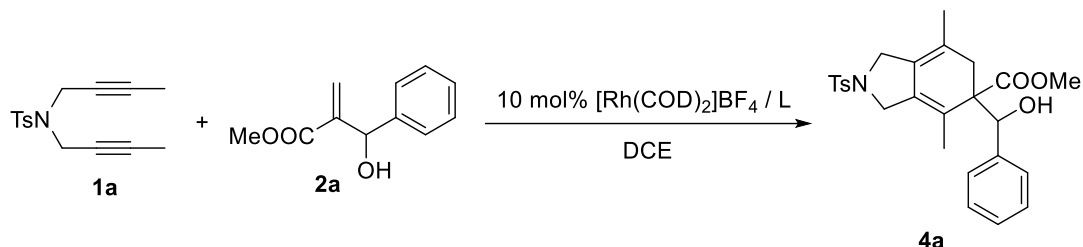
Scheme 3.9. Synthesis of diynes **1h** and **1i**.

All the MBH adducts and the diynes synthesized were fully characterized by the usual analytical techniques (NMR, MS, IR, elemental analysis and melting point).

3.2.3. [2+2+2] Cycloaddition of diynes and Morita-Baylis-Hillman adducts

The feasibility of the cycloaddition was assessed with *N*-tosyl-tethered diyne **1a** and MBH adduct **2a**.¹ The catalytic system of choice was the combination of the cationic rhodium source [Rh(COD)₂]BF₄ with BINAP-type phosphines in a 10 mol% in 1,2-dichloroethane (DCE) as the solvent (Table 3.2).

Table 3.2. Optimization of the [2+2+2] cycloaddition between **1a** and **2a**^[a]

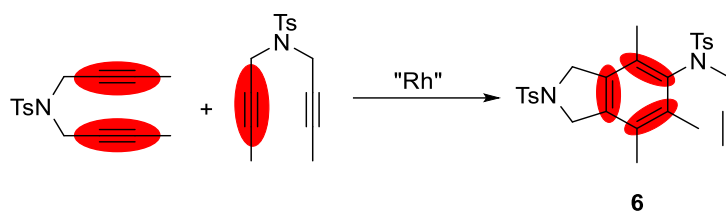


Entry	Ligand	T (°C) / time	Yield/ee ^[b] of 4a (%)
1	(<i>rac</i>)-BINAP	84 / 22h	0 / --
2	(<i>rac</i>)-BINAP	80 (μW) / 10 min	27 / --
3	(<i>R</i>)-BINAP	60 (μW) / 20 min	50 / 93
4	(<i>R</i>)-BINAP	40 (μW) / 40 min	0 / --
5 ^[c]	(<i>R</i>)-BINAP	84 / 4.5 h	55 / 73
6	(<i>R</i>)-H ₈ -BINAP	60 (μW) / 20 min	47 / 95
7	(<i>R</i>)-SEGPHOS	60 (μW) / 20 min	35 / 72
8	(<i>R</i>)-DTBM-SEGPHOS	80 (μW) / 40 min	0 / --
9 ^[d]	(<i>S</i>)-BINAP	60 (μW) / 20 min	24 / 81
10 ^[e]	(<i>R</i>)-BINAP	60 (μW) / 10 min	51 / 94

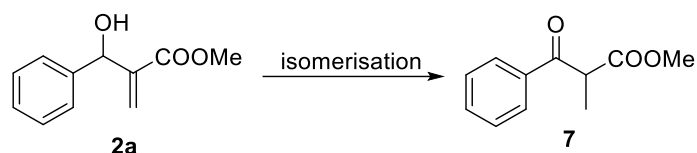
^[a] Conditions: **1a** (1 equiv.), **2a** (1.5 equiv.), DCE (3 mL). ^[b] Enantiomeric excess determined by chiral HPLC. ^[c] Slow addition of the diyne to a mixture of catalyst and **2a** with a syringe pump for 4 h. ^[d] The enantiomer obtained in this case was the opposite of that obtained using (*R*)-BINAP. ^[e] Reaction run in ethanol (3 mL).

In a first attempt, only **6** (Scheme 3.10), an undesired homocoupling of the diyne **1a**, and ketone derivative **7** (Scheme 3.11), resulting from an isomerization MBH adduct, were obtained (entry 1, Table 3.2).

¹ I am grateful to Magda Parera, a previous member of our group, for having performed some of the optimization reactions here.

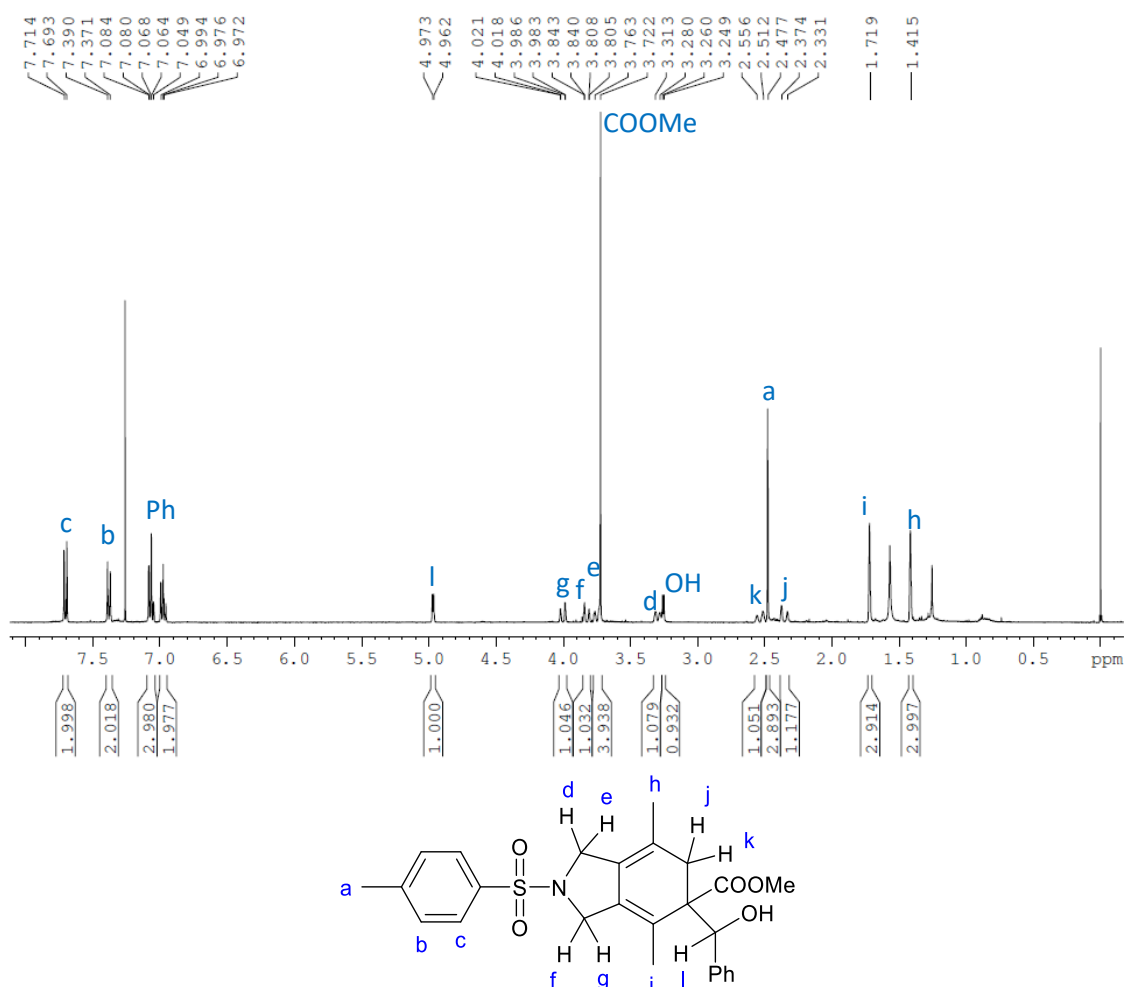


Scheme 3.10. Homocoupling reaction of diene **1a**.



Scheme 3.11. Isomerization of MBH adduct **2a**.

It is well-known that microwave heating can reduce the reaction time, thus avoiding the generation of undesirable products. Therefore, we decided to evaluate the effect of this heating source. The reaction was run at 80°C for 10 minutes (see experimental section for details on the MW experiment conditions). A 27% yield of **4a** was obtained and the formation of both **6** and **7** was reduced (entry 2, Table 3.2).

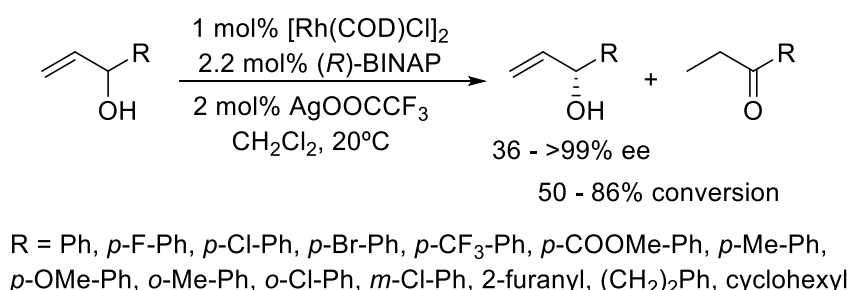


Cycloadduct **4a** contains two chiral carbons, permitting four possible stereoisomers (two pairs of diastereoisomers) to be envisaged. However, $^1\text{H-NMR}$ analysis of **4a** showed the formation of only one of the two possible diastereoisomers, as can be seen in Figure 3.3 where only a set of diastereotopic signals for H_j and H_k is observed. This fact demonstrates the high diastereoselectivity of the process. However, due to free rotation about the C-C bond linking the two stereocentres, it was not possible to determine their relative configuration by NMR spectroscopy.

We then studied the stereoselectivity of this cycloaddition using various chiral phosphines. The use of (*R*)-BINAP at 60°C led to a better yield of **4a** with excellent enantioselectivity in 20 minutes (entry 3, Table 3.2). Having started from racemic MBH adduct **2a**, an enantioenriched cycloadduct was obtained, suggesting that a kinetic resolution process was operative. The recovered unreacted MBH adduct was submitted to chiral HPLC analysis resulting in an e.e. of 17%, which corroborated our hypothesis. The low e.e. obtained can be justified on the grounds of a competing enantiocomplementary isomerization process of the MBH adduct (*vide infra*).

An attempt to reduce the temperature to 40°C resulted in a complete loss of reactivity (entry 4, Table 3.2). We then evaluated the e.e. obtained under conventional heating using slow addition of diyne **1a** to avoid its homodimerization (entry 5, Table 3.2). The yield of **4a** was similar but the enantioselectivity was lower (73% instead of 93%, entries 5 and 3, Table 3.2). Different axially chiral biphosphines were then tested in dichloroethane under microwave heating. Whereas (*R*)-H₈-BINAP provided analogous yields and enantiomeric excesses (entry 6, Table 3.2), the use of both (*R*)-SEGPHOS and especially (*R*)-DTBM-SEGPHOS gave worse results (entries 7 and 8, Table 3.2). As a result, (*R*)- and (*S*)-BINAP were chosen for the rest of the study. (*S*)-BINAP promoted the reaction of the other enantiomer of the MBH adduct to afford **4a** with 81% enantiomeric excess; however, the yield was lower than when (*R*)-BINAP was used (compare entries 3 and 9, Table 3.2).

In all the above experiments, isomerization of **2a** to ketone **7** occurred consistently. A cationic rhodium system with (*R*)-BINAP was described by Zhang et al.⁷⁶, in which a non-coordinating solvent such as dichloromethane (DCM) favours the isomerisation of allylic alcohols to saturated carbonyl compounds (Scheme 3.12). It should be noted that when alcohol-type solvents were used in Zhang's report, the reaction proceeded with less efficiency or did not proceed at all.



Scheme 3.12. Kinetic resolution of allylic alcohols by selective isomerization to the ketone reported by Zhang.

Therefore, we decided to evaluate the effect of the solvent in our reaction. Using EtOH, **4a** was obtained in a 51% yield and with 94% of e.e. and, importantly, no trace of the isomerized compound was detected (entry 10, Table 3.2). Two control experiments were carried out to

determine whether or not the isomerization process was rhodium-catalysed. Treatment of MBH adduct **2a** with the Rh-catalytic system in DCE at 80°C for three hours led to its quantitative conversion into **7**. We then repeated the experiment in EtOH. The MBH adduct was submitted to MW heating in EtOH (10 minutes at 60°C). Starting material alone was recovered, indicating that EtOH prevents isomerization. Additionally, in the reaction of entry 10 (Table 3.2), the recovered MBH adduct was obtained in 43% e.e., confirming that the lower e.e. previously observed (17% ee) originates from the isomerization process.

Single crystals of **4a** were obtained by slow evaporation of a solution consisting of **4a** in a mixture of dichloromethane and pentane. A single X-ray crystallographic analysis of the crystals obtained revealed an (*R*)-configuration for the quaternary stereogenic centre and an (*S*)-configuration for the tertiary alcohol stereogenic centre (Figure 3.4).

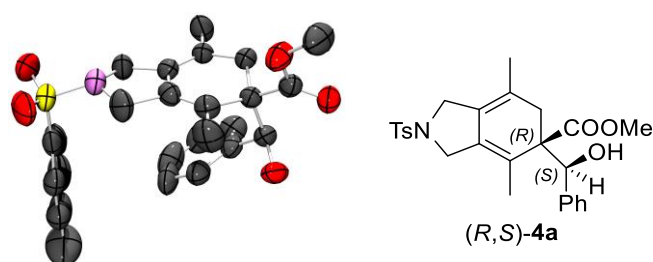
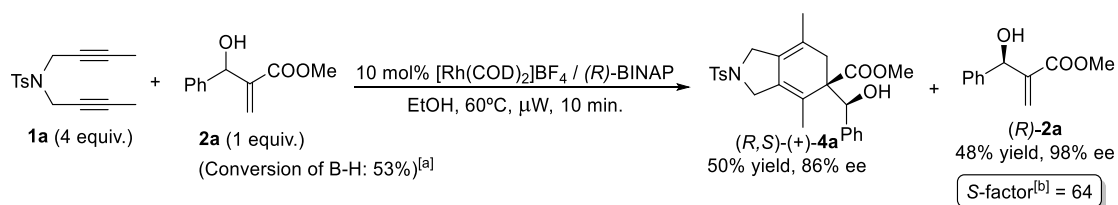


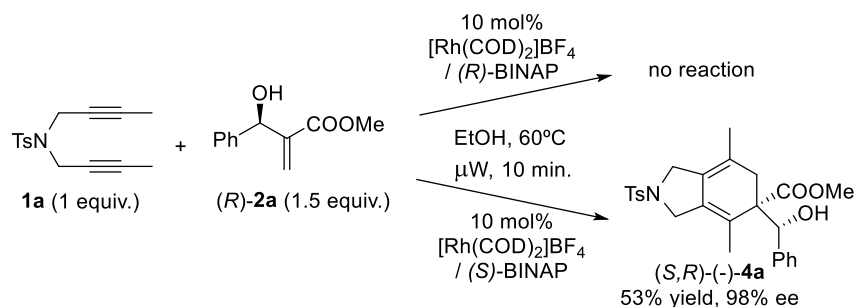
Figure 3.4. ORTEP diagram of cycloadduct (*R,S*)-**4a**.

The kinetic resolution process was then analysed in greater detail. First, a [2+2+2] cycloaddition reaction was set up using an excess of diyne **1a** (Scheme 3.13). We obtained (*R,S*)-**4a** in a 50% yield and 86% e.e., together with an excess of diyne homocoupled compounds and (*R*)-**2a** in a 48% yield and an excellent 98% e.e. The selectivity factor (*S*-factor) for the kinetic resolution of **2a** was determined to be 64, meaning that (*S*)-**2a** reacts 64 times faster than (*R*)-**2a**.⁷⁷ Therefore, the rhodium-catalysed [2+2+2] cycloaddition reaction developed appears to be a potentially efficient way to resolve MBH adducts.



Scheme 3.13. Kinetic resolution of MBH adduct **2a**. ^[a] Conversion of *rac*-**2a** = $ee_{2a}/(ee_{2a} + ee_{4a})$; ^[b] *S*-factor = $\ln[(1-\text{conv})(1-ee_{2a})]/\ln[(1-\text{conv})(1+ee_{2a})]$.

Further insight into the resolution process was gained by treating the enantioenriched MBH adduct (*R*)-**2a** with **1a** in the optimized reaction conditions (entry 10, Table 3.2) with either (*R*)- or (*S*)-BINAP (Scheme 3.14). As expected, no cycloadduct was isolated in the reaction with (*R*)-BINAP. On the other hand, (*S*)-BINAP efficiently promoted the cycloaddition of (*R*)-**2a** to (*S,R*)-**4a**, corroborating the high enantiospecificity of the process.



Scheme 3.14. Cycloaddition reactions with enantioenriched (*R*)-**2a**.

Finally, the cycloaddition of **1a** with **2a** was monitored over time in a reaction carried out under conventional heating, which has a longer reaction time than that run under microwave heating (Figure 3.5). This kinetic experiment revealed a rapid consumption of (*S*)-**2a** to form (*R,S*)-**4a** cycloadduct with a high enantiomeric excess, which did not decrease over time. After approximately 2.5h of reaction, the cycloadduct yield and the e.e. of the MBH adduct reached a plateau indicating that (*R*)-**2a** does not react at a significant rate under the reaction conditions. This experiment constitutes further evidence that the two enantiomers of the MBH adduct show different reactivities under asymmetric Rh/biphosphine catalysis.

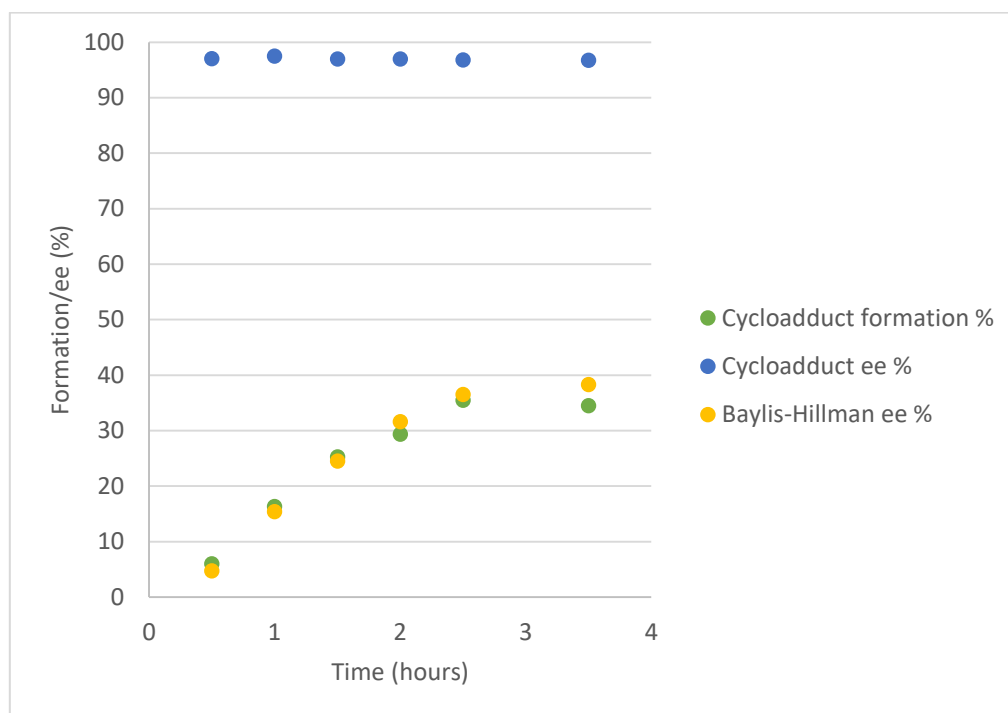


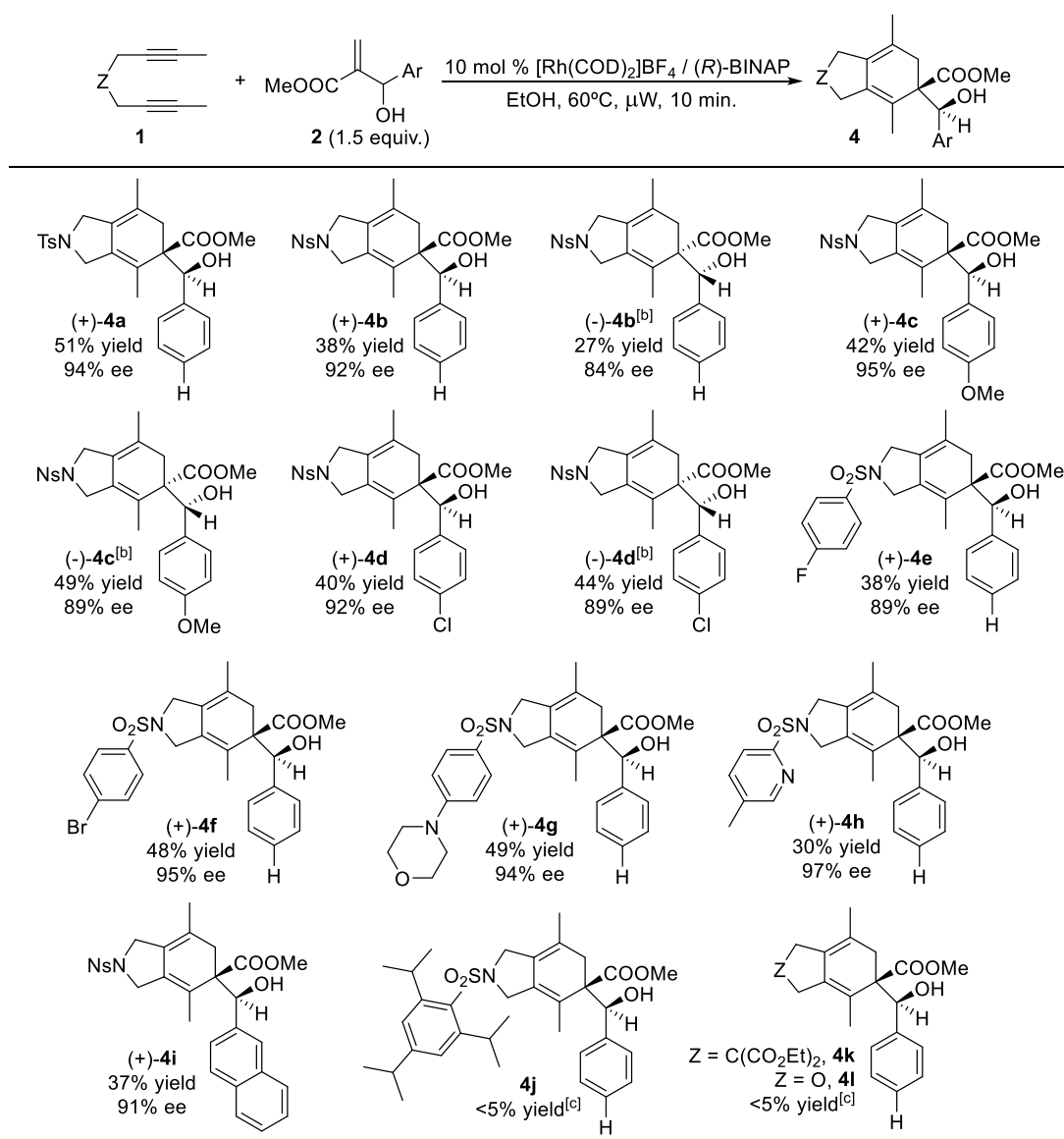
Figure 3.5. Formation of cycloadduct **4a** over time (hours).

In a final set of optimization experiments, the relative amount of the MBH adduct **2a** was modified. Using either 3 or 4 equivalents of **2a**, the yield of **4a** was not improved (41% and 42%, respectively). The reaction shows substrate inhibition when a high excess of MBH adduct is used. Our interpretation is that this inhibition is probably due to coordination of multiple MBH adducts to the rhodium complex. Therefore, we decided to use only 1.5 equivalents of the MBH adduct. In order to study the effect of the hydroxyl group of the MBH adduct in the cycloaddition process, acetyl- and Boc-protected MBH adducts were tested using the optimized reaction

conditions. In neither case was cycloadduct **4a** obtained, indicating that the free hydroxyl group has a determining role in the process.

Having established the background for the kinetic resolution that operates in the described process, we again focused on the stereoselective synthesis of highly functionalized cyclohexadienes, proceeding to evaluate the scope of the reaction varying both the tethers of the diene and the MBH adduct (Scheme 3.15).

A first test showed that the use of diyne **1b**, containing a 4-nitrobenzenesulfonamide (NNs) instead of *N*-tosylsulfonamide, gave the cycloadduct **4b** also with great efficiency. Since NNs group could be deprotected in milder reaction conditions⁷⁸, the study of the scope of the MBH adducts was continued with diyne **1b** (compounds **4b-4d**, Scheme 3.15).

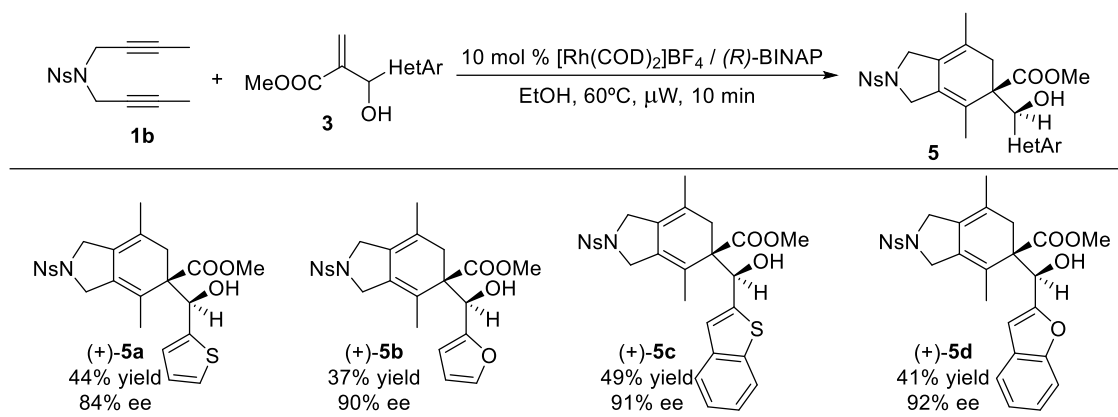


^[a] The cited yields were of isolated products. Enantiomeric excess were determined by chiral HPLC. ^[b] (*S*)-BINAP was used. ^[c] The reaction was carried out at 80°C (MW) for 10 min. Yield estimated by NMR.

Scheme 3.15. Scope of the process^[a]

Substituents in the *para*-position of the phenyl ring of **2** with different electronic demand (OMe, Cl) gave the corresponding cycloadducts **4c** and **4d** with good yields and high enantiomeric excesses. Using the enantiomeric (*S*)-BINAP ligand, (-)-**4b**, (-)-**4c** and (-)-**4d** were obtained in high enantiomeric excesses. We then changed the substituent in the *para* position of the phenyl ring at the sulfonamide tether. Fluoride and bromide substituted diynes led to (+)-**4e** and (+)-**4f** with high enantiomeric excesses (Scheme 3.15). Changing the *para* substituent to a moiety with different electronic properties, such as a morpholine ring, did not affect the yield or the e.e., affording compound (+)-**4g** in a 49% yield with 94% of e.e. A diyne bearing the 5-methyl-2-pyridinesulfonyl group provided (+)-**4h** in a 30% yield with 97% e.e. The presence of a nitrogen atom in the molecule did not seem to affect the process by poisoning the catalyst. An effective reaction was also obtained with an MBH adduct with a naphthalene group (compound **4i**). However, MBH adduct **2a** (Ar = Ph) failed to provide significant amounts of cycloadducts **4j** when the highly hindered diyne **1g**, containing three isopropyl groups on the aryl moiety, was used. Malonate and oxygen tethered diynes **1h** and **1i** were not reactive either with **2a** and cycloadducts **4k** and **4l** were not obtained in significant amounts. MBH **2d**, which has a highly electrowithdrawing nitro group, was not suitable for this reaction either, nor were adducts **2f** and **2g** (see Scheme 3.8), which contain carboxylic acid and amide functions that were not reactive with only homocoupling of the diyne being observed. In the case of cycloadduct **4b**, we tested the effect of increasing the MBH adduct equivalents again. With 2, 3 or 4 equiv. of **2a**, the yield was only improved to 43%, 45% and 56%, respectively.

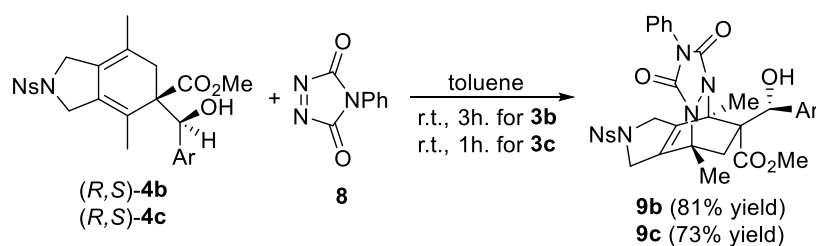
MBH adducts containing heteroaromatic rings such as thiophene, furan, benzothiophene, and benzofuran were then tested as more challenging substrates (Scheme 3.16).



Scheme 3.16. [2+2+2] Cycloaddition reactions between diyne **1b** and Morita-Baylis-Hillman adducts **3**.

In all cases, the corresponding cycloadducts were obtained with high enantioselectivities. Thus, a heteroatom in the MBH adduct did not affect the process and did not poison the rhodium catalyst. However, MBH adduct **3f** containing a pyridine ring (see Scheme 3.7) did not react under the conditions established, in fact this substrate completely inhibited any reaction as only starting material was recovered. The relative and absolute configurations of **4b-4h** and **5a-5d** were tentatively assigned by analogy with (+)-**4a**.

We then exploited the 1,3-cyclohexadiene derivatives generated by the [2+2+2] cycloaddition reaction to access more densely functionalized scaffolds via Diels-Alder reactions⁷⁹ (Scheme 3.17).



Scheme 3.17. Diels-Alder cycloaddition between 1,3-cyclohexadienes **4b** and **4c** and dienophile **8**.

A reactive nitrogen-containing heterodienophile, *N*-phenyltriazolinedione **8**, was reacted with the unactivated and highly substituted cycloadducts **4b** and **4c** in toluene at room temperature, leading to **9b** and **9c**, respectively, in high yields. 2D NMR experiments of the Diels-Alder adducts revealed a highly diastereoselective [4+2] cycloaddition, which took place at the opposite side of the ester group (Figure 3.6). A NOESY experiment showed dipolar coupling between the methylene protons of the six-membered ring and the protons of the CHOH group and aryl ring (red arrows), whereas no coupling between the same methylenic protons and the ester group was observed (green arrows). In both cases, traces of the stereoisomer resulting from the addition of **8** to the same face of the ester group were also observed.

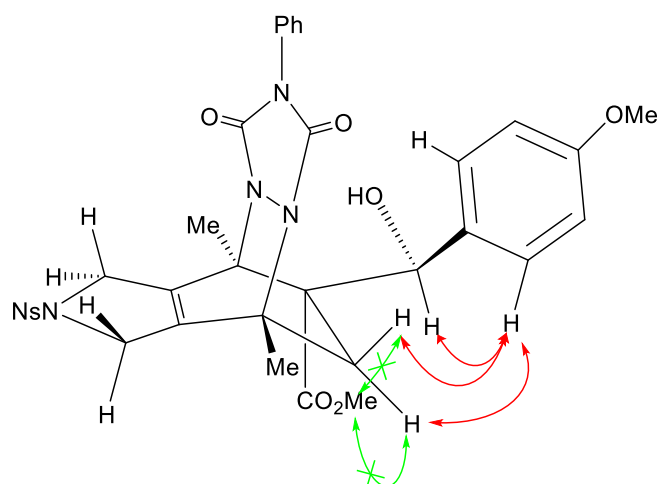


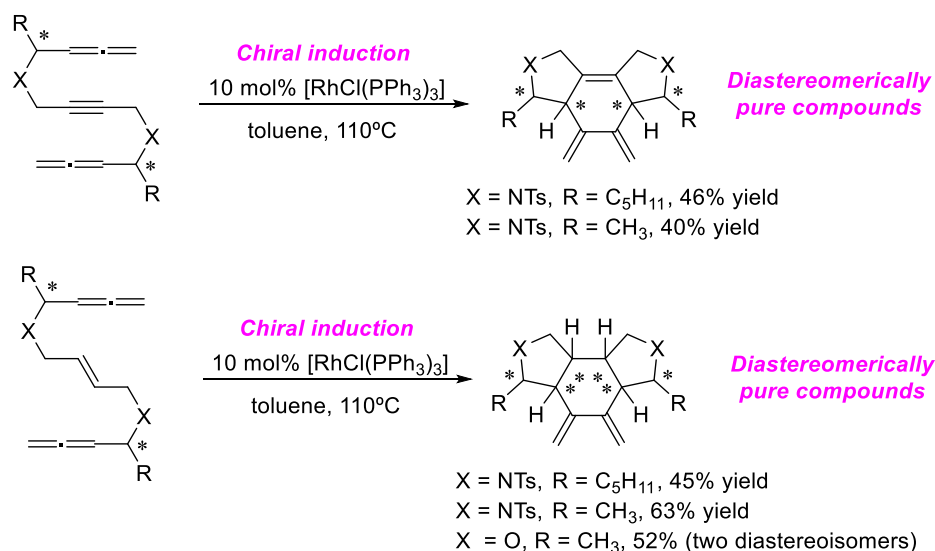
Figure 3.6. Key 2D NOESY contacts for **9c**.

To summarize, we have developed a diastereo- and enantioselective [2+2+2] cycloaddition reaction between diynes and Morita-Baylis-Hillman adducts using a combination of $[\text{Rh}(\text{COD})_2]\text{BF}_4$ and chiral BINAP ligands. A kinetic resolution of the MBH adduct was achieved generating an optically pure 1,3-cyclohexadiene containing vicinal tertiary and quaternary carbon centres. Furthermore, Diels-Alder reactions using these dienes as substrates occurred in a highly diastereoselective fashion to provide densely functionalized polycyclic scaffolds.

Chapter 4. Chiral induction in intramolecular rhodium-catalysed [2+2+2] cycloadditions of optically active allene-yne/ene-allene substrates

This chapter has been published as:

Haraburda, E.; Fernández, M.; Gifreu, A.; Garcia, J.; Parella, T.; Pla-Quintana, A.; Roglans, A. *Adv. Synth. Catal.* **2017**, 359, 506.



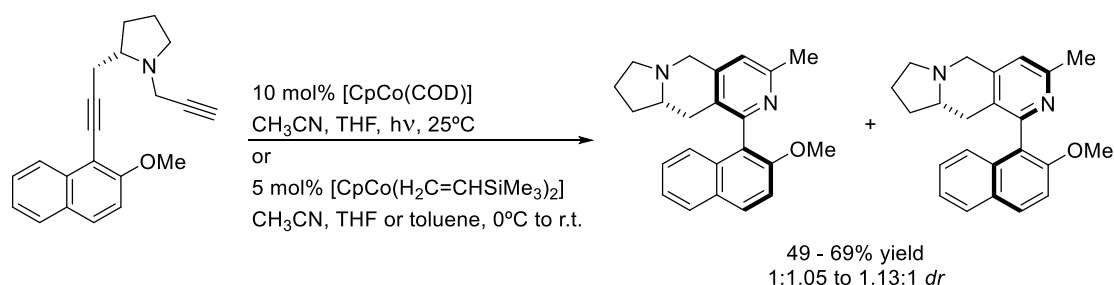
4.1 Precedents

4.1.1. Chirality induction

The production of enantiomerically pure compounds is one of the most desirable goals in modern organic synthesis. Single enantiomers of a chiral compound are highly sought as they are active molecules in many drugs. Among numerous strategies for the production of chiral molecules, asymmetric synthesis, which is defined as the conversion of an achiral starting material to a chiral product in a chiral environment, is currently the most attractive option.⁸⁰

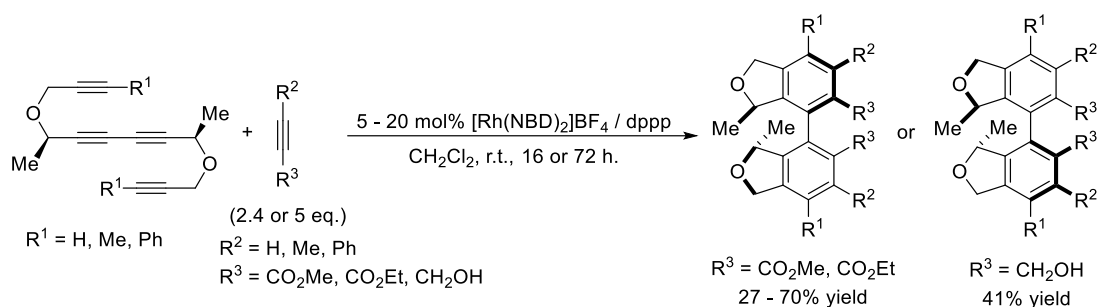
However, studies based on diastereoselective reactions of easily accessible chiral substrates have also been reported and are an alternative to asymmetric synthesis. In section 1.1.2.2 we have already described an example from Malacria's group in which they report axial-to-central chirality transfer from an enantioenriched allenediene.³⁵

Although in chirality transfer processes new chiral elements are created in substitution of the original ones, a most common approach is that the initial inducing stereogenic element is maintained in the final product synthesizing an enantiopure compound by means of a diastereoselective process.⁸¹ This strategy, referred to as chirality induction, has also been applied in [2+2+2] cycloaddition reactions. Hapke et al.⁸² reported in 2012 the cobalt(I)-catalysed [2+2+2] cycloaddition of chiral proline-derived diynes with nitriles, which led to the formation of both atropoisomers of the axially chiral arylpyridines. No large selectivity effects were observed, presumably due to the distance of the proline moiety to the reaction centre, and both atropoisomers were obtained (*dr* ranging from 1:1.05 to 1.13:1). However, this strategy provided access to both diastereomeric atropoisomers, which could easily be separated by column chromatography without the need for chiral catalysts (Scheme 4.1).



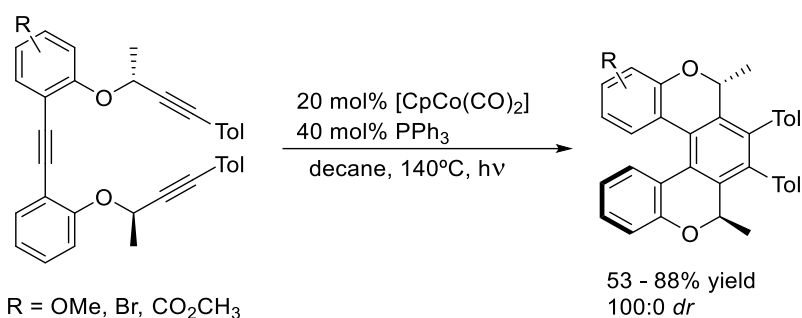
Scheme 4.1. Central to axial chirality induction in the cobalt-catalysed formation of pyridines.

On the other hand, Tanaka et al.⁸³ reported the rhodium(I)-catalysed diastereoselective [2+2+2] cycloaddition of chiral tetraynes with functionalised monoynes to achieve C₂-symmetric axially chiral biaryls (Scheme 4.2). In this case, the reaction was completely diastereoselective leading to enantiopure compounds. Interestingly, the authors demonstrated that the diastereoselectivity of the reaction is under substrate control and not induced even when a chiral ligand is used in the catalytic system.



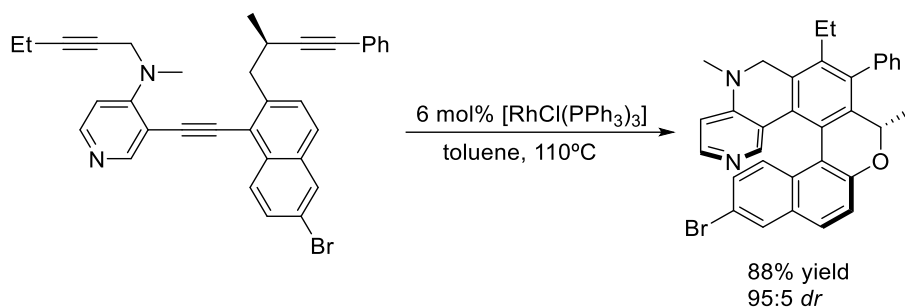
Scheme 4.2. [2+2+2] Cycloaddition of chiral tetraynes with monoynes to achieve axially chiral biaryls

Central-to-helical chirality induction was also demonstrated in several papers by Stará and Starý's group.⁸⁴ They developed a highly stereoselective [2+2+2] cycloaddition of optically pure aromatic triynes producing [7]helicene-like scaffolds in diastereoisomeric ratios up to 100:0. High diastereoselectivities were obtained when a Co(I) complex together with triphenylphosphine was used as catalytic system. The efficient central to axial chirality induction was controlled by the absolute configuration at the asymmetric centre and by the carbon substituents at the alkyne terminus.^{84d,e} The cobalt-catalysed diastereoselective [2+2+2] cycloaddition reaction was then effectively applied to the synthesis of functionalized penta-, hexa-, and heptacyclic helicenes in non-racemic form starting from optically pure triynes. Stará and Starý discovered that theoretical studies could be used to predict the stereochemical outcome of the reaction.^{84c} In a further study, they achieved the synthesis of aromatic hexaynes under cobalt catalysis in a process in which six new cycles of a helicene backbone were formed in a single operation.^{84b} Finally, the same group reported the improvement of the selectivity of their methodology for the preparation of optically pure [5]-, [6]-, and [7]heterohelicenes. Theoretical calculations were used to determine suitable substituents on the terminus of the alkynes so that the cyclisations were highly diastereoselective avoiding the racemisation of the helical compounds (Scheme 4.3).^{84a}



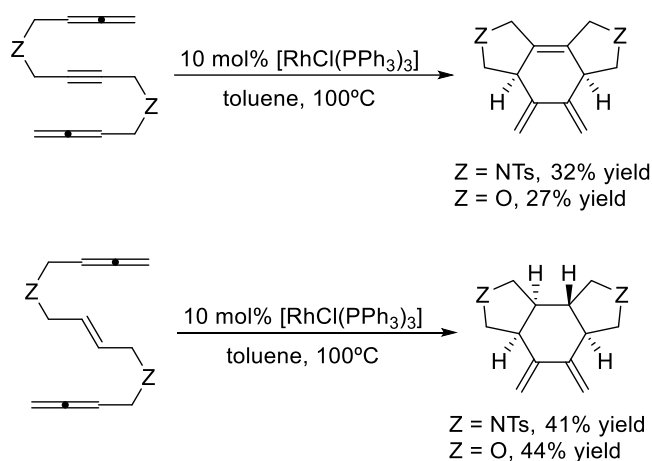
Scheme 4.3. [2+2+2] Cycloaddition of optically pure aromatic triynes to obtain helicene-like scaffolds.

Finally, Carbery et al.⁸⁵ reported the synthesis of helicenoidal-DMAP organocatalysts upon diastereoselective Wilkinson-catalysed [2+2+2] cycloaddition on an optically pure triyne that had a stereogenic centre and that already contained a pyridine ring (Scheme 4.4).



Scheme 4.4. Synthesis of helicene-like DMAP compound by the Wilkinson-catalysed [2+2+2] cycloaddition of an optically pure tryene.

As we saw in section 1.1.2.2, and as part of our continuing interest in the use of allenes as unsaturated substrates for the construction of polycyclic scaffolds by Rh-catalysed cycloaddition reactions,^{3h} our group described the cycloaddition of linear allene-yne-allene and allene-ene-allene substrates promoted by the Wilkinson's complex to afford tricyclic scaffolds featuring exocyclic dienes (Scheme 4.5).



Scheme 4.5. Rhodium(I)-catalysed [2+2+2] cycloaddition of allene-yne/ene-allene substrates.

The process was diastereoselective, furnishing cycloadducts with two or four stereocentres, respectively, as a single diastereoisomer. Cycloadducts were formed by a chemoselective reaction of the inner allene double bond and, therefore, featured an exocyclic diene motif. Given that new stereocentres were generated in the cycloadducts, we tried to obtain optically pure polycycles using combinations of a cationic rhodium source and chiral biphosphine ligands. However, the diastereoselectivity of the reaction dramatically decreased making the process inefficient.

In this chapter we aim to evaluate the synthesis of asymmetric cyclohexane and cyclohexene scaffolds by chirality induction starting from an enantiomerically pure allene-ene/yne-allene substrate under $[\text{RhCl}(\text{PPh}_3)_3]$ catalysis.

4.2 Results and discussion

4.2.1. Synthesis of chiral allene-ene-allene and allene-yne-allene substrates

In order to perform the study of the stereoselective [2+2+2] cycloaddition reaction with chiral bisallene substrates, five model compounds bearing *N*-tosyl- (NTs) and oxygen (O) linkage were

prepared. Two chiral centres were placed in the α -position to the allene functionality, a long C_5H_{11} alkyl chain [(*S,S*)-**10**, (*S,S*)-**11**] and a methyl group [(*R,R*)-**12**, (*R,R*)-**13** and (*S,S*)-**14**] (Figure 4.1).

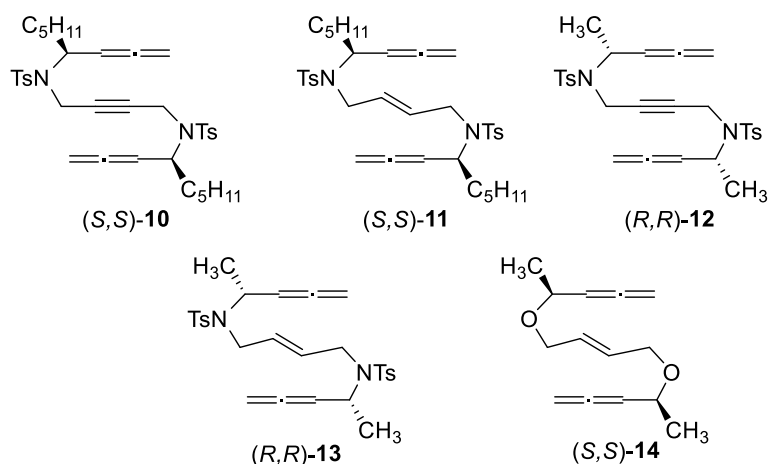
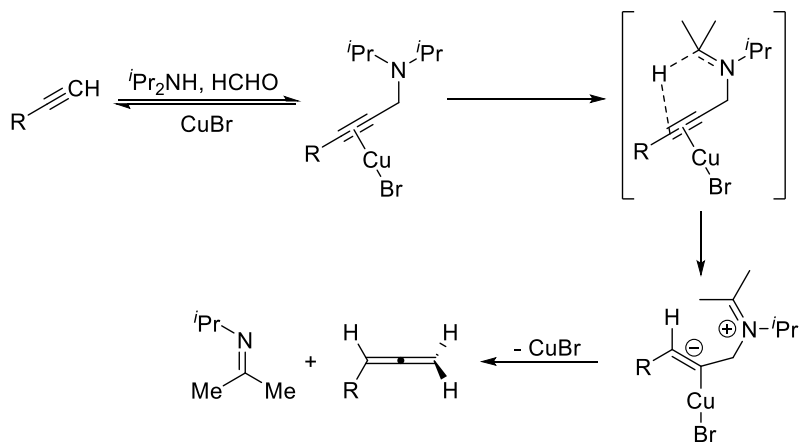


Figure 4.1. Bisallene substrates used.

The synthesis of (*S,S*)-**10** and (*S,S*)-**11** depicted in Scheme 4.7 was performed by a previous member of our group and published in her PhD thesis.⁸⁶ The first step is the transformation of the alkyne moiety of 1-octyn-3-ol to an allene through a Crabbé homologation.⁸⁷ The postulated mechanism of this reaction is depicted in Scheme 4.6.

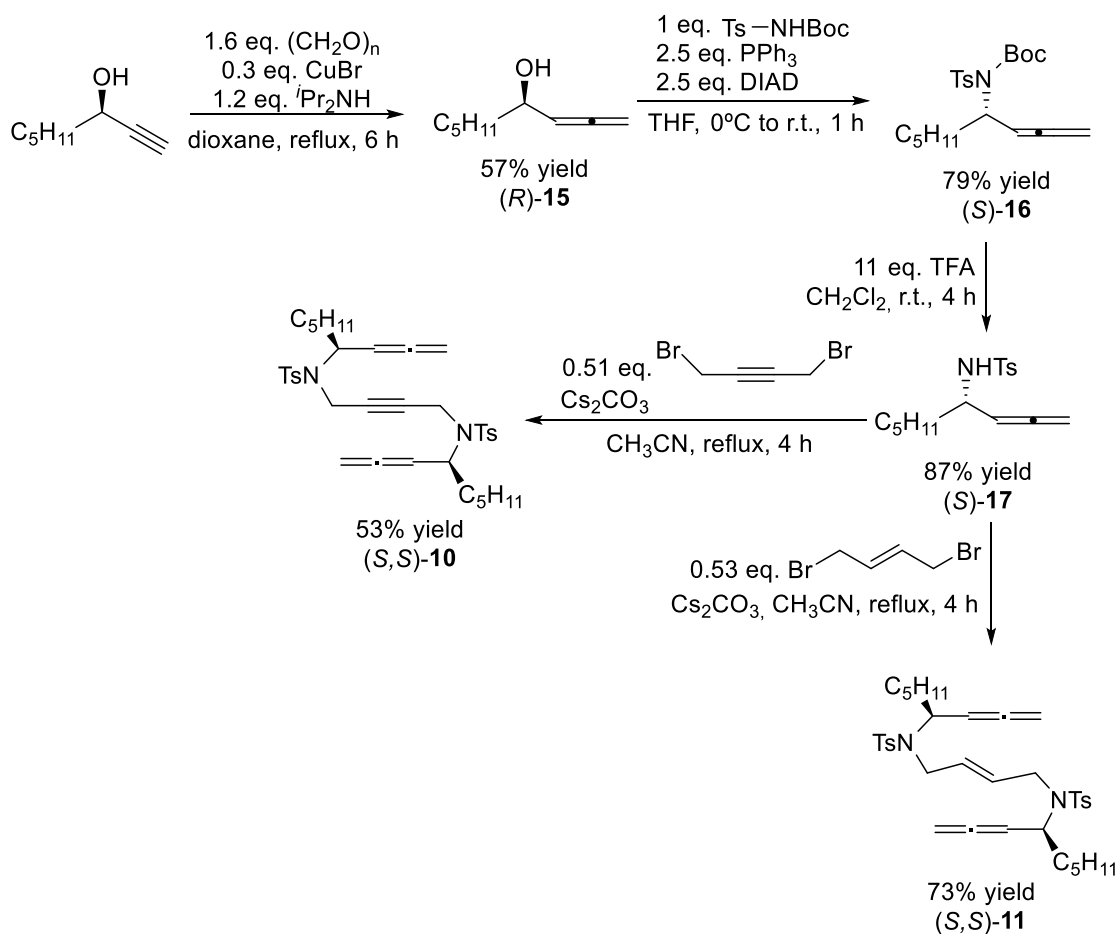


Scheme 4.6. Mechanism of the Crabbé homologation for the synthesis of allenes.

The reaction proceeds via the stepwise formal retro-imino-ene reaction of the Mannich base intermediate initially formed. The main role of the Cu(I) catalyst is the activation of the alkyne towards nucleophilic attack by a formal hydride and the stabilisation of the incipient formation of a vinyl carbanion at the transition state.⁸⁸

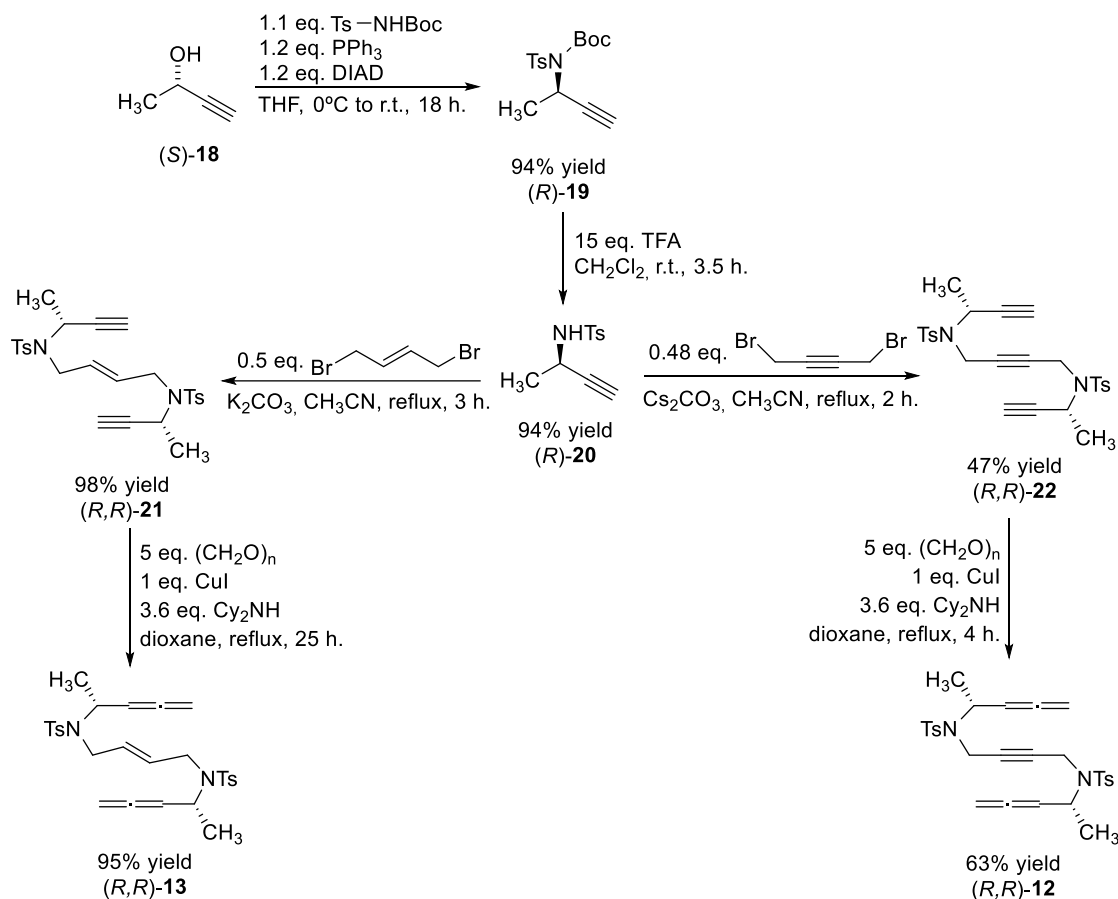
A Mitsunobu reaction on the alcohol of (*R*)-**15** with *N*-(*tert*-butyloxycarbonyl) tosylsulfonamide then inverts the chirality of the molecule, transforming the (*R*) compound into (*S*). Further removal of the Boc group with trifluoroacetic acid (TFA) gives (*S*)-**17** that can be alkylated with either 1,4-dibromobut-2-yne to afford (*S,S*)-**10** or with (*E*)-1,4-dibromo-2-butene to afford (*S,S*)-**11**. Throughout the whole synthetic process the products obtained with the enantiopure alcohol were analysed by chiral HPLC to prove their optical purity. In addition, when the synthesis was

started with the racemic propargylic alcohol, inseparable 1:1 mixtures of *meso* form and racemate of the bisallene derivatives were obtained in both cases.



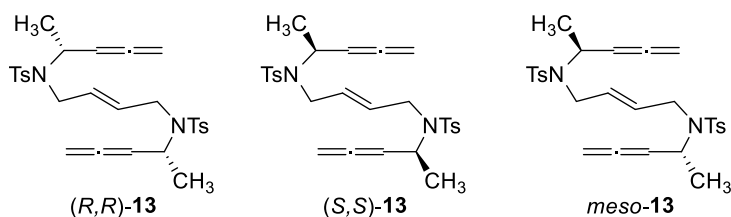
Scheme 4.7. Synthesis of (*S,S*)-**10** and (*S,S*)-**11**.

The synthesis of the methyl-substituted bisallenes (*R,R*)-**12** and (*R,R*)-**13** was then planned following a procedure that is analogous to the one used for the synthesis of (*S,S*)-**10** and (*S,S*)-**11**. However, in this case the Crabbé homologation on the alcohol (*S*)-**18** was not efficient as the corresponding allene was highly volatile and, in consequence, was lost during the work-up of the reaction. In consequence we decided to modify the synthetic strategy and to perform the Crabbé homologation in the last step of the synthesis (Scheme 4.8). Therefore, the first reaction performed was the Mitsunobu reaction of alcohol (*S*)-**18** with *N*-(*tert*-butyloxycarbonyl) tosylsulfonamide, which takes place with an inversion of the configuration of the chiral carbon. Deprotection of the sulfonamide moiety with TFA afforded (*R*)-**20**, which underwent alkylation with either (*E*)-1,4-dibromo-2-butene to afford (*R,R*)-**21** or 1,4-dibromobut-2-yne to afford (*R,R*)-**22**. Both compounds were submitted to Crabbé homologation conditions to afford the corresponding bisallene derivative (*R,R*)-**12** with a 26% overall yield and (*R,R*)-**13** and an 82% overall yield.



Scheme 4.8. Synthesis of (R,R)-12 and (R,R)-13.

The optical purity of (R,R)-13 was checked by chiral HPLC analysis. When the synthesis was performed starting from the racemic alcohol **18**, a mixture of a *meso* form and a racemic mixture of two enantiomers was obtained. Taking into account the two stereogenic centres that bear the molecule, equation 2^n would give us four stereoisomers, but due to the symmetry of the molecule a non-chiral *meso* form is obtained, reducing the number to three stereoisomers (Figure 4.2).

Figure 4.2. Stereoisomers of **13** when the synthesis is performed starting from *rac*-**18**.

The HPLC chromatogram of **13** shows two peaks at retention times of 18.2 and 20.6 minutes, which correspond to the pair of enantiomers, and a third peak at a retention time of 21.9 minutes, with an area twice that of the peaks at 18.2 and 20.6 min., which corresponds to the *meso* form (Figure 4.3).

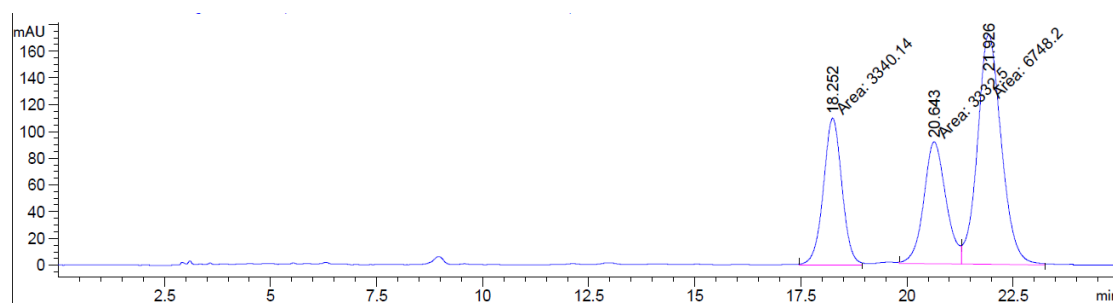


Figure 4.3. HPLC chromatogram of **13**.

On the other hand, when the synthesis was performed starting from the chiral alcohol (*S*)-**18** a single peak for (*R,R*)-**13** at a retention time of 20.4 minutes, which corresponds to one of the stereoisomers obtained in the synthesis of **13**, was observed (Figure 4.4).

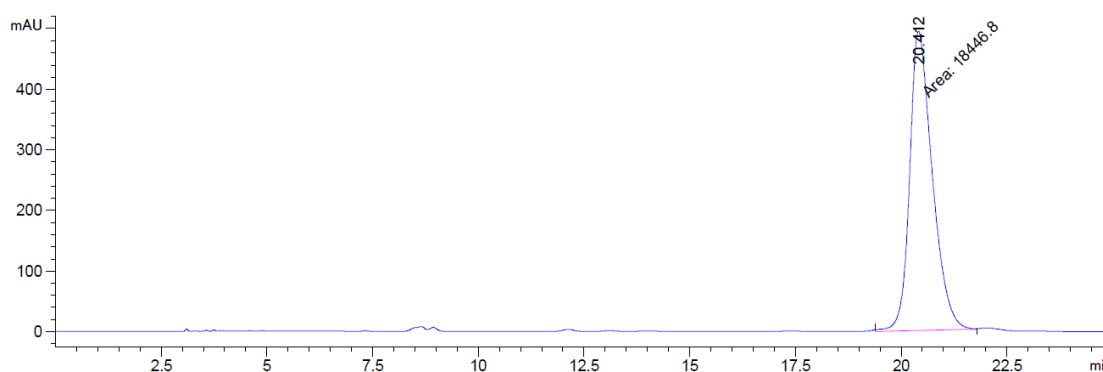
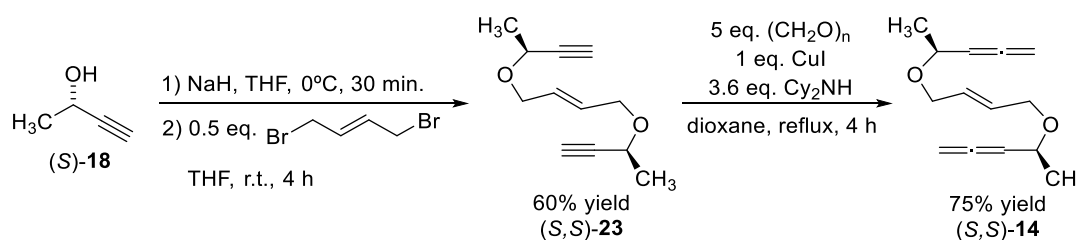


Figure 4.4. HPLC chromatogram of (*R,R*)-**13**.

Finally, the oxygen-tethered bisallene was prepared as depicted in Scheme 4.9. Deprotonation of the alcohol functionality of (*S*)-**18** with sodium hydride and alkylation with (*E*)-1,4-dibromo-2-butene afforded endiyne (*S,S*)-**23** in a 60% yield. The last reaction was the transformation of the alkynes to allenes through a Crabbé homologation to obtain a 75% yield of (*S,S*)-**14**.



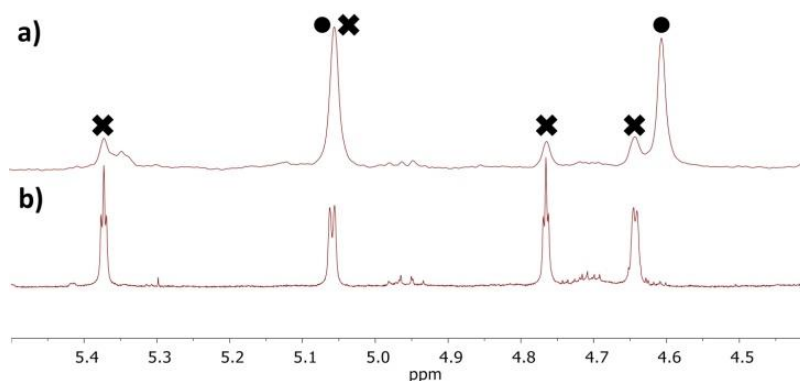
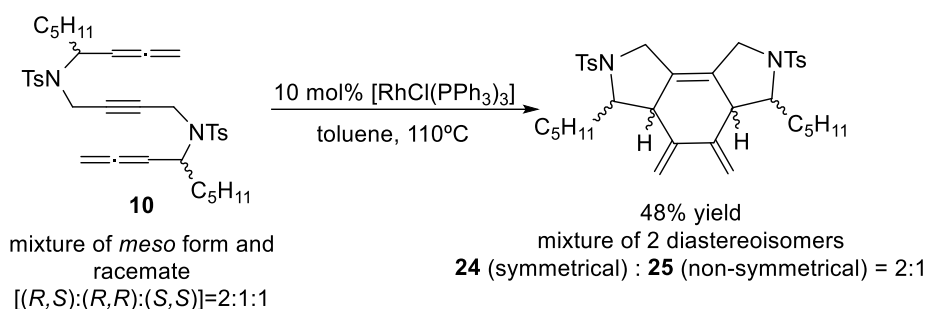
Scheme 4.9. Synthesis of (*S,S*)-**14**.

All the bisallene derivatives were fully characterized by the usual analytical techniques (NMR, MS, IR, elemental analysis and melting point).

4.2.2. [2+2+2] Cycloaddition of allene-yne-allene substrates

After the preparation of the model substrates, their reactivity in the [2+2+2] cycloaddition reaction was evaluated. The use of Wilkinson's catalyst and toluene as the solvent at 110°C was chosen as reaction conditions based on our previous results. The [2+2+2] cycloaddition of substrates **10** and **11** was performed by a previous member of our group and published in her PhD thesis,⁸⁶ but in order to understand the results for the other substrates, the results are also

presented here. We first investigated the reaction of allene-yne-allene **10**, prepared from racemic propargylic alcohol. In this case, only two new stereogenic centres were generated. In the cycloaddition of **10**, two diastereoisomers were formed (Scheme 4.10).



Scheme 4.10. Wilkinson-catalysed [2+2+2] cycloaddition reaction of allene-yne-allene **10**. a) $^1\text{H-NMR}$ spectra of the olefinic part of the cycloadduct mixture from **10** and b) from optically pure (*S,S*)-**10**.

A detailed NMR analysis of the olefinic part of the spectrum revealed that one symmetrical (**24**) (dots) and one non-symmetrical cycloadduct (**25**) (crosses) were formed in a 2:1 ratio.

The cycloaddition of the enantiomerically pure bisallene (*S,S*)-**10** showed a single non-symmetric enantiomer in a 46% yield, which happened to correspond to the minor diastereoisomer **25** obtained in the previous reaction (Scheme 4.10). Taking into account this result, it was concluded that the symmetrical isomer **24** formed when non chiral **10** was used arises from the cycloaddition of the *meso* form. In addition, the major proportion of **24** over **25** indicated that the *meso* form was more reactive than the racemate.

To determine the absolute configuration of the enantiopure cycloadduct, we considered all the stereoisomers that might be generated. The cycloadduct has four stereocentres: two of which are new stereogenic centres generated in the cycloaddition, whereas the other two are transferred from the substrate, maintaining their (*S*) absolute configuration. Figure 4.5 shows the three stereoisomers that could be derived from the relative position of the two hydrogens on the carbon C(3) and C(10). However, we can discard structures **II** and **III** with C_2 symmetry axis, since a non-symmetric compound arises from the NMR spectra analysis. Bidimensional NMR studies were undertaken in order to confirm that the cycloadduct obtained corresponded to structure **I**.

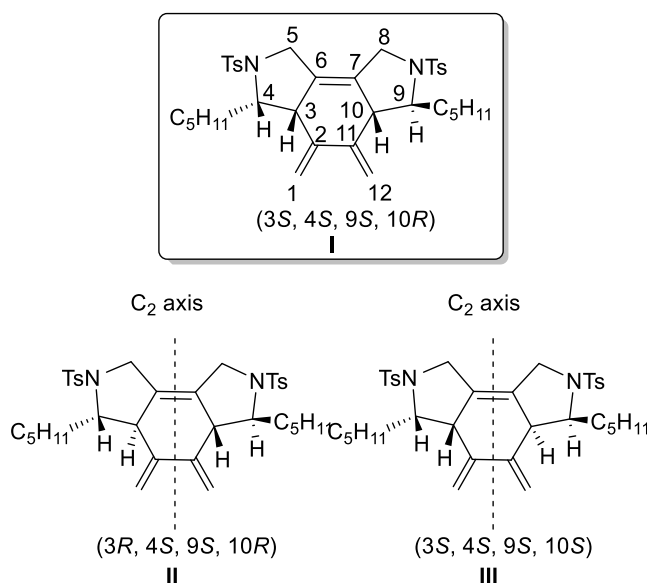


Figure 4.5. Three possible stereoisomers that could be formed upon cycloaddition of (*S,S*)-**10**.

NOESY correlations showed strong dipolar couplings between H(3) and H(4) and, together with the absence of NOE contact between H(3) and the protons on the pentyl chain on C(4) (blue arrows in Figure 4.6), indicated a *cis* relationship between H(3) and H(4). The presence in the NOESY spectrum of NOE cross-peaks between H(10) and the protons of the aliphatic groups in C(9), together with the lack of dipolar coupling between H(10) and H(9), revealed a *trans* relative configuration in the other half of the cycloadduct (green arrows in Figure 4.6). A NOE crosspeak observed between H(3) and H(10) confirmed their *cis* relationship excluding possible structures **II** and **III** (red arrow in Figure 4.6).

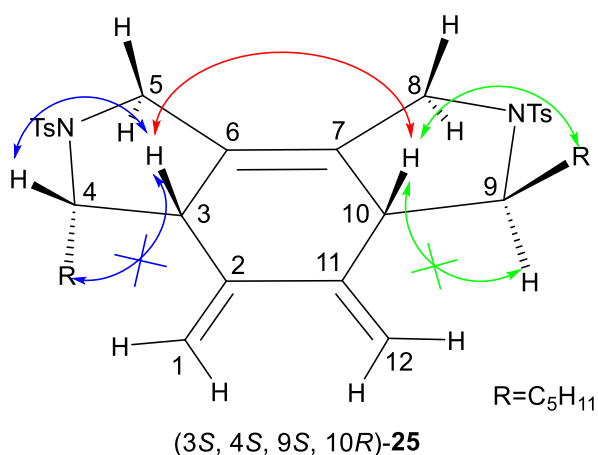
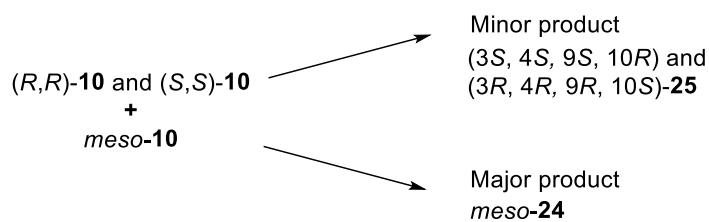


Figure 4.6. Main observed NOESY correlations in good agreement with the proposed structure of **25**.

We then turned our attention to the major diastereoisomer **24** formed in the cycloaddition of **10**, which we expected to be formed from the *meso* compound present in the mixture of substrate **10** (Scheme 4.11).



Scheme 4.11. Stereochemical correlations in the cycloaddition of **10**.

Taking into account that the structure of **24** must have a relative *syn* configuration at the C(4) and C(9) position, the number of possible stereoisomers was reduced to four (Figure 4.7). Structures **IV** and **V** are *meso* forms whereas structures **VI** and **VII** are a pair of enantiomers. Since the major product is symmetrical, the enantiomeric pair can be discarded. The main difference between structure **IV** and **V** is that protons H(3) and H(10) are in a *cis* relative configuration with protons H(4) and H(9), respectively (for structure **IV**, Figure 4.7), or in a *trans* relative configuration (for structure **V**, Figure 4.7).

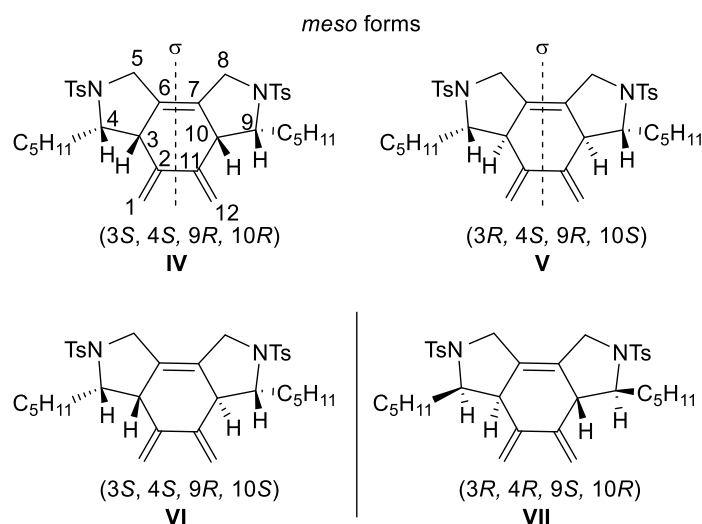


Figure 4.7. Possible stereoisomers of **24**.

After a complete chemical shift assignment of the signals, the dipolar couplings observed in the NOESY spectrum were analysed (Figure 4.8). The olefinic proton signals on C(1) show dipolar coupling with the proton H(3) (green arrow). The strong NOE cross-peak between H(3) and the protons on the pentyl chain in C(4) (blue arrow) fully confirm that the configuration of cycloadduct **24** matches with structure **V**.

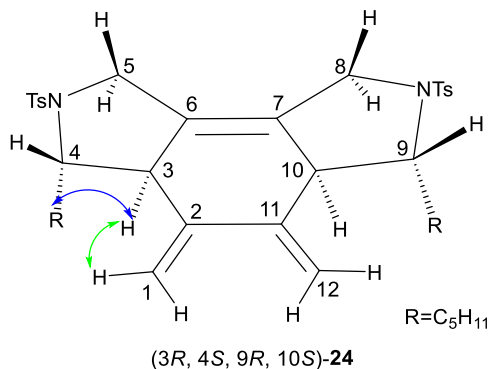
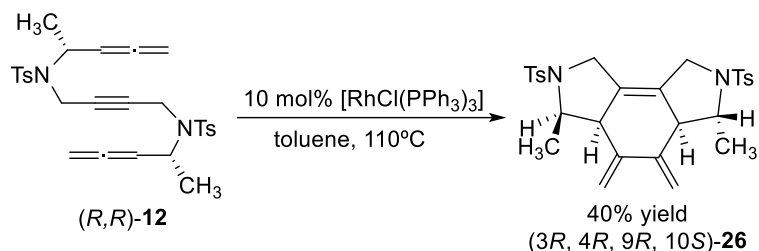


Figure 4.8. Main observed NOESY correlations of cycloadduct **24** supporting the proposed structure.

We then wanted to evaluate the effect on the length of the chain. Bisallene (*R,R*)-**12** underwent [2+2+2] cycloaddition reaction giving the diastereomerically pure (3*R*, 4*R*, 9*R*, 10*S*)-**26** cycloadduct in a 40% yield (Scheme 4.12), demonstrating that the length of the alkyl chain in the substrate has no influence on the diastereoselectivity of the reaction.



Scheme 4.12. Wilkinson-catalysed [2+2+2] cycloaddition reaction of allene-yne-allene (*R,R*)-**12**.

After a complete chemical shift assignment of the signals (Figure 4.9a), the dipolar couplings observed in the NOESY spectrum were analysed (Figure 4.9b).

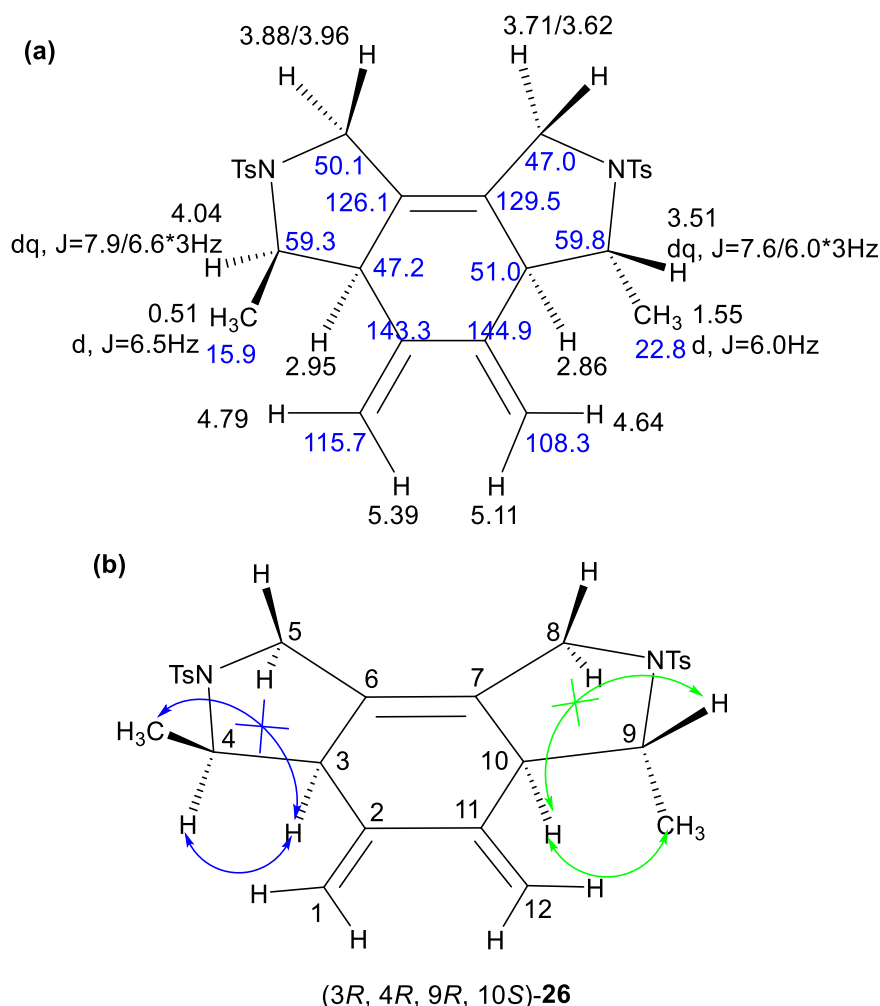


Figure 4.9. a) ¹H-NMR chemical shifts (black) and ¹³C-NMR chemical shifts (blue) of (3*R*, 4*R*, 9*R*, 10*S*)-**26**.
b) Main observed NOESY correlations of cycloadduct **26** supporting the proposed structure.

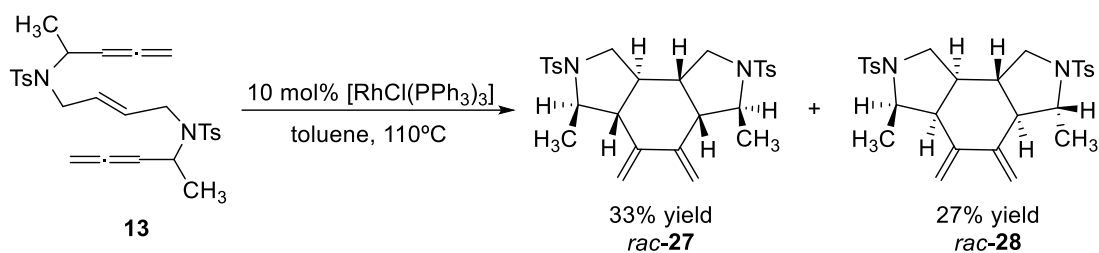
The dipolar coupling between the proton H(3) with H(4), together with the absence of NOE signal between H(3) and the methyl on C(4) indicate a *cis* H(3)-H(4) configuration (blue arrows). A NOE

cross-peak between H(10) and the methyl on C(9) indicate their *cis* relationship, which is further confirmed by the absence of dipolar coupling between H(10) and H(9) (green arrow).

It should be taken into account that the inversion of the configuration of the inducing stereocentres on the bisallene results in the inversion of the configuration of the stereocentres generated upon cycloaddition to give access to both enantiomers of the tricyclic scaffolds with total stereoselectivity.

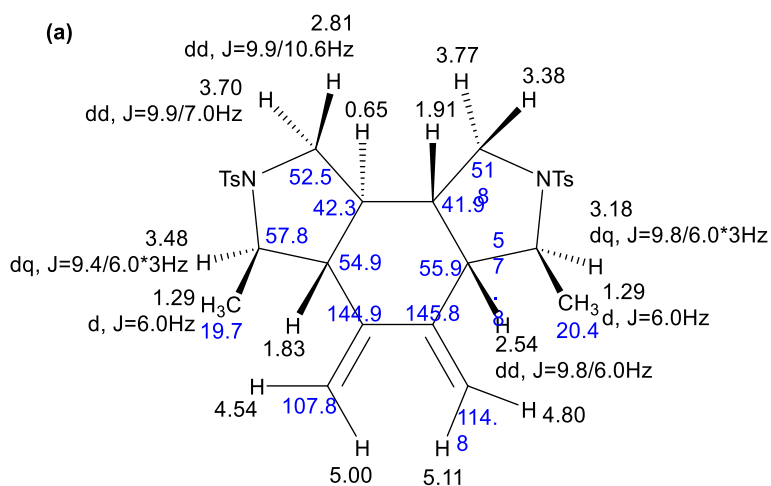
4.2.3. [2+2+2] Cycloaddition of allene-ene-allene substrates

As the next step we studied more challenging substrates. We have demonstrated that a chiral centre in the α -position of the allene moiety induces chirality in stereogenic centres C(3) and C(10). Now we aimed to introduce an *E* double bond in the bisallene in order to generate two more stereogenic centres in the cycloaddition and explore the chiral induction in these two more distant chiral centres. The cycloaddition of allene-ene-allene substrate **13** was evaluated following the same methodology as for cases **10** and **12**. The cycloaddition of **13** (derived from racemic propargylic alcohols containing a mixture of a pair of enantiomers and a *meso* form, see Figure 4.2) was first investigated and the reaction yielded two diastereomeric products, which could be separated by column chromatography, giving a 33% yield of the major isomer and a 27% yield of the minor one (Scheme 4.13).



Scheme 4.13. [RhCl(PPh₃)₃]-catalysed [2+2+2] cycloaddition reaction of **13**.

From the complete set of 1D and 2D NMR spectra recorded both for compounds **27** and **28**, it was concluded that the products formed did not have symmetry as four signals on the 4-6 ppm region of the spectra, where the exomethylene protons appear, were observed. In Figure 4.10 the complete chemical shift assignment as well as the key NOESY contacts observed for **27** are shown.



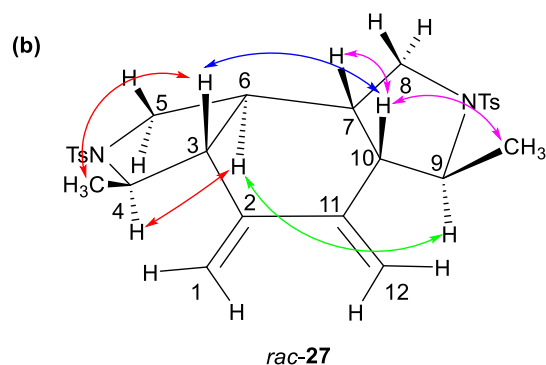


Figure 4.10. a) ^1H -NMR chemical shifts (black) and ^{13}C -NMR chemical shifts (blue) of *rac-27*. b) Main NOESY correlations observed for *rac-27*.

NOE crosspeaks were observed between H(3) and the methyl on C(4), indicating a *cis* relationship, together with dipolar coupling between H(4) and H(6), indicating a *trans* ring fusion (red arrows). A crosspeak between H(3) and H(10) indicates their *cis* relative configuration (blue arrow). Dipolar coupling between H(10) and H(7) and the methyl on C(9) reveal a *cis* ring fusion and a *cis* relationship with the methyl (pink arrows). A crosspeak between H(9) and H(6) indicates their *cis* disposition (green arrow).

In Figure 4.11 the complete chemical shift assignment as well as the key NOESY contacts observed for **28** are shown.

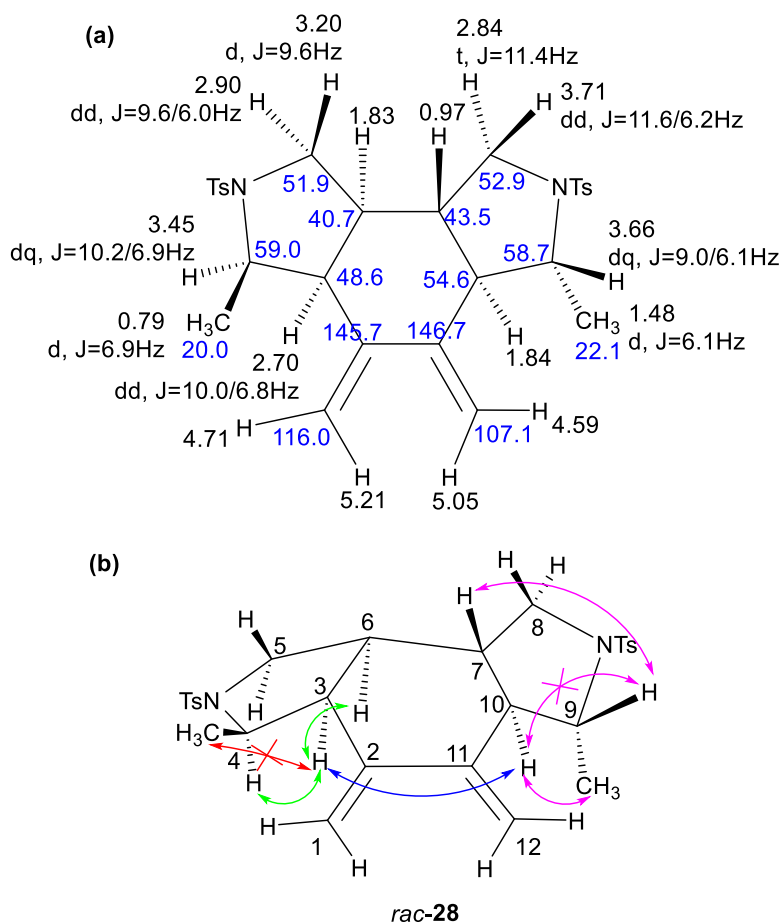


Figure 4.11. a) ^1H -NMR chemical shifts (black) and ^{13}C -NMR chemical shifts (blue) of *rac-28*. b) Main NOESY correlations observed for *rac-28*.

Strong NOE crosspeaks were observed between H(3) and both H(4) and H(6) protons (green arrows), which, together with the absence of NOE between H(3) and the CH₃ on C(4) (red arrow), confirmed the *cis* ring fusion and the *cis* configuration of H(4) with the two protons on the ring junction. An intense dipolar coupling was also observed between protons H(9) and H(7) which, together with the absence of NOE contact between H(10) and H(9), clearly indicate their *trans* configuration. Moreover, dipolar coupling between H(10) and the CH₃ on C(9) confirmed their *cis* disposition (pink arrows). On the other hand, the H(3) proton shows strong NOE with H(10), indicating their relative *cis* relationship (blue arrow). As can be observed, the stereochemistry of the original double bond is maintained since the two protons were found to be in a relative *trans* position in the final cycloadducts.

HPLC analysis of **27** showed two peaks at retention times of 14.8 and 16.6 minutes belonging to its pair of enantiomers (Figure 4.12).

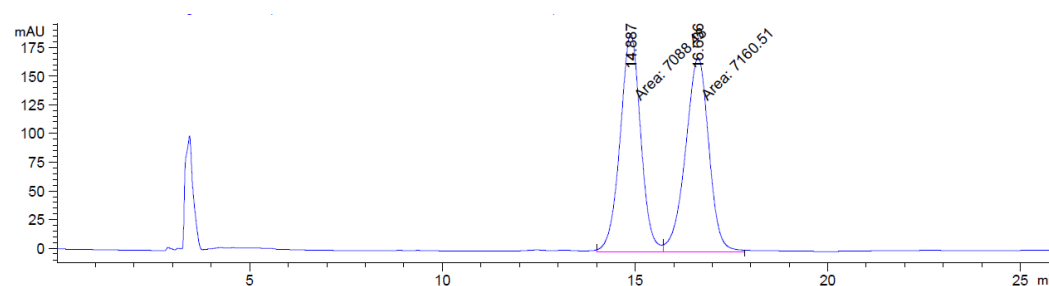


Figure 4.12. HPLC chromatogram of *rac*-**27**.

In the case of isomer **28**, two peaks also appeared, corresponding to the enantiomeric pair, at 18.4 and 32.7 minutes (Figure 4.13).

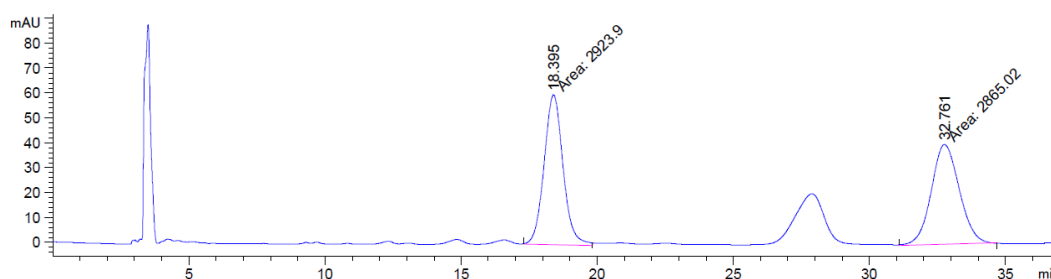
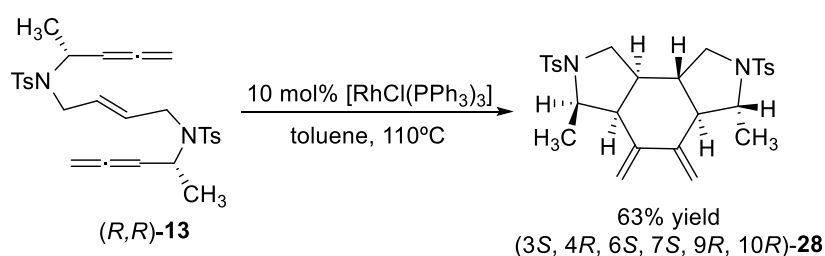


Figure 4.13. HPLC chromatogram of *rac*-**28**.

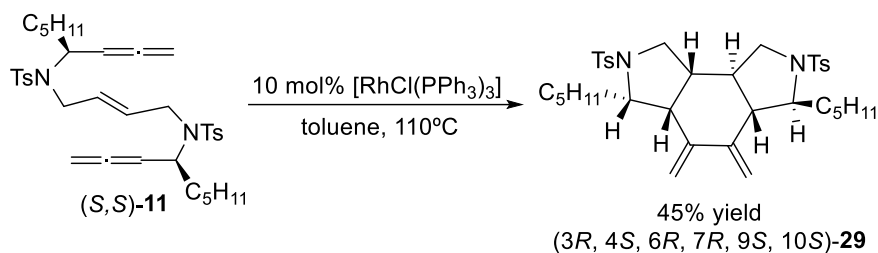
The [2+2+2] cycloaddition of the enantiopure (*R,R*)-**13** bisallene was then analysed (Scheme 4.14).



Scheme 4.14. Wilkinson-catalysed [2+2+2] cycloaddition reaction of allene-ene-allene (*R,R*)-**13**.

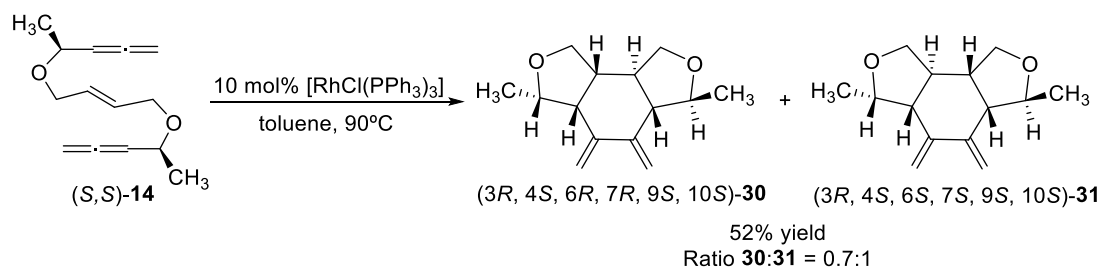
A careful analysis of the 1D and 2D NMR spectroscopic data revealed that the cycloadduct formed was isomer **28**. HPLC analysis of the product showed a single peak, at a retention time of 32.7 minutes, confirming that the cycloadduct obtained is one of the stereoisomers of *rac*-**28**.

At the same time the [2+2+2] cycloaddition of bisallene (*S,S*)-**11** was evaluated (Scheme 4.15). Cycloadduct (*3R, 4S, 6R, 7R, 9S, 10S*)-**29** was obtained in a 45% yield and the same structural characterization as for cycloadduct **28** was performed. As expected, the configuration of **29** was found to be the reverse of that of **28**.



Scheme 4.15. Wilkinson-catalysed [2+2+2] cycloaddition reaction of allene-ene-allene (*S,S*)-**11**.

Finally, we turned our attention to the influence of the tether on the process. Taking the oxygen-tethered compound (*S,S*)-**14** and treating it with [RhCl(PPh₃)₃] in toluene at 90°C, a 52% yield of an inseparable mixture consisting mainly of two cycloadducts, **30** and **31**, was obtained (Scheme 4.16).



Scheme 4.16. Wilkinson-catalysed [2+2+2] cycloaddition reaction of the oxygen-tethered allene-ene-allene (*S,S*)-**14**.

In order to determine the relative configuration of the stereocentres, the following points need to be taken into account. As the [2+2+2] cycloaddition is stereospecific with respect to the *trans* alkene and two of the stereogenic centres are transferred from the substrate, maintaining the (*S*) absolute configuration, only six stereoisomers can be formed upon the cycloaddition of (*S,S*)-**14** (Figure 4.14). Stereoisomers **VIII** and **IX**, which have the two *cis* 5,6-ring fusions, and stereoisomers **X** and **XI**, which have two *trans* 5,6-ring fusions, should be discarded as they bear a C₂ axis of symmetry and, as seen in Figure 4.15, the cycloadducts obtained are non-symmetrical. The two remaining stereoisomers, **XII** and **XIII**, both have a *cis* and a *trans* 5,6-ring fusion that could match the configuration of the products.

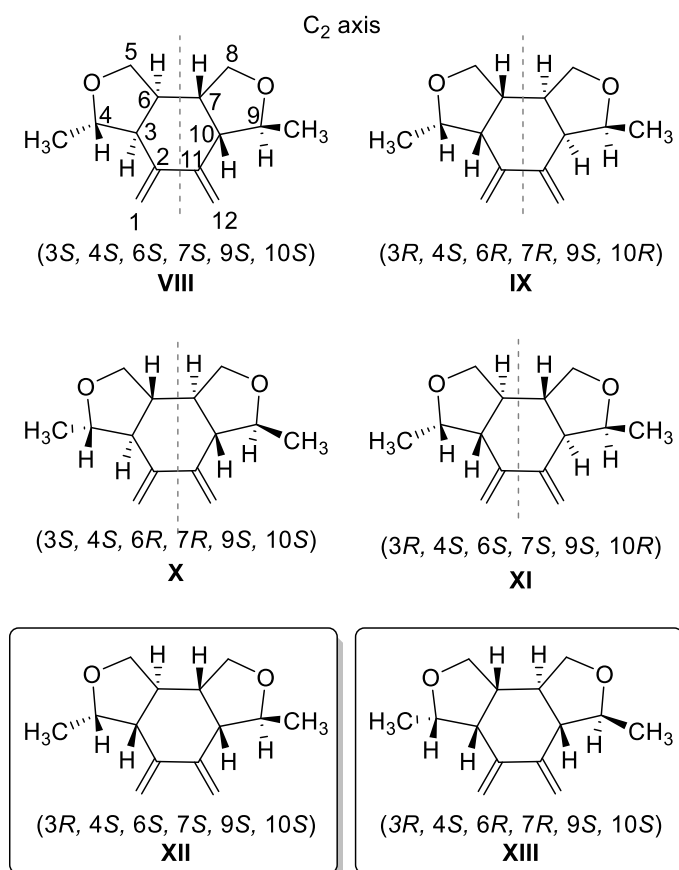


Figure 4.14. Six possible stereoisomers that could be formed upon cycloaddition of (*S,S*)-**14**.

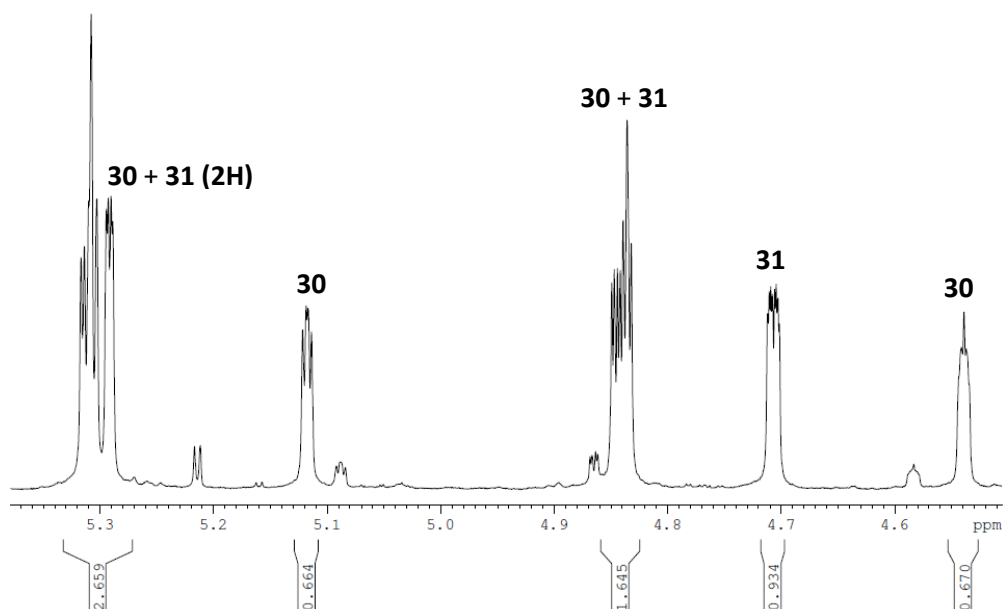


Figure 4.15. $^1\text{H-NMR}$ spectrum of the olefinic part of the cycloadduct mixture from (*S,S*)-**14**.

After careful NMR analysis, we were able to determine that out of the six possible stereoisomers that were likely to have been formed, two asymmetric structures featuring a *trans/cis* ring fusion were mainly obtained (**XIII** for **30** and **XII** for **31**). Moreover, a complete chemical shift assignment for both isomers was also possible (Figure 4.16).

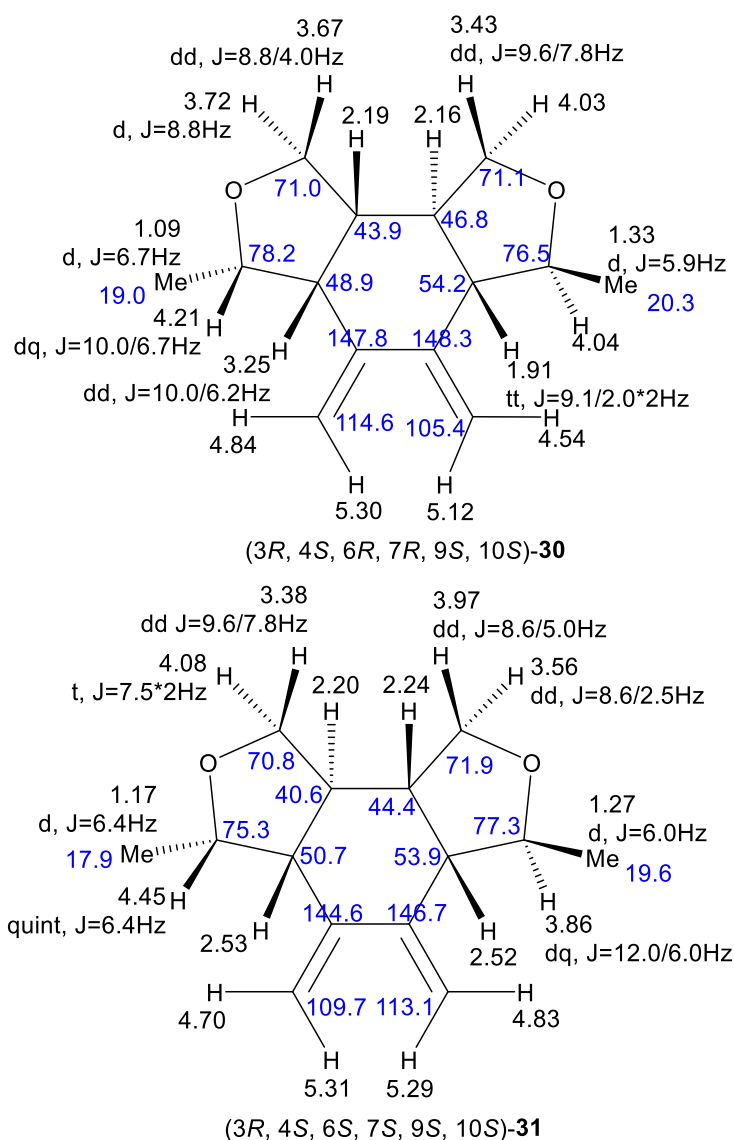
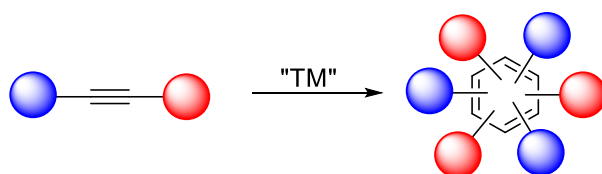


Figure 4.16. ^1H -NMR chemical shifts (black) and ^{13}C -NMR chemical shifts (blue) of (3R, 4S, 6R, 7R, 9S, 10S)-**30** and (3R, 4S, 6S, 7S, 9S, 10S)-**31**.

Apart from the two asymmetric diastereoisomers **30** and **31**, two symmetric diastereoisomers, which could not be completely characterized, were observed in the NMR spectra with a 0.7(**30**) : 1(**31**) : 0.1 : 0.1 ratio. Therefore the tether has a strong influence on the overall stereoselectivity of the process.

Overall, the Wilkinson's complex catalysed the [2+2+2] cycloaddition reaction of allene-yne/ene-allene substrates bearing chiral centres in the α -position of the allene functionality. The enantiomerically pure *N*-tosyl linked bisallenes gave a completely diastereoselective reaction and the product was isolated as a single optically pure enantiomer. When an oxygen-linked substrate was reacted, two diastereoisomers were formed. The built-in chirality present in the allene-yne/ene-allene starting substrates was preserved and used to generate two or four more chiral centres employing the [2+2+2] cycloaddition reaction.

Chapter 5. [2+2+2] Cycloaddition reaction for the synthesis of non-symmetric dendrimers



5.1 Precedents

5.1.1. Dendrimers

Macromolecules can be classified into four major groups: linear, crosslinked, branched and dendritic. The first three groups are traditional synthetic polymers which, as they are polydisperse, do not have uniform structures and molecular weights. On the other hand, dendrimers are nanosized macromolecules that have perfect monodispersity and regular highly-branched structure. The uniform molecular weight and more precise structures of dendrimers compared to classic polymers arise due to the step-by-step, ordered, iterative reaction sequences employed during their synthesis. Their properties can be tuned by designing a controlled synthetic procedure that precisely locates in the structure groups with specific functions; this allows dendrimers to have applications in fields such as chemistry, medicine, biology or materials science.⁸⁹

Dendrimers⁹⁰ consist of three main parts: a multifunctional core (C), branching units (B) and surface groups (S, also called peripheral groups) (Figure 5.1). The number of functional groups on the core determines the multiplicity of the dendrimer. Branching units are multifunctional components which allow the growth of the dendrimer. These units form the regular branched structure of the dendrimer, giving the dendritic shape. The number of branching points from the core towards the dendrimer surface is referred to as the generation number. All dendritic architectures end up with many surface groups. In the three dimensional structure, surface groups form the outer surface of the globular dendritic architecture. As inner layers and the core are highly sterically-hindered, the chemical activity of dendrimers mostly depends on peripheral groups.

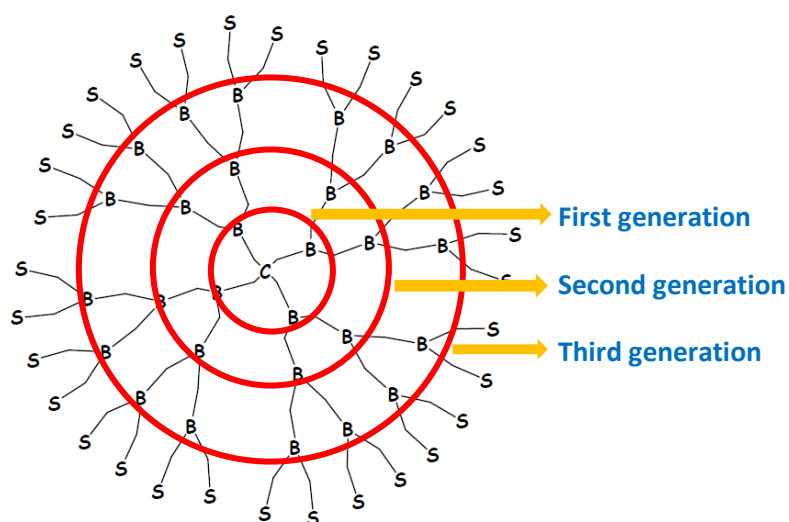


Figure 5.1. Schematic representation of a dendrimer. C: core, B: branching units, S: surface groups.

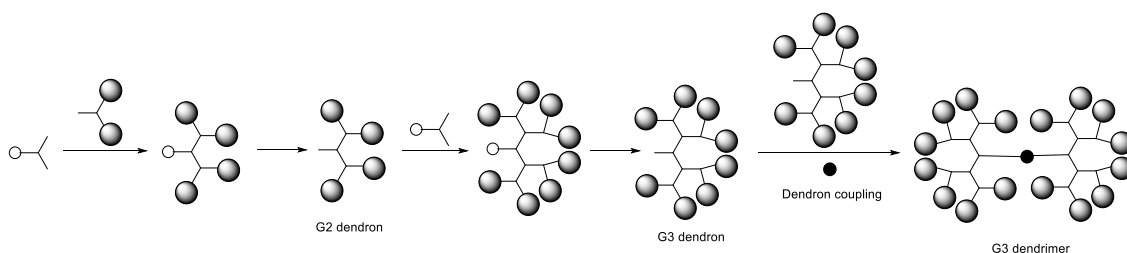
These molecules were first described in 1978 by Vögtle et al.⁹¹ and referred to as “cascade” molecules. In 1981, Denkewalter et al.⁹² claimed the synthesis of macromolecular compounds were composed of at least four successive layers of lysine units, which later were referred to as polylysine dendrimers. In 1985, Newkome et al.⁹³ proposed the synthesis of the same type of molecules, which they called “arborols”, and, in the same year, Tomalia et al.⁹⁴ finally introduced the name of “dendrimers” (from the Greek “dendros”, meaning “tree”, and “meros”, meaning

“part”). Tomalia et al. synthesised, the now widely used Starburst polymers also called polyamidoamine (PAMAM) dendrimers. In 1990, a new type of dendrimer based on polyether was introduced by Fréchet et al.⁹⁵ In 1993, Mülhaupt et al.⁹⁶ and Meijer et al.⁹⁷ simultaneously continued the work initiated by Vögtle, describing the preparation of diaminobutane (DAB) dendrimers. Research into dendrimers has grown enormously since this date, leading to the preparation of new dendrimers, specially using heteroatoms such as silicon⁹⁸ or phosphorus⁹⁹. In 1994, Majoral, Caminade et al.¹⁰⁰ were the first to achieve the synthesis of a neutral phosphorus-containing dendrimer.

5.1.1.1. Synthetic strategies

Dendrimer synthesis is accomplished by following either a convergent or divergent construction approach.

In the convergent synthesis, introduced by Fréchet et al.⁹⁵ in 1990, the synthesis starts with the construction of the dendritic branches, called dendrons, from the surface to the focal point. These dendrons are then attached to the core to obtain a dendrimer of a generation equivalent to that of the dendrons (Scheme 5.1).



Scheme 5.1. Simplified model of the convergent synthesis.

This strategy has the advantage of diminishing the possibility of defects in the dendrimer growth due to incomplete reactions on the surface, as the number of reactions run in each step is small and they are carried out at the focal point. This strategy also avoids the use of a high excess of monomer, easing the purification of the dendrimers. On the other hand, the yield of the reactions is usually low when high generation dendrimers are synthesized, due to the steric hindrance on the focal points that are to be attached to the core. Finally, it is worth noting that with this method it is possible to create asymmetric dendritic structures by attaching two or more different dendrons to the core.

The most characteristic dendrimers synthesized with the convergent methodology are Fréchet's poly(arylether)s¹⁰¹ (Figure 5.2) and Moore's poly(phenylacetylene)s¹⁰² (Figure 5.3).

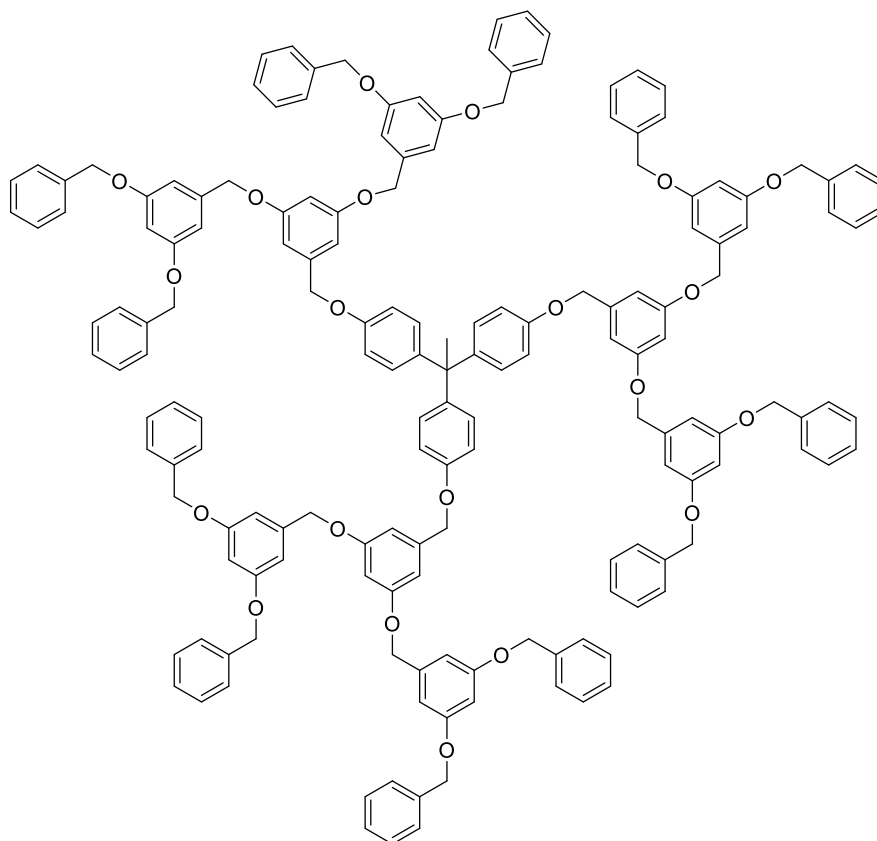


Figure 5.2. Fréchet's poly(aryl ether) dendrimer.

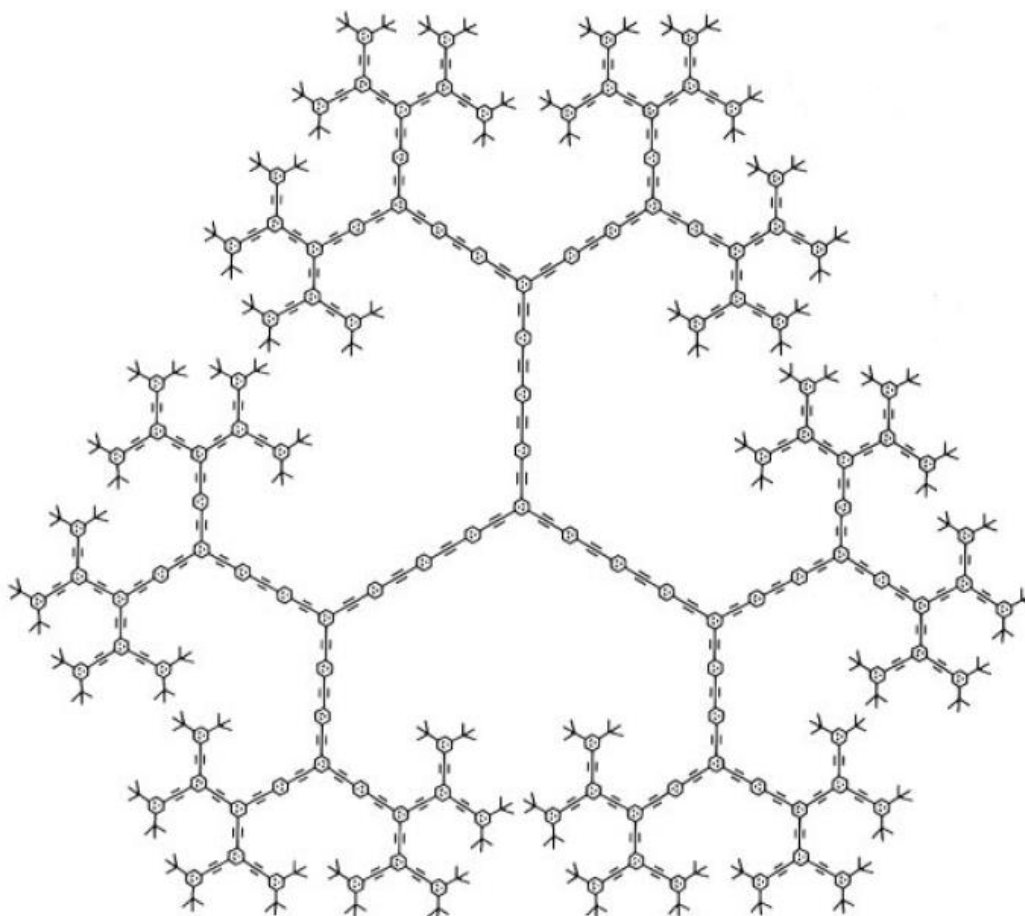
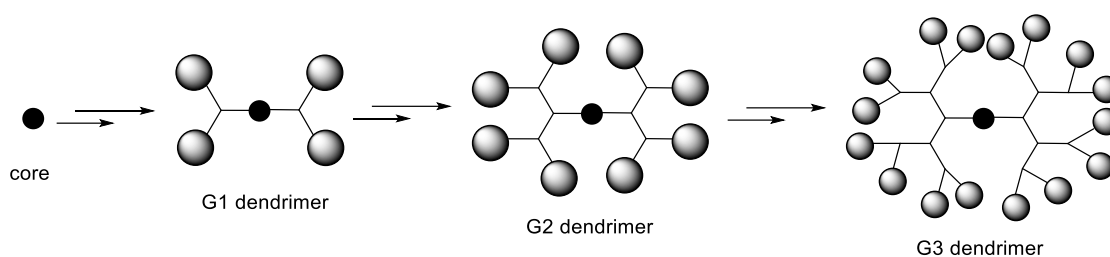


Figure 5.3. Moore's poly(phenylacetylene) dendrimer.

The divergent synthesis, introduced by Tomalia et al.⁹⁴, is based on the growth of the dendrimer from the core to the periphery by an iterative sequence of reactions on the surface of the dendrimer (Scheme 5.2).



Scheme 5.2. Divergent synthesis strategy.

The repetition of these steps allows the simultaneous growth of all the dendritic branches, thus quickly increasing its size. The growth of the dendrimer is limited by the steric hindrance present at the surface level at high generations. This method is the most widely used.

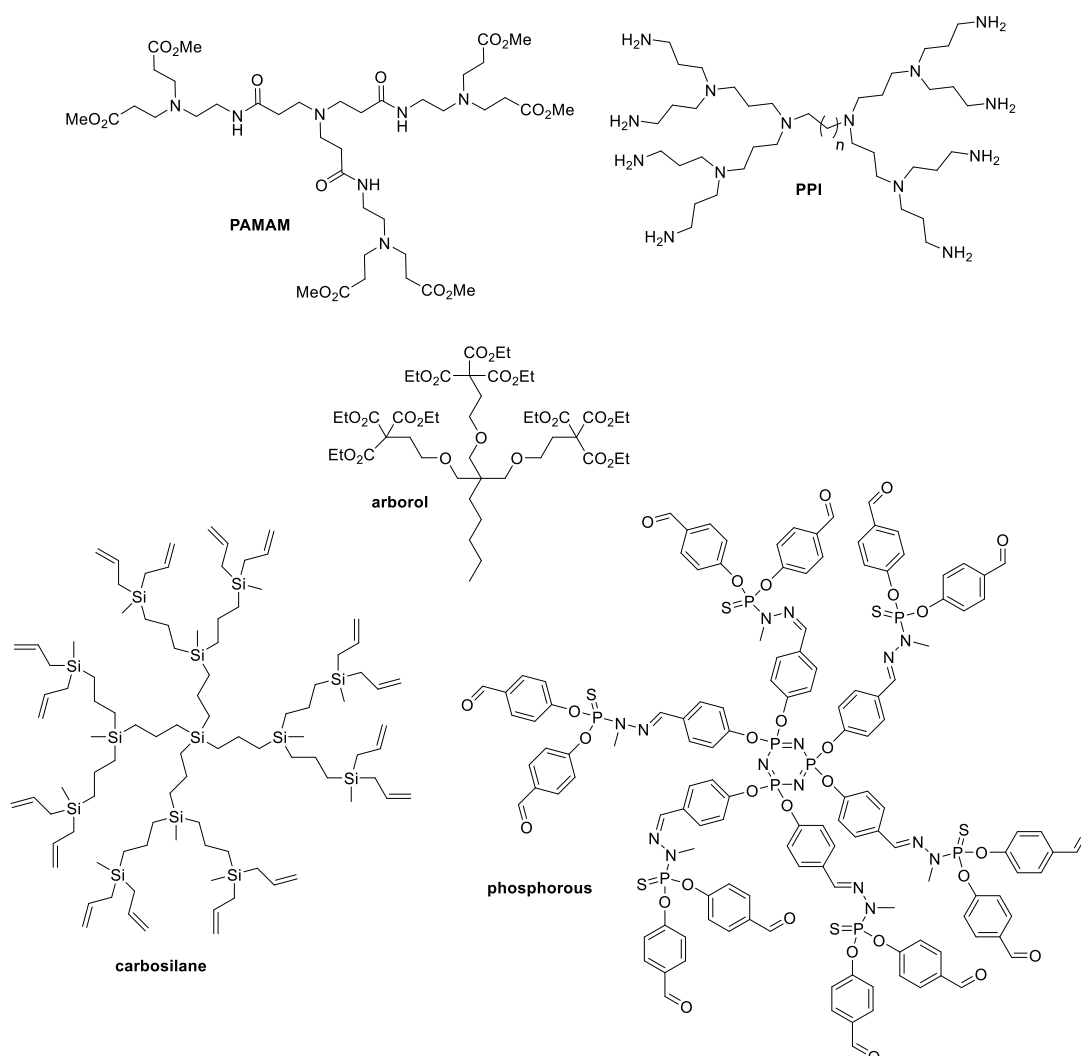
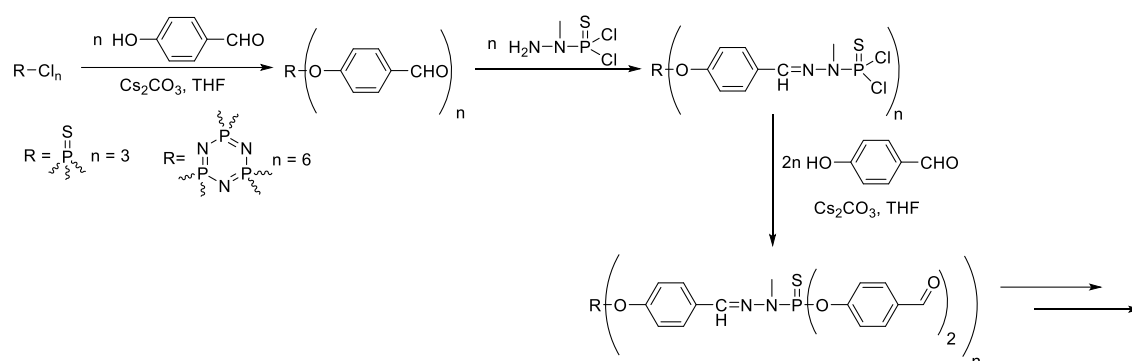


Figure 5.4. Dendrimers synthesized with the divergent method.

The main dendrimers synthesized using this methodology are Tomalia's PAMAMs¹⁰³ (poly(amidoamine)), Meijer's PPIs⁹⁷ (poly(propyleneimine)), Newkome's arborols⁹³, Rebrov's

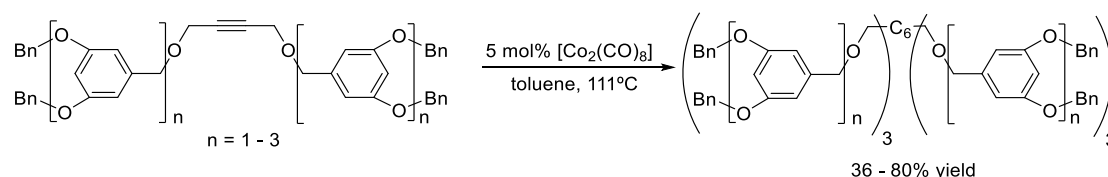
carbosilanes¹⁰⁴, and Majoral's and Caminade's phosphorus-containing dendrimers¹⁰⁵ (Figure 5.4).

As the work that will be presented here arises from a collaboration with Dr. Caminade's group, a few features of the phosphorus-containing dendrimers developed in this group will be explained. The particularity of their dendrimers resides in the phosphorus atom at each branching point that allows a perfect control of the structure by $^{31}\text{P}\{^1\text{H}\}$ -NMR. The phosphorus-containing dendrimers are built by the repetition of two steps: the nucleophilic substitution of the chlorine atom by 4-hydroxybenzaldehyde in basic media, and the condensation of aldehydes with the *N*-methyl dichlorophosphothiohydrazide $\text{H}_2\text{N}-\text{N}(\text{Me})-\text{P}(\text{S})\text{Cl}_2$, which regenerates the $\text{P}(\text{S})\text{Cl}_2$ functions suitable to perform the substitution with phenols again (Scheme 5.3).¹⁰⁶ $^{31}\text{P}\{^1\text{H}\}$ -NMR is a very powerful tool to monitor the nucleophilic substitution step on the dendrimer synthesis. The monosubstitution of one chloride atom induces a deshielding of the signal from *ca.* 63 ppm to *ca.* 69 ppm. The second substitution reaction induces a shielding at *ca.* 61 ppm. Thus, any incomplete substitution is easily detectable by such a method. In their earlier works, the central core consisted of $\text{P}(\text{S})\text{Cl}_3$ (thiophosphoryl trichloride)¹⁰⁰ but it was later replaced by $\text{N}_3\text{P}_3\text{Cl}_6$ (hexachlorocyclotriphosphazene),¹⁰⁷ which allows the number of branches to increase more rapidly.



Scheme 5.3. Synthetic strategy followed by Caminade, Majoral et al.

Besides the previously explained methodologies, our interest in transition-metal catalysed [2+2+2] cycloadditions prompted us to investigate whether this reaction had been used in the construction of dendrimers. We could find only two examples of this particular case. The first was a benzylic ether dendrimer with a benzene core that was synthesised from its acetylenic precursor in 1999 by Fréchet et al.¹⁰⁸ The cycloaddition reaction was carried out in refluxing toluene using dicobalt octacarbonyl as the catalyst (Scheme 5.4).



Scheme 5.4. Poly(aryl ether) dendrimer synthesized by a Co(I)-catalysed [2+2+2] cycloaddition reaction.

As expected, the time required to complete the cycloaddition reaction increased with the generation (from 30 minutes to 48 hours), while the yield decreased because of steric crowding

around the nascent core. Due to the nature of the transformation, the reaction is extremely clean, and no partially reacted products can be formed. Therefore, aside from recovered starting materials, cycloaddition compounds were the only products isolated after reaction, thus facilitating the purification.

The other example found in the literature is by Nierengarten et al.¹⁰⁹ They described the synthesis of fullerodendrimers with hexaphenylbenzene cores and peripheral C₆₀ units (Figure 5.5) by metal-catalysed cycloaddition of the corresponding dendritic bis(aryl)alkyne.

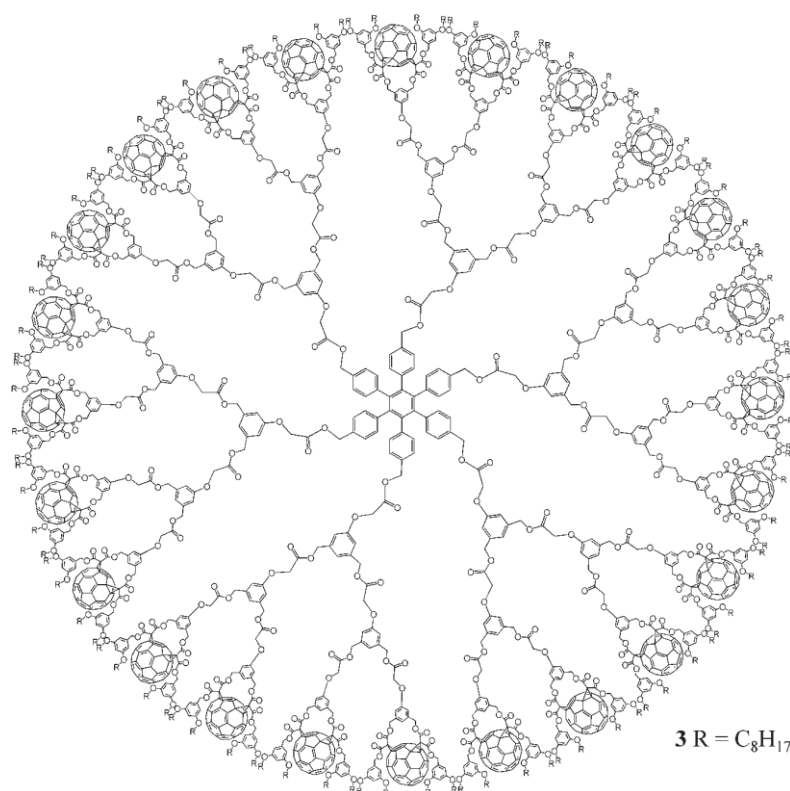


Figure 5.5. Third generation fullerodendrimer.

Treatment of the alkyne precursor with a catalytic amount of [Co₂(CO)₈] in dioxane at room temperature for one day (in the case of the first and second generation dendrimers) or five days (for the third generation one), led to the desired fullerodendrimers in 93%, 62% and 24% yields for the corresponding first, second and third generation.

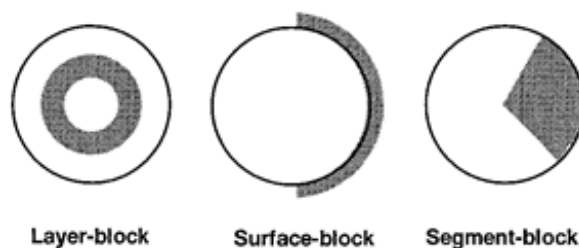


Figure 5.6. Graphic depiction of layer, surface and segment-block dendrimers.

Whereas traditional dendrimers are composed of self-repeating units, the synthesis of dendrimers containing two or more dendritic components, which break with the symmetry of the molecule, can also be achieved. Depending on the distribution of the different functionalities

in the dendrimer, three categories arise: layer-block, surface-block and segment-block dendrimers (Figure 5.6). Hawker and Fréchet¹¹⁰ were pioneers in synthesizing the first dendrimers with this kind of architecture.

5.1.1.2. Layer-block dendrimers

Layer-block dendrimers result from placing concentric layers of different functional groups around the central core moiety. Hawker and Fréchet¹¹¹ reported the first example of this kind of architecture in 1992 (Figure 5.7).

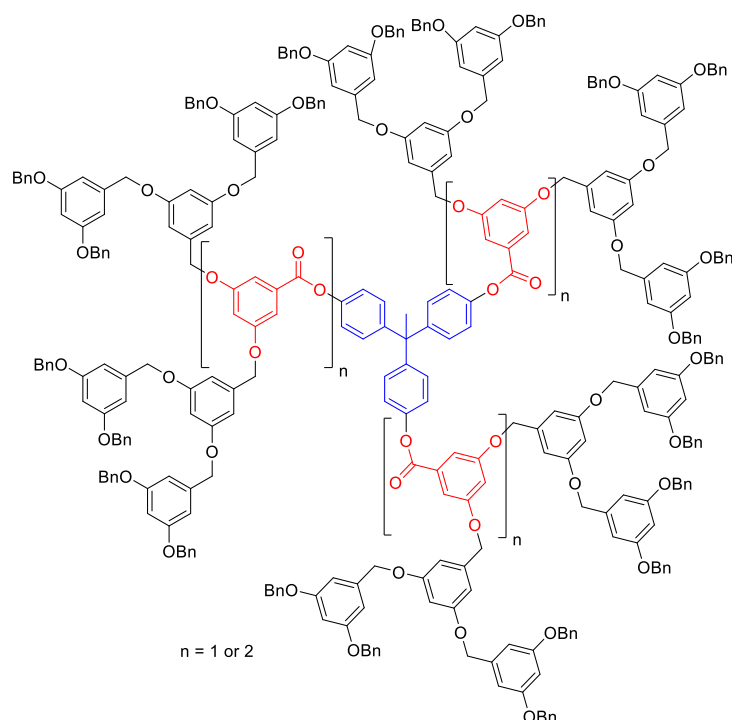


Figure 5.7. First layer-block dendrimer described. The core is represented in blue, aryl ester groups are in red, and aryl ether groups in black.

Two dendrimers containing either one or two layers of arylester functional groups followed by layers of aryether groups were synthesized.

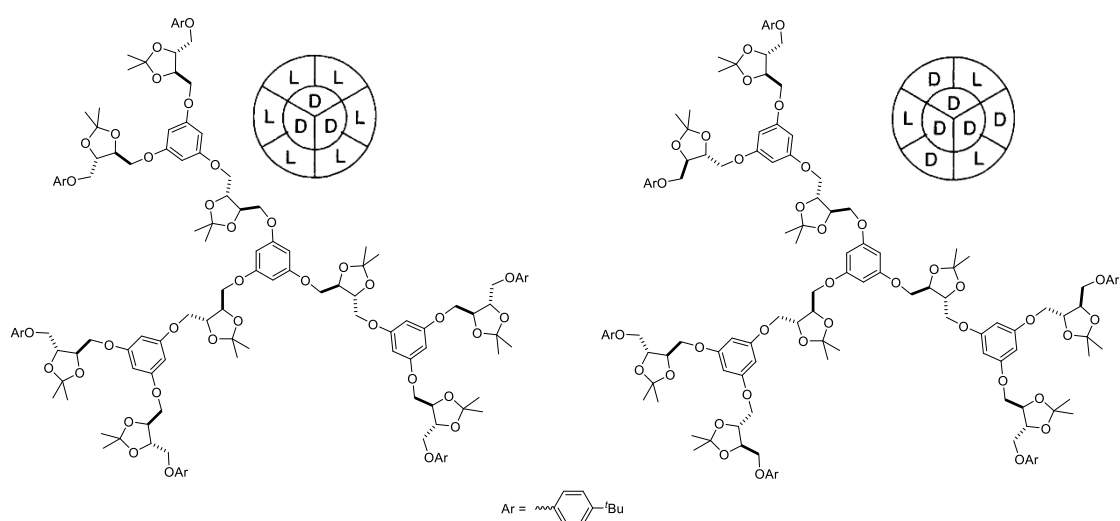
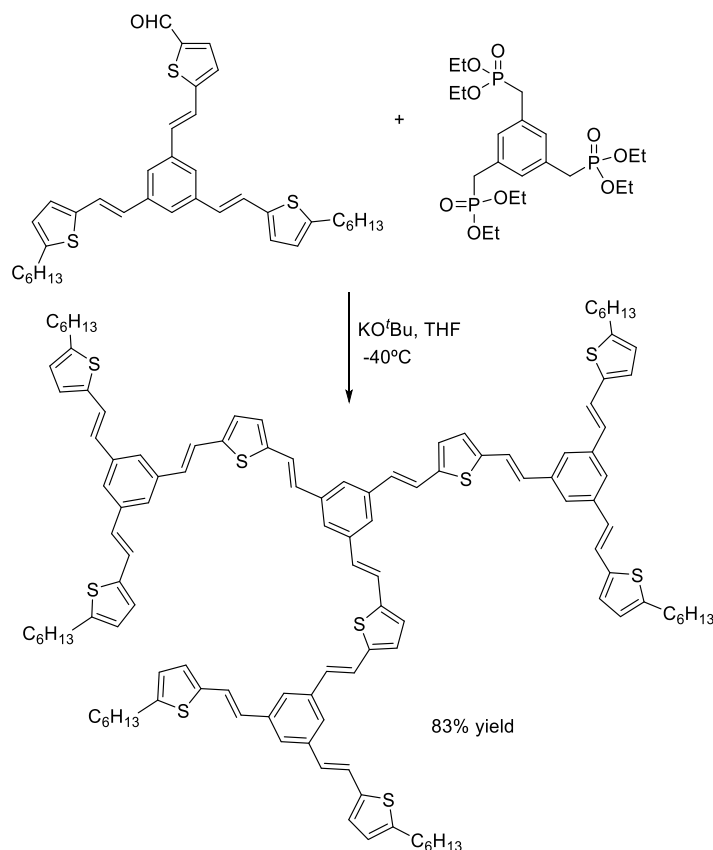


Figure 5.8. Layer-block dendrimer containing units derived from D- and L-tartaric acid.

Chow et al.¹¹² described the synthesis of two different chiral, layer-block dendrimers. The first-generation dendrimers contain units derived from D- and L-tartaric acid with a phloroglucinol core (Figure 5.8). The optical rotational properties of these compounds were studied. It was noted that the chiroptical effect of the L-tartrate chiral unit cancelled that of the D-tartrate unit on a one-to-one basis. As a consequence, the overall molar rotation of the dendritic fragment was proportional to the number of D- or L-tartrate units in excess.



Scheme 5.5. Synthesis of the first generation layer-block π -conjugated dendrimer with alternating thienylenevinylene and phenylenevinylene units by a HWE reaction.

In a more recent work Rodríguez-López et al.¹¹³ reported the synthesis of layer-block π -conjugated dendrimers with alternating thienylenevinylene and phenylenevinylene units. A convergent strategy was followed consisting of the synthesis of the dendrons followed by a Horner-Wadsworth-Emmons (HWE) reaction to attach them to the core (Scheme 5.5). Only the zero and first generation dendrimers could be synthesized as the HWE reaction did not work for the synthesis of the second generation dendrimer. The optical properties of the dendrimers were investigated by UV/Vis and fluorescence spectroscopy. The *meta* relative position between the substituents in the aryls through which the different units are linked prevents efficient delocalization throughout the conjugated backbone. As a result, the UV/Vis spectrum consisted of a superposition of the absorptions due to the different chromophores and all compounds showed absorption wavelengths in the UV or visible region.

5.1.1.3. Surface-block dendrimers

Surface-block dendrimers are characterised by having the same interior building blocks with areas of different functional groups at the surface of the molecules. Hawker and Fréchet's first

surface-block dendrimer¹¹⁴ was based on poly(benzyl ether) repeating units, which were capped with bromide atoms in one or two dendritic wedges (Figure 5.9).

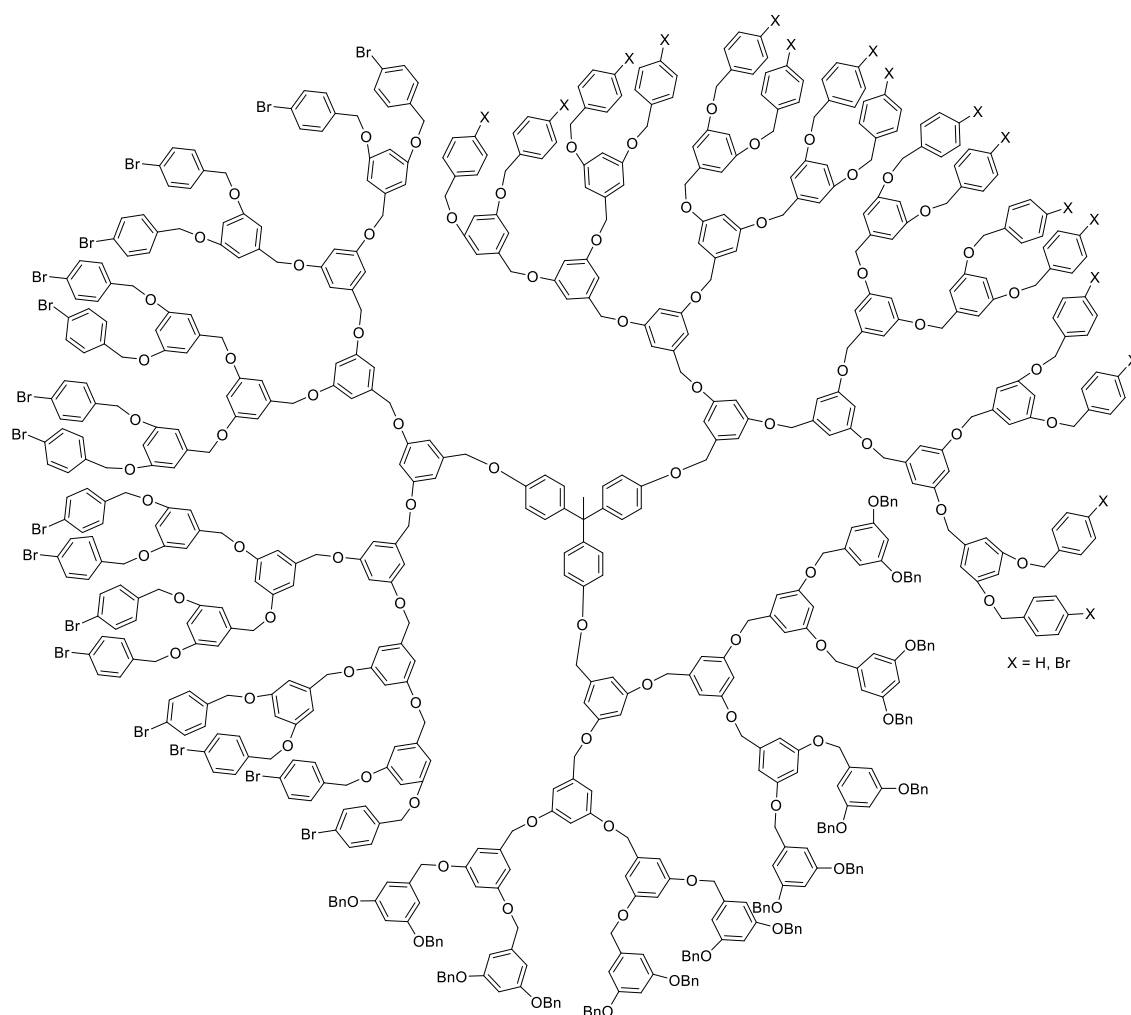


Figure 5.9. First surface-block dendrimer described.

In 2005 Grinstaff et al.¹¹⁵ described a series of amphiphilic surface-block dendrimers synthesized from the natural metabolites of glycerol, succinic acid, and myristic acid (Figure 5.10).

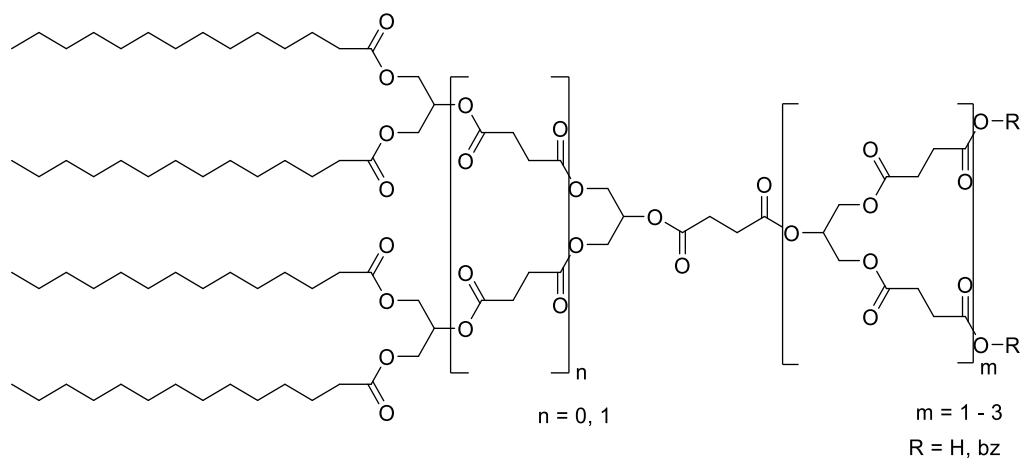
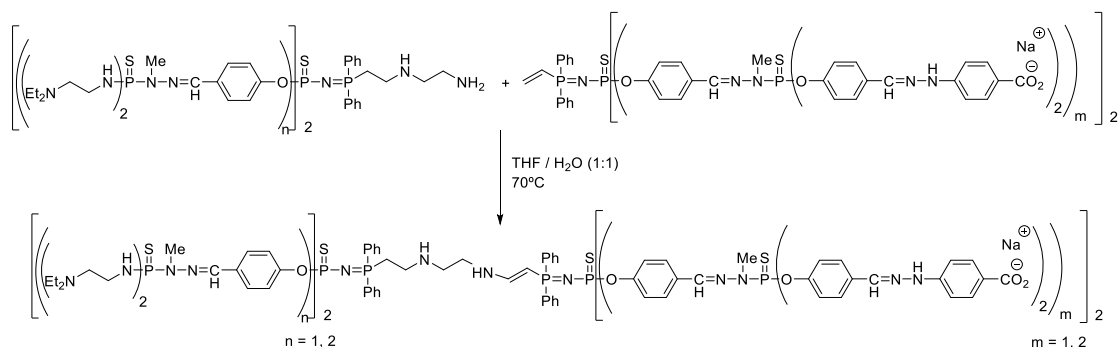


Figure 5.10. Amphiphilic surface-block dendrimer.

The surfaces of these dendrimers displayed different numbers of alkyl chains and carboxylic acids, varying the hydrophobic-to-hydrophilic ratio. In solution these dendritic amphiphiles form supramolecular aggregates. The ability to solubilize hydrophobic molecules was tested and it was seen that these dendrimers are able to entrap pyrene.

Knoll et al., in collaboration with Majoral and Caminade's group,¹¹⁶ described the synthesis of multi-charged phosphorus-containing surface-block dendrimers. Michael-type addition between dendrons bearing vinyl groups and amino groups at the core successfully achieved the desired dendrimers (Scheme 5.6).



Scheme 5.6. Multi-charged phosphorus-containing surface-block dendrimer.

5.1.1.4. Segment-block dendrimers

Segment-block dendrimers are characterised by a radial geometry in which dendritic segments of different functionality emanate from a polyfunctional core. Hawker and Fréchet's first segment-block dendrimer¹¹¹ was based on poly(benzyl ether) and poly(benzyl ester) repeating units (Figure 5.11). The synthesis was carried out using the convergent approach and the final dendrimer contained three pairs of hybrid ester-ether dendritic wedges.

Yamamoto et al.¹¹⁷ assembled a segment-block dendrimer based on the imine formation between two different divergently synthesized aromatic dendrons (Scheme 5.7). This segment-block dendrimer could be used for organic light-emitting diode (OLED) applications. They found that the highest HOMO value was obtained when the highest generations of the dendrons were coupled.

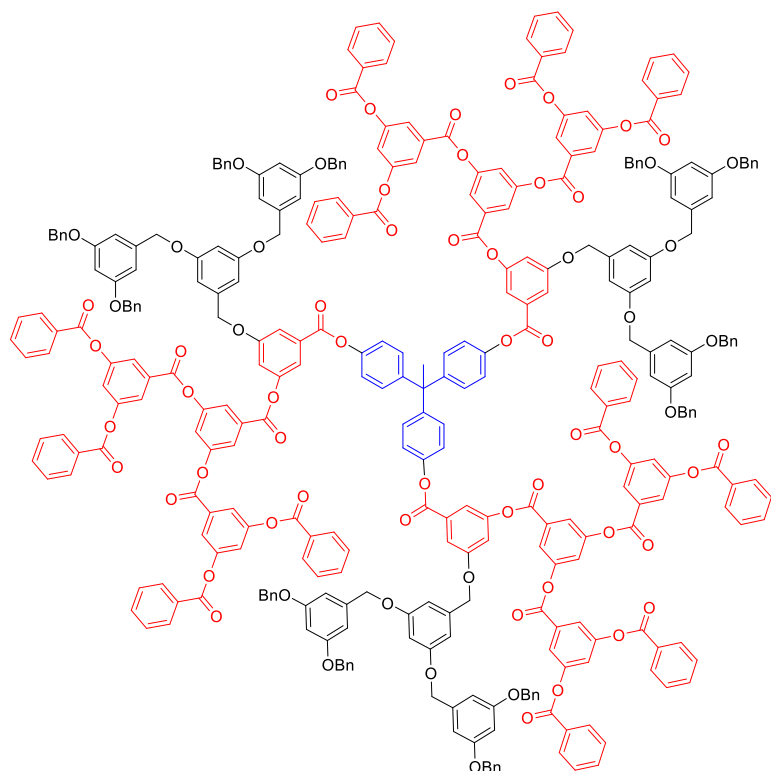
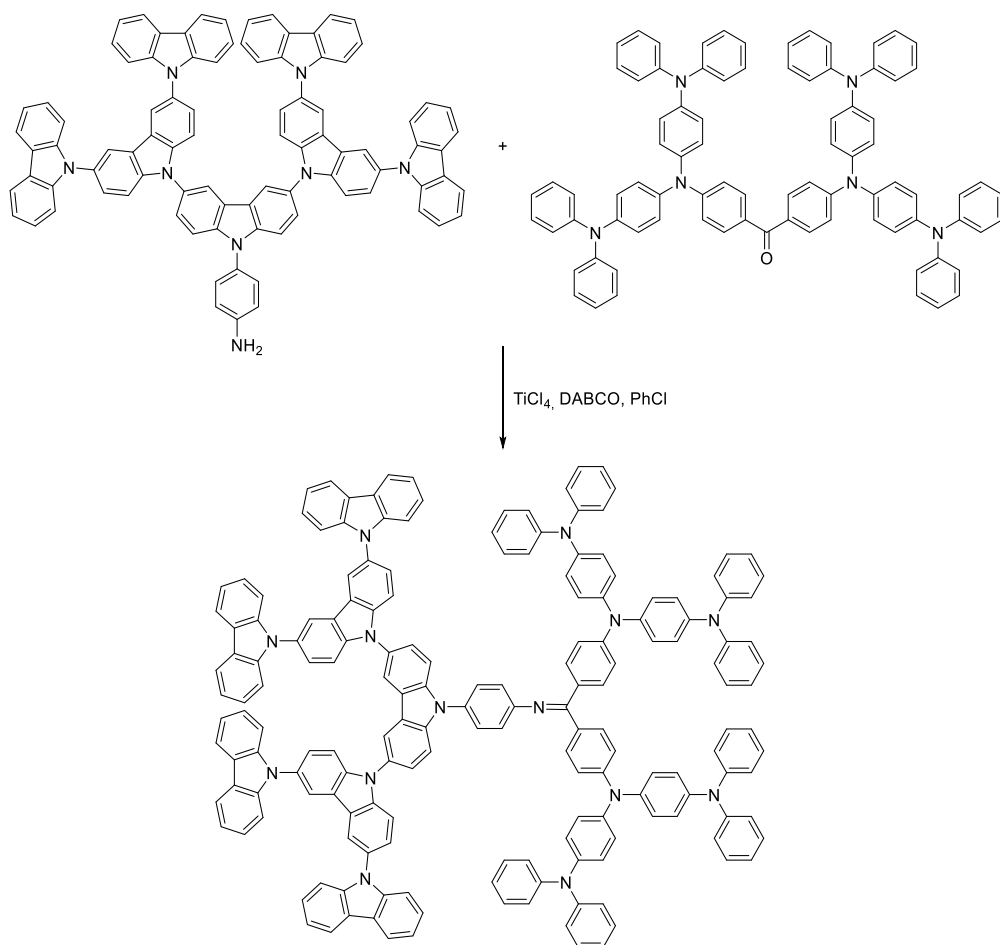
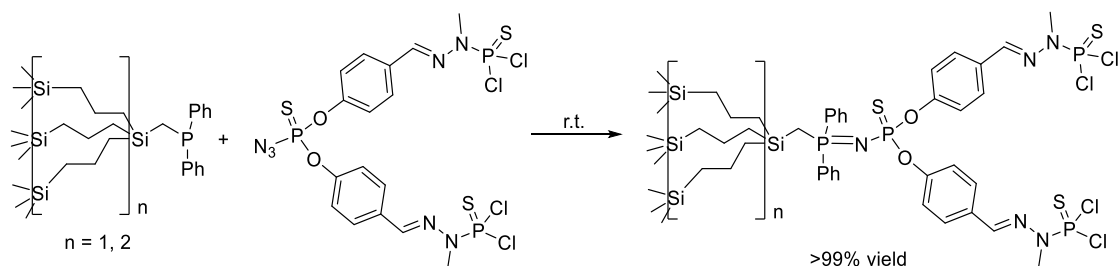


Figure 5.11. First segment-block dendrimer described. The core is represented in blue, arylester groups are in red and arylether groups in black.



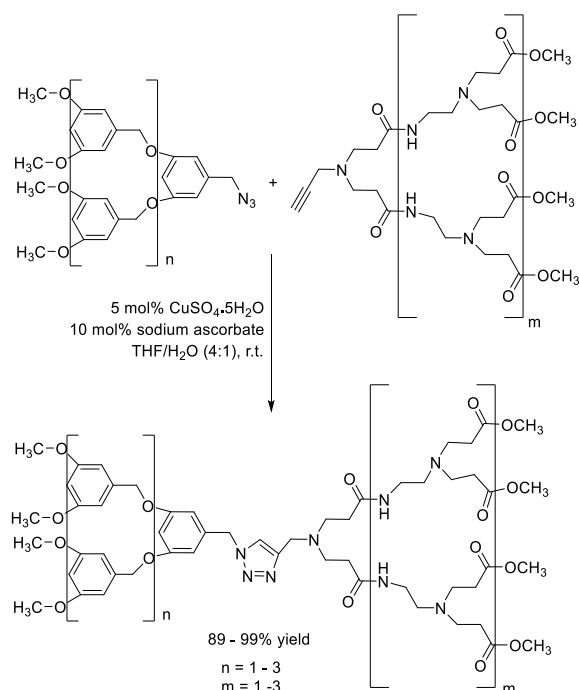
Scheme 5.7. Yamamoto's third generation segment-block dendrimer.

Caminade et al.¹¹⁸ used the Staudinger “click” reaction to synthesize a dendrimer that contained a carbosilane dendron and a phosphorhydrazone dendron (Scheme 5.8). The Staudinger reaction generates a P=N linkage, which is highly sensitive to hydrolysis. However, as the azide is linked to a phosphine sulfide, the connectivity P=N–P=S obtained is stable. The dendrimers could be further functionalised on the phosphorhydrazone side with aldehydes, phenolphosphines and amino bisdiphenylphosphines.



Scheme 5.8. Segment-block dendrimer containing a carbosilane dendron and a phosphorhydrazone dendron.

Cycloaddition reactions have also been used to construct this kind of molecules. The first report on the synthesis of segment block dendrimers by a cycloaddition reaction was in 2006 by Lee et al.¹¹⁹ A Fréchet-type polyether dendron was fused with a Tomalia-type PAMAM dendron by means of a copper-catalysed 1,3-dipolar cycloaddition between an alkyne and an azide (Scheme 5.9).



Scheme 5.9. Segment-block dendrimer synthesized by a copper-catalysed 1,3-dipolar cycloaddition between an alkyne and an azide.

Sanyal et al.¹²⁰ used the Diels-Alder reaction to synthesize dendrimers consisting of polyester and polyaryl ether dendrons (Figure 5.12). Furan functionalised polyaryl ether dendrons were reacted with maleimide functionalized polyester dendrons of the same generation to obtain segment block dendrimers. The exo/endo selectivity for the dendrimers was studied, revealing

that the reaction temperature plays an important role in the stereoselectivity of the product formed. For the first generation dendrimers, it was possible to obtain a pure *exo* product when the cycloaddition was run at 85 °C. However, it was not possible to exclusively obtain an *exo* product for the second and third-generation dendrimers.

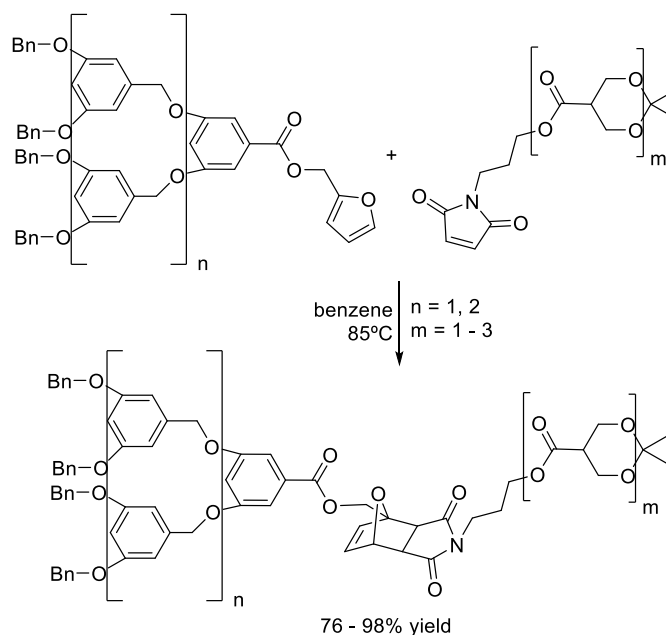


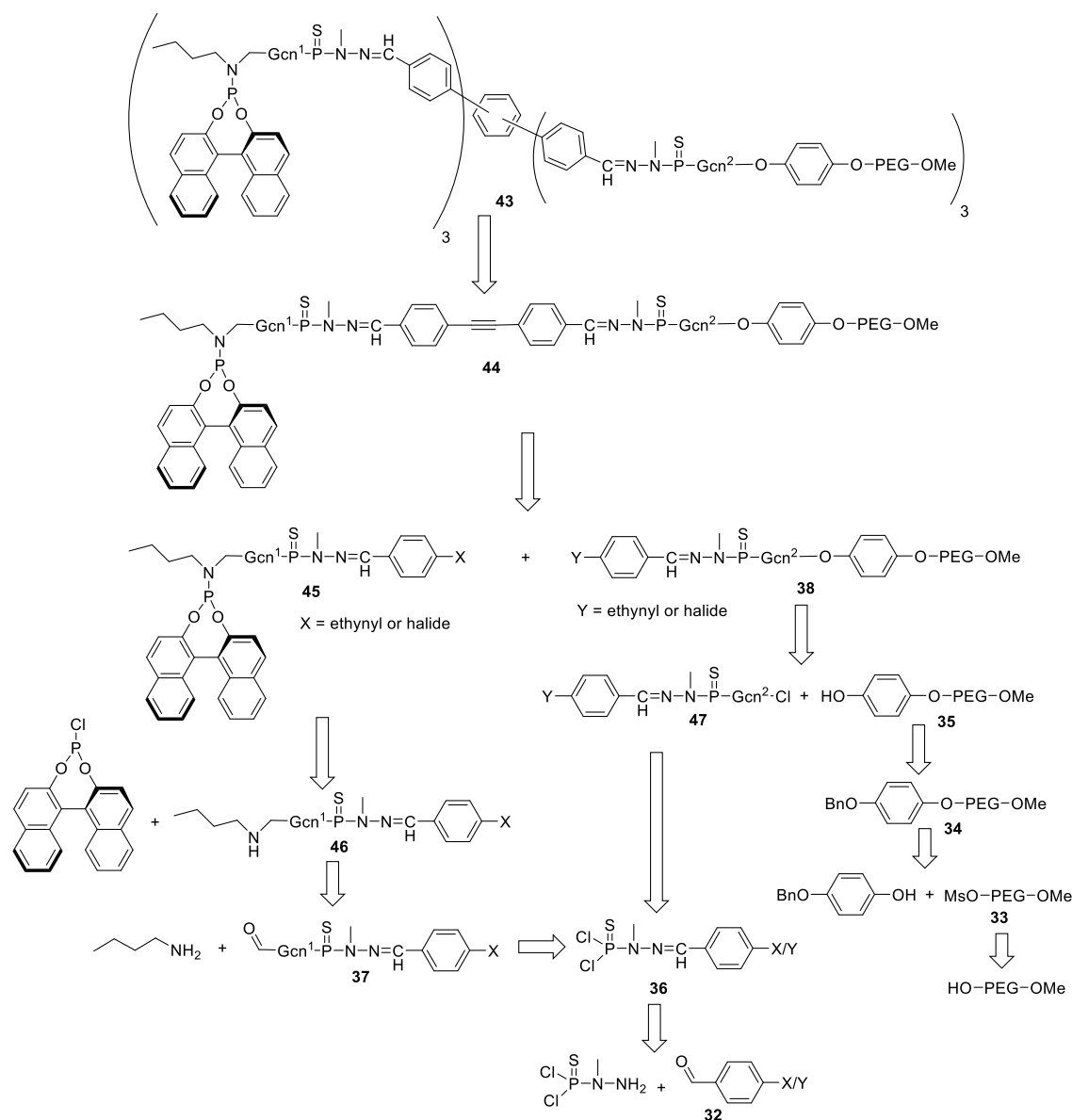
Figure 5.12. Dendrimer containing polyester and polyaryl ether dendrons synthesized with a Diels-Alder reaction.

To the best of our knowledge, dendrimers containing different surfaces or blocks have not been synthesized by a [2+2+2] cycloaddition methodology. Within the framework of a collaboration agreement that our group has with Prof. Caminade's group at the *Laboratoire de Chimie de Coordination* of the CNRS in Toulouse, we decided to explore the [2+2+2] cycloaddition as a tool to synthesize phosphorus-containing dendrimers with different surfaces or blocks. I began this project at Prof. Caminade's laboratories in Toulouse during a three-month stay, which was partially financed by the *Hetero-elements and Coordination Chemistry: from the Concept to Applications (HC3A)* project (*Groupement de Recherche International (GDRI)* between Catalonia and the Midi-Pyrénées), and continued it at the laboratories of the METSO group at the UdG.

5.2 Results and discussion

5.2.1. Synthesis of a surface-block dendrimer

Inspired by the excellent results achieved in our previous collaboration with Caminade's group in which phosphoramidite-containing dendrimers were used as ligands for the rhodium catalysed [2+2+2] cycloaddition reaction (see Scheme 1.39 in section 1.1.3.1),⁴⁷ we aimed to synthesize surface-block dendrimers bearing two different functional groups: the first would contain the already described phosphoramidite ligand and the second a water-solubilising fragment that would provide the dendrimer with water solubility to perform catalysis in water. Among all the strategies that have already been used in Caminade's group to synthesize water-soluble dendrimers,¹²¹ such as the use of quaternary ammonium salts and poly(ethylene glycol) (PEG) chains, PEG was chosen due to its more neutral character. The retrosynthetic analysis for the preparation of the dendrimer is depicted in Scheme 5.10.

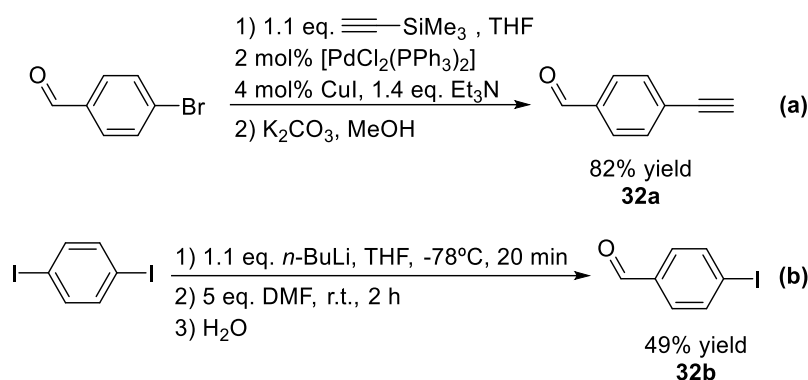


Scheme 5.10. Retrosynthetic analysis of the surface-block dendrimer.

The key step of the synthesis is the formation of the core of the dendrimer by means of a [2+2+2] cycloaddition of **44** containing an internal alkyne, which can be assembled through a Sonogashira reaction of an aryl alkyne and an aryl halide (**45** and **38**). Fragment **45** is an analogue of the dendrimer used in the previous work,⁴⁷ so the synthesis had already been established: the phosphoramidite moiety will be introduced through the commercially available BINOL-chlorophosphite by a nucleophilic substitution on the butylamine functionality (**46**), which in turn will arise from a reductive elimination of the corresponding imine, formed on an aldehyde residue of **37**. The partner fragment **38** can be assembled by a nucleophilic substitution of the phenol derivative **35** on a chloride residue on **47**. Both intermediates **37** and **47** can be formed through a common intermediate **36**, which can be constructed by the condensation of a benzaldehyde derivative **32** and *N*-methyl-dichlorophosphorhydrazine. The route to obtain phenol **35** had already been optimised by Yiqian Wei, a previous member of Caminade's group.¹²² The free alkoxy group will be obtained from the corresponding benzyl-protected compound **34**. The poly(ethylene glycol) chain can be introduced by a base-mediated

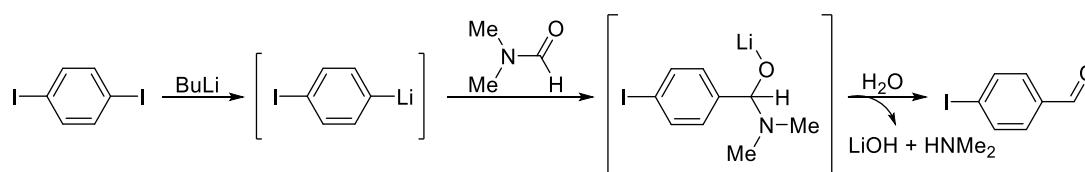
nucleophilic substitution of 4-(benzyloxy)phenol on the mesyl-derivative **33**, which can be formed from the commercially available poly(ethylene glycol) methyl ether.

In a first step, the precursors needed were synthesized, starting with aldehydes **32a**¹²³ and **32b**¹²⁴. These compounds contain on one side alkyne or halide moieties, which are necessary for the Sonogashira reaction, and on the other side feature the aldehyde function, which permits the growth of the dendrimer. The synthesis was carried out according to already described procedures as is shown in Scheme 5.11. The synthesis of 4-ethynylbenzaldehyde (equation a) consists, first, on a Sonogashira reaction between 4-bromobenzaldehyde and ethynyltrimethylsilane, followed by the deprotection of the acetylene moiety to give compound **32a** in an 82% yield



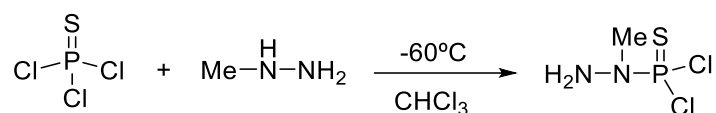
Scheme 5.11. Synthesis of 4-ethynylbenzaldehyde (equation a) and 4-iodobenzaldehyde (equation b).

4-Iodobenzaldehyde was synthesized through a Bouveault aldehyde synthesis on 4-diodobenzene (Scheme 5.11, Equation b). The mechanism of this reaction is depicted in Scheme 5.12. In a first step, the aryl-lithium compound is generated, which subsequently adds to DMF to form a hemiaminal intermediate that can easily be hydrolysed to give the desired aldehyde. A 49% yield of **32b** could be obtained using this method.



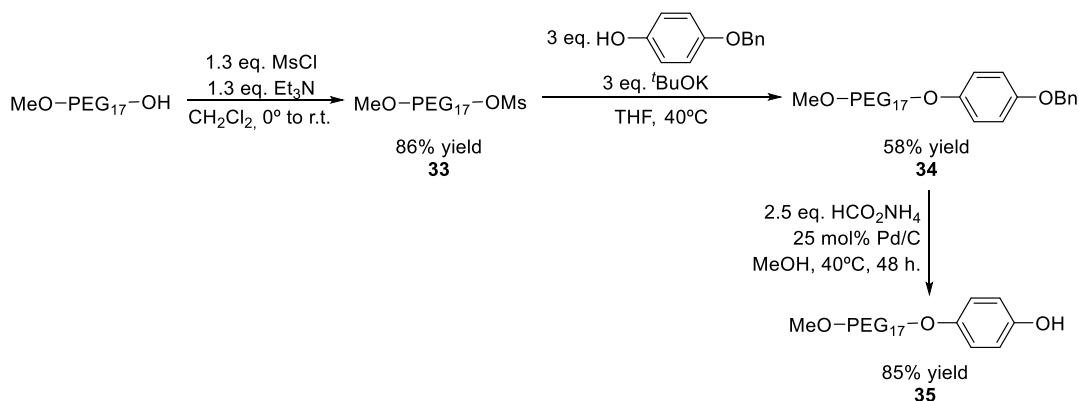
Scheme 5.12. Mechanism of the Bouveault aldehyde synthesis.

N-methyl-dichlorophosphorhydrazine was then prepared. This compound will provide the branching points and phosphorus structure of the dendrimer. Its preparation is probably the most difficult step in the synthesis of phosphorus dendrimers, as the monosubstitution of phosphoryl trichloride needs highly precise reaction conditions. The synthesis of the compound is achieved by a drop-by-drop addition of a solution of *N*-methylhydrazine in chloroform over another solution in chloroform of phosphoryl trichloride, with the temperature being controlled in the -65°C and -60°C range (Scheme 5.13).



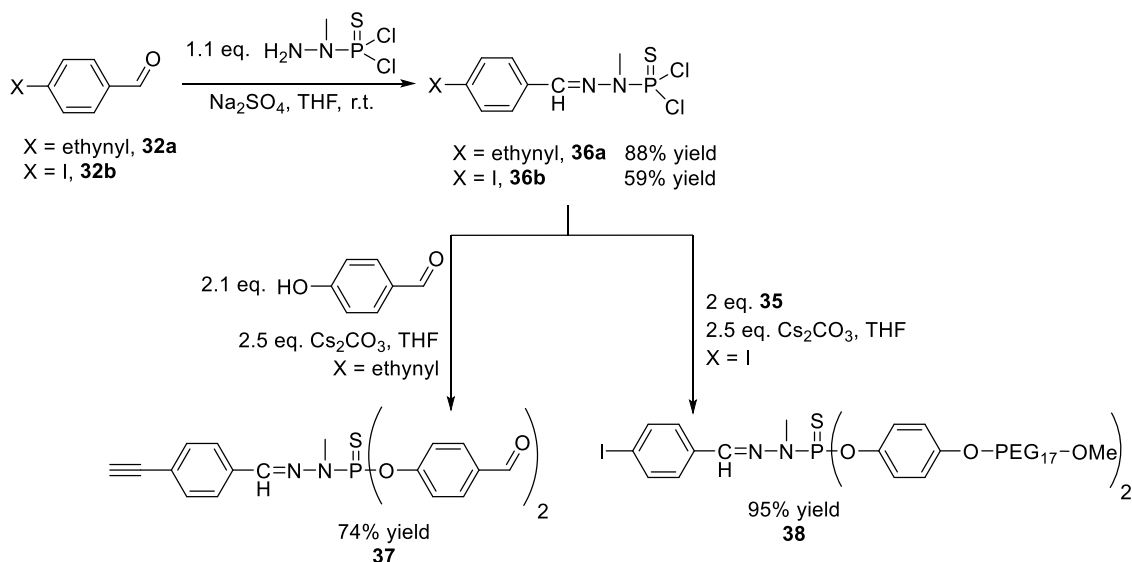
Scheme 5.13. Synthesis of *N*-methyl-dichlorophosphorhydrazine.

Finally, the phenolated PEG fragment **35**, which is necessary to provide water solubility, was synthesized following the route depicted in Scheme 5.14. The commercially available poly(ethylene glycol) methyl ether, with an average mass of 750 g/mol (which corresponds to approximately seventeen units of ethylene glycol), was reacted with mesyl chloride to afford compound **33**. Next, a nucleophilic substitution on the mesylated alcohol with 4-(benzyloxy)phenol afforded the benzyl-protected compound **34**, which was removed by means of a reduction catalysed by Pd/C and hydrogen formed in situ to obtain a 42% overall yield of the phenol derivative **35**. It should be taken into account that the yields given are calculated from the average mass of the molecules.



Scheme 5.14. Synthesis of the poly(ethylene glycol) derivative **35**.

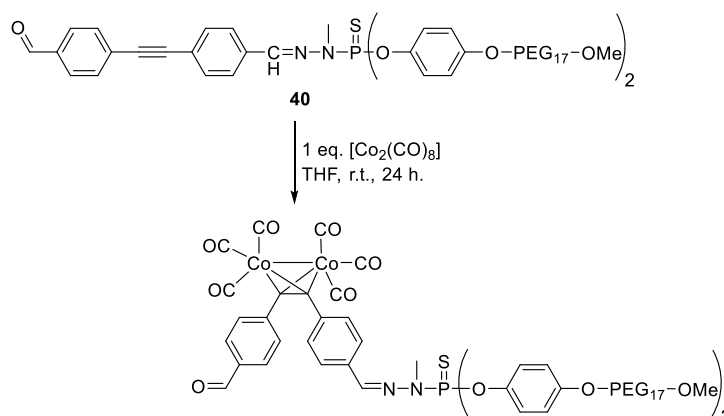
Once all the starting materials had been synthesized, the dendrons containing the phosphorus-based skeleton were prepared according to the route depicted in Scheme 5.15.



Scheme 5.15. Synthesis of the phosphorus-containing moieties **37** and **38**.

First, the benzaldehyde derivatives **32** were reacted with *N*-methyl-dichlorophosphorhydrazine affording the corresponding imine derivatives **36**. From compounds **36**, the corresponding phenol compound was introduced by nucleophilic substitution on the chloride atoms under basic conditions. For **36a**, 4-hydroxybenzaldehyde was chosen to afford dendron **37**, which in further reactions would contain the phosphoramidite ligand. In **36b** the synthesized PEG derivative **35** was introduced to provide the dendron that should enhance the hydrophilicity.

aerobic atmosphere and are generally catalytically competent in cycloaddition reactions. To check whether the instability of the $[\text{Co}_2(\text{CO})_8]$ complex used was responsible for the failure of the cycloaddition, the Co complex of compound **40** was synthesized as shown in Scheme 5.18.

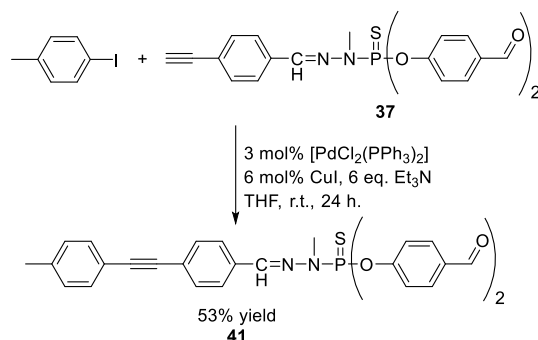


Scheme 5.18. Preparation of the Co complex of **40**.

This complex was then used as the catalyst for the [2+2+2] cycloaddition. However, starting material was also recovered. Catalytic systems based on rhodium were also tested. Mitsudo, Suga et al.¹²⁵ used a catalytic system consisting of a mixture of catalytic amounts of RhCl_3 and Pr_2NEt to promote the [2+2+2] cycloaddition reaction of di(furan-2-yl)acetylenes, however, it was not effective in our case. We also tested the complex $[\text{RhCl}(\text{CO})_2]_2$ as its structure is similar to that of the dicobalt octacarbonyl compound, but this was not effective either.

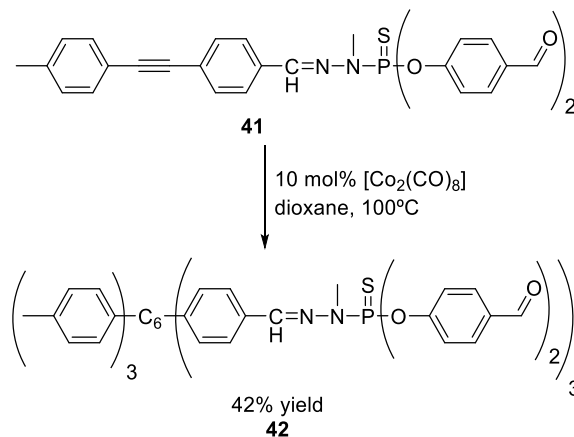
In the cobalt-catalysed reactions it was observed that a green residue sticking to the glass of the reaction vessel appeared when the reaction mixture was removed. Leitner et al.¹²⁶ reported the formation of green Co nanoparticles stabilized by poly(ethylene glycol), obtained by thermal decomposition of $[\text{Co}_2(\text{CO})_8]$ in PEG at 80-100°C. Taking this report into account, we believe that the PEG moiety of the dendron assists in the decomposition of the cobalt catalyst, thus rendering it inactive.

In order to check whether the problem arises from the phosphorus skeleton or the PEG chain, a simpler derivative containing the phosphorhydrazone moiety was synthesized. Compound **37** was reacted with 4-iodotoluene under Sonogashira conditions to afford derivative **41** (Scheme 5.19).



Scheme 5.19. Synthesis of the model substrate **41**.

This compound was then submitted to Co-catalysed [2+2+2] cycloaddition reaction conditions, as shown in Scheme 5.20. The reaction proved to be effective, affording compound **42** in a 42% yield. The signals corresponding to the internal alkyne at 88.5 and 91.7 ppm in the ^{13}C -NMR spectrum of **41** disappeared and signals in the aromatic region appeared. A peak in the ESI-MS at m/z 1657.6, corresponding to $[\text{M}+\text{H}]^+$, can be observed.



Scheme 5.20. Co-catalysed [2+2+2] cycloaddition reaction of **41**.

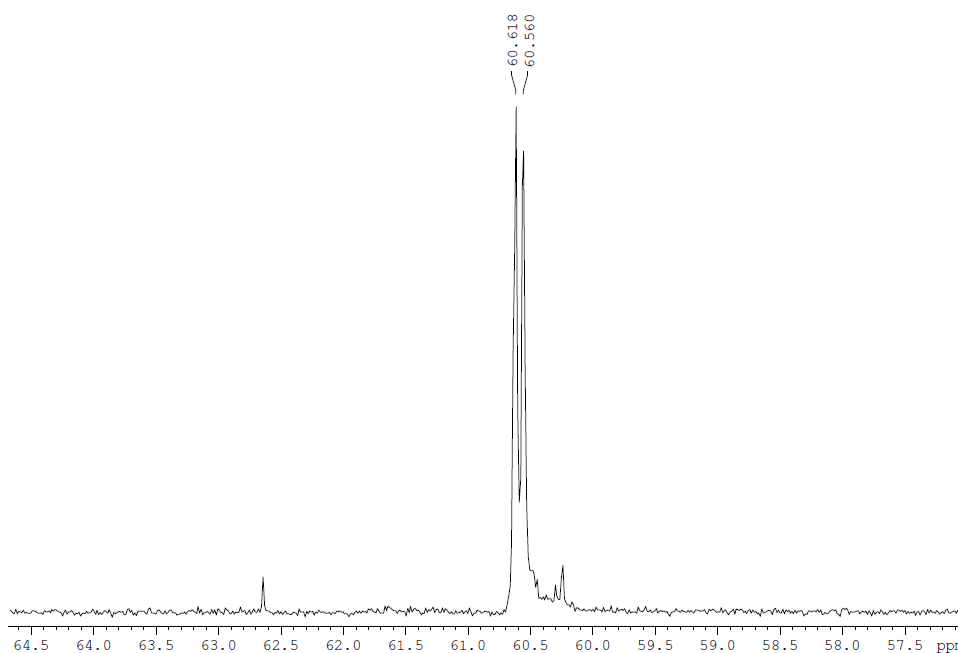
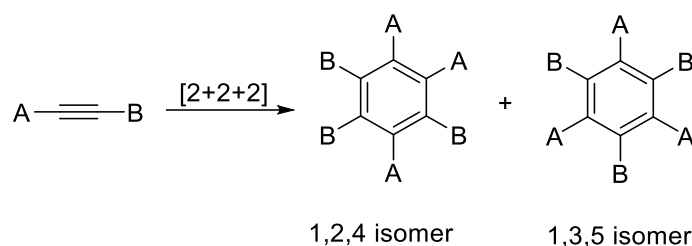


Figure 5.14. $^{31}\text{P}\{^1\text{H}\}$ -NMR of **42**.

In the $^{31}\text{P}\{^1\text{H}\}$ -NMR spectrum of **41** only a single peak appears. However, the $^{31}\text{P}\{^1\text{H}\}$ -NMR spectrum of **42** shows two different phosphorus peaks at 60.5 and 60.6 (Figure 5.14). A similar splitting is observed for the aldehyde and methyl signals in the ^1H -NMR spectrum.

The [2+2+2] cycloaddition reaction may form the two different isomers schematically represented in Scheme 5.21. Whereas for the 1,3,5-isomer we would expect only one phosphorus signal, the 1,2,4-isomer should provide three different signals.



Scheme 5.21. Possible isomers formed in the [2+2+2] cycloaddition reaction.

One possible explanation is that the phosphorus atoms are relatively far from the central aromatic group, so they should only be sensitive to large differences and, in consequence, only two signals in a 1:2 ratio for the 1,2,4 isomer were to be expected. When A is between two B it can be presumed that the chemical shift is the same for position 4 in the 1,2,4 isomer, and positions 1,3,5 in the 1,3,5 isomer. Furthermore, when A is between A and B (positions 1 and 2 on the 1,2,4 isomer), another signal (a single signal for both) should be observed, thus only two signals for a mixture of isomers can be expected. As the signals have a 1:1 ratio in the $^{31}\text{P}\{^1\text{H}\}$ -NMR, it can be assumed that a mixture comprising about 75% of isomer 1,2,4 and 25% of isomer 1,3,5 was obtained.

At this point, it can be concluded that the problem of reactivity of **40** must have been due to the PEG moiety and, thus, that [2+2+2] cycloaddition cannot be performed on a dendron already containing the PEG functional group. Therefore, our synthetic strategy had an orthogonality problem.

5.2.2. Synthesis of a segment-block dendrimer

In order to solve this drawback, and maintaining our objective of preparing a water soluble dendrimer, we decided to change the type of dendrimer synthesized. In order to circumvent the orthogonality issue, we decided to change the phosphoramidite ligand, which is constructed on a benzaldehyde capped dendron, for a 1,3,5-triaza-7-phosphaadamantane (PTA) ligand (Figure 5.15), which is attached to a chloromethylbenzene moiety, while maintaining the PEG groups as water-solubilizing moieties.

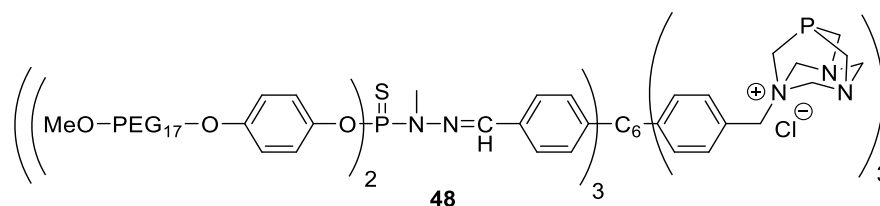
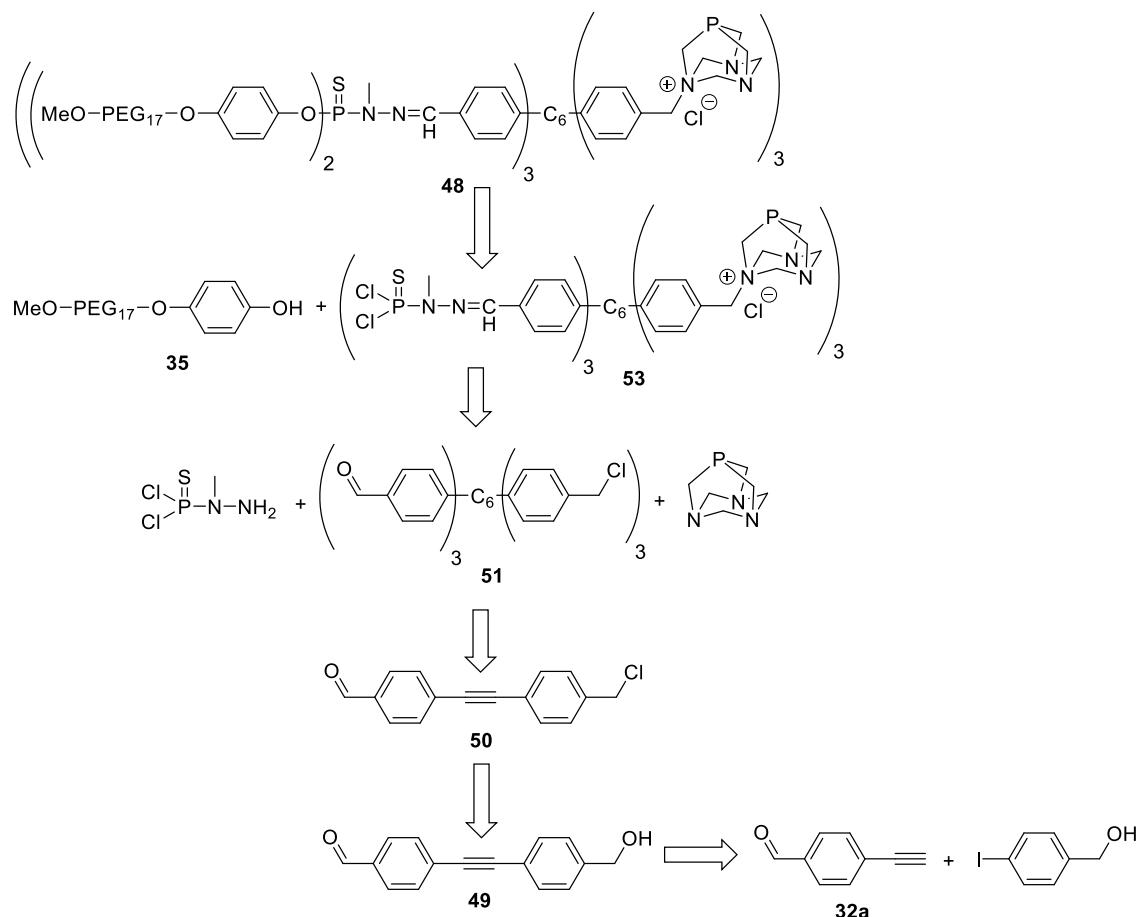


Figure 5.15. Segment-block dendrimer containing PTA ligands and poly(ethylene glycol) chains.

Caminade et al.¹²⁷ have previously synthesized phosphorus dendrimers containing PTA ligands on the surface and have used them as ligands for ruthenium and rhodium, giving good results in the isomerisation of allylic alcohols and the hydration of alkynes. Moreover, Ru(II)-arene complexes with PTA ligands have shown important anticarcinogenic activity.¹²⁸

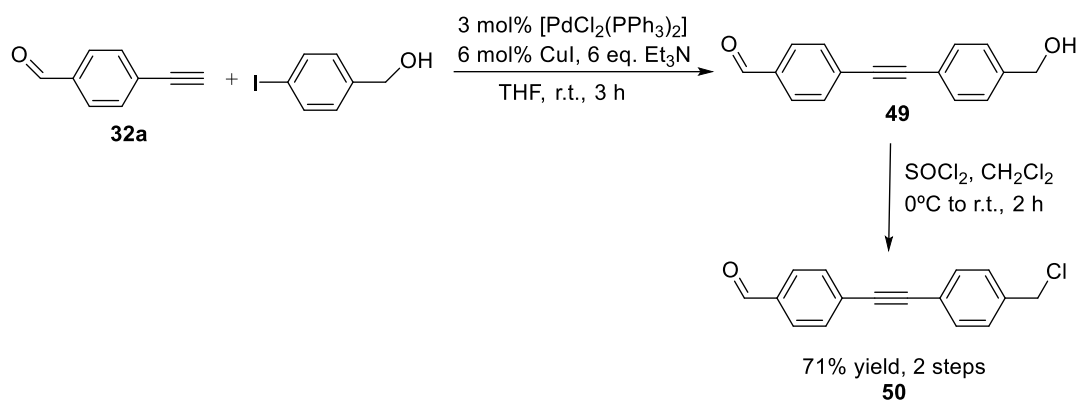
The retrosynthetic pathway is depicted in Scheme 5.22. The core will be formed by means of a [2+2+2] cycloaddition, but in order to avoid incompatibility problems with the functionality of the molecule, it will be assembled in an early stage of the synthesis. The PEG moiety of **48** will

be introduced by formation of the phenolate under basic conditions and its reaction over **53** as previously explained. The PTA will be introduced by alkylation on one of the nitrogen atoms with the CH_2Cl group of **51** and the *N*-methyl-dichlorophosphorhydrazine group will react with the aldehyde residue to give the corresponding imine. **51** will be the molecule synthesized by the [2+2+2] cycloaddition reaction from **50**, as no incompatibility between functional groups is expected. The chlorine atom on **50** will be introduced from the alcohol precursor **49**, which in turn will be synthesized by a Sonogashira reaction between 4-ethynylbenzaldehyde (**32a**) and 4-iodobenzyl alcohol.

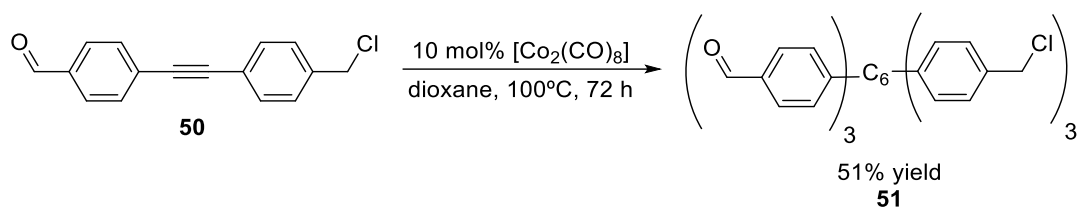


Scheme 5.22. Retrosynthetic analysis for dendrimer **48**.

The synthetic route to obtain derivative **50** is depicted in Scheme 5.23. Compound **49** was obtained by a Sonogashira coupling between 4-ethynylbenzaldehyde and 4-iodobenzyl alcohol. As this compound is highly insoluble in CH_2Cl_2 , purification was performed by washing it with this solvent. The hydroxide was then transformed to a chloride using thionyl chloride. The overall yield for these two steps is 71%.

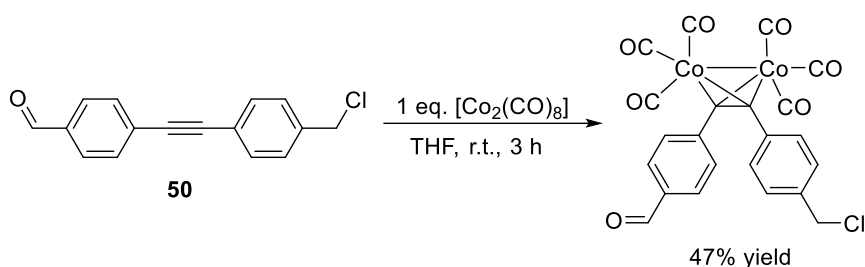
Scheme 5.23. Synthesis of **50**.

Using the $[\text{Co}_2(\text{CO})_8]$ complex, **50** was submitted to cycloaddition conditions. A 51% yield of cyclized product **51** was obtained after three days in refluxing dioxane (Scheme 5.24).

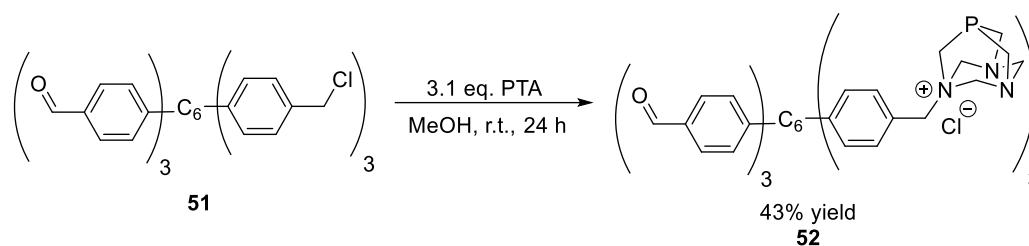
Scheme 5.24. Co-catalysed [2+2+2] cycloaddition of **50**.

Derivative **51** was characterised by ^1H and ^{13}C -NMR and ESI-MS. The ^1H -NMR spectrum showed the same signals as compound **50** but split into two, indicating that a mixture of isomers was formed. The ^{13}C -NMR spectrum showed no presence of acetylenic carbons and a group of new aromatic carbons. Two peaks related to the product appeared in the ESI-MS spectrum: the first at m/z 785.2, corresponding to $[\text{M}+\text{Na}]^+$, and the second at m/z 819.3, corresponding to $[\text{M}+\text{CH}_3\text{OH}+\text{Na}]^+$.

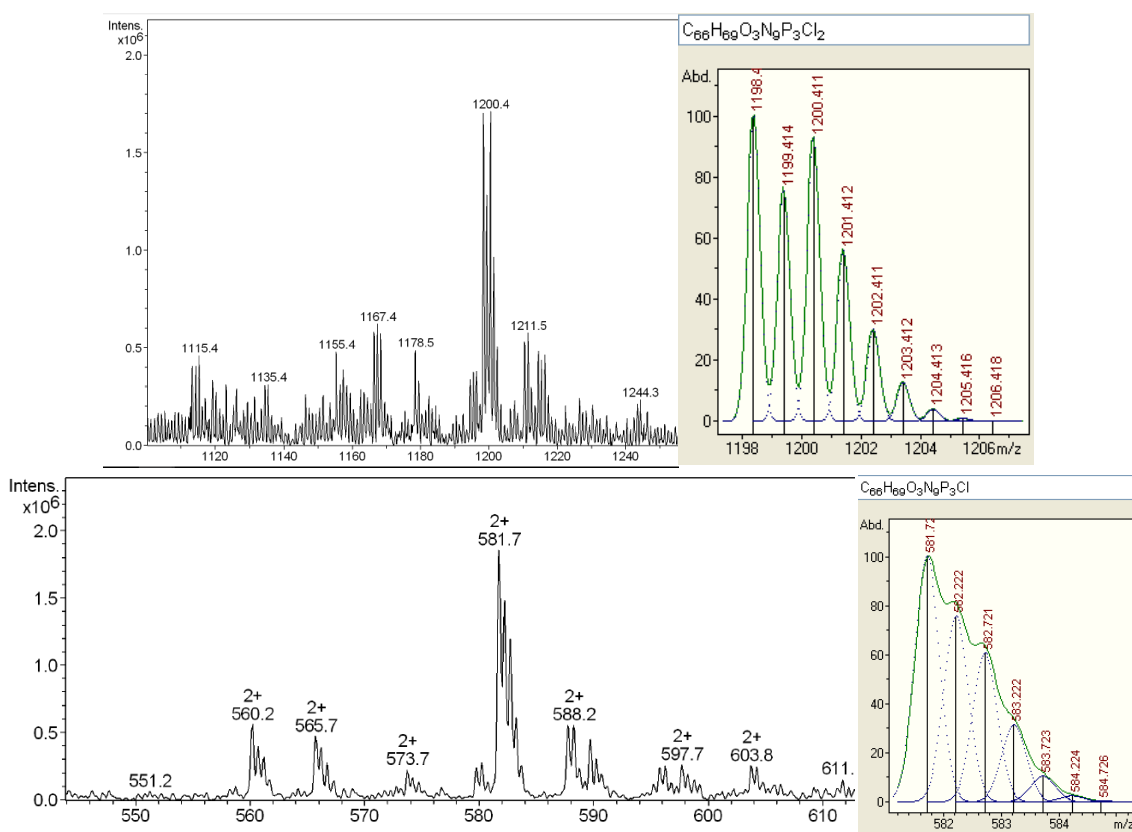
In order to try to improve the yield, the cobalt complex of compound **50** was also prepared (Scheme 5.25). However, no significant difference was observed when the complex was used as the catalyst for the [2+2+2] cycloaddition reaction.

Scheme 5.25. Synthesis of the cobalt complex of **50**.

The reaction with PTA was then assessed. Compound **51** was dissolved together with three equivalents of PTA in MeOH and was stirred for 24 hours at room temperature (Scheme 5.26).

Scheme 5.26. Alkylation of **51** with PTA.

A 43% yield of compound **52** was obtained. The ESI-MS spectrum of **52** showed a peak at m/z 1200.4 corresponding to $[\text{M}-\text{Cl}]^+$ and at m/z 581.7, corresponding to $[\text{M}-2\text{Cl}]^{2+}$ (Figure 5.16).



In this case, three signals in the $^{31}\text{P}\{^1\text{H}\}$ -NMR were observed (Figure 5.17). The PTA is closer to the central aromatic ring than the P=S in compound **42**, and it is also bulkier. For both reasons, signals that were equivalent in **42** become non-equivalent for compound **52**, thus a larger number of signals should be observed. If the same approximate ratio of 75% of 1,2,4 and 25% of 1,3,5 is expected, either 4 signals with intensity 1:1:1:1 or three signals with intensity 2:1:1 (if two of them are superimposed) should be observed. This latter scenario seems to be the one observed.

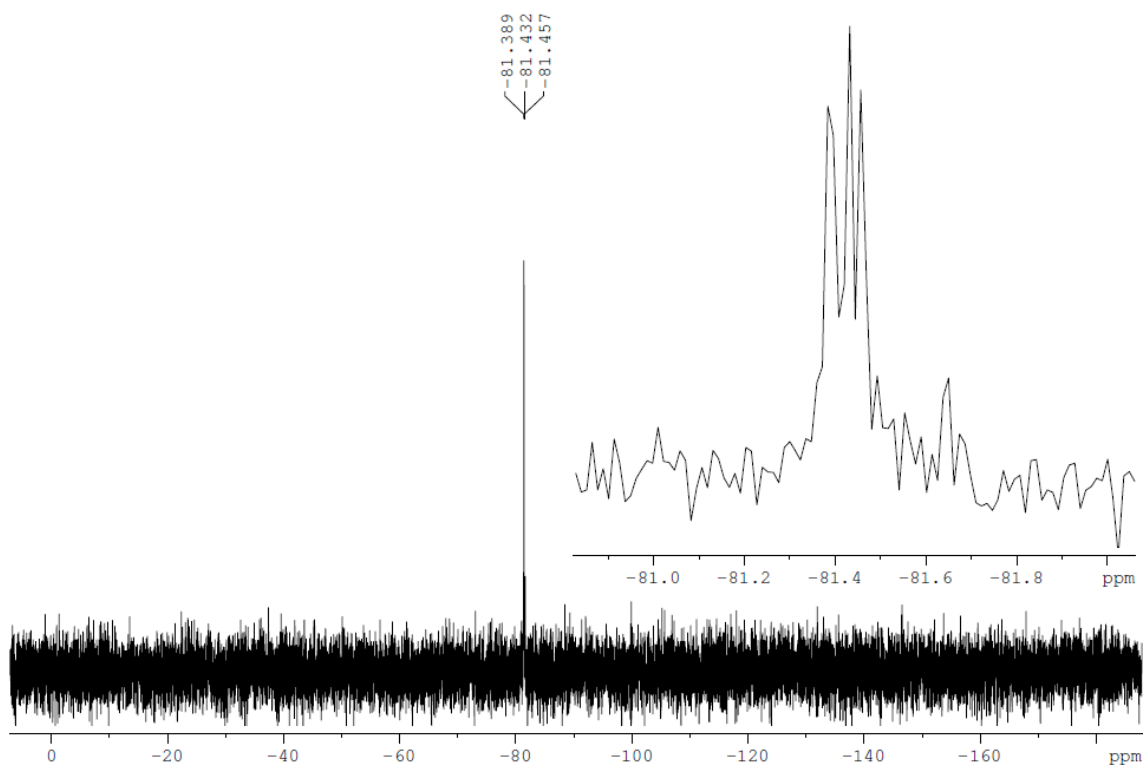


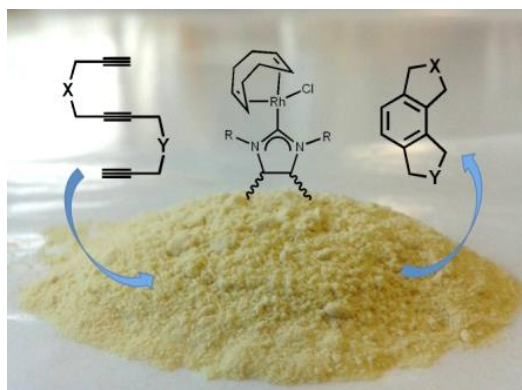
Figure 5.17. $^{31}\text{P}\{^1\text{H}\}$ -NMR spectrum of **52**.

In summary, we were not able to synthesize a surface-block dendrimer containing PEG and phosphoramidite moieties by means of a Co-catalysed [2+2+2] cycloaddition reaction to construct the core. The incompatibility between the PEG and the cobalt catalyst and the lack of orthogonality of the synthetic route prompted us to change our strategy as well as the target molecule itself. Therefore, in the second part of the chapter, we aimed to prepare a segment-block dendrimer containing PTA ligands and PEG moieties. In this case, we were able to develop a successful strategy that allowed us to prepare a dendrimer containing a PTA ligand on one segment. However, due to lack of time the poly(ethylene glycol) moiety could not be introduced.

Chapter 6. Rhodium-NHC hybrid silica materials as recyclable catalysts for [2+2+2] cycloaddition reactions

This chapter has been published as:

Fernández, M.; Ferré, M.; Pla-Quintana, A.; Parella, T.; Pleixats, R.; Roglans, A. *Eur. J. Org. Chem.* **2014**, 6242.



6.1 Precedents

6.1.1. Organic-inorganic hybrid silica materials

Hybrid materials are constituted by organic components or networks mixed at the molecular level with an inorganic skeleton. Such a material combines the properties of both organic and inorganic compounds and has attracted many scientists since the beginning of the industrial era. Some of the oldest and most famous organic-inorganic hybrids come from the paint and polymer industries.¹²⁹ The properties of these materials are not just an addition of the individual contributions from the comprising elements, which makes them a very interesting class of solids. The coexistence of the two different domains can be beneficial, resulting in new physical properties.

Consequently, numerous organic-inorganic hybrid materials have been developed over the past decades,¹³⁰ providing a great variety of applications, in diverse fields, one of them in catalysis.¹³¹ The immobilization of homogeneous catalysts on hybrid materials offers many advantages in catalytic applications.¹³² First, catalysts that are supported within the inorganic matrix can be easily separated from the reaction mixture, thus reducing the contamination of the product by catalyst traces and simplifying the purification process. Secondly, the easy recovery of the heterogenized catalysts allows their reuse for further reaction batches offering eco-friendly advantages, with less consumption of the often costly and/or toxic catalysts. Among many inorganic solids, polymeric silicon oxide is one of the most frequently used catalyst supports due to its chemical, thermal and mechanical stability.

The chemical nature of both phases directly affects the chemical and textural properties in the final material. Depending on the interaction between the organic and the inorganic part, hybrid silica materials can be divided into two families:¹³³

(a) **Class I** materials, in which either the organics are entrapped (or embedded) in the inorganic matrix without any interaction, or the organic and inorganic components are linked together through non-covalent weak bonds such as hydrogen bonds and van der Waals, hydrophobic or ionic interactions (Figure 6.1). As the strength of these interactions is weak, the two phases of these materials can be separated by techniques such as extraction of the organic components with an organic solvent.

(b) **Class II** materials, in which the organic and inorganic components are linked together through strong covalent or ion-covalent chemical bonds (Figure 6.1). As a result, they form a unique continuous phase.

In catalysis, Class II materials are preferred to Class I. Catalyst leaching and the difficulties in controlling the loading of the organics in Class I materials prompted researchers to concentrate their investigations mainly on Class II materials.

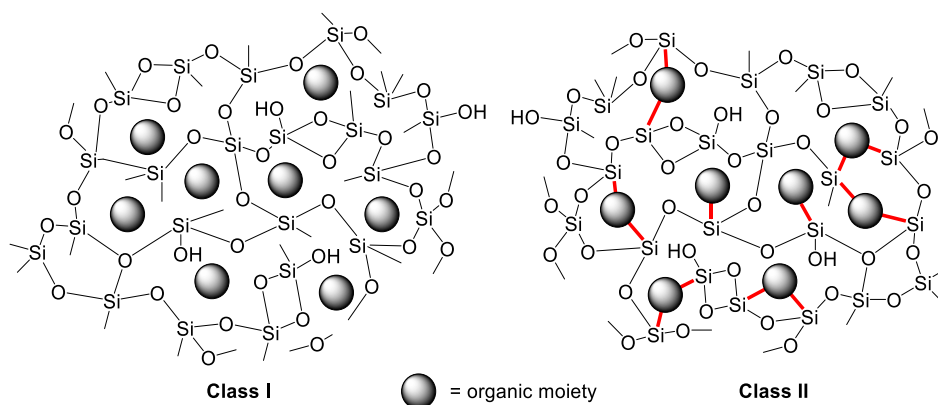


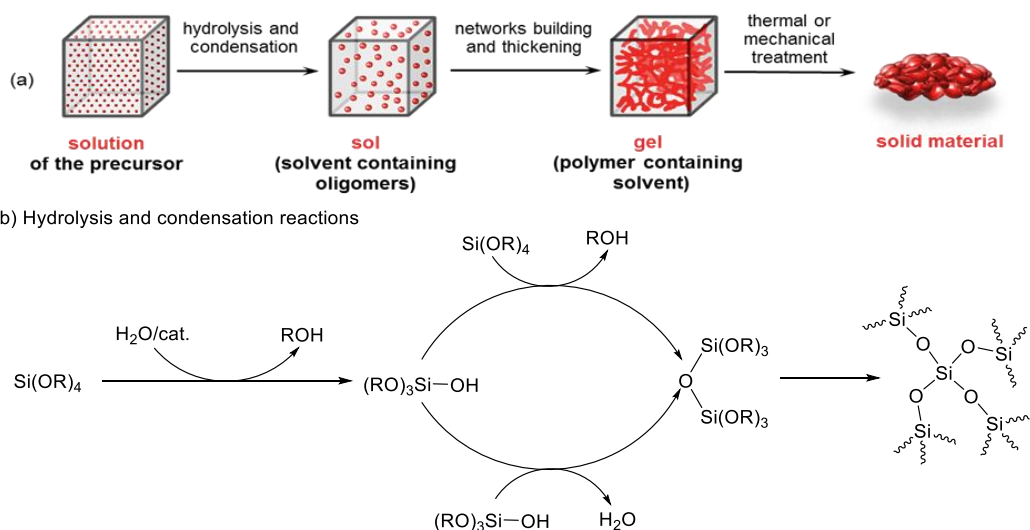
Figure 6.1. Hybrid silica material classification.

6.1.1.1. Preparation of organic-inorganic hybrid silica materials.

Two of the most common methods to synthesize hybrid silica materials are the sol-gel process and the grafting method.

The sol-gel process allows the preparation of pure inorganic materials in a reproducible way.¹³⁴ It can be carried out using inorganic precursors, such as chlorides, nitrates or sulfates, but the most versatile methodology typically involves the use of alkoxides and, of these, the use of alkoxysilanes is particularly common.

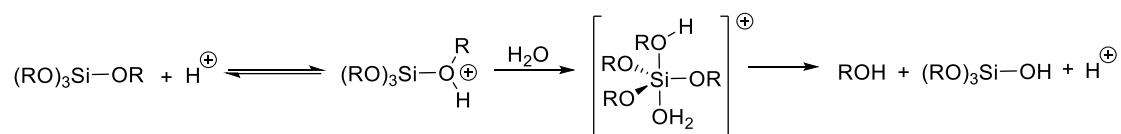
The process starts when a tetraalkoxysilane such as tetraethoxysilane (TEOS) is catalytically hydrolyzed in a solvent (ethanol, THF, DMF...) to give colloidal silanol and siloxane species, oligomers and other small clusters (*sol* in Scheme 6.1a). These clusters condense to form more siloxane bridges, then small particles, and eventually tridimensional networks that entrap the solvent to form a gel. On a macroscopic scale, gelation is the thickening of the initial solution into an elastic solid (a gel). However, this is not the end of the process. During the gel's aging process, hydrolysis and condensation continue (Scheme 6.1b) and the network stiffens, limiting the flow of the pore liquid. Although the system seems virtually unaffected, polymerization, coarsening and phase transformation occur. Finally, the gel is dried and after a thermal or mechanical treatment the material is obtained as a powder, called xerogel.



Scheme 6.1. a) Physics and b) chemistry of the sol-gel process.

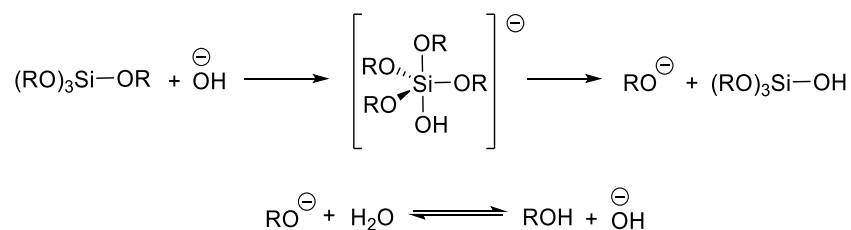
The properties of the final material, such as the surface area, strongly depend on the experimental parameters used in the sol-gel process. Therefore, any small change in the temperature, solvent, concentration or the catalyst can significantly affect the properties of the final hybrid material. The nucleophilic attack of water to the silicon atom in the first step takes place through a different mechanism depending on whether the catalyst used is acidic, basic or nucleophilic (F⁻, *N*-methylimidazole, HMPA).¹³⁵ The mechanism for each type of catalyst can be summarized as follows:

(a) *Acidic catalysis*: the nucleophilic attack of water (or silanol) occurs after the reversible protonation of an alkoxy group and generates a pentacoordinate intermediate that is able to lose an alcohol molecule (Scheme 6.2).



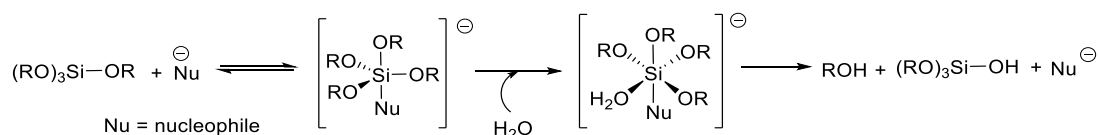
Scheme 6.2. Hydrolysis of tetraalkoxysilane promoted by acidic catalysis.

(b) *Basic catalysis*: in the presence of hydroxide anions, a nucleophilic attack to the tetraalkoxysilane occurs through an anionic pentacoordinate intermediate, from which an alkoxide group is eliminated (Scheme 6.3).



Scheme 6.3. Hydrolysis of tetraalkoxysilane promoted by basic catalysis.

(c) *Nucleophilic catalysis*: the nucleophile coordinates to the silicon centre of a tetraalkoxysilane generating an anionic pentacoordinate intermediate. This intermediate shows higher reactivity towards nucleophilic substitution. Water and silanol coordinate this intermediate and form a hexacoordinate transition state, which evolves to give an alcohol and a silanol and to regenerate the catalyst (Scheme 6.4). Many bases can act as nucleophilic catalysts (anions such as hydroxide and fluoride).

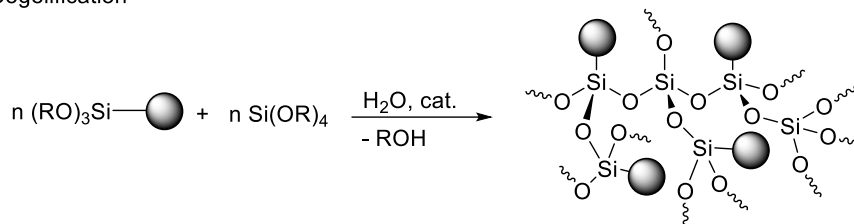


Scheme 6.4. Hydrolysis of tetraalkoxysilane promoted by nucleophilic catalysis.

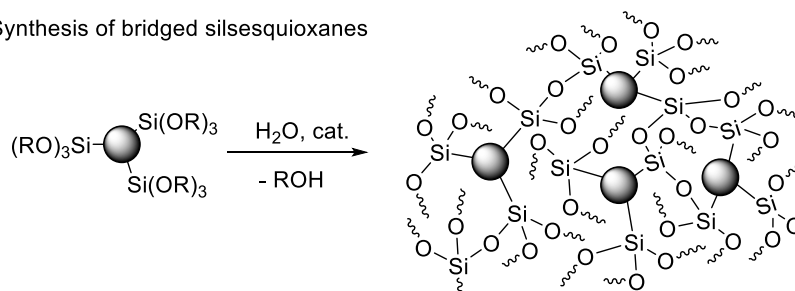
The organic moiety in an organic-inorganic hybrid material can be directly incorporated during the sol-gel process by co-gelification of an organotrialkoxysilane and tetraalkoxysilane.¹³⁶ After hydrolysis and condensation, the final solid will contain organic groups dispersed in the silica matrix (Scheme 6.5a).¹³⁷ Importantly, when the organic compound bears two or more trialkoxysilyl groups, the sol-gel process can be performed without the addition of

tetraalkoxysilane (Scheme 6.5b).¹³⁸ These organosilicas are also called bridged silsesquioxanes, and are inherently homogeneous solids.¹³⁹

(a) Cogelification



(b) Synthesis of bridged silsesquioxanes



Scheme 6.5. a) Cogelification and b) Synthesis of bridged silsesquioxanes.

One of the most important characteristics of silica materials is their porosity. This property gives rise to three materials, categorised by their pore size: microporous (pore size < 20 Å), mesoporous (20 – 500 Å) and macroporous (> 500 Å). The control of the porosity or surface area is not possible when materials are prepared by simple condensation or polycondensation sol-gel processes in organic solvents (e.g. alcohols, THF, DMF) and amorphous materials with wide pore distribution are obtained in these cases. This lack of control of the pore size distribution and other drawbacks can be overcome through the use of surfactants during the sol-gel reaction.¹⁴⁰

Surfactants are organic compounds with hydrophobic hydrocarbon chains and a hydrophilic polar head. In aqueous media, these molecules organize in micelles, with the hydrophobic and non-polar chains at the inner side of the sphere and the polar heads oriented towards the exterior, due to the non-compatibility of the hydrocarbon chains with water and the compatibility of the polar head towards water. Depending on the nature of the surfactant as well as its concentration and the temperature of the solution, micelles interact with each other to form spherical, cylindrical, tubular or bilayer type structures, which can pack in tridimensional structures with different patterns (e.g. spherical, hexagonal, cubic, lamellar).¹⁴¹ These micelles act as a template and, due to electrostatic interactions, the hydrolysis and condensation reactions of the sol-gel process take place at the surface of these micelles (Scheme 6.6). The electrostatic interaction between the surfactant or template (T) and the charged silicon species formed (S) is strongly affected by the medium.¹⁴² Therefore, when the sol-gel reaction is performed under basic conditions, cationic surfactants such as ammonium salts are commonly used (T^+S^- interaction), whereas under acidic conditions, anionic surfactants such as sulfates or phosphonates are preferred (T^-S^+).¹⁴³ Under nucleophilic catalysis in a neutral medium, surfactants without charge (long chain alkyl amines, polyoxyethylene oxides or amphiphilic block copolymers) are often used as the interaction with the silicon substrate occurs through hydrogen bonding (T^0S^0). Neutral poly(ethylene oxide)-poly(propylene oxide) block copolymers,

This method has the advantage that the mesostructure of the starting phase is usually retained when the organic fragment is attached. Two drawbacks are the reduction of porosity that results from the addition of the organic residue and the difficulty of achieving a homogeneous distribution of the organic groups.

6.1.1.2. Characterization of hybrid silica materials

As has already been mentioned, the properties of the materials obtained by the sol-gel process strongly depend on the experimental conditions. Therefore, techniques which allow their physical and chemical characterization are needed in order to understand the activity of functionalized silica materials.¹⁴⁷ Chemical analyses provide information about the amount of organic and/or metal fragments loaded in the material. Physical parameters such as surface area, pore size distribution, material morphology or texture are very important in catalysis as they affect reagent and product diffusion and the accessibility to the catalytic centre. A brief summary of the different techniques used to characterize the materials is presented here.

6.1.1.2.1. Thermogravimetric analysis (TGA)

This analytical technique is used to determine changes in the mass of a material as a function of temperature.¹⁴⁸ It provides an idea of thermal stability of a given material, including structural decomposition, oxidation, corrosion and moisture adsorption/desorption. In hybrid materials it is used to determine the loading of inorganic and organic components. The record is the thermogravimetric (TG) curve, where the mass is plotted on the ordinate and temperature (T) or time (t) on the abscissa (Figure 6.2).

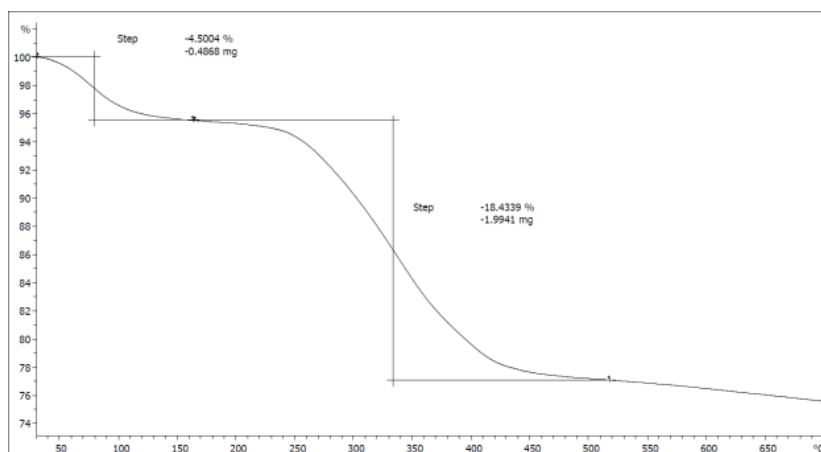


Figure 6.2. Thermogravimetric curve for **M1** (see section 6.2.1.4).

In the TG curve of hybrid materials the first weight loss corresponds to the thermodesorption of physically adsorbed water from the silica surface (temperatures in the range of 20 – 200 °C).¹⁴⁹ The second weight loss can be attributed to a combination of two processes: first, the condensation of silanol groups and the cross-linking of surface silanol with some organic functionality, and second, the thermal decomposition of the chemically-bonded organic groups. At temperatures exceeding 700°C the organic component of hybrid materials is destroyed completely and so the inorganic content of the hybrid material can be determined from the residual mass.

This technique gives us an insight to the stability of the organic fragment of the hybrid material since some functional groups decompose at low temperatures (*i.e.* azides, carbamates or thioureas)¹⁵⁰ whereas others are stable enough to resist pyrolysis at low temperatures without degrading any covalently bound organic moiety.¹⁵¹ The nature of the organic moiety will also affect the choice and control of other experimental parameters, such as the temperature gradient (typically between 5 and 10 °C/min) and the atmosphere under which the analysis is performed (e.g. air, argon).

6.1.1.2.2. Elemental analysis

The chemical composition of hybrid materials is determined by elemental analysis. The carbon, hydrogen, nitrogen, sulphur, chlorine, bromine and iodine present in organic fragments can be analysed by combustion. The presence of other elements such as silicon or metals can be quantified by inductively coupled plasma (ICP) analysis. The amount of organic fragments found is usually lower than the expected value because of incomplete incorporation in the hybrid material. This fact can be rationalized taking into account that the hydrolysis rate is lower for organotrialkoxysilanes with respect to tetraalkoxysilanes. Within the group of tetraalkoxysilanes, the hydrolysis rate decreases in the following order: tetramethoxysilane (TMOS) > tetraethoxysilane (TEOS) > tetrapropoxysilane (TPOS) > tetrabutoxysilane (TBOS). The degree of condensation also contributes to the difference between theoretical and experimental values, since some alkoxy groups are not hydrolysed and some silanol groups may not condense. Discrepancy between the two values may also arise from traces of surfactant or high-boiling point solvent remaining in the material after the processing.

6.1.1.2.3. ²⁹Si and ¹³C Solid State Nuclear Magnetic Resonance (SSNMR)

²⁹Si-SSNMR confirms the existence of a covalent bond between silicon and the organic component and provides information about the degree of condensation in the hybrid material. During the sol-gel process a great variety of silicon species are formed containing different numbers of Si-O-Si bonds. These species lead to structures that give signals with different chemical shifts in the ²⁹Si-SSNMR spectrum depending on the alkoxy groups bonded to the silicon atom (Figure 6.3).

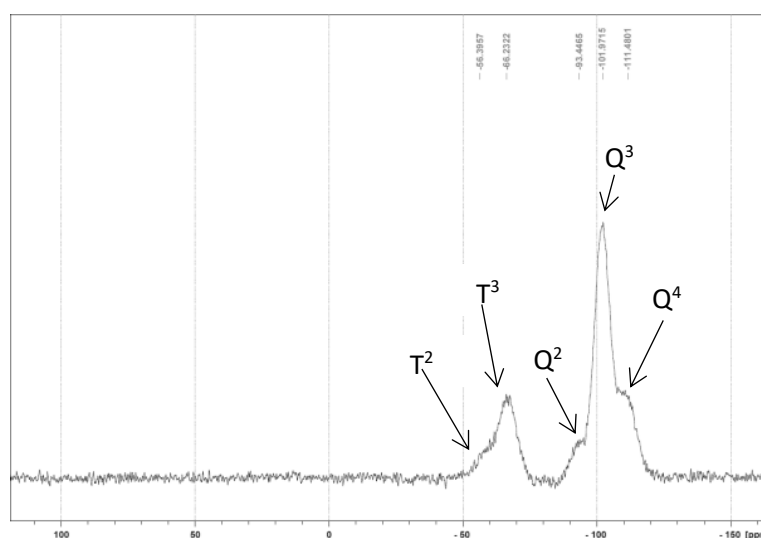


Figure 6.3. Example of ²⁹Si-SSNMR of material **M1** (see section 6.2.1.4).

These signals are classified as monofunctional silicon (M), which come from monoalkoxysilanes; difunctional (D), from dialkoxysilanes; trifunctional (T), from trialkoxysilanes; and quadrifunctional (Q), from tetraalkoxysilanes. In addition, numeric superindices are used to indicate the degree of condensation (Figure 6.4). For instance, 0 if condensation did not occur; 1 if only one alkoxy group has condensed; 2 if two alkoxy groups have condensed and so on. The nature of the organic moiety (e.g. alkyl, aryl etc.) or of the catalyst used in the sol-gel process can also affect the chemical shift.

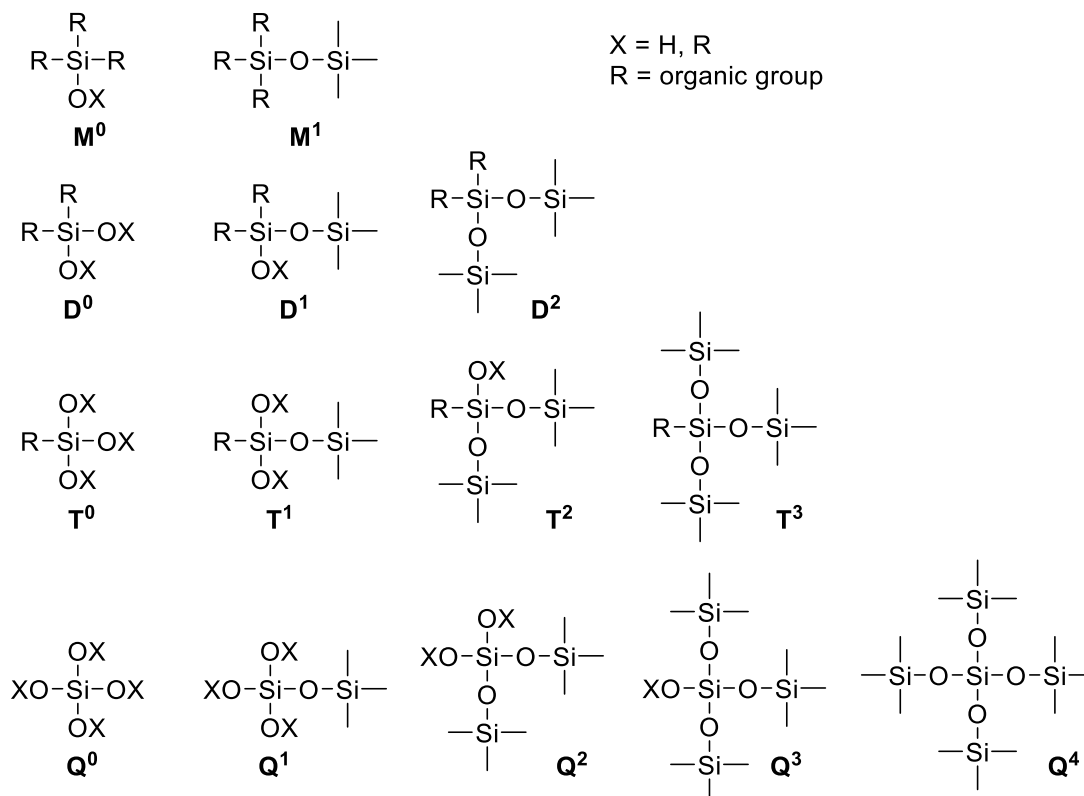


Figure 6.4. Silicon environments and their corresponding label in the ^{29}Si -SSNMR.

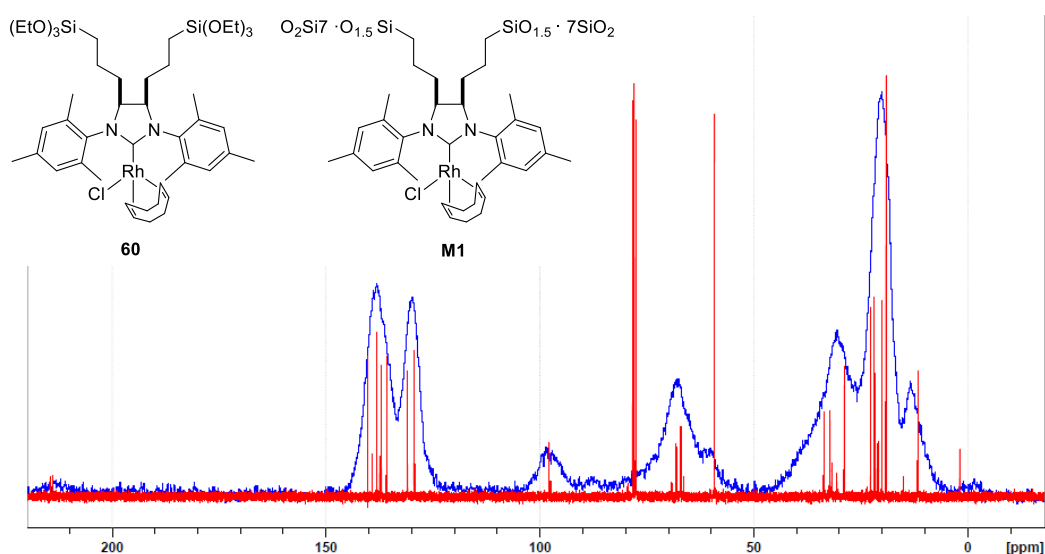


Figure 6.5. Comparison of ^{13}C -NMR of compound **60** in CDCl_3 solution (red) and ^{13}C -CP-MAS of material **M1** (blue, see section 6.2.1.4).

^{13}C -SSNMR is quite useful to check that the organic functionality has been loaded in the final material. The ^{13}C -SSNMR spectrum appears to be similar to the common ^{13}C -NMR in solution but the former has broader peaks (Figure 6.5). This technique provides qualitative information for the identification of organic functional groups. Unlike the spectrum recorded in solution, signals of different carbon atoms easily overlap.

It must be taken into account that ^{13}C and ^{29}Si solid state NMR suffer from low sensitivity.¹⁵² In fact, functionalized silicon sites of type T^n are often too diluted to be readily observed in the ^{29}Si -SSNMR. Generally, for high dilution of the organic component in the hybrid material (tetraalkoxysilane/organotrialkoxysilane ratio > 10), the spectrum mainly provides information about the Q^n and proton-rich sites (Si-OH). ^{13}C -SSNMR suffers from a similar drawback and, therefore, when the organic component is highly diluted, little evidence is normally obtained regarding the incorporation of the organic moiety.

6.1.1.2.4. Surface area analysis

Gas adsorption-desorption measurements are used for determining the surface area, the average pore size, and the pore size and pore volume distributions of a variety of different solid materials. *Adsorption* is the process by which atoms or molecules are weakly bound to the surface of a solid, and form a layer at the interface. Its counterpart, *desorption*, denotes the reverse process, in which the amount of adsorbed atoms or molecules decreases.

N_2 -sorption analyses are performed at 77 K from thoroughly degassed samples. The adsorption isotherm is built by adding controlled doses of nitrogen gas to the cold sample, and monitoring the corresponding relative pressure in the surrounding environment (p/p^0). When p/p^0 reaches 1, spontaneous liquefaction of N_2 occurs. Under these conditions, consecutive molecular layers of nitrogen can be adsorbed on the solid surface. In monolayer adsorption, all the adsorbed molecules are in contact with the surface layer of the sample, whereas in multilayer adsorption, the adsorption space accommodates more than one layer of molecules, so that not all adsorbed molecules are in direct contact with the surface layer of the sample. The surface area of a given sample, for example a hybrid material, may be calculated from monolayer adsorption. Therefore, it is necessary to quantify the amount of N_2 adsorbed in a unimolecular layer.

The graph representing the relationship, at constant temperature, between the amount adsorbed and the equilibrium pressure of the gas is known as the adsorption-desorption isotherm.¹⁵³ In some cases, a hysteresis loop is observed when adsorption and desorption curves do not coincide. In 1940, S. Brunauer, L.S. Deming, W.E. Deming and E. Teller classified isotherms in five different types. Later, in 1985, the International Union of Pure and Applied Chemistry (IUPAC) expanded this classification to six types.¹⁵⁴ Types I, II and IV are the most frequently observed (Figure 6.6).

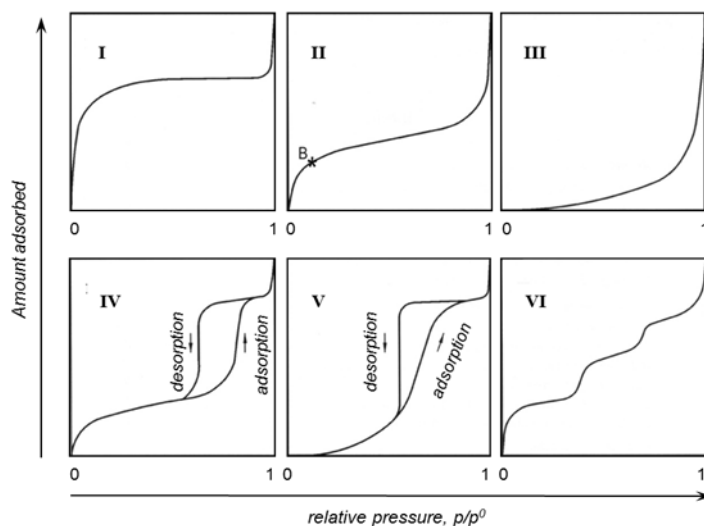


Figure 6.6. Types of isotherm according to the IUPAC rules.¹⁵⁴

(a) Type I isotherms are given by microporous solids with relatively small external surfaces, where adsorption takes place at low relative pressures.

(b) Type II isotherms are normally obtained with non-porous or macroporous solids. Some mesoporous solids also give this adsorption curve when monolayer adsorption is observed at a low relative pressure and saturation at a high relative pressure, but without a hysteresis loop. The interaction between adsorbate and adsorbent is strong. Point B represents the beginning of the almost linear middle section of the isotherm. It is often taken to indicate the stage at which monolayer coverage is complete and multilayer adsorption is about to begin.

(c) Type III isotherms are observed in systems with weak adsorbate-adsorbent interactions. Type III is not common, but a number of systems (for example, nitrogen on polyethylene) show this profile. These isotherms do not exhibit point B due to their convex curvature over the entire range of pressure,

(d) Type IV isotherms are generally given by mesoporous materials. They have a characteristic hysteresis loop, which is associated with capillary condensation taking place in mesopores, and the limiting uptake over a range of high relative pressure. In Type IV isotherms there is an important increase in the amount adsorbed at upper-intermediate relative pressure and the filling mechanism corresponds to a *monolayer-multilayer* adsorption.

(e) Type V isotherms arise from a deviation of Type IV. Adsorption-desorption is observed at relative pressure $p/p^0 \approx 0.5$.

(f) Type VI isotherms are obtained when stepwise multilayer adsorption on uniform non-porous surfaces occurs. The sharpness of the steps depends on the system and the temperature, whereas the step-height represents the monolayer capacity of each adsorbed layer. These isotherms are typically obtained with argon or krypton on graphitised carbon at liquid nitrogen temperature.

Many hybrid materials show adsorption isotherms which are actually a combination of types I-VI. Mesoporous materials can also contain a certain number of micropores, which in a Type IV

isotherm can be recognized because of the higher adsorption that is observed at low relative pressure.

The hysteresis appearing in the multilayer range of isotherms is usually associated with capillary condensation in mesoporous structures. This phenomenon occurs when the gas is first adsorbed in pores, where it can condense to the liquid state after sufficient gas is supplied. Such hysteresis loops may exhibit a variety of shapes classified by IUPAC in four types, of which types H1 and H2 are the most frequent (Figure 6.7). Although the factors affecting adsorption hysteresis are not fully understood, the shapes of hysteresis loops have often been identified as having specific pore structures.

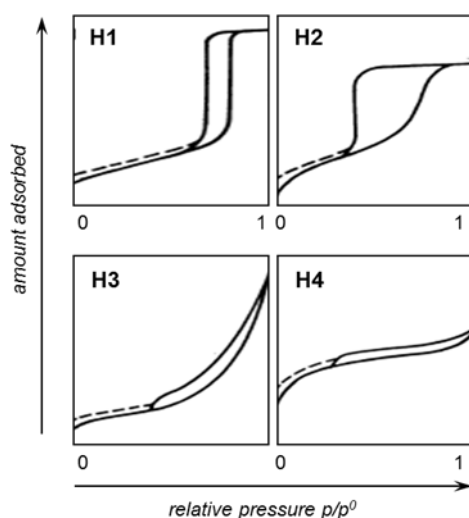


Figure 6.7. Types of hysteresis loops according to the IUPAC rules.¹⁵⁴

(a) *Type H1* has adsorption and desorption branches that are almost parallel and is often associated with a specific pore structure. Mesoporous materials such as SBA-15, MCM-41 and MCM-48 exhibit this type of hysteresis.

(b) *Type H2* has a hysteresis loop that is difficult to interpret and is representative of highly disordered materials. The desorption branch normally presents a more pronounced slope with respect to the adsorption branch.

(c) *Type H3* is observed in aggregates of plate-like particles giving rise to slit-shaped pores. An aggregate is an assembly of loosely coherent particles.

(d) A *Type H4* loop is associated with narrow slit-like pores.

The curve shape gives information about the pore size (p/p^0 from the hysteresis point), the pore volume (the area limited by adsorption and desorption curves) and the diameter distribution (related with the slope of the hysteresis).

Several mathematical transformations have been developed to transform the adsorption isotherm data into a calculated surface area but the Brunauer-Emmett-Teller (BET)¹⁵⁵ method is the most widely used, although it is not suitable for the measurement of the specific surface area of microporous materials. The Barrett-Joyner-Halenda (BJH)¹⁵⁶ method determines the

pore size distribution, while the t-Plot calculation provides information about the contribution of micro- and mesopores in the material.

6.1.1.2.5. Powder X-ray diffraction

The organization of hybrid materials can be measured with the powder X-ray diffraction (PXRD) technique. Under irradiation, the interaction of the repeating planes of a sample with an incident beam is described by Bragg's law:

$$n \cdot \lambda = 2 d_{hkl} \sin \theta$$

In this equation, θ stands for the angle between the incident beam and the plane, d_{hkl} represents the distance between two consecutive identical planes, and λ is the incident beam wavelength (Figure 6.8).

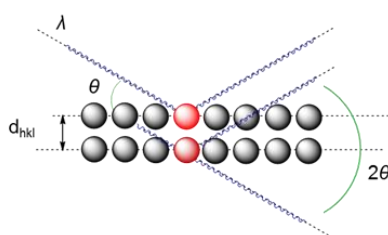


Figure 6.8. Schematic representation of Bragg's law.

The distance between planes can be determined from the incident beam and the measured dispersion angles. Normally, the PXRD plot represents the intensity (I) with respect to a parameter called q , which is calculated as follows $q = \frac{4\pi \sin \theta}{\lambda}$. The relationship between q and d is the following: $q = 2\theta / d$. When a material is organized, well-defined peaks can be observed in the plot and from their pattern (Figure 6.9) it is possible to know the type of organization (e.g. hexagonal, lamellar, cubic, worm-like, etc.). On the other hand, amorphous materials do not allow clear signals to be obtained.

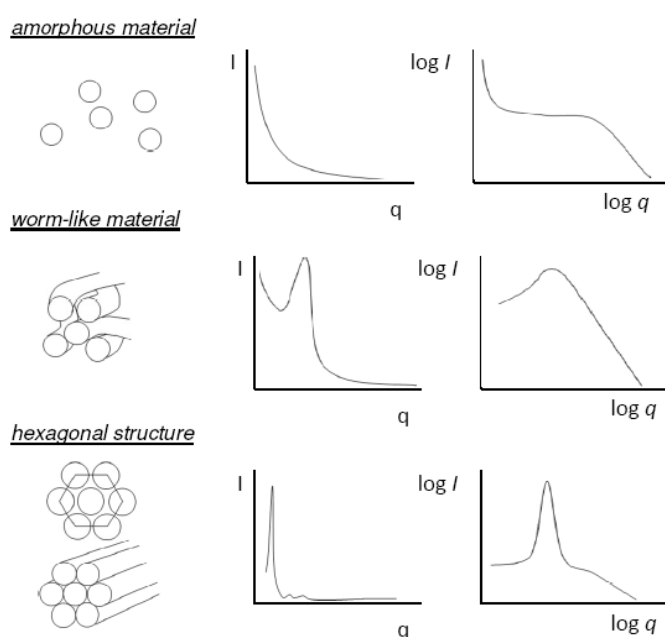


Figure 6.9. Examples of powder X-ray diffraction patterns.

To conclude it should be mentioned that only the combination of several different techniques allows full characterization of hybrid materials. Usually the information provided by the different analyses is compared in order to better understand the effect of the structure and morphology on the properties of hybrid materials.

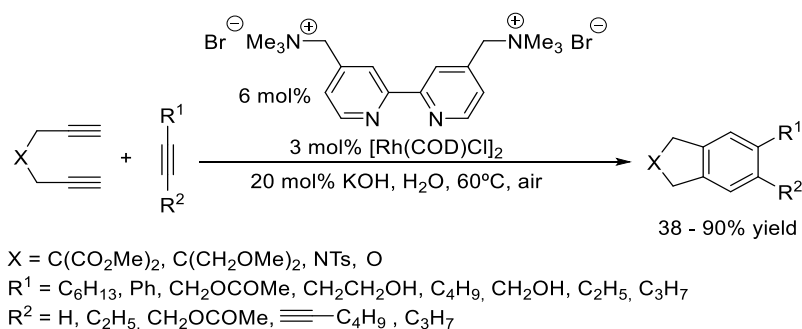
6.1.2. Recyclable catalysts in [2+2+2] cycloadditions

One of the most important challenges in transition metal catalysis is the recovery and reuse of the catalyst. The use of ionic liquids, or molten salts, as immobilizing agents represent the first cases in which the catalyst in [2+2+2] cycloaddition reactions was recovered and reused. The ability of the molten salts to immobilize catalysts favours their recovery at the end of the process.¹⁵⁷ Tagliatesta et al.^{157a} studied the recyclability of Ru-porphyrin catalyst in ionic liquids in the cyclooligomerization of arylethyne. The ionic liquids tested were 1-butyl-3-methylimidazolium hexafluorophosphate, {[Bmim][PF₆]} and 1-octyl-3-methyl-imidazolium hexafluorophosphate, {[Omim][PF₆]}]. The system proved to be recyclable for up to 5 runs with no effect on the yields.

Our group^{157b} contributed to this field by studying the [2+2+2] cycloaddition of unsaturated azamacrocycles catalysed by rhodium and palladium complexes in molten tetra-*n*-butylammonium bromide. When Wilkinson's catalyst was tested, the cycloisomerised product was obtained in excellent yields, but when the catalyst was used in two more runs the yield dropped. When palladium(II) chloride and palladium(II) acetate were used the result was quite similar, good yields were obtained for the first run, but when it was tried in further runs the yield dropped. A TEM analysis was performed when PdCl₂ was used revealing palladium nanoparticles as the active catalytic species.

Yu et al.^{157c} reported the use of gold nanoparticles functionalized with palladium(II) on the surface as a catalyst for the intermolecular [2+2+2] cycloaddition of monoalkynes. They studied the intermolecular reaction in {[Bmim][PF₆]} under microwave irradiation. The catalyst could be reused up to nine times and a gradual decrease in the yield was observed from the fifth cycle onwards.

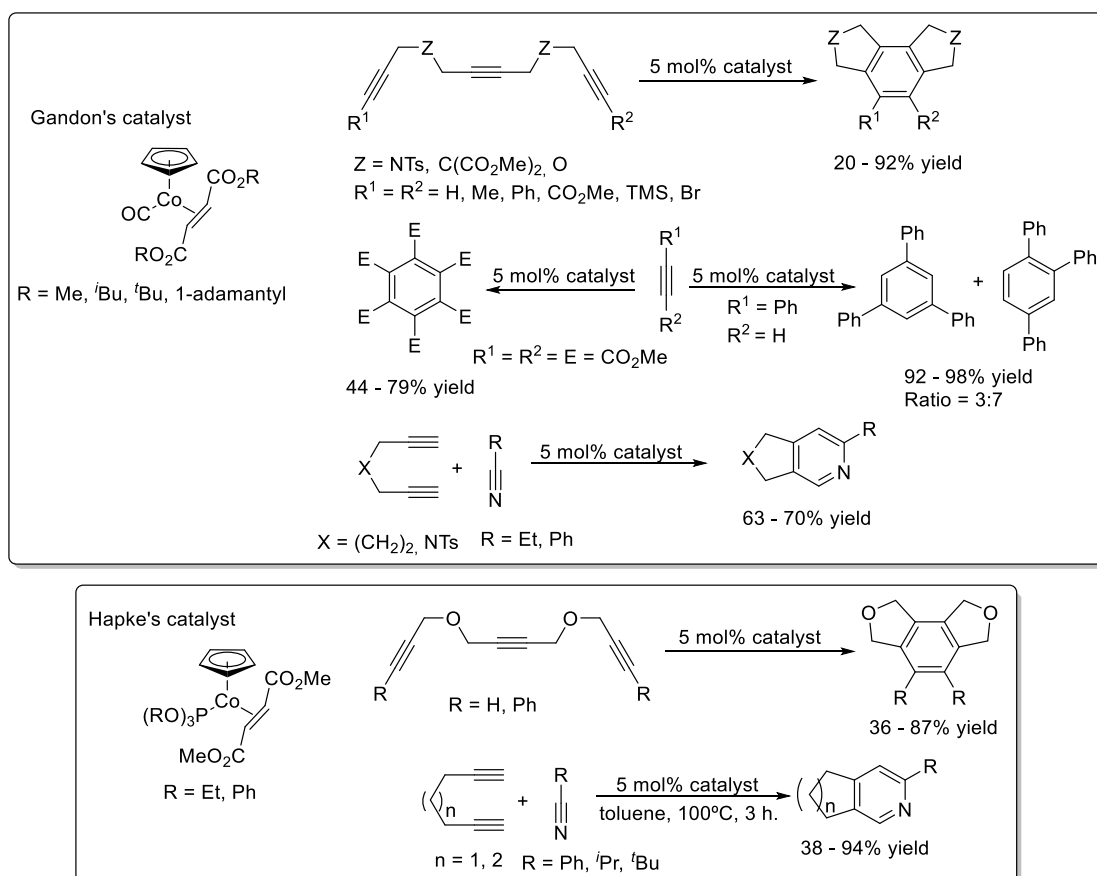
Tsai et al.¹⁵⁸ described the use of a catalytic system consisting of [Rh(COD)Cl]₂/cationic bipyridine in the [2+2+2] cycloaddition reaction of different 1,6-diynes and monoalkynes in aqueous media in the presence of air (Scheme 6.8). The catalyst was recovered by simple liquid-liquid extraction and the aqueous phase could be reused three times, although the metallic complex was gradually deactivated.



Scheme 6.8. Rh-catalysed [2+2+2] cycloaddition reaction in aqueous media.

Air-stable complexes that can be recovered by column chromatography have also been reported as suitable recyclable catalysts for the [2+2+2] cycloaddition. Two examples featuring [CpCoL(fumarate)] complexes have been studied.¹⁵⁹ In 2008 Gandon et al.^{159a} reported the use of [CpCo(CO)(fumarate)] complexes in the intramolecular and intermolecular [2+2+2] cycloaddition of alkynes, and in the partial intramolecular version between diynes and nitriles to form pyridines (Scheme 6.9). The catalyst could be recovered by column chromatography with undiminished catalytic activity.

In 2013 Hapke et al.^{159b} used a similar catalytic system but changing the CO ligand for a phosphite (P(OR)₃). This catalytic system proved to be effective in the intramolecular [2+2+2] cycloaddition of triynes and in the partial intramolecular version between diynes and nitriles to form pyridines (Scheme 6.9). The complex could be isolated quantitatively after at least three successive cycles by column chromatography without any observable decrease in the yield of the cyclotrimerisation product.

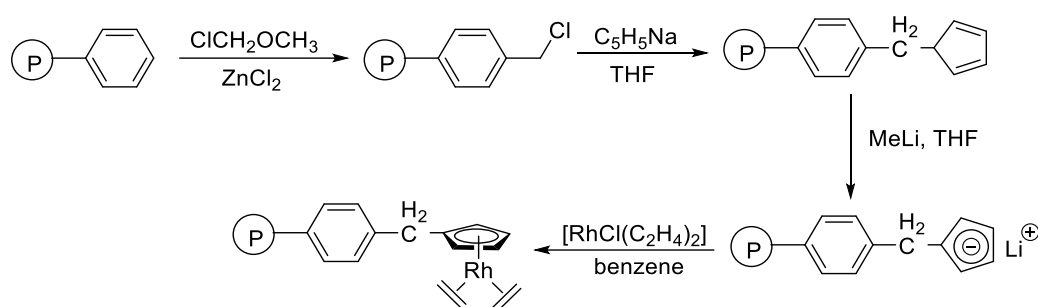


Scheme 6.9. Air-stable [CpCoL(fumarate)] complexes for [2+2+2] cycloaddition reactions.

Although homogeneous catalysts offer many advantages over heterogeneous catalysts, such as better activity and chemoselectivity, one of the most commonly employed strategies when facing the problem of the recovery and reuse of the catalyst is to immobilize it on an insoluble support.¹⁶⁰ In the particular case of [2+2+2] cycloaddition reactions, there are few examples of this kind of supported catalyst in the literature.

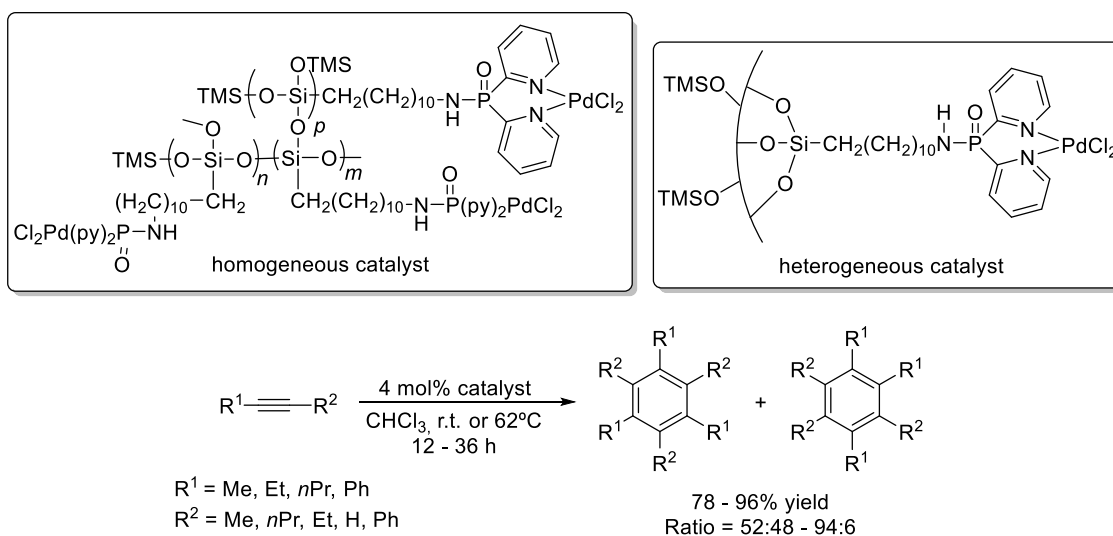
The first support used for metal-catalysed [2+2+2] cycloadditions was polystyrene.¹⁶¹ Ingrosso et al.^{161a} reported polystyrene immobilized [CpRh(C₂H₄)₂] complexes for the synthesis of pyridine

derivatives (Scheme 6.10). Although several problems were observed (low activity and chemoselectivity, as well as poor durability of the heterogeneous catalysts), these represent the first heterogeneous catalysts for the synthesis of pyridines.



Scheme 6.10. Synthesis of a polystyrene immobilized $[\text{CpRh}(\text{C}_2\text{H}_4)_2]$ complex.

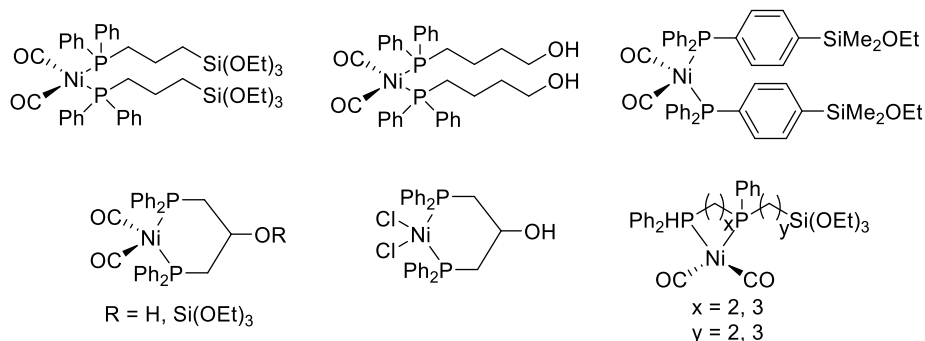
Silica supported catalysts have also been used in [2+2+2] cycloaddition reactions as a strategy to recover the catalyst by simple filtration.¹⁶² Yu et al.^{162c} described the preparation and characterization of homogeneous and heterogeneous Pd(II) complexes tethered to a polysiloxane skeleton. The solubility of the palladium complexes is controlled by the molecular weight and degree of cross-linking of the polysiloxane skeleton (Scheme 6.11). These complexes proved to be effective in the intermolecular [2+2+2] cycloaddition of monoalkynes, affording the cycloadducts in excellent yields. Moreover, the complexes could be recovered and recycled up to six times with no effect on the conversion.



Scheme 6.11. Pd(II) complexes tethered to a polysiloxane skeleton for [2+2+2] cycloadditions.

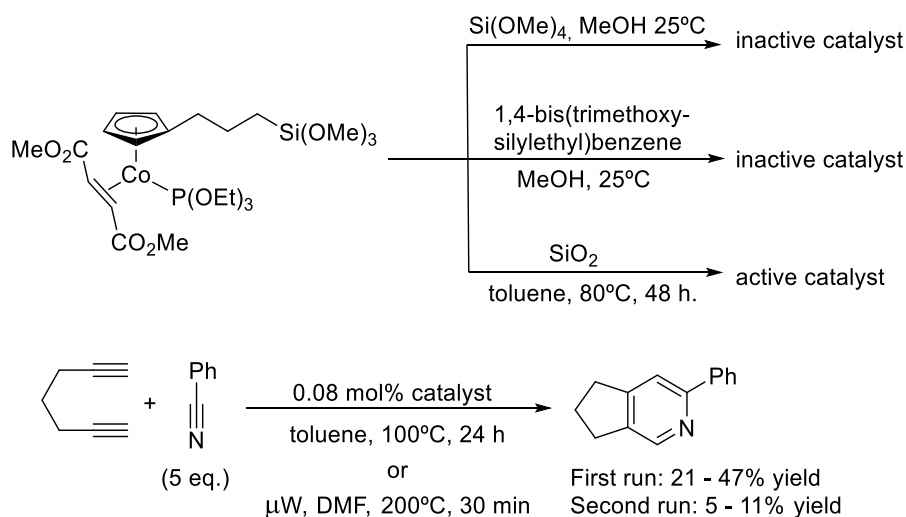
Blümel et al.^{162b} described nickel catalysts with phosphine ligands bearing alkyl chains capped with alkoxy-silyl or alcohol groups (Scheme 6.12). These ligands were immobilized on commercially available silica and used as catalysts in the cyclotrimerization of phenylacetylene. On studying the solvent effect on the immobilized catalysts, it was found to play an important role as the amount of detached ligand depended on the solvent used. Moreover, for complexes that did not contain triethoxysiloxane groups, the immobilization on silica was weak (C-O-Si bonding is much weaker than Si-O-Si bonds) and were readily cleaved in the presence of organic solvents or water. Besides these particular cases, all the immobilized catalysts presented similar activity. The immobilized catalyst was recovered by simple filtration and was reused up to twelve

times, although with a gradual decrease in the conversion. The selectivity of the immobilized catalysts was also affected in the recycling experiments: in a first run all catalysts presented high selectivity towards the 1,2,4-cycloadduct, but the ratio between the 1,2,4-cycloadduct and 1,3,5-cycloadduct gradually diminished until plateauing at a 1:1 ratio.



Scheme 6.12. Ni-complexes immobilised on silica.

At about the same time that the results that will be presented in this chapter were carried out, Hapke's group^{162a} reported a cobalt-supported catalyst for [2+2+2] cycloadditions. They modified the previously described fumarate complex (Scheme 6.9) with a propyltrimethylsilyl group in order to obtain silica-supported catalysts. Two heterogeneous catalysts were synthesized by using the sol-gel method and one by using the grafting method (Scheme 6.13). Only the catalyst obtained from the grafting method was active in the partial intramolecular [2+2+2] cycloaddition between a diyne and a nitrile. A possible explanation could be that the catalysts obtained with the sol-gel methodology have smaller pore size, thus avoiding the penetration of the starting materials in the silica matrix. Although the grafted complex shows moderate activity in the first cycle, the yield drops in consecutive runs.



Scheme 6.13. Silica-immobilized Co-catalyst for the [2+2+2] cycloaddition between diynes and nitriles.

Finally, and as was explained in section 1.1.3.1, our group in collaboration with Caminade's group reported the use of phosphoramidite-type dendrimers as suitable ligands for the rhodium-catalysed [2+2+2] cycloaddition reaction.⁴⁷ The dendrimers used could be recovered by precipitation when hexanes were added to the reaction mixture at the end of the reaction.

By simple filtration the dendrimers were recovered and reused up to three cycles with no effect on the yield or enantiomeric excess of the reaction studied.

Given the importance of the recovery of the catalyst and the few previous reports found in the particular case of the transition metal catalysed [2+2+2] cycloaddition reactions, and in the framework of a collaboration with Dr. Pleixats' group of the *Universitat Autònoma de Barcelona*, we envisaged the heterogeneization of rhodium-based catalysts by the sol-gel and grafting methodologies, and their application in the [2+2+2] cycloaddition of alkynes. In previous works Pleixats' group reported transition-metal catalysts immobilized on organic-inorganic hybrid silica materials through an NHC ligand. Using this methodology they have been able to immobilize ruthenium catalysts for methathesis reactions,^{131h} palladium catalysts for Suzuki, Heck and Sonogashira reactions,¹³¹ⁱ and gold catalysts for the rearrangement of allylic esters and the cycloisomerization of γ -alkynoic acids.^{131b}

6.2 Results and discussion

6.2.1. Preparation of the hybrid silica materials

As a first step, we aimed to synthesize two different imidazolium-derived salts bearing trialkoxysilyl groups (Figure 6.10).

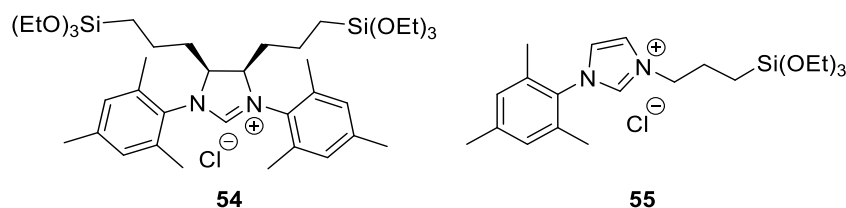
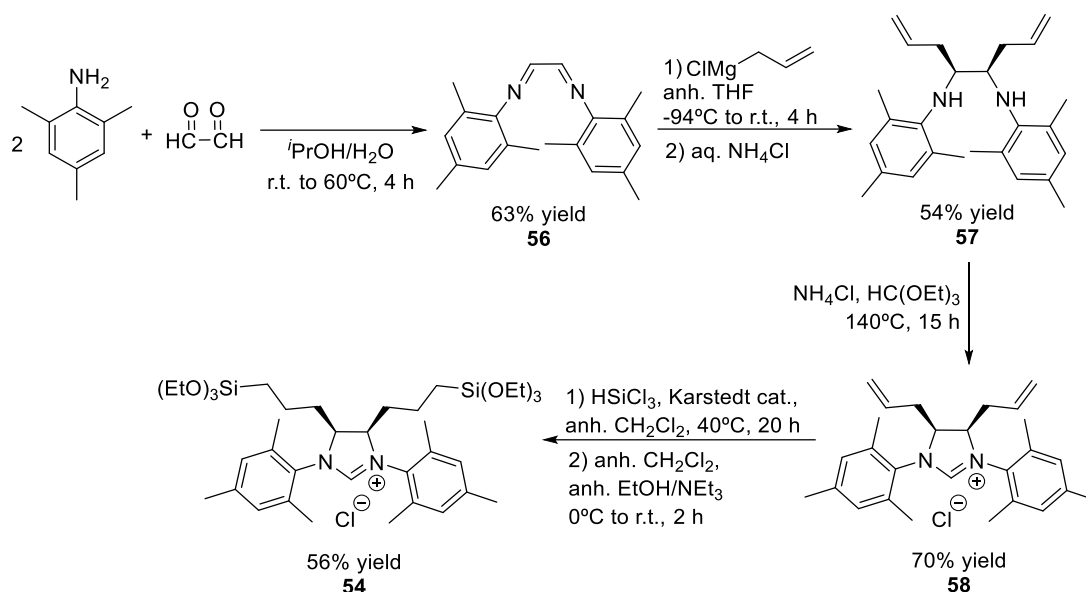


Figure 6.10. Imidazolium salts **54** and **55** containing triethoxysilyl groups.

Imidazolium salt **54** contains two trialkoxysilyl groups, attached through a propyl chain to the carbon backbone of a dihydro-imidazolium ring. On the other hand, imidazolium salt **55** consists of one trialkoxysilyl group attached, also through a propyl chain, to one of the nitrogen atoms of the imidazole ring. These salts will then be used as ligands for rhodium and to synthesize hybrid organic-inorganic silicas.

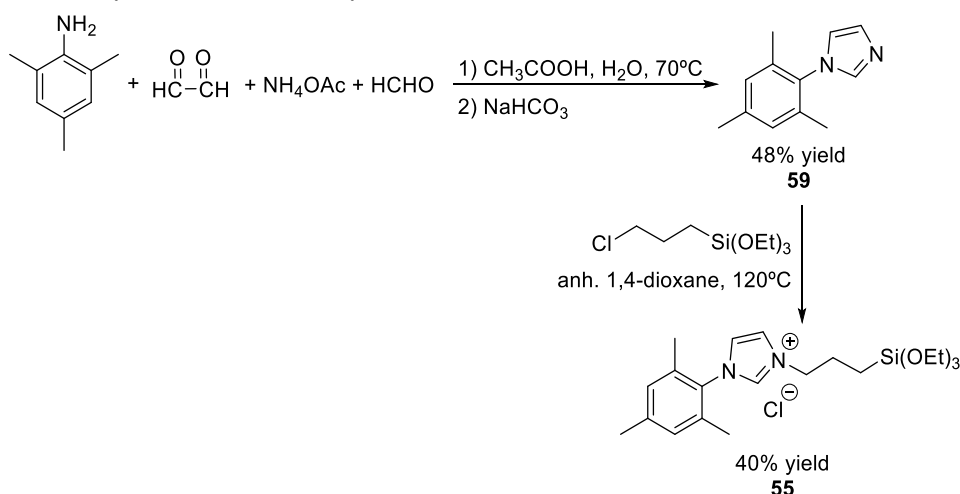
6.2.1.1. Synthesis of the N-heterocyclic carbene (NHC) ligand precursors

The synthesis for the bisilylated salt **54** is summarized in Scheme 6.14. The first step was the formation of the bisimine **56** from the condensation of glyoxal and 2,4,6-trimethylaniline.¹⁶³ Subsequent addition of two equivalents of allylmagnesium chloride afforded a mixture of diastereoisomers, from which the pure *meso* compound **57** could be isolated with a 54% yield by crystallization, as previously reported.¹⁶⁴ Diamine **57** underwent cyclization using triethylorthoformate and ammonium chloride to give a 70% yield of the corresponding dihydroimidazolium salt **58**. Finally, **54** was obtained by an hydrosilylation reaction of **58** with trichlorosilane in CH_2Cl_2 in the presence of Pt Karstedt catalyst and further treatment with anhydrous EtOH and NEt_3 .



Scheme 6.14. Synthetic pathway for imidazolium salt **54**.

The synthesis of monosilylated imidazolium salt **55** is summarized in Scheme 6.15. 1-mesitylimidazole **59** was prepared by a Debus-Radziszewski synthesis using 2,4,6-trimethylaniline, glyoxal, formaldehyde and ammonium acetate in aqueous acetic acid solution. The next step was carried out under the conditions described by Dastgir et al.,¹⁶⁵ which consisted of the alkylation of the imidazole ring with 3-(chloropropyl)triethoxysilane in refluxing dioxane to obtain a 40% yield of the monosilylated imidazolium salt **55**.



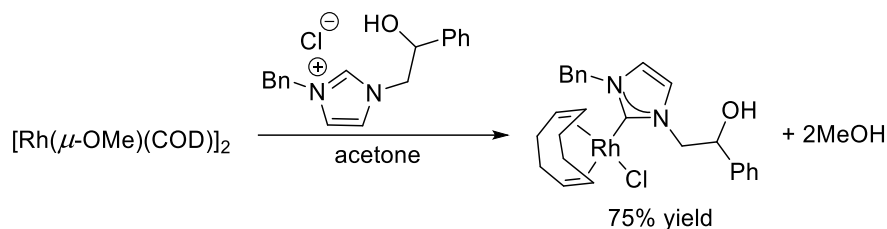
Scheme 6.15. Synthetic pathway for imidazolium salt **55**.

6.2.1.2. Synthesis of Rh-carbene complexes **60** and **61**

The first attempt to synthesize the Rh-carbene complex with imidazolium salt **54** followed the method described by Dastgir et al.¹⁶⁵ This method consisted of the treatment of the imidazolium salt with Ag₂O to afford NHC-Ag(I) complex followed by transmetalation with [Rh(μ-Cl)(COD)]₂ dimer. However, in our case only decomposition to elemental silver and the recovery of **54** were observed.

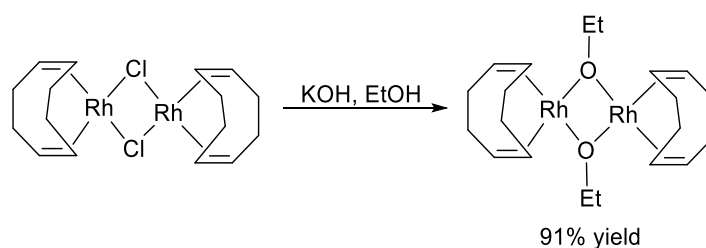
Recently, Esteruelas et al.¹⁶⁶ have described an alternative method which used complex [Rh(μ-OMe)(COD)]₂ to form the corresponding Rh-carbene complex directly. The methoxide anion

deprotonates the imidazolium ring, releasing methanol from the metal centre. Subsequent coordination of the resulting NHC ligand and the chloride anion to the rhodium atom affords the desired Rh-carbene complex (Scheme 6.16).



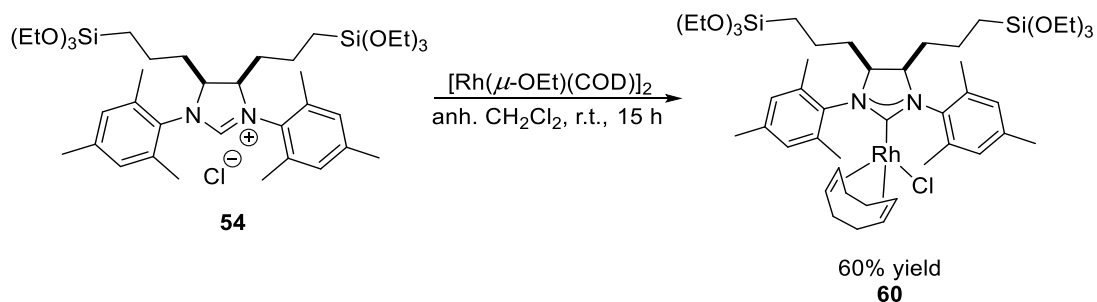
Scheme 6.16. Synthesis of Rh-NHC complex described by Esteruelas et al.

As the imidazolium salts synthesized bear triethoxysilyl groups, and in order to avoid side-reactions, we decided to use the analogous ethoxy-complex to that synthesized by Esteruelas. Given that $[\text{Rh}(\mu\text{-OEt})(\text{COD})]_2$ complex is not commercially available, we prepared it in our laboratory by a nucleophilic substitution of the chlorides of the $[\text{Rh}(\mu\text{-Cl})(\text{COD})]_2$ dimer for ethoxides (Scheme 6.17).¹⁶⁷



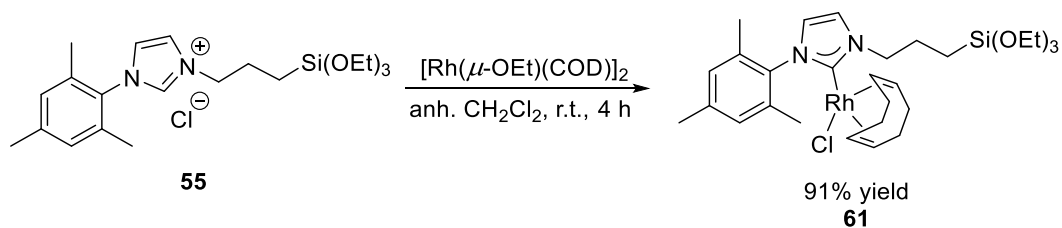
Scheme 6.17. Synthesis of $[\text{Rh}(\mu\text{-OEt})(\text{COD})]_2$

When imidazolium salt **54** was mixed with $[\text{Rh}(\mu\text{-OEt})(\text{COD})]_2$ in anhydrous dichloromethane at room temperature for 15 hours, the desired complex **60** was obtained in a 60% yield (Scheme 6.18).



Scheme 6.18. Synthesis of NHC-rhodium complex **60**.

Applying the same procedure to imidazolium salt **55** a 91% yield of the monosilylated rhodium complex **61** was obtained in 4 hours (Scheme 6.19).



Scheme 6.19. Synthesis of NHC-rhodium complex **61**.

6.2.1.3. Spectroscopic characterization of Rh-NHC complexes **60** and **61**

Both complexes **60** and **61** were fully characterized by ESI-HRMS, ^1H and ^{13}C -NMR. ESI-HRMS spectra of complex **60** showed a peak at $m/z = 925.4470$, corresponding to $[\text{M-Cl}]^+$. The same behaviour was observed for complex **61**, which showed a peak at $m/z = 601.233$, which also corresponded to the same chloride loss.

As a result of hindered rotation around the carbene carbon-rhodium bond, two different sets of signals in a 4:1 ratio are observed in the ^1H and ^{13}C -NMR spectra of complex **60**. Six different signals corresponding to the methyl groups in the aromatic ring can be seen in the ^1H -NMR spectrum: the major isomer presented three signals at 2.26, 2.30 and 2.63 ppm whereas the signals corresponding to the minor isomer appeared at 2.29, 2.36, and 2.52 ppm (Figure 6.11).

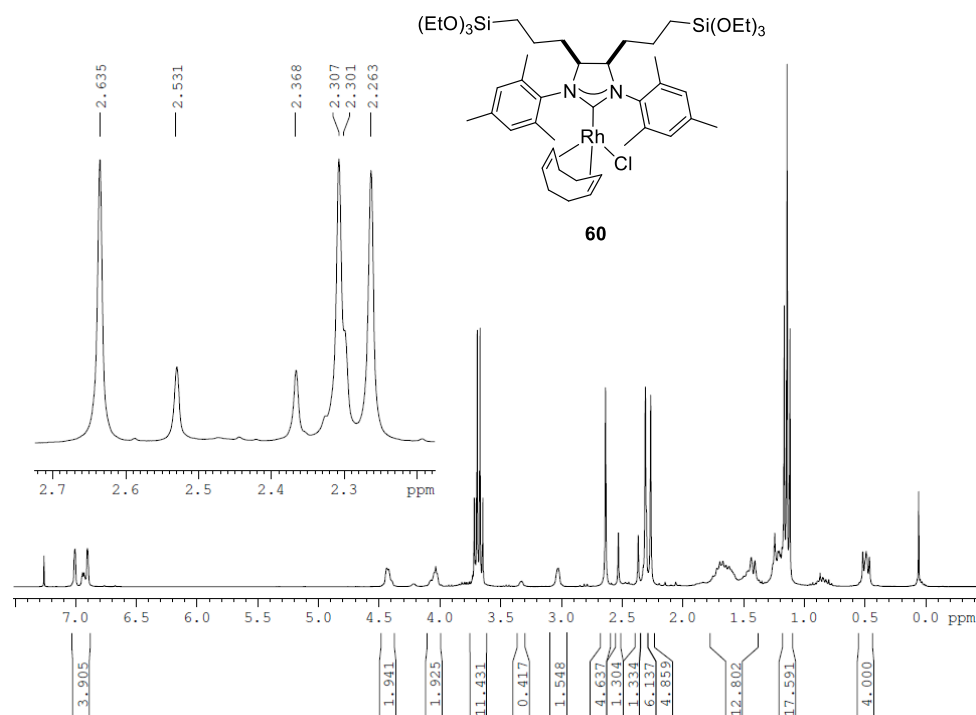


Figure 6.11. ^1H -NMR of complex **60**.

The ^{13}C -NMR spectrum displays two sets of doublets: at 67.1 ppm ($J_{\text{Rh-C}} = 14.5$ Hz, major isomer) and 68.3 ppm ($J_{\text{Rh-C}} = 14.0$ Hz, minor isomer), corresponding to the methylene carbons of the COD ligand, and at 96.8 ppm ($J_{\text{Rh-C}} = 6.9$ Hz, major isomer) and 96.5 ppm ($J_{\text{Rh-C}} = 7.0$ Hz, minor isomer), corresponding to the olefinic carbons of the COD ligand. The carbene carbon atom of the NHC ligand coordinated to Rh appeared as a doublet at 213.2 ppm with a coupling constant of $J_{\text{Rh-C}} = 48.0$ Hz (Figure 6.12). High-temperature ^1H -NMR experiments at up to 95°C were carried out in an unsuccessful attempt to observe the interconversion between the two isomers. The formation of two diastereoisomers has previously been described by Köhler et al.¹⁶⁸ in the synthesis of a Rh complex derived from 4,5-diallyl-1,3-dimesityl-4,5-dihydroimidazolium chloride, which in our case is a precursor of the synthesis of **54**. In this study, the authors also found that no dynamic process was observed by variable-temperature ^1H -NMR experiments up to 70°C.

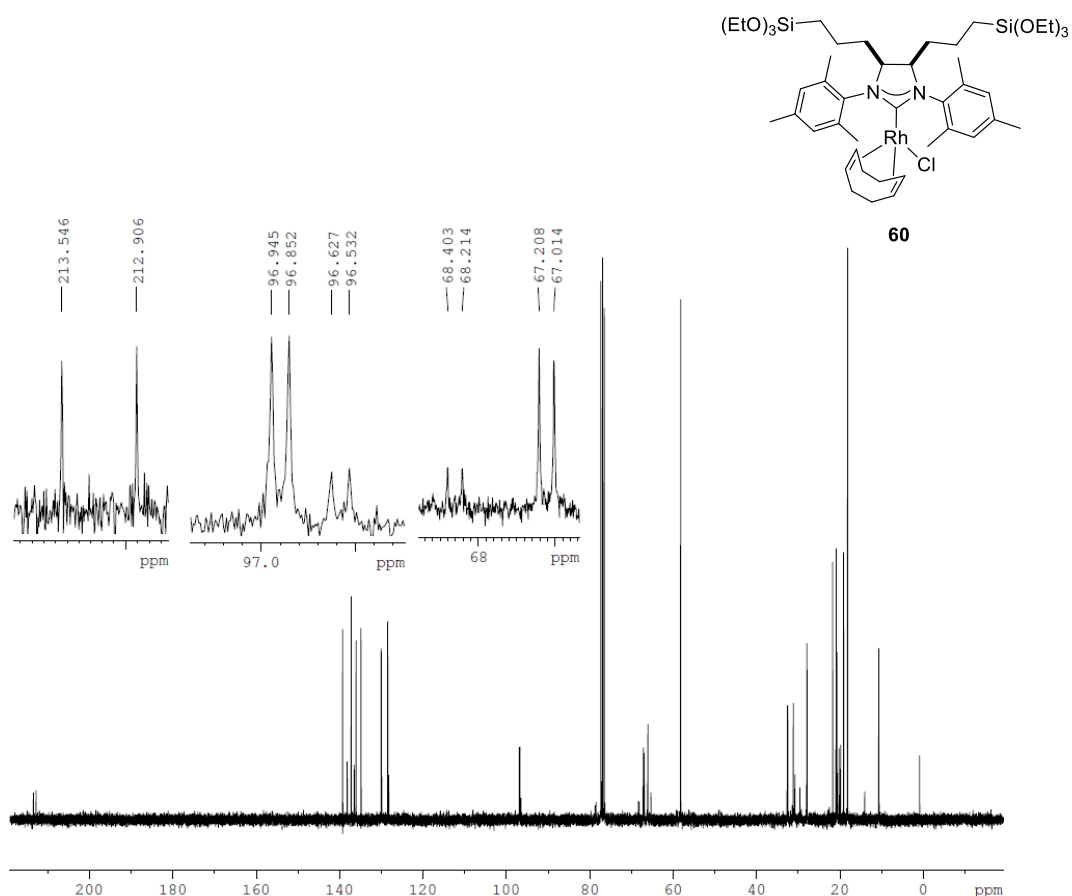


Figure 6.12. ^{13}C -NMR of complex **60**.

In an attempt to identify the relative geometry of the two diastereoisomers, NOESY experiments were planned. Since Rh complex **60** containing triethoxysilyl groups is prone to be hydrolyzed under air conditions, the NMR study was performed with the already described Rh-carbene complex derived from the allylic precursor of imidazolium salt **54** (named **60-allyl**), which analogously gives a double set of signals with a 4:1 isomers ratio. The square planar rhodium complexes feature the carbene ligand in a perpendicular orientation to the square-plane of the complex and *cis* to the chlorine atom. Both diastereoisomers have a plane of symmetry corresponding to the square-plane of the complex. The NOESY data reveal that the two allyl chains of the major isomer point to the Cl atom while in the minor isomer they point to the COD ligand (Figure 6.13).

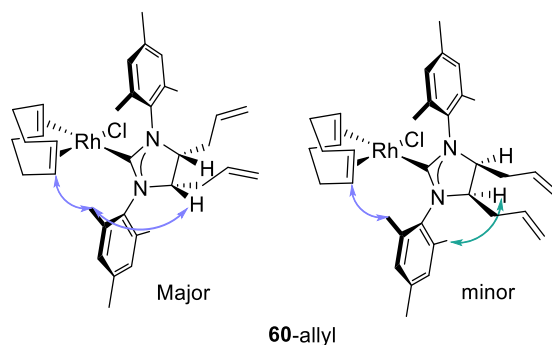


Figure 6.13. Representation of the two isomers of **60-allyl** showing the major NOESY correlations observed.

Whereas in the major isomer both the olefin COD proton and the H of the NHC core give a cross-peak with the same *ortho* methyl of the mesityl, in the minor isomer both protons correlate to a different *ortho* methyl of the mesityl which is perpendicular to the dihydroimidazole ring. These results can be extrapolated to allow us to conclude that the same type of structures would be found in complex **60**.

In the $^1\text{H-NMR}$ spectra of complex **61** (Figure 6.14), three different methyl and two aromatic signals corresponding to the mesityl ring were observed. The methylene group attached to the second nitrogen atom of the NHC ligand appeared overlapped with COD ligand signals at around 2 ppm. Overlapping was also found at 1.5 ppm between the signals of the central CH_2 unit of the silylated chain and protons of the cyclooctadiene ligand. The CH_2 group next to the Si atom appeared at 0.77 ppm as a triplet.

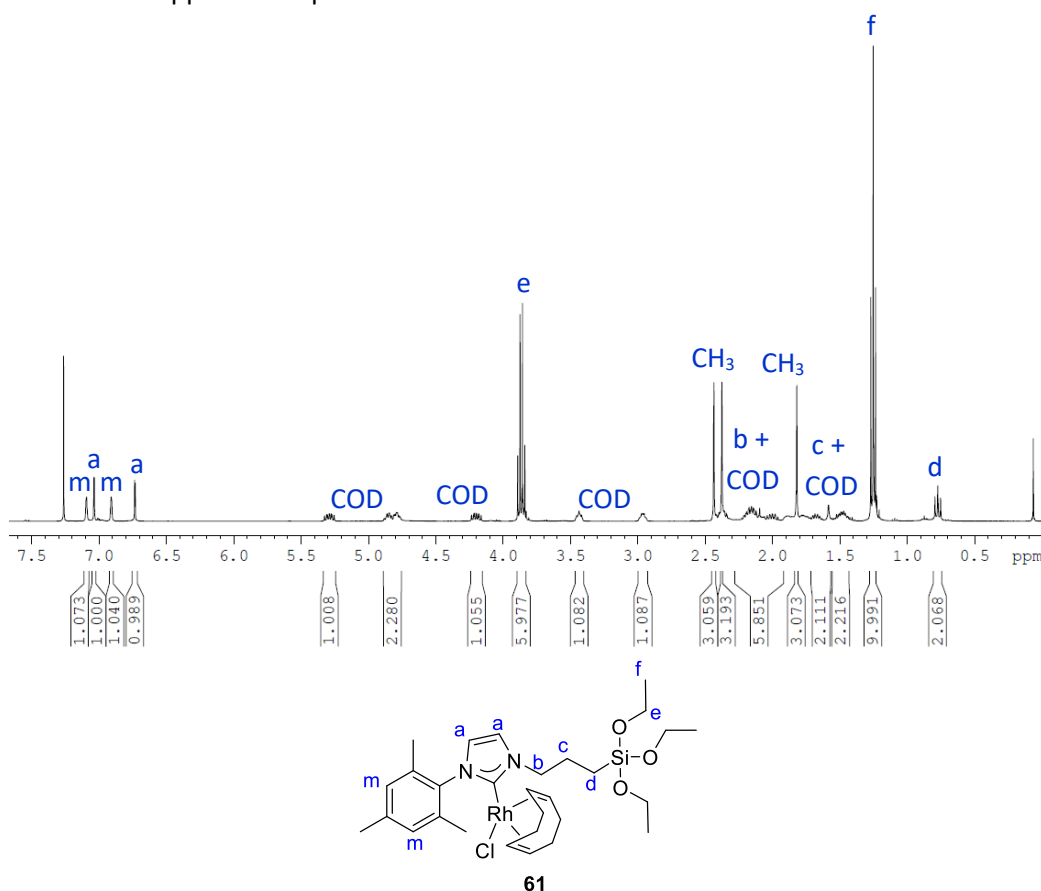


Figure 6.14. $^1\text{H-NMR}$ spectrum of complex **61**.

In the $^{13}\text{C-NMR}$ spectrum (Figure 6.15), two doublets at 96.7 and 96.9 ppm corresponded to the olefinic carbons of the COD ligand (Rh-C coupling constants of 7.3 Hz and 7.1 Hz, respectively).

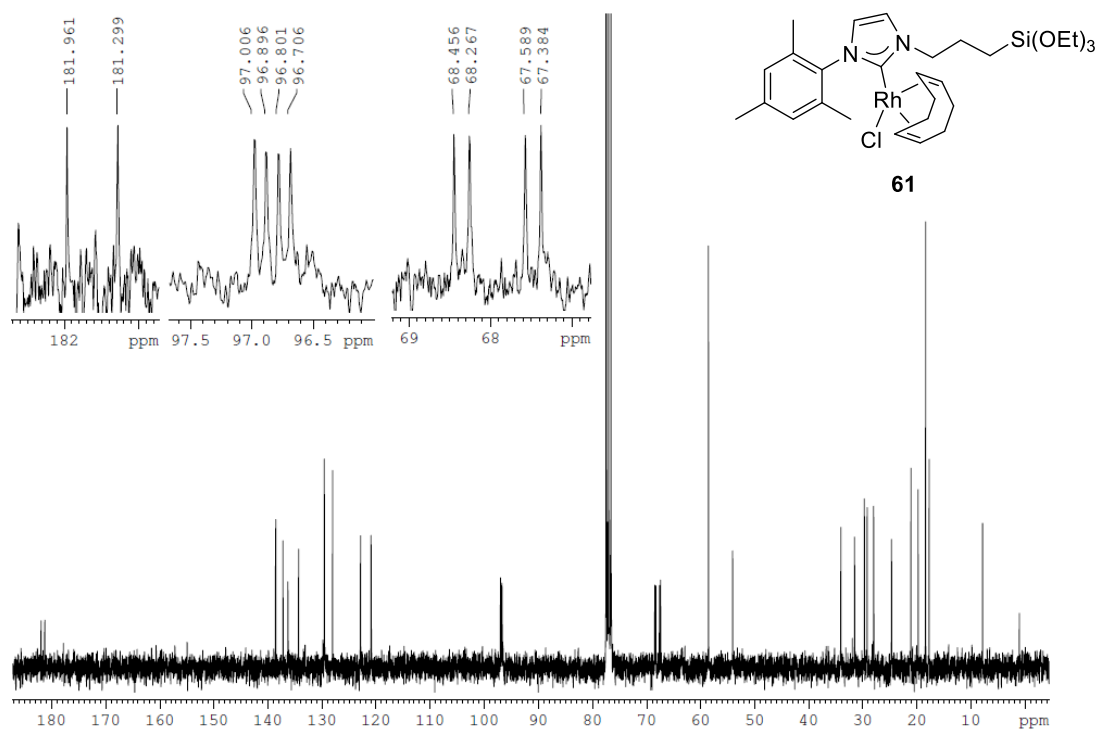
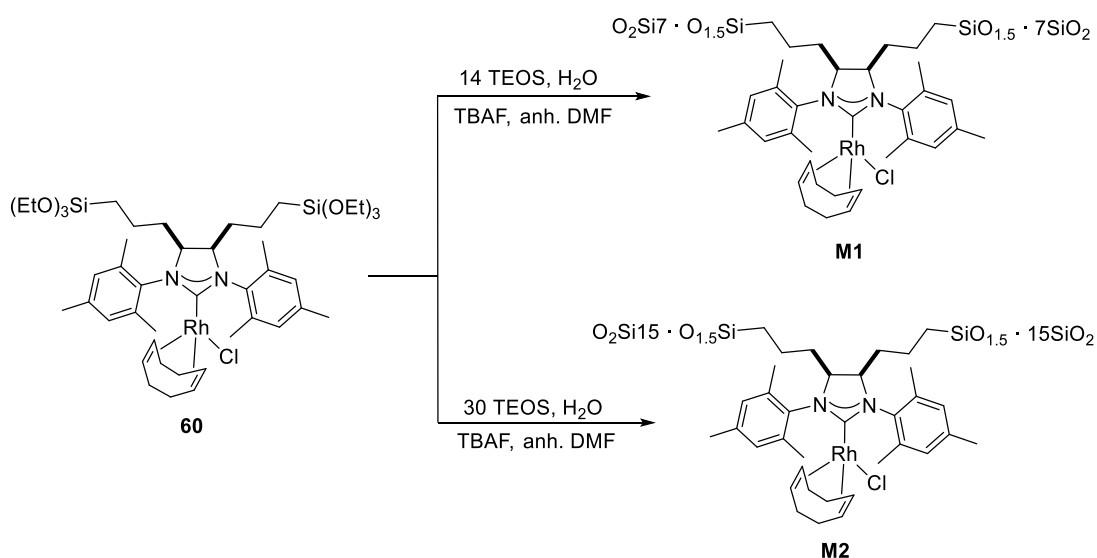


Figure 6.15. ^{13}C -NMR spectrum of complex **61**.

6.2.1.4. Preparation of organic-inorganic hybrid silica materials

Once the NHC-Rh complexes **60** and **61** were obtained and fully characterized, the organic-inorganic hybrid silica materials were prepared.

Two different materials were prepared from complex **60** by cogelification with tetraethoxysilane: one with a molar ratio of **60** and TEOS 1:14 (**M1**) and another with a molar ratio of 1:30 (**M2**) (Scheme 6.20).



Scheme 6.20. Preparation of hybrid silica materials **M1** and **M2**.

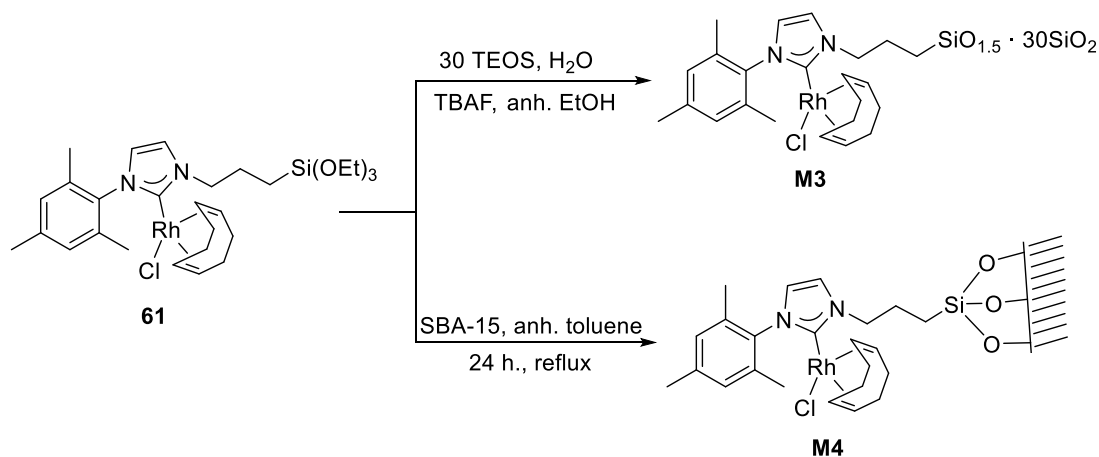
The reactions were performed under nitrogen atmosphere in anhydrous DMF at room temperature under nucleophilic conditions using a stoichiometric amount of water (with respect

to the ethoxy groups) and tetrabutylammonium fluoride as the catalyst (1 mol% with respect to Si). Both solutions gellified after one hour and were aged for six days at room temperature under nitrogen atmosphere (Figure 6.16). They were then filtered and washed successively with ethanol, acetone and anhydrous diethyl ether. The resulting powders were dried overnight under vacuum at 40°C to afford both materials as an orange powder.



Figure 6.16. Gel formed with complex **60** and TEOS (molar ratio 1:30).

With complex **61** two different materials were also prepared, this time using different methods: one by cogelification with tetraethoxysilane at molar ratio 1:30 (**M3**) and the other by grafting with SBA-15 (**M4**) (Scheme 6.21). The procedure to obtain **M3** was the same as that described for complex **60**. **M4** was prepared using the grafting method: complex **61** and SBA-15 were heated in anhydrous toluene at reflux for 24 hours under nitrogen atmosphere. The suspension was treated with the same procedure as **M1** and **M2**.



Scheme 6.21. Preparation of hybrid silica materials **M3** and **M4**.

6.2.1.5. Characterization of hybrid silica materials

The materials were characterized by solid state ²⁹Si NMR and ¹³C-NMR (only for **M1**), N₂-sorption measurements (BET method), thermogravimetric analysis (TGA) and elemental analysis, and the amount of rhodium was determined by inductively coupled plasma (ICP). Analytical data is summarized in Table 6.1 and textural data in Table 6.2.

Table 6.1. Analytical data of materials **M1-M4**.

	²⁹ Si CP MAS NMR					TGA ^[a] %	% Rh	mmol Rh/g
	T ²	T ³	Q ²	Q ³	Q ⁴			
M1	-56.3	-66.2	-93.4	-101.9	-111.4	77.06	4.47	0.435
M2	-55.7	-65.6	-92.5	-101.7	-110.2	80.66	2.93	0.285
M3	--	-65.1	-91.6	-101.8	-111.3	75.98	3.15	0.306
M4	--	--	--	--	--	84.30	1.03	0.100

^[a] Residual mass measured in the TGA analysis.

The covalent incorporation of the organosilane in the hybrid materials was ascertained by ²⁹Si CP MAS solid-state NMR. The ²⁹Si spectra of **M1-M3** showed two sets of chemical shifts: T units at around -55 to -67 ppm, resulting from the hydrolysis-condensation of monomers **60** and **61**, and Q units ranging from -90 to -112 ppm, corresponding to the condensed TEOS, as exemplified by the ²⁹Si solid-state NMR of **M1** (Figure 6.17).

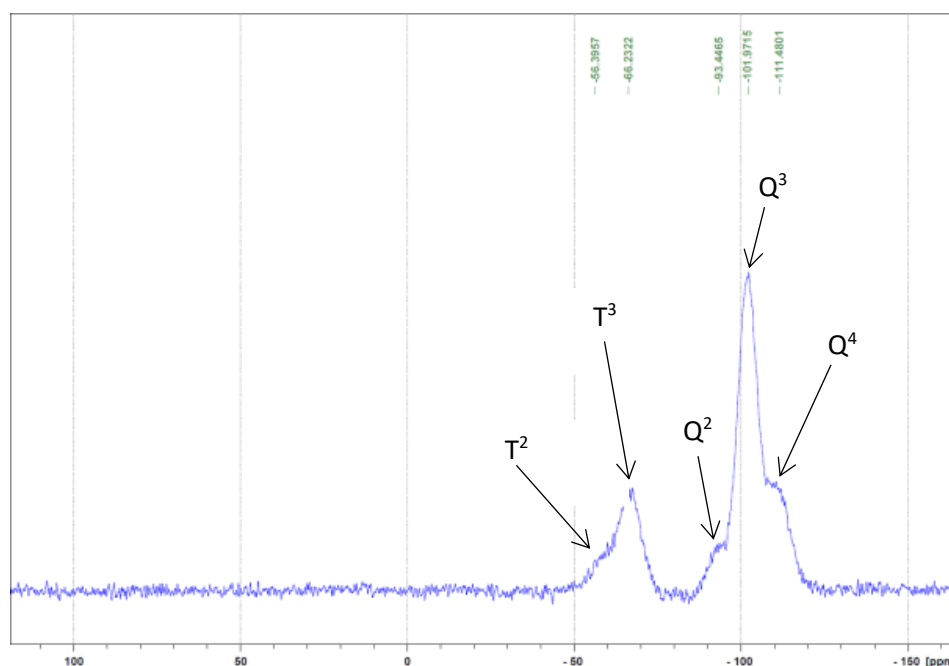


Figure 6.17. ²⁹Si-NMR in solid state of **M1**.

Only the solid-state ¹³C-NMR of **M1** was performed, as for the other materials, **M2-M4**, the high dilution of the organic moiety in the inorganic matrix precluded the observation of signals in ¹³C solid-state NMR. Significant absorptions appeared at 13.3 ppm (CH₂-Si), which confirmed the covalently bonded ligand to silica, and at 213.3 ppm, attributable to the carbenic carbon of the NHC ligand coordinated to the rhodium (C-Rh) (Figure 6.18).

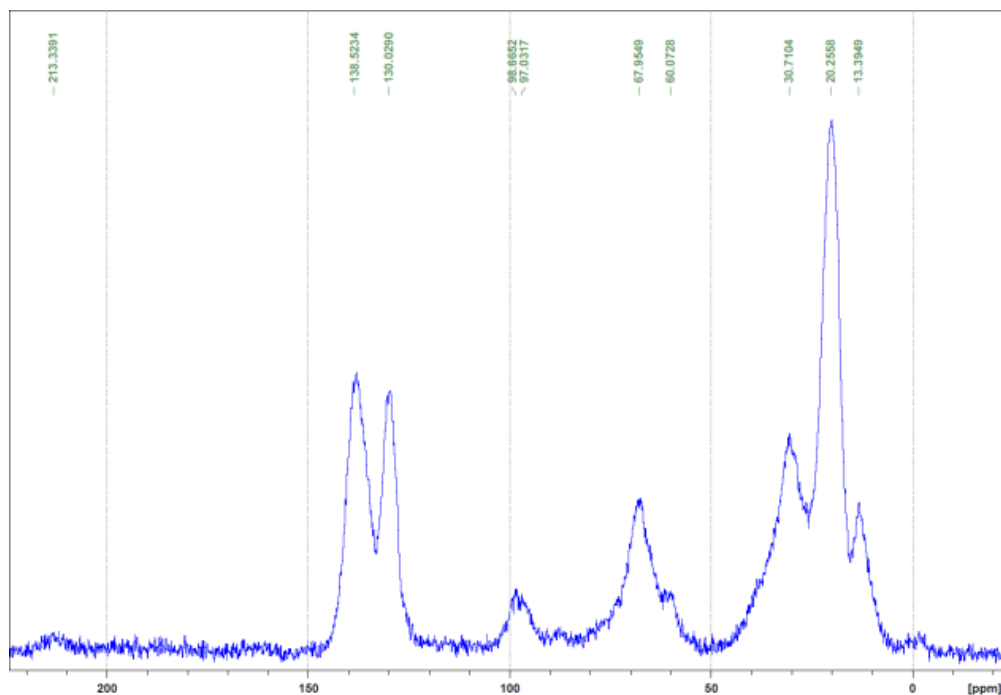


Figure 6.18. ^{13}C -NMR in solid state of **M1**.

The TGA curves of all materials showed a weight decrease of less than 5% below 200 °C, which was attributed to the loss of the physisorbed water and the remaining uncondensed ethoxy groups. A more significant weight loss was then found in the 250-500 °C range, assigned to the decomposition of the organometallic constituent (Figure 6.19).

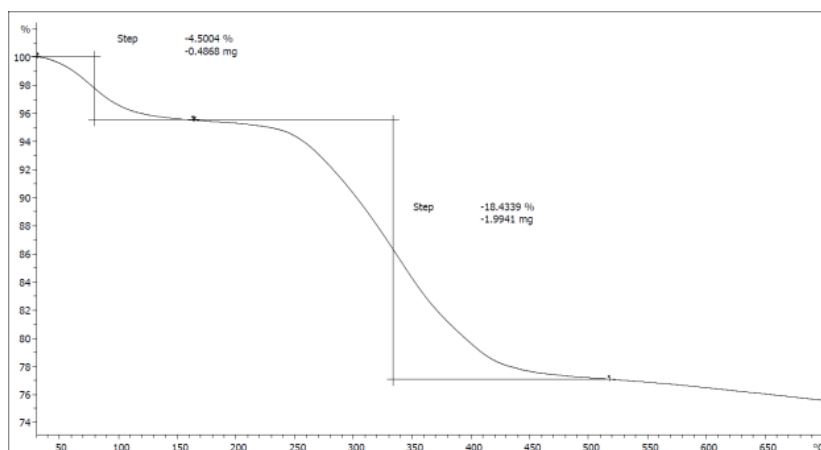


Figure 6.19. TGA curve of **M1**.

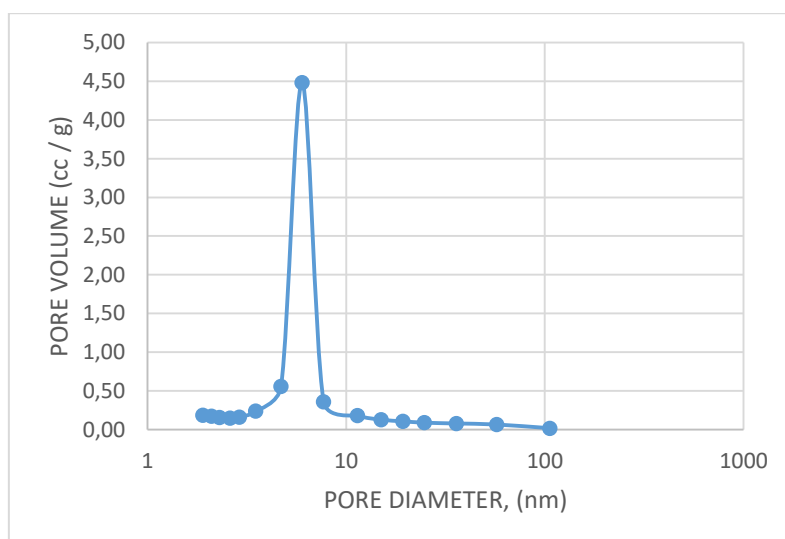
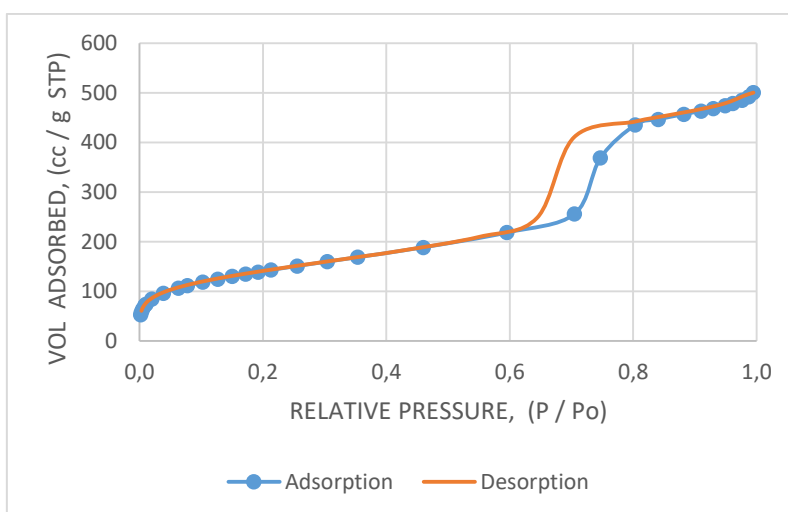
The rhodium content of the materials was determined by ICP-MS after digesting the materials in a mixture of aqua regia and fluorhydric acid under microwave irradiation. The values found were consistent with those that were expected: 4.47% for **M1**, 2.93% for **M2**, 3.15% for **M3** and 1.03% for **M4**. In the case of **M2**, the fact that it is a more diluted material than **M1** explains why less rhodium was detected. With the grafting method, a smaller amount of complex is linked to the silica compared to the cogelification process, therefore **M4** presented lower rhodium content than the other materials (Table 6.1). We obtained a molar ratio Rh/N of 0.4 for material **M4** from the analytical data, which was close to the expected 0.5 value. Lower experimental molar ratios for the other materials **M1-M3** were found, indicating that partial decomplexation had occurred in the formation of materials by the sol-gel process.

Table 6.2. Textural data of materials **M1-M4**.

	S_{BET} (m^2g^{-1})	$\varnothing_{\text{pore}}$ [\AA]	V_{pore} ^[a] (cm^3g^{-1})
M1	453	^[b]	0.230 (0.209)
M2	493	20-30 ^[c]	0.280 (0.088)
M3	325	^[d]	0.232 (0.071)
M4	512	58.8	0.774 (0.044)

^[a] Total pore volume at p/p^0 0.99 (p/p^0 0.8 for **M3**). The contribution of micropores to the V_{pore} is given in brackets. ^[b] Micropores, type I isotherm. ^[c] Type IV isotherm. ^[d] Type II isotherm.

N_2 -sorption measurements revealed a significant porosity for all the materials and high surface areas, ranging from 325 to 512 $\text{m}^2 \text{g}^{-1}$, were obtained. The functionalized mesostructured silica **M4** prepared by grafting exhibited the highest surface area, with a rather sharp pore size distribution centred at around 59 \AA (Figure 6.20) and a type IV isotherm typical for mesoporous materials (Figure 6.21).

**Figure 6.20.** Pore size distribution of **M4**.**Figure 6.21.** N_2 adsorption-desorption isotherm of **M4**.

A powder X-ray diffractogram of **M4** confirmed that the original 2D hexagonal mesostructure of the parent silica had not been affected by the grafting. However, the BET surface area decreased significantly from $732 \text{ m}^2 \text{ g}^{-1}$ for parent SBA-15-type silica to $512 \text{ m}^2 \text{ g}^{-1}$ for **M4**, in a clear indication that precursor **60** had successfully been grafted to the parent silica and filled the pores.

For the materials derived from sol-gel methodologies, their N_2 adsorption-desorption isotherm and the pore size distribution plot are explained below.

M1 was found to be a microporous solid (type I isotherm, Figure 6.22) and the pore diameter distribution is centred around 24 \AA (Figure 6.23).

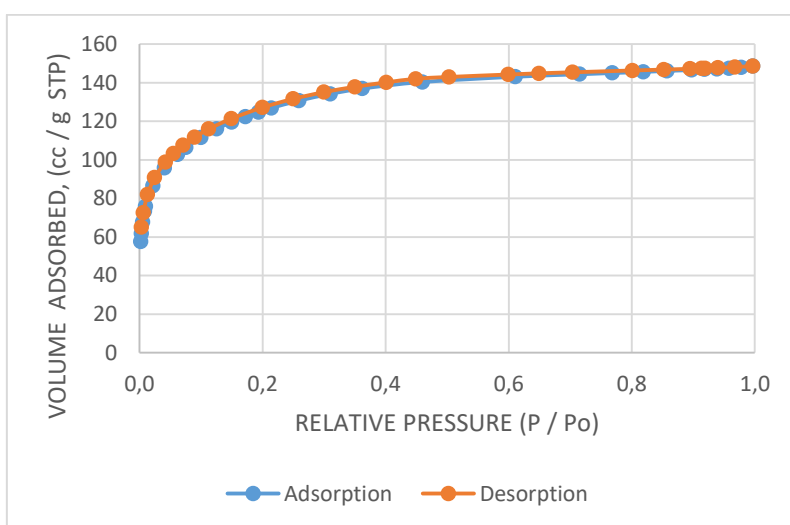


Figure 6.22. N_2 adsorption-desorption isotherm of **M1**.

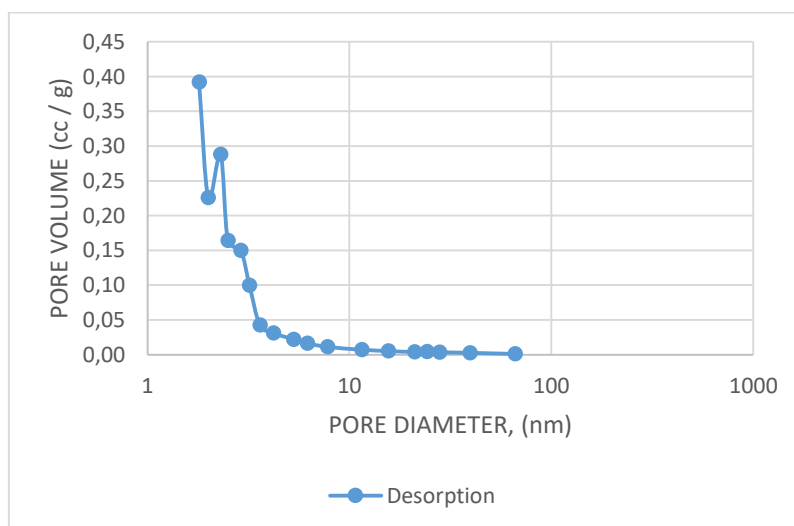


Figure 6.23. Pore size distribution of **M1**.

M2 exhibited a type IV isotherm (Figure 6.24) with a pore size distribution centred around $20\text{-}30 \text{ \AA}$ (Figure 6.25).

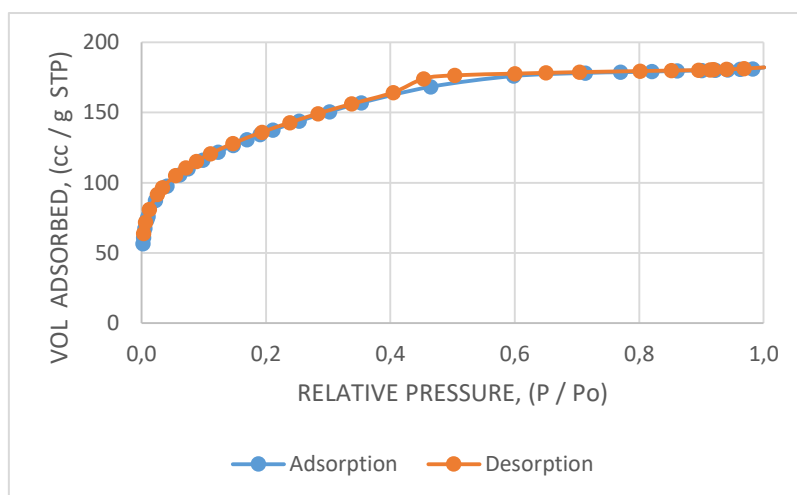


Figure 6.24. N₂ adsorption-desorption isotherm of **M2**.

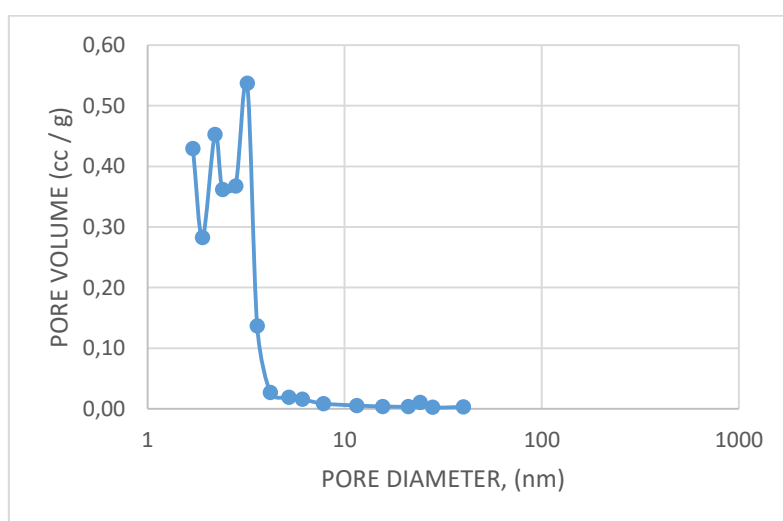


Figure 6.25. Pore size distribution of **M2**.

M3 presented a type II isotherm according to the IUPAC rules (Figure 6.26).¹⁵⁴

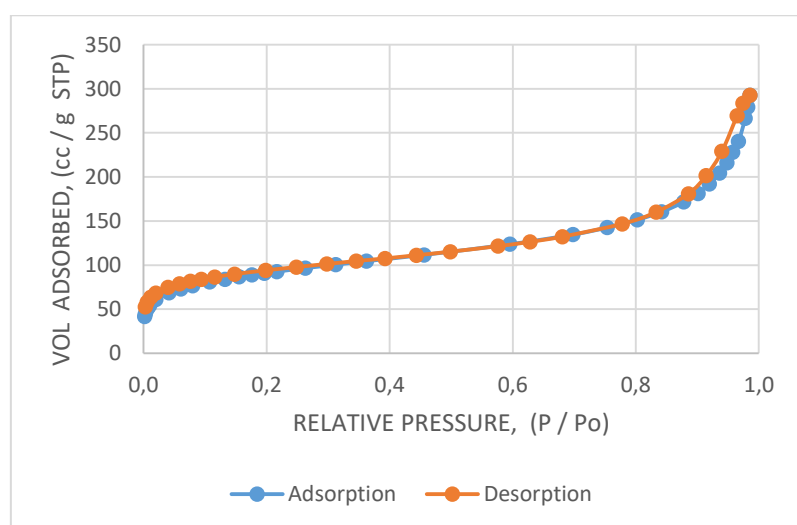


Figure 6.26. N₂ adsorption-desorption isotherm of **M3**.

In the case of **M3** the large amount of nitrogen adsorbed at $p/p^0 > 0.8$ arises from nitrogen that condenses in the voids between particles. The pore size distribution of the material is highly irregular (Figure 6.27).

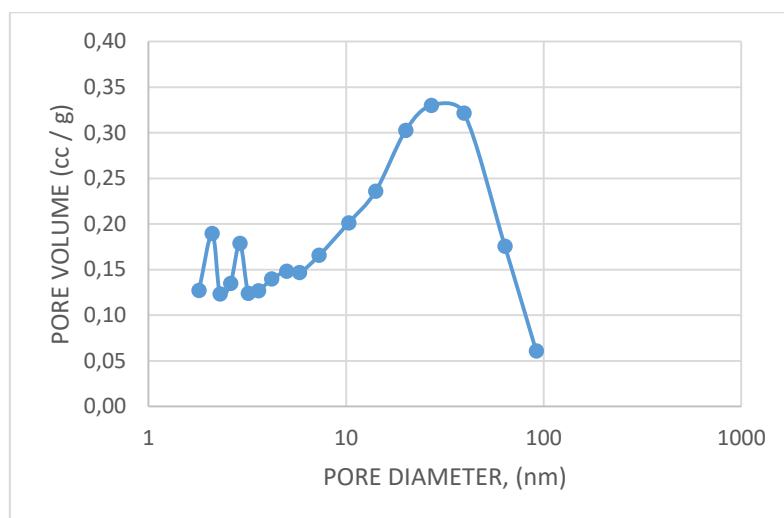


Figure 6.27. Pore size distribution of **M3**.

6.2.2. Catalytic tests of the rhodium-containing hybrid silica materials in [2+2+2] cycloaddition reactions

Once the rhodium hybrid silica materials were prepared and characterized, we investigated whether they had catalytic activity in the [2+2+2] cycloaddition reaction and their recovery and reuse were evaluated.

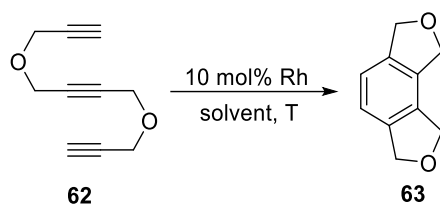
The supported catalysts were tested in the total intramolecular version of the [2+2+2] cycloaddition reaction. The catalyst loading used was 10 mol% of Rh and the reactions were carried out without an inert atmosphere, testing different solvents, without previous purification, and at different temperatures. The catalyst was recovered by filtration and evaporation of the organic phase afforded the cycloadduct. The heterogeneous Rh-complex was then washed with dichloromethane and diethyl ether and used in a subsequent cycle.

The [2+2+2] cycloaddition reaction of the O-tethered triyne **62** was used as a benchmark reaction to establish the best operating conditions of the catalysts. All of the hybrid silica materials efficiently promoted the [2+2+2] cycloaddition reaction of **62**. The results obtained are presented in Table 6.3.

When material **M2** was first tested, the reactions were carried out at room temperature using three different solvents (toluene, DCE and ethanol), but after three hours of reaction only starting material had been obtained (entries 1-3, Table 6.3). As the reaction temperature was increased to 80°C for all solvents, the reactions were completed after 3-5 hours (entries 4, 6, 8, Table 6.3). It can be seen that ethanol is clearly the best solvent as the cyclized product was obtained in an almost quantitative yield (entry 8, Table 6.3). In addition, using ethanol as the solvent, a good yield of the product could still be obtained from a second cycle, although after a longer reaction time (entry 9, Table 6.3). On the other hand, the yields in DCE and toluene

were low in the second cycle (entries 5, 7, Table 6.3). We therefore decided to continue performing the cycloaddition reactions using EtOH as the solvent.

Table 6.3. Catalytic performance of hybrid silica materials in the [2+2+2] cycloaddition of triyne **62**.



Entry	Material	Cycle	Solvent	T (°C)	t (h.)	Yield of 63 (%) ^[a]
1	M2	1	toluene	r.t.	3	-
2	M2	1	DCE	r.t.	3	-
3	M2	1	ethanol	r.t.	3	-
4	M2	1	toluene	80	5	61
5	M2	2	toluene	80	30	16 ^[b]
6	M2	1	DCE	80	3	69
7	M2	2	DCE	80	30	10 ^[b]
8	M2	1	ethanol	80	3	98
9	M2	2	ethanol	80	22	84
10	M2	3	ethanol	80	28	92
11	M2	4	ethanol	80	33	95
12	M1	1	ethanol	80	4	77
13	M3	1	ethanol	80	3	85
14	M4	1	ethanol	80	2.5	85
15	M4	2	ethanol	80	16	85
16	M4	3	ethanol	80	19	92
17	M4	4	ethanol	80	23.5	93
18	M4	5	ethanol	80	24.5	89
19	M4	6	ethanol	80	48	95

^[a] Isolated yield. ^[b] Calculated by ¹H-NMR.

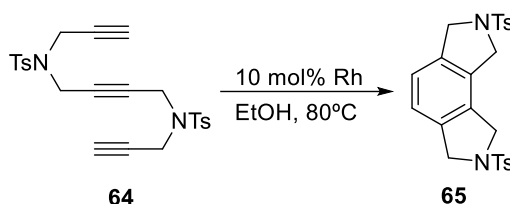
When the other materials were tested, it was observed that **M1** gave the lowest yield (entry 12, Table 6.3) whereas **M3** and **M4** showed similar activity (entries 13-14, Table 6.3).

The recyclability of the best materials (**M2** and **M4**) was then assessed. **M2** was reused successfully for four cycles and **M4** for 6 cycles. In both cases, the reaction time was longer for each cycle but the yield was not affected (entries 8-11, 14-19, Table 6.3).

The amount of rhodium leaching was determined for the four materials by ICP-OES analysis. After complete conversion of **62** to **63**, the reaction mixture was filtered and the rhodium content in the concentrated final product was 5200 ppm for **M1**, 7950 ppm for **M2**, 6580 ppm for **M3** and 9140 ppm for **M4**, which corresponds to metal losses of 5.7% for **M1**, 12.2% for **M2**, 8.4% for **M3** and 12.15% for **M4** with respect to the initial amount of rhodium added as the catalyst.

These high values of rhodium in the product are consistent with the results obtained when hot-filtration tests were performed, as they demonstrated that the catalytic activity partially follows a homogeneous pathway for both cogelificated and grafted materials. A mixture consisting of **M2** and tryine **62** was filtered after 20 minutes of reaction (83% GC conversion). After a further two hours of reaction time, the conversion increased to 96%. The same procedure was followed with **M4** and **62**: after 30 minutes of reaction (52% GC conversion) the mixture was filtered and after a further two hours of reaction, the conversion increased to 65%.

Table 6.4. Catalytic performance of hybrid silica materials in the [2+2+2] cycloaddition of tryine **64**.



Entry	Material	Cycle	t (h.)	Yield of 65 (%) ^[a]
1	M1	1	7	-
2	M2	1	5	92
3	M2	2	67	42 ^[b]
4	M3	1	7	-
5	M4	1	4	99
6	M4	2	16	96
7	M4	3	23	98
8	M4	4	25	98

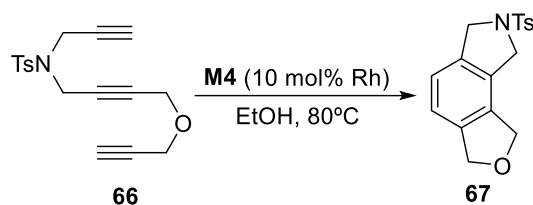
^[a]Isolated yield. ^[b]Calculated by ¹H-NMR.

Our next step was to explore the scope of the reaction. The cycloaddition of the *N*-tosyl-tethered triyne **64** was tested with the four materials under the optimized reaction conditions (EtOH, 80°C). The results are shown in Table 6.4.

M1 and **M3** did not show any activity in the cycloaddition of triyne **64** after seven hours of reaction (entries 1 and 4, Table 6.4). **M2** showed good activity in the first cycle, but in the second the reaction had still not finished after 67 hours of reaction (only 42% yield of the final product was obtained) (entries 2 and 3, Table 6.4). On the other hand, **M4** showed the best activity, the catalyst could be reused for four cycles without any reduction in the yields although reaction times became successively longer (entries 5-8, Table 6.4).

Substrate **66**, which contains two different tethers, was then tested with **M4** as it had shown the best activity so far (Table 6.5). Almost quantitative yields of **67** were obtained in five successive cycles (entries 1-5, Table 6.5), although reaction times substantially increased after the first run.

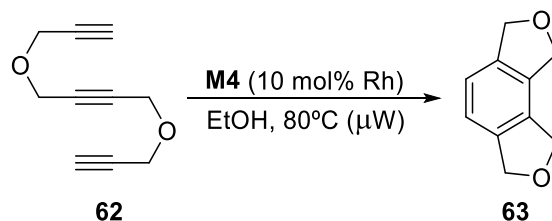
Table 6.5. Catalytic performance of hybrid silica materials in the [2+2+2] cycloaddition of triyne **66**.



Entry	Cycle	t (h.)	Yield of 67 (%) ^[a]
1	1	3	99
2	2	19	96
3	3	24	97
4	4	31	99
5	5	42	98

^[a] Isolated yield

Table 6.6. Catalytic performance of hybrid silica material **M4** under microwave irradiation.



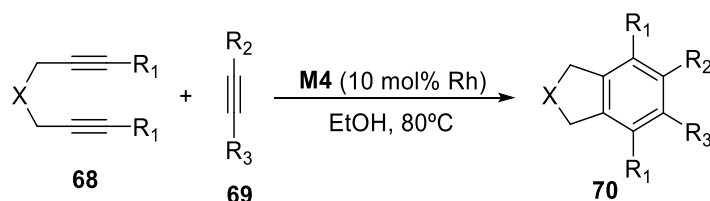
Entry	Cycle	t (min.)	Yield of 63 (%) ^[a]
1	1	15	77
2	2	45	84
3	3	80	88
4	4	120	80

^[a] Isolated yield.

In order to shorten the reaction times, especially after the first cycle, we decided to carry out the cycloaddition under microwave irradiation, which has found an increasing number of applications in organic synthesis and catalysis as an alternative to conventional heating in recent years.¹⁶⁹ We used this heating system in the cycloaddition of triyne **62** to afford tricyclic derivative **63** using catalyst **M4** in EtOH at 80°C (Table 6.6). As shown in Table 6.6 microwave heating efficiently promotes the cycloaddition reaction of triyne **62** giving excellent yields of **63** in significantly shorter reaction times compared with conventional heating. As an example, when comparing entry 17 of Table 6.3 with entry 4 of Table 6.6, we observe that the reaction time is reduced from 1 day to just 120 minutes in the fourth cycle.

Finally, we wanted to test the catalytic activity of material **M4** in the partial intramolecular version of the [2+2+2] cycloaddition reaction between several diynes **68** and monoalkynes **69**. We used the same optimized reaction conditions as for the cycloaddition of triynes. Both terminal (entries 1-4, Table 6.7) and non-terminal (entries 5-6, Table 6.7) diynes with different tethers were active in this process. However, with non-terminal diynes it was necessary to heat the reaction at 110°C using *n*-BuOH as the solvent as they are less reactive than terminal diynes. Both monosubstituted and disubstituted alkynes **69** also gave good yields of the cycloadducts. In addition, the reusability of **M4** was assessed in the reaction of entry 1, giving an 85% yield of cycloadduct **70aa** in 4.5 hours.

Table 6.7. Catalytic performance of hybrid silica material **M4** in the [2+2+2] cycloaddition between diynes **68** and monoalkynes **69**.



Entry	68 (X, R ₁)	69 (R ₂ , R ₃)	Reaction time (h)	Yield of 70 (%) ^[a]
1	68a (O, H)	69a (CH ₂ OH, H)	2	70aa (100)
	68a (O, H)	69a (CH ₂ OH, H)	4.5	70aa (85) ^[b]
2	68a (O, H)	69b (Ph, H)	1	70ab (50)
3	68b (NTs, H)	69a (CH ₂ OH, H)	3	70ba (100)
4	68b (NTs, H)	69b (Ph, H)	5	70bb (72)
5 ^[c]	1i (O, CH ₃)	69a (CH ₂ OH, H)	2.5	70ia (100)
6 ^[c]	1i (O, CH ₃)	69c (CH ₂ OH, CH ₂ OH)	5	70ic (71) ^[d]

^[a] Isolated yield. ^[b] Second batch. ^[c] Reaction run in *n*-BuOH at 110°C. ^[d] Yield calculated by ¹H-NMR spectroscopy.

As a summary, rhodium(I) complexes bearing an *N*-heterocyclic carbene ligand functionalized with either two silylated groups at the saturated carbon backbone (complex **60**) or one silylated

group at the nitrogen (complex **61**) were synthesized by reacting the corresponding imidazolium salts with $[\text{Rh}(\mu\text{-OEt})(\text{COD})]_2$. Hybrid silica materials were obtained by cogelification of complexes **60** and **61** with different amounts of tetraethoxysilane, effectively affording hybrid silica materials **M1-M3**. Monosilylated rhodium complex **61** was also grafted on to the mesostructured silica SBA-15 giving material **M4**. The materials obtained were fully characterized with the standard solid state techniques, making it possible to check that the structure of the catalytic site was maintained in the solid. Furthermore, the rhodium content of the materials was determined by inductively coupled plasma. Their catalytic activity was evaluated in the [2+2+2] cycloaddition reaction of triyne substrates, which afforded tricyclic polysubstituted benzene derivatives. After screening the reaction conditions, ethanol at 80°C was found to be optimal for the catalytic system giving excellent yields of cycloadducts. It is possible to separate the catalytic system from the reaction mixture by simple filtration affording an analytically pure product. The catalyst can be reused up to six times without loss of yield of the cycloadducts. The catalytic activity of material **M4** was also tested in the cycloaddition reaction between diynes and monoalkynes resulting in good yields of the corresponding cycloadducts. These compounds were obtained with a high level of purity after filtration of the catalyst and evaporation of the solvent.

Chapter 7. General conclusions

In this thesis, challenging substrates have been involved in the transition-metal catalysed [2+2+2] cycloaddition reaction and new catalysts for this reaction have been prepared. We can draw the following conclusions from these studies:

- 1) The [2+2+2] cycloaddition reaction of diynes with Morita-Baylis-Hillman adducts afforded enantiopure and highly functionalized 1,3-cyclohexadiene scaffolds containing quaternary and tertiary carbons. In Chapter 3 we reported that the reaction proceeded using a combination of a cationic rhodium catalyst with BINAP. Moreover, the reaction proceeded through a kinetic resolution of the MBH adduct and the process could be used to generate optically pure MBH adducts. The cycloadducts obtained were suitable for Diels-Alder reactions to provide densely functionalized polycyclic scaffolds.
- 2) The Wilkinson-catalysed [2+2+2] cycloaddition reaction of allene-yne/ene-allene substrates bearing chiral centres at the α -position of the allene functionality proceeds through a chiral induction process. In Chapter 4 we used the chiral induction method to access optically pure cycloadducts. The process was highly dependent on the tether as when oxygen-tethered substrates were used a mixture of diastereoisomers was obtained.
- 3) The Co-catalysed [2+2+2] cycloaddition reaction can be used to form the core of dendrimers when non-symmetric dendrimers are sought. However, in Chapter 5 we demonstrated that the Co-catalysed [2+2+2] cycloaddition reaction was not effective in the presence of poly(ethylene glycol) chains, as the catalyst decomposes. At first, the synthesis of a surface-block dendrimer containing a poly(ethylene glycol) on one side and a phosphoramidite moiety on the other was attempted. Due to the incompatibility with the catalyst and the lack of orthogonality of our synthetic strategy we decided to substitute the phosphoramidite moiety with PTA to introduce orthogonality in our synthesis. With this change, the Co-catalysed [2+2+2] cycloaddition reaction was performed at an early stage of the synthesis and PTA was introduced.
- 4) Hybrid silica materials in which Rh(I)-NHC complexes were immobilized were active in the [2+2+2] cycloaddition of alkynes. In Chapter 6 the materials were prepared by either the sol-gel or grafting methodologies and were characterized by the usual techniques. The materials were recovered by simple filtration and were reused in further reactions, although the reaction time increased in each cycle.

Chapter 8. Methods

8.1 General materials and instrumentation

Materials

Unless otherwise noted, materials were obtained from commercial suppliers and used without further purification. All reactions requiring anhydrous conditions were conducted in oven dried glassware under a dry nitrogen atmosphere. Dichloromethane, hexane and THF were degassed and dried under nitrogen atmosphere through solvent purification columns (MBraun, SPS-800). Anhydrous toluene was purchased from Sigma-Aldrich. DMF was distilled under reduced pressure using 4Å molecular sieves as a drying agent. Solvents were removed under reduced pressure with a rotatory evaporator.

Spectroscopy

NMR spectroscopy: ^1H , ^{13}C and ^{31}P NMR spectra were measured on a Bruker Avance III 400 [^1H (400 MHz), ^{13}C (100 MHz) and ^{31}P (162 MHz)], Bruker DPX300 [^1H (300 MHz), ^{13}C (75 MHz) and ^{31}P (121.5 MHz)] NMR spectrometers of the Serveis Tècnics de Recerca of the Universitat de Girona or on the spectrometers of the Laboratoire de Chimie de Coordination. Chemical shifts (δ) for ^1H and ^{13}C were referenced to internal solvent resonances and reported relative to SiMe_4 . ^{29}Si and ^{13}C CP-MAS solid state NMR spectra were performed at 79.5 MHz (^{29}Si) and 100.6 MHz (^{13}C) in a wide-bore AMX400 apparatus of the Universitat Autònoma de Barcelona.

IR spectroscopy: IR spectra were measured on a FT-IR spectrophotometer Mattson-Galaxy Satellite, using a MKII Golden Gate Single Reflection ATR System of the Chemistry Department of the Universitat de Girona.

Powder X-ray diffraction was performed using a Bruker AXS D8 Advance instrument with a copper X-ray tube and $\{\text{NaI}(\text{Tl})\}$ detector.

Spectrometry

Mass spectrometry: Electrospray Ionization Mass Spectrometry spectra were registered in an Esquire 6000 Trap LC/MS (Bruker Daltonics) with an electrospray ionization source of the Serveis Tècnics de Recerca of the Universitat de Girona.

High Resolution Mass Spectrometry (ESI-HRMS) were registered in a Bruker Micro TOF-Q spectrometer with a quadrupole-Time-Of-Flight hybrid analyzer of the Serveis Tècnics de Recerca of the Universitat de Girona.

Chromatography

Thin Layer Chromatography (TLC) was performed with pre-coated (0.20 mm width) chromatography plates Alugram Sil G/UV254.

Column chromatography was performed using Panreac silica gel with a particle size of 40-63 μm . High Performance Liquid Chromatography (HPLC) was performed using a CHIRALPAK AD-H, IA or IC column (4.6 x 250 mm, 5 μm) on an Agilent Technologies 1260 Infinity instrument, with a VWD detector.

Elemental analysis

Elemental analysis were registered on a PerkinElmer type 2400 analyzer in the Serveis Tècnics of the Universitat de Girona.

Inductively Coupled Plasma analysis was performed using a quadrupole-based ICP-MS system (Agilent 7500c, Agilent Technologies) equipped with an octupole collision reaction cell.

Thermogravimetric analysis was performed using a SDTA851e Mettler Toledo instrument under synthetic air, with a heating rate of 10°C/min from 30 to 700°C.

Melting points were measured in a SMP10 apparatus from Stuart without any correction.

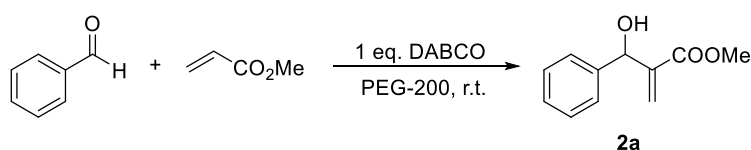
Microwave-assisted reactions were performed with a single mode Discover S-Class labstation microwave (CEM) (0-300 W). Time, temperature, and power were controlled with Synergy software. All experiments were performed on temperature control mode, which was monitored through an infrared sensor in the floor of the cavity.

Optical rotation measurements were obtained on a Jasco P-2000 polarimeter of the Universitat de Barcelona.

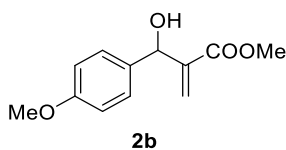
Surface areas were determined by the Brunauer-Emmett-Teller (BET) method from N₂ adsorption-desorption isotherms obtained with a Micrometrics ASAP2000 analyzer after degassing samples for 30 hours at 55°C under vacuum.

8.2. Experimental procedure for the products synthesised in Chapter 3

8.2.1. Synthesis of Morita-Baylis-Hillman substrates

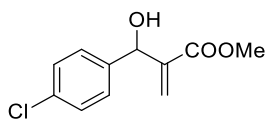


General procedure for **2** and **3**: In a 50 mL round bottom flask, a mixture of benzaldehyde (1.01 mL, 9.90 mmol), methyl acrylate (1.35 mL, 15.0 mmol) and DABCO (1.12 g, 9.98 mmol) in polyethylene glycol (PEG) with an average molecular weight of 200 g/mol (10 mL) was stirred at room temperature for 29 hours until completion (TLC monitoring). Water (10 mL) was then added to the reaction mixture and the product was extracted with ethyl ether (4×10 mL). The combined organic layer was dried over anhydrous Na₂SO₄ and concentrated in vacuum conditions. The residue was purified by column chromatography on silica gel using a mixture of hexanes/ethyl acetate (8:2) as the eluent to afford methyl 2-hydroxy(phenyl)methylacrylate **2a** (1.4 g, 74% yield) as a colourless oil. **Molecular formula**: C₁₁H₁₂O₃; **MW**: 192.21 g/mol; **m.p.**: 39°C (lit.¹⁷⁰: viscous oil); **¹H-NMR (300 MHz, CDCl₃) δ (ppm)** 3.16 (d, ³J_{H,H} = 5.5 Hz, 1H, OH), 3.70 (s, 3H, COOCH₃), 5.54 (d, ³J_{H,H} = 5.5 Hz, 1H, CHOH), 5.83 (m, 1H, CHCH=C), 6.32 (m, 1H, CHCH=C), 7.24-7.39 (m, 5H, CH-Ar); **ESI-MS (m/z)**: 175.0 [M-H₂O+H]⁺, 215 [M+Na]⁺.



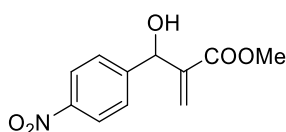
Methyl 2-(hydroxy(4-methoxyphenyl)methyl)acrylate (72% yield), colourless solid. **Molecular formula**: C₁₂H₁₄O₄; **MW**: 222.24 g/mol; **m.p.**: 60°C (lit.¹⁷⁰: 54-56°C); **¹H-NMR (300 MHz, CDCl₃) δ (ppm)** 2.90 (d, ³J_{H,H} = 4.5 Hz, 1H, OH), 3.71 (s, 3H, COOCH₃), 3.79 (s, 3H, OCH₃), 5.52 (bs, 1H, CHOH), 5.84 (m, 1H, CHCH=C), 6.32 (m, 1H, CHCH=C), 6.86 (d, ³J_{H,H} = 8.7

Hz, 2H, *CH*-Ar), 7.28 (d, $^3J_{\text{H,H}} = 8.7$ Hz, 2H, *CH*-Ar); **ESI-MS (*m/z*)**: 205.0 [*M*-H₂O+H]⁺, 245.0 [*M*+Na]⁺.



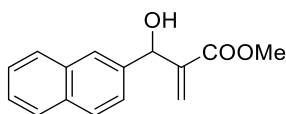
2c

Methyl 2-(hydroxy(4-chlorophenyl)methyl)acrylate (63% yield), colourless solid. **Molecular formula**: C₁₁H₁₁O₃Cl; **MW**: 226.66 g/mol; **m.p.**: 46°C (lit.¹⁷⁰: 42°C); **¹H-NMR (400 MHz, CDCl₃) δ (ppm)** 3.16 (d, $^3J_{\text{H,H}} = 5.4$ Hz, 1H, *OH*), 3.71 (s, 3H, COOCH₃), 5.51 (d, $^3J_{\text{H,H}} = 5.4$ Hz, 1H, *CHOH*), 5.82 (m, 1H, *CHCH=C*), 6.33 (m, 1H, *CHCH=C*), 7.30 (s, 4H, *CH*-Ar); **ESI-MS (*m/z*)**: 209.0 [*M*-H₂O+H]⁺, 249.0 [*M*+Na]⁺.



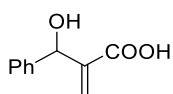
2d

Methyl 2-(hydroxy(4-nitrophenyl)methyl)acrylate (51% yield), yellow solid. **Molecular formula**: C₁₁H₁₁NO₅; **MW**: 237.21 g/mol; **m.p.**: 72°C (lit.¹⁷⁰: 74°C); **¹H-NMR (400 MHz, CDCl₃) δ (ppm)** 3.42 (d, $^3J_{\text{H,H}} = 6.0$ Hz, 1H, *OH*), 3.72 (s, 3H, COOCH₃), 5.62 (d, $^3J_{\text{H,H}} = 6.0$ Hz, 1H, *CHOH*), 5.87 (m, 1H, *CHCH=C*), 6.38 (m, 1H, *CHCH=C*), 7.55 (m, 2H, *CH*-Ar), 8.17 (m, 2H, *CH*-Ar).



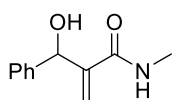
2e

Methyl 2-(hydroxy(2-naphthyl)methyl)acrylate (24% yield), colourless solid. **Molecular formula**: C₁₅H₁₄O₃; **MW**: 242.27 g/mol; **m.p.**: 100°C (lit.¹⁷¹: 97.0-97.3°C); **¹H-NMR (400 MHz, CDCl₃) δ (ppm)**: 3.15 (d, $^3J_{\text{H,H}} = 5.2$ Hz, 1H, *OH*), 3.72 (s, 3H, COOCH₃), 5.74 (d, $^3J_{\text{H,H}} = 5.2$ Hz, 1H, *CHOH*), 5.87 (m, 1H, *CHCH=C*), 6.38 (m, 1H, *CHCH=C*), 7.45-7.49 (m, 3H, *CH*-Ar), 7.81-7.87 (m, 4H, *CH*-Ar); **ESI-MS (*m/z*)**: 225.0 [*M*-H₂O+H]⁺, 265.0 [*M*+Na]⁺.



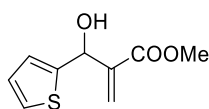
2f

2-(hydroxy(phenyl)methyl)acrylic acid¹⁷² (63% yield), colourless solid. **Molecular formula**: C₁₀H₁₀O₃; **MW**: 178.18 g/mol; **¹H-NMR (400 MHz, DMSO-d₆) δ (ppm)** 3.35 (bs, 1H, *OH*), 5.41 (s, 1H, *CHOH*), 5.93 (s, 1H, *CHCH=C*), 6.15 (s, 1H, *CHCH=C*), 7.21-7.30 (m, 5H, *CH*-Ar), 12.43 (bs, 1H, COOH).



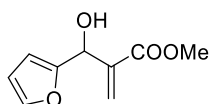
2g

2-(hydroxy(phenyl)methyl)-N-methylacrylamide (81% yield), colourless oil. **Molecular formula**: C₁₁H₁₃NO₂; **MW**: 191.23 g/mol; **¹H-NMR (300 MHz, CDCl₃) δ (ppm)** 2.77 (d, $^3J_{\text{H,H}} = 4.8$ Hz, 3H, NHCH₃), 4.15 (bs, 1H), 5.40 (s, 1H), 5.52 (s, 1H), 5.83 (s, 1H), 6.42 (bs, 1H), 7.26-7.36 (m, 5H, *CH*-Ar).



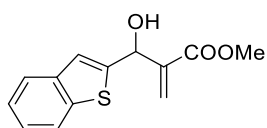
3a

Methyl 2-(hydroxy(2-thienyl)methyl)acrylate (60% yield), yellow oil (lit.¹⁷⁰: yellow viscous oil). **Molecular formula:** C₉H₁₀O₃S; **MW:** 198.24 g/mol; **¹H-NMR (400 MHz, CDCl₃) δ (ppm)** 3.40 (dd, ³J_{H,H} = 6.7 Hz, ⁵J_{H,H} = 2.6 Hz, 1H, OH), 3.75 (s, 3H, COOCH₃), 5.76 (d, ³J_{H,H} = 6.7 Hz, 1H, CHOH), 5.94 (m, 1H, CHCH=C), 6.35 (m, 1H, CHCH=C), 6.93-6.96 (m, 2H, CH-Ar), 7.25 (m, 1H, CH-Ar); **ESI-MS (m/z):** 181.0 [M-H₂O+H]⁺, 221.0 [M+Na]⁺.



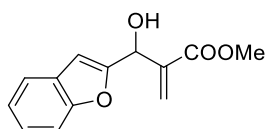
3b

Methyl 2-(hydroxy(2-furyl)methyl)acrylate (41% yield), yellow oil (lit.¹⁷⁰: viscous oil). **Molecular formula:** C₉H₁₀O₄; **MW:** 182.17 g/mol; **¹H-NMR (400 MHz, CDCl₃) δ (ppm)** 3.22 (d, ³J_{H,H} = 6.6 Hz, 1H, OH), 3.74 (s, 3H, COOCH₃), 5.57 (d, ³J_{H,H} = 6.6 Hz, 1H, CHOH), 5.93 (m, 1H, CHCH=C), 6.24 (m, 1H, CH-Ar), 6.32 (m, 1H, CH-Ar), 6.37 (m, 1H, CHCH=C), 7.35 (m, 1H, CH-Ar); **ESI-MS (m/z):** 165.0 [M-H₂O+H]⁺, 205 [M+Na]⁺.



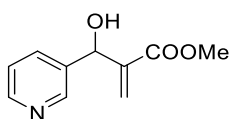
3c

Methyl 2-(hydroxy(2-benzothienyl)methyl)acrylate (17% yield), colourless solid. **Molecular formula:** C₁₃H₁₂O₃S; **MW:** 248.30 g/mol; **m.p.:** 95°C; **¹H-NMR (300 MHz, CDCl₃) δ (ppm)** 3.66 (d, ³J_{H,H} = 7.0 Hz, 1H, OH), 3.82 (s, 3H, COOCH₃), 5.88 (d, ³J_{H,H} = 7.0 Hz, 1H, CHOH), 6.07 (m, 1H, CHCH=C), 6.40 (s, 1H, CHCH=C), 7.18 (s, 1H, CH-Ar), 7.25-7.35 (m, 2H, CH-Ar), 7.69 (m, 1H, CH-Ar), 7.78 (m, 1H, CH-Ar); **¹³C-NMR (75 MHz, CDCl₃) δ (ppm)** 52.3, 70.6, 121.3, 122.5, 123.6, 124.3, 127.0, 139.6, 139.8, 140.6 (2C), 146.5, 166.5; **ESI-MS (m/z):** 231.0 [M-H₂O+H]⁺, 271.0 [M+Na]⁺; **IR (ATR) (cm⁻¹)** 3292, 2954, 1717; **EA** calculated for C₁₃H₁₂O₃S: C, 62.89, H, 4.87, found: C, 63.14; H, 4.91.



3d

Methyl 2-(hydroxy(2-benzofuryl)methyl)acrylate (15% yield), brown oil (lit.¹⁷³: light yellow oil). **Molecular formula:** C₁₃H₁₂O₄; **MW:** 232.24 g/mol; **¹H-NMR (300 MHz, CDCl₃) δ (ppm)** 3.37 (d, ³J_{H,H} = 6.1 Hz, 1H, OH), 3.77 (s, 3H, COOCH₃), 5.71 (d, ³J_{H,H} = 6.1 Hz, 1H, CHOH), 6.02 (m, 1H, CHCH=C), 6.45 (m, 1H, CHCH=C), 6.67 (m, 1H, CH-Ar), 7.18-7.30 (m, 2H, CH-Ar), 7.45 (m, 1H, CH-Ar), 7.54 (m, 1H, CH-Ar); **ESI-MS (m/z):** 215.0 [M-H₂O+H]⁺, 255.0 [M+Na]⁺.



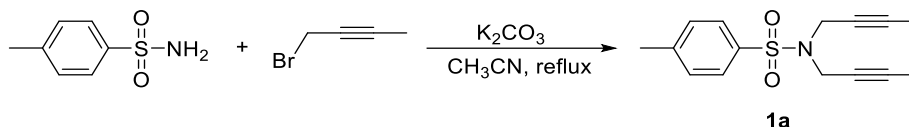
3e

Methyl 2-(hydroxy(3-pyridyl)methyl)acrylate¹⁷⁰ (88% yield), colourless solid. **Molecular formula:** C₁₀H₁₁NO₃; **MW:** 193.20 g/mol; **¹H-NMR (400 MHz, CDCl₃) δ (ppm):** 3.72 (s, 4H, CO₂CH₃ + OH), 5.60 (s, 1H, CHOH), 5.91 (m, 1H, CHHC), 6.38 (m, 1H, CHHC), 7.26 (dd,

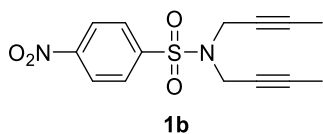
$^3J_{\text{H,H}} = 8.0$ Hz, $^4J_{\text{H,H}} = 4.8$ Hz, 1H, *CH*-pyr), 7.72 (m, 1H, *CH*-pyr), 8.48 (dd, $^3J_{\text{H,H}} = 4.8$ Hz, $^3J_{\text{H,H}} = 1.6$ Hz, 1H, *CH*-pyr), 8.56 (d, $^3J_{\text{H,H}} = 2.20$ Hz, 1H, *CH*-pyr).

8.2.2. Synthesis of diyne substrates

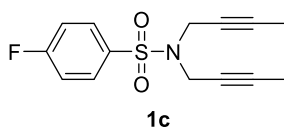
8.2.2.1. Synthesis of sulfonamide diynes



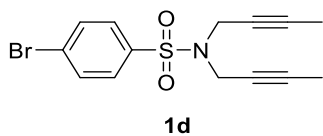
General procedure for **1**: In a 250 mL round bottom flask, a mixture of (4-methylphenyl)sulfonamide (1.20 g, 7.00 mmol) and K_2CO_3 (4.97 g, 35.96 mmol) in acetonitrile (60 mL) was heated at reflux. 1-Bromo-2-butyne (1.22 mL, 13.93 mmol) was then added slowly and the reaction mixture was stirred at reflux for 4 hours until completion (TLC monitoring). The salts were filtered off and the solvent was evaporated. The residue was purified by column chromatography on silica gel using a mixture of hexanes/dichloromethane (1:5) as the eluent to afford *N,N*-bis(2-butynyl)-(4-methylphenyl)sulfonamide **1a**¹⁷⁴ (1.79 g, 93% yield) as a yellow solid. **Molecular formula**: $\text{C}_{15}\text{H}_{17}\text{NO}_2\text{S}$; **MW**: 275.37 g/mol; **m.p.**: 83–84°C; **$^1\text{H-NMR}$ (300 MHz, CDCl_3) δ (ppm)** 1.64 (t, $^5J_{\text{H,H}} = 2.4$ Hz, 6H, $\text{CH}_3\text{C}\equiv\text{C}$), 2.42 (s, 3H, $\text{CH}_3\text{-Ts}$), 4.07 (q, $^5J_{\text{H,H}} = 2.4$ Hz, 4H, CH_2N), 7.29 (d, $^3J_{\text{H,H}} = 8.1$ Hz, 2H, *CH*-Ts(CH_3)), 7.71 (d, $^3J_{\text{H,H}} = 8.1$ Hz, 2H, *CH*-Ts(SO_2)); **ESI-MS (m/z)**: 276.1 [$\text{M}+\text{H}$]⁺, 298.1 [$\text{M}+\text{Na}$]⁺.



***N,N*-bis(2-butynyl)-(4-nitrophenyl)sulfonamide** (79% yield), yellow solid. **Molecular formula**: $\text{C}_{14}\text{H}_{14}\text{N}_2\text{O}_4\text{S}$; **MW**: 306.34 g/mol; **m.p.**: 99–100°C (lit.¹⁷⁵: 109–110°C); **$^1\text{H-NMR}$ (400 MHz, CDCl_3) δ (ppm)** 1.64 (t, $^5J_{\text{H,H}} = 2.4$ Hz, 6H), 4.12 (q, $^5J_{\text{H,H}} = 2.4$ Hz, 4H), 8.02 (d, $^3J_{\text{H,H}} = 9.2$ Hz, 2H), 8.33 (d, $^3J_{\text{H,H}} = 9.2$ Hz, 2H); **ESI-MS (m/z)**: 307.0 [$\text{M}+\text{H}$]⁺, 329.0 [$\text{M}+\text{Na}$]⁺.

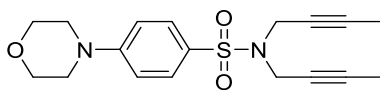


***N,N*-bis(2-butynyl)-(4-fluorophenyl)sulfonamide** (90% yield), yellow solid. **Molecular formula**: $\text{C}_{14}\text{H}_{14}\text{NO}_2\text{SF}$; **MW**: 279.33 g/mol; **m.p.**: 74–76°C; **$^1\text{H-NMR}$ (300 MHz, CDCl_3) δ (ppm)** 1.64 (t, $^5J_{\text{H,H}} = 2.4$ Hz, 6H), 4.06 (q, $^5J_{\text{H,H}} = 2.4$ Hz, 4H), 7.13–7.19 (m, 2H), 7.81–7.86 (m, 2H); **$^{13}\text{C-NMR}$ (100 MHz, CDCl_3) δ (ppm)** 3.33, 36.7, 71.3, 81.9, 115.7 (d, $^2J_{\text{C,F}} = 22.3$ Hz), 130.7 (d, $^3J_{\text{C,F}} = 9.3$ Hz), 134.7 (d, $^4J_{\text{C,F}} = 3.4$ Hz), 165.3 (d, $^1J_{\text{C,F}} = 253.0$ Hz); **ESI-MS (m/z)**: 280.0 [$\text{M}+\text{H}$]⁺, 302.0 [$\text{M}+\text{Na}$]⁺; **IR (ATR) (cm^{-1})** 3107, 2922, 1589, 1493, 1336, 1168; **EA** calculated for $\text{C}_{14}\text{H}_{14}\text{O}_2\text{NSF}$: C, 60.20, H, 5.05, N, 5.01, found: C, 59.94; H, 5.02, N, 5.12.



***N,N*-bis(2-butynyl)-(4-bromophenyl)sulfonamide** (84% yield), yellow solid. **Molecular formula**: $\text{C}_{14}\text{H}_{14}\text{NO}_2\text{SBr}$; **MW**: 340.24 g/mol; **m.p.**: 72–74°C (lit.¹⁷⁶: pale

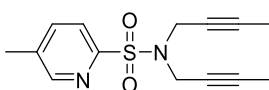
yellow oil); $^1\text{H-NMR}$ (300 MHz, CDCl_3) δ (ppm) 1.66 (t, $^5J_{\text{H,H}} = 1.6$ Hz, 6H), 4.07 (q, $^5J_{\text{H,H}} = 1.6$ Hz, 4H), 7.63 (d, $^3J_{\text{H,H}} = 6.6$ Hz, 2H), 7.70 (d, $^3J_{\text{H,H}} = 6.6$ Hz, 2H); **ESI-MS** (m/z): 340.0 - 342.0 $[\text{M}+\text{H}]^+$.



1e

***N,N*-bis(2-butynyl)-(4-morpholinylphenyl)sulfonamide** (72%

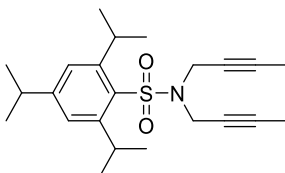
yield), yellow solid. **Molecular formula:** $\text{C}_{18}\text{H}_{22}\text{N}_2\text{O}_3\text{S}$; **MW:** 346.44 g/mol; **m.p.:** 137-139°C; $^1\text{H-NMR}$ (300 MHz, CDCl_3) δ (ppm) 1.66 (t, $^5J_{\text{H,H}} = 2.1$ Hz, 6H), 3.25-3.28 (m, 4H), 3.83-3.87 (m, 4H), 4.05 (q, $^5J_{\text{H,H}} = 2.1$ Hz, 4H), 6.87 (d, $^3J_{\text{H,H}} = 9.1$ Hz, 2H), 7.69 (d, $^3J_{\text{H,H}} = 9.1$ Hz, 2H); $^{13}\text{C-NMR}$ (75 MHz, CDCl_3) δ (ppm) 3.70 (2C), 36.6 (2C), 47.7 (2C), 66.6 (2C), 71.9 (2C), 81.5 (2C), 113.5, 113.6, 127.5, 129.7, 129.9, 154.0; **ESI-MS** (m/z): 347.1 $[\text{M}+\text{H}]^+$; **IR (ATR)** (cm^{-1}) 2967, 2829, 1590, 1332, 1152; **EA** calculated for $\text{C}_{18}\text{H}_{22}\text{O}_3\text{N}_2\text{S}$: C, 62.40, H, 6.40, N, 8.09, found: C, 62.50; H, 6.42, N, 8.32.



1f

***N,N*-bis(2-butynyl)-(5-methyl-2-pyridyl)sulfonamide** (79% yield),

colourless solid. **Molecular formula:** $\text{C}_{14}\text{H}_{16}\text{N}_2\text{O}_2\text{S}$; **MW:** 276.35 g/mol; **m.p.:** 78-79°C; $^1\text{H-NMR}$ (400 MHz, CDCl_3) δ (ppm) 1.59 (t, $^5J_{\text{H,H}} = 2.4$ Hz, 6H), 2.40 (s, 3H), 4.22 (q, $^5J_{\text{H,H}} = 2.4$ Hz, 4H), 7.66 (m, 1H), 7.85 (d, $^3J_{\text{H,H}} = 8.4$ Hz, 1H), 8.50 (m, 1H); $^{13}\text{C-NMR}$ (100 MHz, CDCl_3) δ (ppm) 3.37, 18.4, 37.3, 71.7, 81.2, 122.7, 137.0, 137.6, 150.1, 154.5; **ESI-MS** (m/z): 277.1 $[\text{M}+\text{H}]^+$, 299.1 $[\text{M}+\text{Na}]^+$; **IR (ATR)** (cm^{-1}) 1346, 1170, 1103; **EA** calculated for $\text{C}_{14}\text{H}_{16}\text{O}_2\text{N}_2\text{S}$: C, 60.85, H, 5.84, N, 10.14, found: C, 60.71; H, 5.85, N, 10.07.

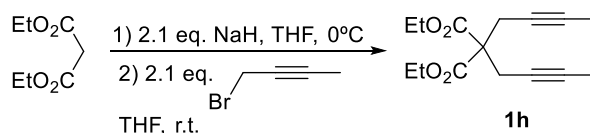


1g

***N,N*-bis(2-butynyl)-(2,4,6-triisopropylphenyl)sulfonamide** (90% yield),

colourless solid. **Molecular formula:** $\text{C}_{23}\text{H}_{33}\text{NO}_2\text{S}$; **MW:** 387.58 g/mol; **m.p.:** 134-135°C; $^1\text{H-NMR}$ (400 MHz, CDCl_3) δ (ppm) 1.245 (d, $^3J_{\text{H,H}} = 7.0$ Hz, 12H, $\text{CH}(\text{CH}_3)_2$), 1.248 (d, $^3J_{\text{H,H}} = 7.0$ Hz, 6H), 1.78 (t, $^5J_{\text{H,H}} = 2.2$ Hz, 6H, $\text{CH}(\text{CH}_3)_2$), 2.90 (sept, $^3J_{\text{H,H}} = 7.0$ Hz, 1H, $\text{CH}(\text{CH}_3)_2$), 4.04 (q, $^5J_{\text{H,H}} = 2.2$ Hz, 4H), 4.10 (sept, $^3J_{\text{H,H}} = 7.0$ Hz, 2H, $\text{CH}(\text{CH}_3)_2$), 7.15 (s, 2H); $^{13}\text{C-NMR}$ (100 MHz, CDCl_3) δ (ppm) 3.69, 23.6, 24.8, 29.4, 34.3, 35.2, 72.7, 81.1, 124.0, 130.8, 151.8, 153.3; **EA** calculated for $\text{C}_{23}\text{H}_{33}\text{NO}_2\text{S}$: C, 71.28, H, 8.58, N, 3.61, found: C, 71.15; H, 8.52, N, 4.05.

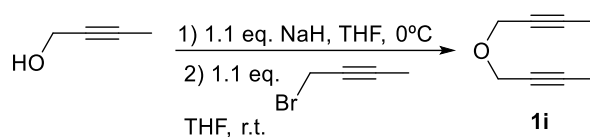
8.2.2.2. Synthesis of diyne 1h



In a 50 mL two-necked round bottom flask, under nitrogen atmosphere, NaH (272 mg, 6.80 mmol) was washed with hexanes (3 x 5 mL) and dried under vacuum. A solution of diethyl malonate (0.5 mL, 3.23 mmol) in THF (20 mL) was then added and cooled at 0°C. After 30

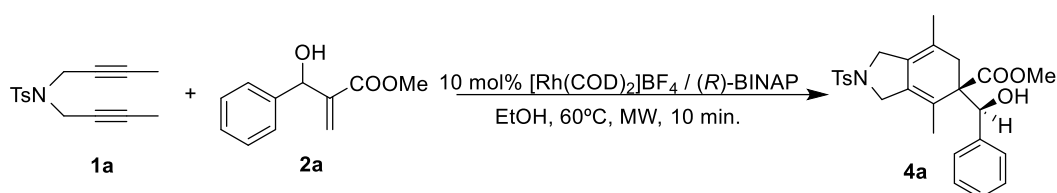
minutes a solution of 1-bromo-2-butyne (0.6 mL, 6.80 mmol) in THF (5 mL) was added and the reaction was stirred at room temperature for 24 hours (TLC monitoring). A saturated aqueous solution of NH_4Cl was added and the aqueous phase was extracted with ethyl acetate (3 x 15 mL). The organic phase was dried with anhydrous sodium sulfate, filtered and evaporated under reduced pressure. The reaction crude was purified by column chromatography using a mixture of hexanes/ethyl acetate (10:1) as the eluent to afford **1h** (0.70 g, 82% yield) as a yellow oil. **Molecular formula:** $\text{C}_{15}\text{H}_{20}\text{O}_4$; **MW:** 264.32 g/mol; **$^1\text{H-NMR}$ (300 MHz, CDCl_3) δ (ppm)** 1.20 (t, $^3J_{\text{H,H}} = 6.9$ Hz, 6H, $\text{CO}_2\text{CH}_2\text{CH}_3$), 1.70 (t, $^5J_{\text{H,H}} = 2.4$ Hz, 6H, $\text{C}\equiv\text{C-CH}_3$), 2.83 (q, $^5J_{\text{H,H}} = 2.4$ Hz, 4H, $\text{CH}_2\text{-C}\equiv\text{C-}$), 4.16 (q, $^3J_{\text{H,H}} = 6.9$ Hz, 4H, $\text{CO}_2\text{CH}_2\text{CH}_3$).

8.2.2.3. Synthesis of diyne **1i**



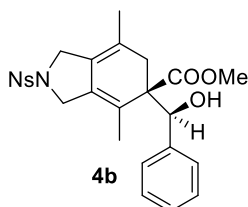
In a 25 mL two-necked round bottom flask, under nitrogen atmosphere, NaH (181 mg, 4.52 mmol) was washed with hexanes (3 x 5 mL) and dried under vacuum. A solution of 2-butyne-1-ol (0.3 mL, 4.52 mmol) in THF (5 mL) was then added and cooled at 0°C . After 30 minutes a solution of 1-bromo-2-butyne (0.4 mL, 4.52 mmol) in THF (5 mL) was added and the reaction was stirred at room temperature for 6 hours (TLC monitoring). A saturated aqueous solution of NH_4Cl was added and the aqueous phase was extracted with ethyl acetate (3 x 15 mL). The organic phase was dried with anhydrous sodium sulfate, filtered and evaporated under reduced pressure. The reaction crude was purified by column chromatography using a mixture of hexanes/ethyl acetate (10:1) as the eluent to afford **1i** (0.36 g, 65% yield) as a yellow oil. **Molecular formula:** $\text{C}_8\text{H}_{10}\text{O}$; **MW:** 122.16 g/mol; **$^1\text{H-NMR}$ (300 MHz, CDCl_3) δ (ppm)** 1.84 (t, $^5J_{\text{H,H}} = 2.3$ Hz, 6H, $\text{C}\equiv\text{C-CH}_3$), 4.17 (q, $^5J_{\text{H,H}} = 2.3$ Hz, 4H, $\text{CH}_2\text{-C}\equiv\text{C-}$)

8.2.3. Rh-catalysed [2+2+2] cycloaddition between diynes and MBH adducts.



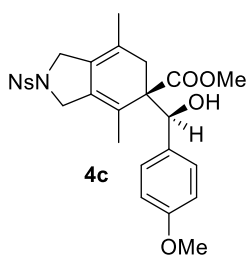
General procedure for **4** and **5**: A stirred mixture of $[\text{Rh}(\text{COD})_2]\text{BF}_4$ (4.1 mg, 0.01 mmol, 0.1 equiv.) and (*R*)-BINAP (6.3 mg, 0.01 mmol, 0.1 equiv.) in dichloromethane (2 mL) was degassed under nitrogen. Hydrogen gas was introduced to the catalyst solution and stirred for 30 minutes. The resulting mixture was concentrated to dryness. Ethanol (3 mL) was then added and the solution was stirred under nitrogen atmosphere. The solution was introduced to a 10 mL screw-capped vial. To this solution Baylis-Hillman adduct **2a** (28.8 mg, 0.15 mmol, 1.5 equiv.) and diyne **1a** (27.6 mg, 0.1 mmol, 1 equiv.) were then added under nitrogen atmosphere. The vial was then placed inside the cavity of the microwave synthesizer. The reaction mixture was heated at 60°C for 10 minutes (TLC monitoring). The solvent was then evaporated and the residue was purified by column chromatography on silica gel using a mixture of hexanes/ethyl acetate (8:2) as the eluent to give compound **4a** (23.7 mg, 51% yield, 94% ee) as a colourless solid. **Molecular**

formula: C₂₆H₂₉NO₅S; **MW:** 467.58 g/mol; **m.p.:** 75-77°C; **¹H-NMR (400 MHz, CDCl₃) δ (ppm)** 1.41 (s, 3H, CH₃), 1.72 (s, 3H, CH₃), 2.35 (d, ²J_{H,H} = 17.4 Hz, 1H, CHH-C-CH₃), 2.47 (s, 3H, CH₃-Ts), 2.52 (d, ²J_{H,H} = 17.4 Hz, 1H, CHH-C-CH₃), 3.25 (d, ³J_{H,H} = 4.4 Hz, 1H, OH), 3.29 (d, ²J_{H,H} = 13.2 Hz, 1H, CHHN), 3.72 (s, 3H, COOCH₃), 3.75 (m, 1H, CHHN), 3.82 (dd, ²J_{H,H} = 14.0 Hz, ⁴J_{H,H} = 1.2 Hz, 1H, CHHN), 4.00 (dd, ²J_{H,H} = 14.0 Hz, ⁴J_{H,H} = 1.2 Hz, 1H, CHHN), 4.97 (d, ³J_{H,H} = 4.4 Hz, 1H, CHOH), 6.97-7.00 (m, 2H, Ph), 7.04-7.09 (m, 3H, Ph), 7.38 (d, ³J_{H,H} = 8.0 Hz, 2H, CH-Ts(CH₃)), 7.70 (d, ³J_{H,H} = 8.0 Hz, 2H, CH-Ts(SO₂)); **¹³C-NMR (100 MHz, CDCl₃) δ (ppm)** 17.6, 18.9, 21.6, 35.9, 50.1, 51.0, 52.5, 58.0, 77.7, 119.6, 122.2, 125.8, 127.0, 127.2, 127.9, 128.0, 129.7, 132.8, 133.1, 139.7, 143.8, 176.2; **ESI-MS (m/z):** 468.1 [M+H]⁺, 490.1 [M+Na]⁺, 957.3 [2M+Na]⁺; **IR (ATR) (cm⁻¹)** 3507, 2919, 1726, 1341, 1159; **EA** calculated for C₂₆H₂₉NO₅S·2H₂O: C, 62.01, H, 6.60, N, 2.78, found: C, 62.25; H, 6.04; N, 3.17. Enantiomeric excess was determined with **HPLC** analysis (Chiralpak AD-H column (4.6 x 250 mm, 5 μm); 1 mL/min flow rate of a 50% 2-propanol : 50% heptane mobile phase during 20 min.; λ = 254 nm.; Rt = 8 min for major isomer and Rt = 15 min for minor isomer). **[α]_D²⁰** +15.1 (c 0.00205, CH₂Cl₂).



Compound **4b** (38% yield, 92% ee), yellow solid. **Molecular formula:**

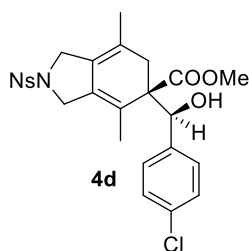
C₂₅H₂₆N₂SO₇; **MW:** 498.55 g/mol; **m.p.:** 64-65°C; **¹H-NMR (400 MHz, CDCl₃) δ (ppm)** 1.42 (s, 3H, CH₃), 1.76 (s, 3H, CH₃), 2.34-2.46 (m, 2H, CH₂CCH₃), 3.16 (d, ³J_{H,H} = 4.0 Hz, 1H, OH), 3.43 (d, ²J_{H,H} = 13.2 Hz, 1H, CHHN), 3.68 (s, 3H, CO₂CH₃), 3.79 (d, ²J_{H,H} = 13.2 Hz, 1H, CHHN), 3.92 (dd, ²J_{H,H} = 14.0 Hz, ⁴J_{H,H} = 1.2 Hz, 1H, CHHN), 4.02 (dd, ²J_{H,H} = 14.0 Hz, ⁴J_{H,H} = 1.2 Hz, 1H, CHHN), 5.02 (d, ³J_{H,H} = 4.0 Hz, 1H, CHOH), 7.02-7.13 (m, 5H, Ph), 7.97 (d, ³J_{H,H} = 9.0 Hz, 2H, CH-Ts(SO₂)), 8.40 (d, ³J_{H,H} = 9.0 Hz, 2H, CH-Ts(NO₂)); **¹³C-NMR (75MHz, CDCl₃) δ (ppm)** 17.6 (CH₃), 18.7 (CH₃), 35.4 (CH₂CCH₃), 50.1 (CH₂N), 51.2 (CH₂N), 52.5 (CO₂CH₃), 57.9 (CCO₂CH₃), 77.3 (CHOH), 120.5 (CCH₃), 123.2 (C=CCH₃), 124.4 (CH-Ns(NO₂)), 125.0 (CCH₃), 127.0 (CH-Ph), 127.3 (CH-Ph), 128.0 (CH-Ph), 128.9 (CH-Ns(SO₂)), 132.2 (C=CCH₃), 139.7 (C-Ph), 142.2 (C-SO₂), 150.3 (C-NO₂), 175.6 (CO₂CH₃); **ESI-MS (m/z):** 481.1 [M-H₂O+H]⁺, 521.2 [M+Na]⁺; **IR (ATR) (cm⁻¹)** 3461, 2922, 1721, 1529, 1348, 1165; **EA** calculated for C₂₅H₂₆N₂SO₇·0.5H₂O: C, 59.16, H, 5.36, N, 5.52, found: C, 58.97, H, 5.30, N, 5.54. Enantiomeric excess was determined with **HPLC** analysis (Chiralpak AD-H column (4.6 x 250 mm, 5 μm); 1 mL/min flow rate of a 50% 2-propanol : 50% heptane mobile phase during 20 min.; λ = 254 nm.; Rt = 10.9 min for major isomer and Rt = 15.7 min for minor isomer). **[α]_D²⁰** +21.3 (c 0.0028, CH₂Cl₂).



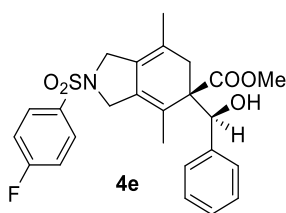
Compound **4c** (42% yield, 95% ee), brown solid. **Molecular formula:**

C₂₆H₂₈N₂O₈S; **MW:** 528.58 g/mol; **m.p.:** 59-60°C; **¹H-NMR (300 MHz, CDCl₃) δ (ppm)** 1.45 (s, 3H), 1.77 (s, 3H), 2.39 (bs, 2H), 3.07 (d, ³J_{H,H} = 3.6 Hz, 1H), 3.49 (d, ²J_{H,H} = 12.0 Hz, 1H), 3.68 (s, 3H), 3.73 (s, 3H), 3.87 (d, ²J_{H,H} = 12.0 Hz, 1H), 3.92 (d, ²J_{H,H} = 14.1 Hz, 1H), 4.03 (d, ²J_{H,H} = 14.1 Hz, 1H),

4.98 (d, $^3J_{\text{H,H}} = 3.6$ Hz, 1H), 6.60 (d, $^3J_{\text{H,H}} = 8.7$ Hz, 2H), 7.02 (d, $^3J_{\text{H,H}} = 8.7$ Hz, 2H), 7.97 (d, $^3J_{\text{H,H}} = 9.4$ Hz, 2H), 8.39 (d, $^3J_{\text{H,H}} = 9.4$ Hz, 2H); $^{13}\text{C-NMR}$ (75MHz, CDCl_3) δ (ppm) 17.5, 19.1, 35.2, 50.3, 51.2, 52.5, 55.3, 57.8, 76.7, 112.7, 120.7, 123.3, 124.4, 124.8, 128.0, 128.7, 131.7, 132.1, 142.0, 150.3, 159.3, 175.5; IR (ATR) (cm^{-1}) 3460, 2920, 1719, 1529, 1512, 1348, 1164; ESI-MS (m/z): 511.1 $[\text{M}-\text{H}_2\text{O}+\text{H}]^+$, 551.1 $[\text{M}+\text{Na}]^+$; ESI-HRMS (m/z) calculated for $[\text{C}_{26}\text{H}_{28}\text{N}_2\text{O}_8\text{S}+\text{Na}]^+$: 551.1459, found: 551.1419. Enantiomeric excess was determined with HPLC analysis (Chiralpak AD-H column (4.6 x 250 mm, 5 μm); 1 mL/min flow rate of a 70% 2-propanol : 30% heptane mobile phase during 30 min.; $\lambda = 254$ nm.; Rt = 11 min for major isomer and Rt = 20 min for minor isomer). $[\alpha]_{\text{D}}^{20} +15.9$ (c 0.0026, CH_2Cl_2).

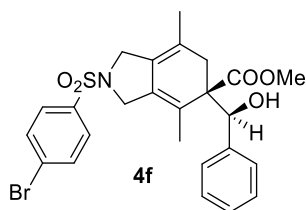


Compound **4d** (40% yield, 92% ee), brown solid. **Molecular formula:** $\text{C}_{25}\text{H}_{25}\text{N}_2\text{O}_7\text{SCl}$; **MW:** 532.99 g/mol; **m.p.:** 70°C; $^1\text{H-NMR}$ (300 MHz, CDCl_3) δ (ppm) 1.43 (s, 3H), 1.76 (s, 3H), 2.30 (d, $^2J_{\text{H,H}} = 17.2$ Hz, 1H), 2.50 (d, $^2J_{\text{H,H}} = 17.2$ Hz, 1H), 3.26 (d, $^3J_{\text{H,H}} = 3.7$ Hz, 1H), 3.33 (d, $^2J_{\text{H,H}} = 13.8$ Hz, 1H), 3.71 (s, 3H), 3.81-3.87 (m, 2H), 4.08 (d, $^2J_{\text{H,H}} = 12.9$ Hz, 1H), 4.97 (d, $^3J_{\text{H,H}} = 3.7$ Hz, 1H), 6.94 (d, $^3J_{\text{H,H}} = 8.5$ Hz, 2H), 7.02 (d, $^3J_{\text{H,H}} = 8.5$ Hz, 2H), 7.99 (d, $^3J_{\text{H,H}} = 9.0$ Hz, 2H), 8.42 (d, $^3J_{\text{H,H}} = 9.0$ Hz, 2H); $^{13}\text{C-NMR}$ (75MHz, CDCl_3) δ (ppm) 17.7, 19.0, 35.7, 50.2, 51.1, 52.7, 57.8, 77.2, 120.1, 123.0, 124.6, 125.1, 127.2, 128.3, 128.7, 132.4, 133.7, 138.1, 142.0, 150.3, 175.8; IR (ATR) (cm^{-1}) 3492, 2921, 1719, 1528, 1347, 1164; ESI-MS (m/z): 515.1 $[\text{M}-\text{H}_2\text{O}+\text{H}]^+$, 533.0 $[\text{M}+\text{H}]^+$, 555.1 $[\text{M}+\text{Na}]^+$; ESI-HRMS (m/z) calculated for $[\text{C}_{25}\text{H}_{25}\text{N}_2\text{O}_7\text{SCl}+\text{Na}]^+$: 555.0963, found: 555.0926. Enantiomeric excess was determined with HPLC analysis (Chiralpak AD-H column (4.6 x 250 mm, 5 μm); 1 mL/min flow rate of a 50% 2-propanol : 50% heptane mobile phase during 20 min.; $\lambda = 254$ nm.; Rt = 9 min for major isomer and Rt = 14 min for minor isomer). $[\alpha]_{\text{D}}^{20} +10.2$ (c 0.0024, CH_2Cl_2)

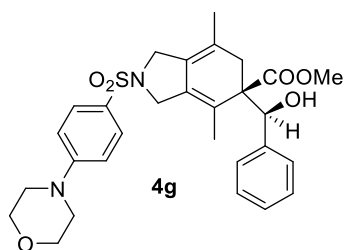


Compound **4e** (38% yield, 89% ee), colourless solid. **Molecular formula:** $\text{C}_{25}\text{H}_{26}\text{NSO}_5\text{F}$; **MW:** 471.54 g/mol; **m.p.:** 69-71 °C; $^1\text{H-NMR}$ (300 MHz, CDCl_3) δ (ppm) 1.42 (s, 3H), 1.74 (s, 3H), 2.36 (d, $^2J_{\text{H,H}} = 17.7$ Hz, 1H), 2.51 (d, $^2J_{\text{H,H}} = 17.7$ Hz, 1H), 3.25 (d, $^3J_{\text{H,H}} = 3.6$ Hz, 1H), 3.30 (d, $^2J_{\text{H,H}} = 13.2$ Hz, 1H), 3.71 (s, 3H), 3.75 (d, $^2J_{\text{H,H}} = 13.2$ Hz, 1H), 3.82 (d, $^2J_{\text{H,H}} = 14.0$ Hz, 1H), 3.99 (d, $^2J_{\text{H,H}} = 14.0$ Hz, 1H), 4.99 (d, $^3J_{\text{H,H}} = 3.6$ Hz, 1H), 6.99-7.11 (m, 5H), 7.22-7.28 (m, 2H), 7.80-7.85 (m, 2H); $^{13}\text{C-NMR}$ (75 MH, CDCl_3) δ (ppm) 17.6, 18.9, 35.8, 50.1, 51.0, 52.5, 57.9, 77.6, 116.4 (d, $^3J_{\text{C,F}} = 22.4$ Hz, 2C), 119.9, 122.6, 125.5, 127.0, 127.2, 127.9, 130.5, 132.2 (d, $^4J_{\text{C,F}} = 3.3$ Hz), 132.8, 139.6, 165.4 (d, $^1J_{\text{C,F}} = 253.4$ Hz), 176.0; ESI-MS (m/z): 454.1 $[\text{M}-\text{H}_2\text{O}+\text{H}]^+$, 472.1 $[\text{M}+\text{H}]^+$; IR (ATR) (cm^{-1}) 3510, 2922, 1724, 1345, 1166; ESI-HRMS (m/z) calculated for $[\text{C}_{25}\text{H}_{26}\text{NSO}_5\text{F}+\text{Na}]^+$: 494.1408, found: 494.1403. Enantiomeric excess was determined with HPLC analysis (Chiralpak AD-H column (4.6 x 250 mm, 5 μm); 1 mL/min flow rate of a 40% 2-propanol : 60% heptane

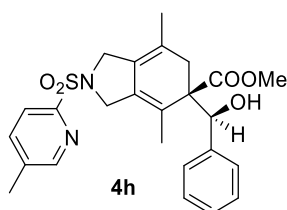
mobile phase during 16 min.; $\lambda = 254$ nm.; $R_t = 8.5$ min for major isomer and $R_t = 13.2$ min for minor isomer); $[\alpha]^{20}_D +5.0$ (c 0.00265, CH_2Cl_2)



Compound **4f** (48% yield, 95% ee), colourless solid. **Molecular formula:** $\text{C}_{25}\text{H}_{26}\text{NSO}_5\text{Br}$; **MW:** 532.45 g/mol; **m.p.:** 75-77 °C; **$^1\text{H-NMR}$ (300 MHz, CDCl_3) δ (ppm)** 1.41 (s, 3H), 1.74 (s, 3H), 2.35 (d, $^2J_{\text{H,H}} = 17.5$ Hz, 1H), 2.50 (d, $^2J_{\text{H,H}} = 17.5$ Hz, 1H), 3.25 (d, $^3J_{\text{H,H}} = 4.1$ Hz, 1H), 3.30 (d, $^2J_{\text{H,H}} = 12.9$ Hz, 1H), 3.71 (s, 3H), 3.72 (m, 1H), 3.81 (d, $^2J_{\text{H,H}} = 12.7$ Hz, 1H), 3.99 (d, $^2J_{\text{H,H}} = 12.7$ Hz, 1H), 4.98 (d, $^3J_{\text{H,H}} = 4.1$ Hz, 1H), 7.01-7.10 (m, 5H), 7.63-7.74 (m, 4H); **$^{13}\text{C-NMR}$ (75 MHz, CDCl_3) δ (ppm)** 17.7, 18.9, 35.8, 50.1, 51.1, 52.5, 58.0, 77.6, 120.0, 122.6, 125.4, 127.0, 127.2, 127.9, 128.0, 129.3, 132.4, 132.6, 134.9, 139.6, 176.0; **ESI-MS (m/z):** 514.0–516.0 $[\text{M}-\text{H}_2\text{O}+\text{H}]^+$, 532.0-534.0 $[\text{M}+\text{H}]^+$; **IR (ATR) (cm^{-1})** 3512, 2950, 1723, 1345, 1161; **EA** calculated for $\text{C}_{25}\text{H}_{26}\text{NSO}_5\text{Br}$: C, 56.40, H, 4.92, N, 2.63, found: C, 56.85, H, 5.35, N, 2.72. Enantiomeric excess was determined with **HPLC** analysis (Chiralpak AD-H column (4.6 x 250 mm, 5 μm); 1 mL/min flow rate of a 40% 2-propanol : 60% heptane mobile phase during 22 min.; $\lambda = 254$ nm.; $R_t = 9.6$ min for major isomer and $R_t = 19.3$ min for minor isomer); $[\alpha]^{20}_D +21.5$ (c 0.0034, CH_2Cl_2)

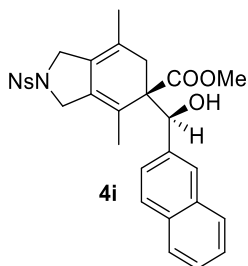


Compound **4g** (49% yield, 94% ee), colourless solid. **Molecular formula:** $\text{C}_{29}\text{H}_{34}\text{N}_2\text{SO}_6$; **MW:** 538.66 g/mol; **m.p.:** 94-96 °C; **$^1\text{H-NMR}$ (300 MHz, CDCl_3) δ (ppm)** 1.41 (s, 3H), 1.71 (s, 3H), 2.35 (d, $^2J_{\text{H,H}} = 17.7$ Hz, 1H), 2.50 (d, $^2J_{\text{H,H}} = 17.7$ Hz, 1H), 3.26-3.33 (m, 5H), 3.70 (s, 3H), 3.72 (m, 1H), 3.79-3.88 (m, 6H), 3.96 (d, $^2J_{\text{H,H}} = 13.5$ Hz, 1H), 4.98 (d, $^3J_{\text{H,H}} = 4.2$ Hz, 1H), 6.94-7.10 (m, 7H), 7.68 (d, $^3J_{\text{H,H}} = 9.0$ Hz, 2H); **$^{13}\text{C-NMR}$ (75 MHz, CDCl_3) δ (ppm)** 17.5, 18.9, 35.7, 47.7, 50.0, 51.0, 52.5, 57.9, 66.6, 77.4, 113.9, 119.5, 122.2, 124.6, 125.9, 127.0, 127.2, 127.8, 129.6, 129.8, 133.3, 139.7, 154.1, 176.1; **ESI-MS (m/z):** 521.2 $[\text{M}-\text{H}_2\text{O}+\text{H}]^+$, 539.2 $[\text{M}+\text{H}]^+$; **IR (ATR) (cm^{-1})** 3505, 2922, 1725, 1591, 1336, 1154; **EA** calculated for $\text{C}_{29}\text{H}_{34}\text{N}_2\text{SO}_6$: C, 64.66, H, 6.36, N, 5.20, found: C, 64.18, H, 6.26, N, 4.99. Enantiomeric excess was determined with **HPLC** analysis (Chiralpak AD-H column (4.6 x 250 mm, 5 μm); 1 mL/min flow rate of a 70% 2-propanol : 30% heptane mobile phase during 27 min.; $\lambda = 254$ nm.; $R_t = 9.4$ min for major isomer and $R_t = 24.3$ min for minor isomer); $[\alpha]^{20}_D +12.0$ (c 0.0036, CH_2Cl_2)

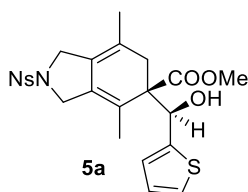


Compound **4h** (30% yield, 97% ee), colourless solid. **Molecular formula:** $\text{C}_{25}\text{H}_{28}\text{N}_2\text{SO}_5$; **MW:** 468.57 g/mol; **m.p.:** 48-50 °C; **$^1\text{H-NMR}$ (400 MHz, CDCl_3) δ (ppm)** 1.43 (s, 3H), 1.65 (s, 3H), 2.41 (m, 1H), 2.44 (s, 3H), 2.51 (d, $^2J_{\text{H,H}} = 17.6$ Hz, 1H), 3.30 (d, $^3J_{\text{H,H}} = 3.2$ Hz, 1H),

3.65 (m, 1H), 3.69 (s, 3H), 3.96 (d, $^2J_{\text{H,H}} = 12.8$ Hz, 1H), 4.14 (d, $^2J_{\text{H,H}} = 14.2$ Hz, 1H), 4.20 (d, $^2J_{\text{H,H}} = 14.2$ Hz, 1H), 4.97 (s, 1H), 7.04-7.13 (m, 5H), 7.70 (d, $^3J_{\text{H,H}} = 8.2$ Hz, 1H), 7.83 (d, $^3J_{\text{H,H}} = 8.2$ Hz, 1H), 8.54 (s, 1H); $^{13}\text{C-NMR}$ (75 MHz, CDCl_3) δ (ppm) 17.6, 18.7, 19.0, 35.8, 50.8, 51.8, 52.5, 58.0, 77.0, 119.7, 122.4, 122.9, 126.1, 127.1, 127.4, 127.9, 133.3, 137.4, 138.0, 139.9, 150.7, 153.3, 176.1; **IR (ATR)** (cm^{-1}) 3508, 2921, 1725, 1341, 1168; **ESI-MS** (m/z): 469.0 $[\text{M}+\text{H}]^+$; **EA** calculated for $\text{C}_{25}\text{H}_{28}\text{N}_2\text{SO}_5 \cdot 2\text{H}_2\text{O}$: C, 59.51, H, 6.39, N, 5.55, found: C, 59.96, H, 5.63, N, 5.64. Enantiomeric excess was determined with **HPLC** analysis (Chiralpak AD-H column (4.6 x 250 mm, 5 μm); 1 mL/min flow rate of a 40% 2-propanol : 60% heptane mobile phase during 20 min.; $\lambda = 254$ nm.; $R_t = 9$ min for major isomer and $R_t = 14$ min for minor isomer); $[\alpha]_D^{20} +5.6$ (c 0.0035, CH_2Cl_2).

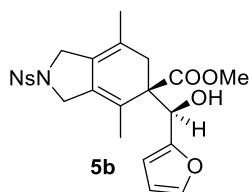


Compound **4i** (37% yield, 91% ee), yellow solid. **Molecular formula**: $\text{C}_{29}\text{H}_{28}\text{N}_2\text{SO}_7$; **MW**: 548.61 g/mol; **m.p.**: 65-67°C; $^1\text{H-NMR}$ (400 MHz, CDCl_3) δ (ppm) 1.35 (s, 3H), 1.82 (s, 3H), 2.46 (bs, 2H), 3.10 (d, $^2J_{\text{H,H}} = 12.0$ Hz, 1H), 3.30 (d, $^3J_{\text{H,H}} = 3.8$ Hz, 1H), 3.68 (m, 1H), 3.70 (s, 3H), 3.88 (dd, $^2J_{\text{H,H}} = 14.0$ Hz, $^4J_{\text{H,H}} = 1.2$ Hz, 1H), 4.04 (dd, $^2J_{\text{H,H}} = 14.0$ Hz, $^4J_{\text{H,H}} = 1.2$ Hz, 1H), 5.21 (d, $^3J_{\text{H,H}} = 3.8$ Hz, 1H), 7.22 (dd, $^3J_{\text{H,H}} = 8.6$ Hz, $^4J_{\text{H,H}} = 1.8$ Hz, 1H), 7.37-7.45 (m, 2H), 7.49 (d, $^3J_{\text{H,H}} = 8.6$ Hz, 1H), 7.58 (s, 1H), 7.66-7.69 (m, 2H), 7.90 (d, $^3J_{\text{H,H}} = 9.0$ Hz, 2H), 8.36 (d, $^3J_{\text{H,H}} = 9.0$ Hz, 2H); $^{13}\text{C-NMR}$ (75MHz, CDCl_3) δ (ppm) 17.6, 18.9, 35.4, 50.1, 51.1, 52.5, 58.0, 77.3, 120.6, 123.4, 124.4, 124.9, 125.9, 126.1, 126.5, 126.7, 127.4, 127.7, 127.9, 128.6, 132.3, 132.6, 133.0, 137.1, 142.1, 150.2, 175.6; **ESI-MS** (m/z): 531.1 $[\text{M}-\text{H}_2\text{O}+\text{H}]^+$; **IR (ATR)** (cm^{-1}) 3509, 2920, 1721, 1528, 1347, 1164; **EA** calculated for $\text{C}_{29}\text{H}_{28}\text{N}_2\text{SO}_7 \cdot 1.5\text{H}_2\text{O}$: C, 60.51, H, 5.43, N, 4.87, found: C, 60.48, H, 5.10, N, 4.99. Enantiomeric excess was determined with **HPLC** analysis (Chiralpak IA column (4.6 x 250 mm, 5 μm); 1 mL/min flow rate of a 50% 2-propanol : 50% hexane mobile phase during 22 min.; $\lambda = 254$ nm.; $R_t = 14$ min for major isomer and $R_t = 20$ min for minor isomer); $[\alpha]_D^{20} +6.2$ (c 0.0015, CH_2Cl_2).



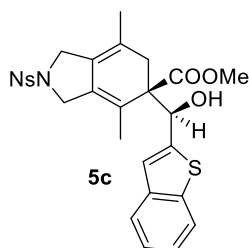
Compound **5a** (44% yield, 84% ee), yellow solid. **Molecular formula**: $\text{C}_{23}\text{H}_{24}\text{N}_2\text{O}_7\text{S}_2$; **MW**: 504.57 g/mol; **m.p.**: 49-50°C; $^1\text{H-NMR}$ (400 MHz, CDCl_3) δ (ppm) 1.55 (s, 3H), 1.65 (s, 3H), 2.44-2.54 (m, 2H), 3.15 (d, $^3J_{\text{H,H}} = 5.4$ Hz, 1H), 3.71 (s, 3H), 3.81 (d, $^2J_{\text{H,H}} = 13.6$ Hz, 1H), 3.93 (d, $^2J_{\text{H,H}} = 13.6$ Hz, 1H), 4.03 (s, 2H), 5.28 (s, $^3J_{\text{H,H}} = 5.4$ Hz, 1H), 6.82-6.87 (m, 2H), 7.09 (dd, $^3J_{\text{H,H}} = 4.8$ Hz, $^4J_{\text{H,H}} = 1.6$ Hz, 1H), 8.01 (d, $^3J_{\text{H,H}} = 9.0$ Hz, 2H), 8.39 (d, $^3J_{\text{H,H}} = 9.0$ Hz, 2H); $^{13}\text{C-NMR}$ (75MHz, CDCl_3) δ (ppm) 17.0, 19.0, 34.9, 50.3, 51.2, 52.4, 57.6, 72.3, 120.2, 123.9, 124.3, 124.7, 124.9, 125.3, 126.0, 128.6, 132.4, 142.2, 143.2, 150.2, 174.7; **IR (ATR)** (cm^{-1}) 3490, 2921, 1711, 1528, 1348, 1164; **ESI-MS** (m/z): 487.1 $[\text{M}-\text{H}_2\text{O}+\text{H}]^+$, 527.1 $[\text{M}+\text{Na}]^+$; **ESI-HRMS** (m/z) calculated for $[\text{C}_{23}\text{H}_{24}\text{N}_2\text{O}_7\text{S}_2+\text{Na}]^+$: 527.0917, found: 527.0908. Enantiomeric excess was determined with **HPLC** analysis (Chiralpak AD-H column (4.6 x 250 mm, 5 μm); 1 mL/min flow

rate of a 10% 2-propanol : 90% heptane mobile phase during 18 min.; $\lambda = 254$ nm.; $R_t = 11$ min for major isomer and $R_t = 15$ min for minor isomer); $[\alpha]^{20}_D +12.8$ (c 0.00435, CH_2Cl_2)



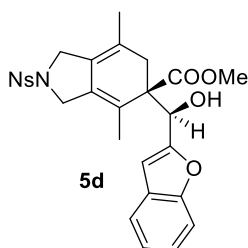
Compound **5b** (37% yield, 90% ee), yellow solid. **Molecular formula:**

$\text{C}_{23}\text{H}_{24}\text{N}_2\text{SO}_8$; **MW:** 488.51 g/mol; **m.p.:** 63-64°C; **$^1\text{H-NMR}$ (300 MHz, CDCl_3) δ (ppm)** 1.54 (s, 3H), 1.61 (s, 3H), 2.46 (d, $^2J_{\text{H,H}} = 17.4$ Hz, 1H), 2.58 (d, $^7J_{\text{H,H}} = 17.4$ Hz, 1H), 3.25 (d, $^3J_{\text{H,H}} = 6.7$ Hz, 1H), 3.70 (s, 3H), 3.93-4.03 (m, 4H), 4.93 (d, $^3J_{\text{H,H}} = 6.7$ Hz, 1H), 6.13 (m, 1H), 6.24 (m, 1H), 7.22 (m, 1H), 8.01 (d, $^3J_{\text{H,H}} = 9.0$ Hz, 2H), 8.38 (d, $^3J_{\text{H,H}} = 9.0$ Hz, 2H); **$^{13}\text{C-NMR}$ (75MHz, CDCl_3) δ (ppm)** 16.5, 19.2, 35.3, 50.5, 51.2, 52.5, 57.1, 69.5, 107.9, 110.5, 120.6, 123.8, 124.5, 124.9, 128.7, 131.9, 141.7, 142.4, 150.3, 153.7, 174.9; **ESI-MS (m/z):** 471.1 $[\text{M}-\text{H}_2\text{O}+\text{H}]^+$, 511.1 $[\text{M}+\text{Na}]^+$; **IR (ATR) (cm^{-1})** 3506, 2920, 1719, 1528, 1348, 1164; **EA** calculated for $\text{C}_{23}\text{H}_{24}\text{N}_2\text{SO}_8 \cdot 0.5\text{H}_2\text{O}$: C, 55.53, H, 5.07, N, 5.63, found: C, 55.11, H, 4.81, N, 5.48. Enantiomeric excess was determined with **HPLC** analysis (Chiralpak AD-H column (4.6 x 250 mm, 5 μm); 1 mL/min flow rate of a 50% 2-propanol : 50% heptane mobile phase during 15 min.; $\lambda = 254$ nm.; $R_t = 9.0$ min for major isomer and $R_t = 9.9$ min for minor isomer). $[\alpha]^{20}_D +18.6$ (c 0.0026, CH_2Cl_2).



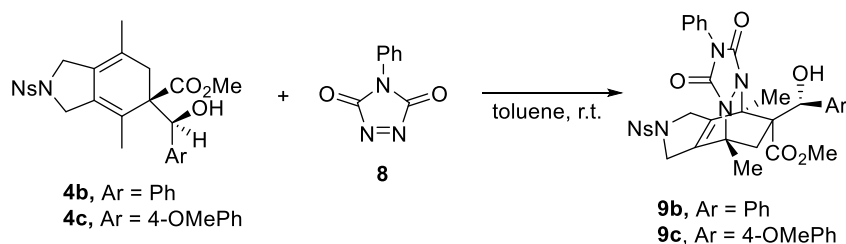
Compound **5c** (49% yield, 91% ee), yellow solid. **Molecular formula:**

$\text{C}_{27}\text{H}_{26}\text{N}_2\text{S}_2\text{O}_7$; **MW:** 554.63 g/mol; **m.p.:** 70°C; **$^1\text{H-NMR}$ (400 MHz, CDCl_3) δ (ppm)** 1.53 (s, 3H), 1.70 (s, 3H), 2.41 (d, $^2J_{\text{H,H}} = 17.6$ Hz, 1H), 2.58 (d, $^2J_{\text{H,H}} = 17.6$ Hz, 1H), 3.40 (d, $^3J_{\text{H,H}} = 4.8$ Hz, 1H), 3.70 (m, 1H), 3.71 (s, 3H), 3.90 (dd, $^2J_{\text{H,H}} = 13.2$ Hz, $^4J_{\text{H,H}} = 1.2$ Hz, 1H), 4.01 (s, 2H), 5.38 (d, $^3J_{\text{H,H}} = 4.8$ Hz, 1H), 7.05 (s, 1H), 7.24-7.32 (m, 2H), 7.61-7.65 (m, 2H), 7.95 (d, $^3J_{\text{H,H}} = 9.0$ Hz, 2H), 8.34 (d, $^3J_{\text{H,H}} = 9.0$ Hz, 2H); **$^{13}\text{C-NMR}$ (75MHz, CDCl_3) δ (ppm)** 16.7, 19.2, 34.7, 50.4, 51.3, 52.6, 57.6, 72.5, 120.2, 122.15, 122.16, 123.5, 124.3, 124.43, 124.45, 124.48, 124.7, 128.8, 132.6, 138.9, 139.4, 142.2, 144.2, 150.2, 174.4; **ESI-MS (m/z):** 537.0 $[\text{M}-\text{H}_2\text{O}+\text{H}]^+$, 577.1 $[\text{M}+\text{Na}]^+$; **IR (ATR) (cm^{-1})** 3485, 2919, 1725, 1527, 1347, 1164; **EA** calculated for $\text{C}_{27}\text{H}_{26}\text{N}_2\text{S}_2\text{O}_7 \cdot \text{H}_2\text{O}$: C, 56.63, H, 4.93, N, 4.89, found: C, 56.88, H, 4.82, N, 5.24. Enantiomeric excess was determined with **HPLC** analysis (Chiralpak IA column (4.6 x 250 mm, 5 μm); 1 mL/min flow rate of a 30% 2-propanol : 70% hexane mobile phase during 33 min.; $\lambda = 254$ nm.; $R_t = 24$ min for major isomer and $R_t = 29$ min for minor isomer); $[\alpha]^{20}_D +19.8$ (c 0.0048, CH_2Cl_2)

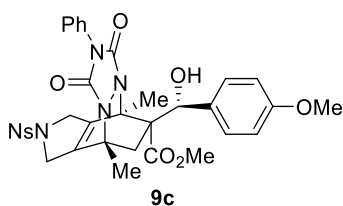


Compound **5d** (41% yield, 92% ee), yellow solid. **Molecular formula:** $C_{27}H_{26}N_2SO_8$; **MW:** 538.57 g/mol; **m.p.:** 84-86°C; **1H -NMR (400 MHz, $CDCl_3$) δ (ppm)** 1.54 (s, 3H), 1.66 (s, 3H), 2.50 (d, $^2J_{H,H} = 17.6$ Hz, 1H), 2.56 (d, $^2J_{H,H} = 17.6$ Hz, 1H), 3.39 (d, $^3J_{H,H} = 5.8$ Hz, 1H), 3.51 (d, $^2J_{H,H} = 12.2$ Hz, 1H), 3.74 (s, 3H), 3.85 (d, $^3J_{H,H} = 12.2$ Hz, 1H), 4.01 (bs, 2H), 5.14 (d, $^3J_{H,H} = 5.8$ Hz, 1H), 6.52 (s, 1H), 7.15-7.23 (m, 2H), 7.27 (m, 1H), 7.40 (m, 1H), 7.97 (d, $^3J_{H,H} = 9.0$ Hz, 2H), 8.38 (d, $^3J_{H,H} = 9.0$ Hz, 2H); **^{13}C -NMR (75MHz, $CDCl_3$) δ (ppm)** 16.9, 19.1, 35.2, 50.2, 51.2, 52.6, 57.0, 70.7, 104.6, 111.0, 120.0, 120.9, 123.0, 123.6, 124.3, 124.4, 124.7, 127.8, 128.7, 132.1, 142.2, 150.2, 154.3, 156.3, 174.9; **ESI-MS (m/z):** 521.1 $[M-H_2O+H]^+$, 561.14 $[M+Na]^+$; **IR (ATR) (cm^{-1})** 3491, 2916, 1724, 1528, 1347, 1164; **EA** calculated for $C_{27}H_{26}N_2SO_8 \cdot H_2O$: C, 58.27, H, 5.07, N, 5.03, found: C, 58.28, H, 4.58, N, 4.85. Enantiomeric excess was determined with **HPLC** analysis (Chiralpak AD-H column (4.6 x 250 mm, 5 μ m); 1 mL/min flow rate of a 10% 2-propanol : 90% heptane mobile phase during 20 min.; $\lambda = 254$ nm.; Rt = 14 min for major isomer and Rt = 16 min for minor isomer); **$[\alpha]^{20}_D + 7.1$** (c 0.0015, CH_2Cl_2)

8.2.4. Diels-Alder cycloaddition between 1,3-cyclohexadienes **4** and 4-phenyl-1,2,4-triazoline-3,5-dione.



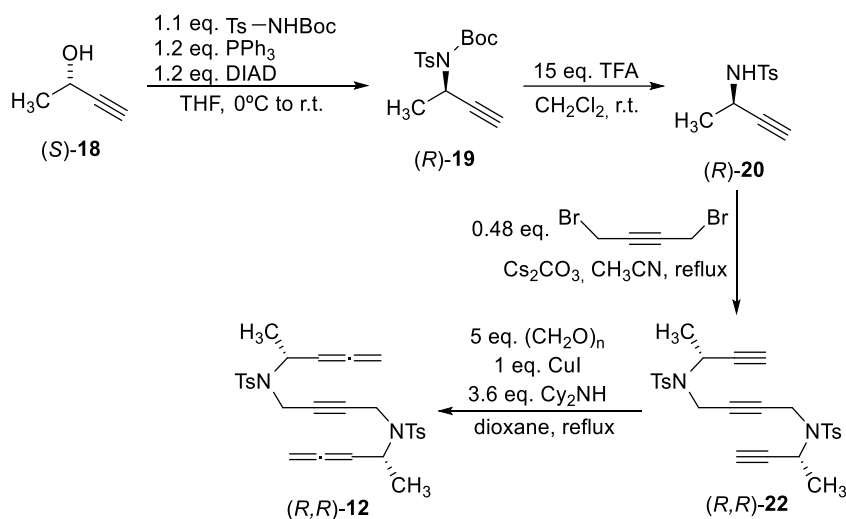
General procedure for **9**: In a 10 mL round bottom flask, a mixture of cycloadduct **4b** (20.0 mg, 0.04 mmol) and 4-phenyl-1,2,4-triazoline-3,5-dione **8** (7.5 mg, 0.04 mmol) in toluene (1 mL) was stirred at room temperature for 3 hours until completion (TLC monitoring). The solvent was then evaporated and the residue was purified by preparative TLC using a mixture of hexanes/ethyl acetate (1:1) as the eluent to give compound **9b** (22.1 mg, 81% yield) as a light-brown solid. **Molecular formula:** $C_{33}H_{31}N_5O_9S$; **MW:** 673.70 g/mol; **m.p.:** 65-67°C; **1H -NMR (400 MHz, $CDCl_3$) δ (ppm)** 1.96 (s, 3H), 2.23 (d, $^2J_{H,H} = 13.6$ Hz, 1H), 2.32 (s, 3H), 2.79 (d, $^2J_{H,H} = 13.6$ Hz, 1H), 3.03 (d, $^3J_{H,H} = 2.9$ Hz, 1H), 3.30 (s, 3H), 3.98 (m, 1H), 4.25-4.45 (m, 3H), 5.51 (d, $^3J_{H,H} = 2.9$ Hz, 1H), 7.19-7.43 (m, 10H), 8.00 (d, $^3J_{H,H} = 9.0$ Hz, 2H), 8.38 (d, $^3J_{H,H} = 9.0$ Hz, 2H). **^{13}C -NMR (100MHz, $CDCl_3$) δ (ppm)** 15.1, 18.9, 36.0, 52.5, 53.3, 53.7, 58.1, 61.9, 64.1, 72.6, 124.8, 126.2, 127.0, 128.5, 128.7, 129.1, 131.3, 137.6, 139.7, 140.5, 143.2, 150.1, 150.4, 151.2, 170.7. **IR (ATR) (cm^{-1})** 3446, 2920, 1756, 1689, 1529, 1348, 1165; **ESI-MS (m/z):** 674.2 $[M+H]^+$; **ESI-HRMS (m/z)** calculated for $[C_{33}H_{31}N_5O_9S+Na]^+$: 696.1735, found: 696.1725.



Compound **9c** (73% yield), light-brown solid. **Molecular formula:** $C_{34}H_{33}N_5O_{10}S$; **MW:** 703.70 g/mol; **m.p.:** 59–61°C; **1H -NMR (600 MHz, $CDCl_3$) δ (ppm) (major)** 1.92 (s, 3H), 2.20 (d, $^2J_{H,H} = 13.5$ Hz, 1H), 2.25 (s, 3H), 2.72 (d, $^3J_{H,H} = 13.5$ Hz, 1H), 3.22 (bs, 1H), 3.29 (s, 3H), 3.74 (s, 3H), 4.00 (m, 1H), 4.23–4.37 (m, 3H), 5.36 (bs, 1H), 6.75 (d, $^3J_{H,H} = 9.0$ Hz, 2H), 7.05 (d, $^3J_{H,H} = 9.0$ Hz, 2H), 7.25–7.37 (m, 5H), 7.97 (d, $^3J_{H,H} = 9.0$ Hz, 2H), 8.32 (d, $^3J_{H,H} = 9.0$ Hz, 2H); **(minor)** 1.66 (d, $^2J_{H,H} = 13.2$ Hz, 1H), 1.84 (s, 3H), 2.10 (s, 3H), 2.52 (d, $^2J_{H,H} = 13.2$ Hz, 1H), 3.06 (bs, 1H), 3.64 (s, 3H), 3.70 (s, 3H), 4.23 (m, 1H), 4.23–4.37 (m, 2H), 4.43 (m, 1H), 5.19 (bs, 1H), 6.75 (d, $^3J_{H,H} = 8.4$ Hz, 2H), 6.94 (d, $^3J_{H,H} = 8.4$ Hz, 2H), 7.25–7.37 (m, 5H), 7.94 (d, $^3J_{H,H} = 8.7$ Hz, 2H), 8.30 (d, $^3J_{H,H} = 8.7$ Hz, 2H); **^{13}C -NMR (150 MHz, $CDCl_3$) δ (ppm) (major)** 14.9, 18.6, 35.9, 52.3, 53.1, 53.5, 55.2, 58.0, 61.8, 63.5, 71.6, 113.5, 124.6, 126.1, 128.1, 128.4, 129.0, 131.2, 132.0, 137.8, 140.1, 142.9, 149.2, 150.2, 150.4, 159.4, 170.7 **(minor)** 15.0, 18.9, 38.1, 52.0, 52.7, 54.5, 55.2, 58.5, 60.5, 63.9, 71.2, 113.7, 124.6, 126.1, 127.8, 128.4, 129.0, 131.2, 131.5, 136.1, 138.8, 143.4, 149.2, 150.2, 150.4, 159.5, 171.6; **IR (ATR) (cm^{-1})** 3463, 2951, 1755, 1689, 1529, 1348, 1166; **ESI-MS (m/z):** 686.1 $[M-H_2O+H]^+$, 704.1 $[M+H]^+$; **ESI-HRMS (m/z):** calculated for $[C_{34}H_{33}N_5O_{10}S+Na]^+$: 726.1840, found: 726.1823

8.3. Experimental procedure for the products synthesised in Chapter 4

8.3.1. Synthesis of allene-yne-allene (*R,R*)-12



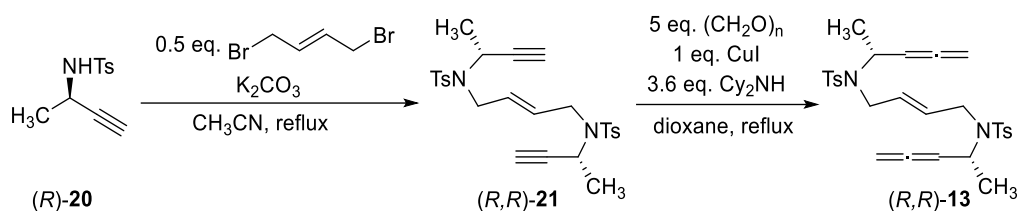
In a 100 mL round bottom flask, a mixture of *N*-(*tert*-butoxycarbonyl)-*p*-toluenesulfonamide (3.87 g, 14.26 mmol), triphenylphosphine (4.50 g, 17.16 mmol) and (*S*)-3-butyn-2-ol, (*S*)-**18**, (1.12 mL, 14.11 mmol) in anhydrous tetrahydrofuran (50 mL) was stirred and cooled to 0°C. Diisopropyl azodicarboxylate (3.09 mL, 15.69 mmol) was then added dropwise and the reaction mixture was stirred overnight at room temperature (TLC monitoring). The solvent was removed under reduced pressure and the crude was purified by column chromatography using a mixture of hexanes/ethyl acetate (20:1) as the eluent to afford (*R*)-**19**¹⁷⁷ (4.32 g, 94% yield) as a yellow oil. **Molecular formula:** $C_{16}H_{21}NO_4S$; **MW:** 323.41 g/mol; **1H -NMR (400 MHz, $CDCl_3$) δ (ppm)** 1.36 (s,

9H, $\text{CH}_3\text{-Boc}$), 1.75 (d, $^3J_{\text{H,H}} = 7.0$ Hz, 3H, CH_3), 2.38 (d, $^4J_{\text{H,H}} = 2.4$ Hz, 1H, CHN), 2.44 (s, 3H, $\text{CH}_3\text{-Ts}$), 5.48 (dq, $^3J_{\text{H,H}} = 7.0$ Hz, $^4J_{\text{H,H}} = 2.4$ Hz, 1H, $\text{HC}\equiv\text{C}$), 7.31 (d, $^3J_{\text{H,H}} = 8.4$ Hz, 2H, CH-Ts), 7.85 (d, $^3J_{\text{H,H}} = 8.4$ Hz, 2H, CH-Ts).

In a 250 mL two-necked round bottom flask, a mixture of (*R*)-**19**, (4.32 g, 11.22 mmol) and trifluoroacetic acid (13 ml, 169.77 mmol) in dichloromethane (50 mL) was stirred at room temperature for 3.5 h (TLC monitoring). A saturated aqueous solution of NaHCO_3 was added and the aqueous phase was extracted with dichloromethane (3 x 50 mL). The organic phase was dried with anhydrous sodium sulfate, filtered and evaporated under reduced pressure. The residue was purified by column chromatography using a mixture of hexanes/ethyl acetate (8:2) as the eluent to give (*R*)-**20**¹⁷⁸ (2.37 g, 94 %yield) as a colourless solid. **Molecular formula:** $\text{C}_{11}\text{H}_{13}\text{NO}_2\text{S}$; **MW:** 223.29 g/mol; **m.p.:** 79-80°C; **$^1\text{H-NMR}$ (400 MHz, CDCl_3) δ (ppm)** 1.43 (d, $^3J_{\text{H,H}} = 6.8$ Hz, 3H, CH_3), 2.09 (d, $^4J_{\text{H,H}} = 2.4$ Hz, 1H, CHN), 2.43 (s, 3H, $\text{CH}_3\text{-Ts}$), 4.19 (ddq, $^3J_{\text{H,H}} = 8.8$ Hz, $^4J_{\text{H,H}} = 6.8$ Hz, $^5J_{\text{H,H}} = 2.4$ Hz, 1H, NH), 4.63 (d, $^4J_{\text{H,H}} = 8.8$ Hz, 1H, $\text{HC}\equiv\text{C}$), 7.30 (d, $^3J_{\text{H,H}} = 8.0$ Hz, 2H, CH-Ts), 7.78 (d, $^3J_{\text{H,H}} = 8.0$ Hz, 2H, CH-Ts); **$[\alpha]_{\text{D}}^{22} +83.2$ (c 1.4, CHCl_3).**

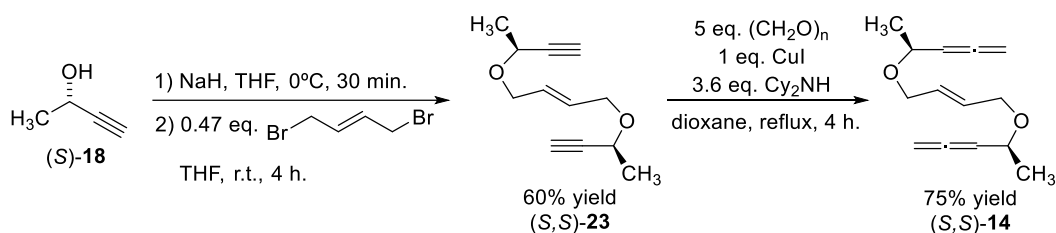
In a 25 mL two-necked round bottom flask, a mixture of (*R*)-**20** (0.2 g, 0.90 mmol), 1,4-dibromobut-2-yne (0.09 g, 0.43 mmol) and cesium carbonate (1.46 g, 4.5 mmol) in acetonitrile (10 mL) was heated at reflux for 2 h (TLC monitoring). The insoluble salts were filtered off and the solvent was removed under reduced pressure. The reaction crude was purified by column chromatography using a mixture of hexanes/ethyl acetate of increasing polarity (10:1-9:1) as the eluent to give (*R,R*)-**22** (0.104 g, 47% yield) as a colourless solid. **Molecular formula:** $\text{C}_{26}\text{H}_{28}\text{N}_2\text{O}_4\text{S}_2$; **MW:** 496.64 g/mol; **m.p.:** 99-101°C; **$^1\text{H-NMR}$ (400 MHz, CDCl_3) δ (ppm)** 1.41 (d, $^3J_{\text{H,H}} = 7.2$ Hz, 6H, CH_3), 2.21 (d, $^4J_{\text{H,H}} = 2.4$ Hz, 2H, $\text{HC}\equiv\text{C}$), 2.40 (s, 6H, $\text{CH}_3\text{-Ts}$), 3.92 (d, $^2J_{\text{H,H}} = 16.8$ Hz 2H, NCH_2), 4.14 (d, $^2J_{\text{H,H}} = 16.4$ Hz, 2H, NCH_2), 4.82 (qd, $^3J_{\text{H,H}} = 7.2$ Hz, $^4J_{\text{H,H}} = 2.4$ Hz, 2H, CHN), 7.28 (d, $^3J_{\text{H,H}} = 8.2$ Hz, 4H, CH-Ts), 7.72 (d, $^3J_{\text{H,H}} = 8.2$ Hz, 4H, CH-Ts); **$^{13}\text{C-NMR}$ (75 MHz, CDCl_3) δ (ppm)** 21.7 (CH_3), 22.0 (CH_3), 33.7 (NCH_2), 46.1 (NCH), 73.7 (C-alkyne), 80.0 (C-alkyne), 81.0 (C-alkyne), 127.7 (CH-Ts), 129.7 (CH-Ts), 136.5 (C-Ts), 143.8 (C-Ts); **IR (ATR) ν (cm^{-1})** 3272, 2920, 1326, 1163; **ESI-MS (m/z):** 497.2 [$\text{M}+\text{H}$]⁺, 514.2 [$\text{M}+\text{NH}_4$]⁺; **ESI-HRMS (m/z):** calculated for $[\text{C}_{26}\text{H}_{28}\text{N}_2\text{O}_4\text{S}_2 + \text{Na}]^+$: 519.1383, found 519.1398; **$[\alpha]_{\text{D}}^{22} +100.0$ (c 0.69, CHCl_3)**

In a 10 mL two-necked round bottom flask, a mixture of (*R,R*)-**22** (0.070 g, 0.15 mmol), paraformaldehyde (0.023 g, 0.76 mmol) and copper(I) iodide (0.028 g, 0.15 mmol) in dioxane (3 mL) was stirred and heated at reflux. Dicyclohexylamine (0.10 mL, 0.50 mmol) was then added and the reaction was stirred for 4 hours (TLC monitoring). The reaction crude was purified by column chromatography using a mixture of hexanes/ethyl acetate (15:1) as the eluent to afford (*R,R*)-**12** (0.05 g, 63% yield) as a colourless oil. **Molecular formula:** $\text{C}_{28}\text{H}_{32}\text{N}_2\text{O}_4\text{S}_2$; **MW:** 524.69 g/mol; **$^1\text{H-NMR}$ (400MHz, CDCl_3) δ (ppm)** 1.17 (d, $^3J_{\text{H,H}} = 6.8$ Hz, 6H, CH_3), 2.41 (s, 6H, $\text{CH}_3\text{-Ts}$), 3.82 (d, $^2J_{\text{H,H}} = 16.6$ Hz, 2H, NCH_2), 4.04 (d, $^2J_{\text{H,H}} = 16.6$ Hz, 2H, NCH_2), 4.49-4.57 (m, 2H, $\text{HC}=\text{C}=\text{CH}_2$), 4.78 (dd, $^2J_{\text{H,H}} = 3.7$ Hz, $^4J_{\text{H,H}} = 1.3$ Hz, 2H, $\text{HC}=\text{C}=\text{CH}_2$), 4.80 (dd, $^2J_{\text{H,H}} = 3.7$ Hz, $^4J_{\text{H,H}} = 1.7$ Hz, 2H, $\text{HC}=\text{C}=\text{CH}_2$), 5.00 (dq, $^3J_{\text{H,H}} = 6.8$ Hz, $^3J_{\text{H,H}} = 4.8$ Hz, 2H, CHN), 7.30 (d, $^3J_{\text{H,H}} = 8.2$ Hz, 4H, CH-Ts), 7.77 (d, $^3J_{\text{H,H}} = 8.2$ Hz, 4H, CH-Ts); **$^{13}\text{C-NMR}$ (75 MHz, CDCl_3) δ (ppm)** 18.0 (CH_3), 21.6 ($\text{CH}_3\text{-Ts}$), 32.4 (NCH_2), 51.7 (NCH), 78.0 (C-alkyne), 80.2 ($\text{HC}=\text{C}=\text{CH}_2$), 91.7 ($\text{HC}=\text{C}=\text{CH}_2$), 127.5 (CH-Ts), 129.7 (CH-Ts), 137.8 (C-Ts), 143.5 (C-Ts), 208.7 ($\text{HC}=\text{C}=\text{CH}_2$); **IR (ATR) ν (cm^{-1})** 2922, 1952, 1330, 1150; **ESI-MS (m/z):** 542.2 [$\text{M}+\text{NH}_4$]⁺; **ESI-HRMS (m/z):** calculated for $[\text{C}_{28}\text{H}_{32}\text{N}_2\text{O}_4\text{S}_2 + \text{Na}]^+$: 547.1696, found 547.1715; **$[\alpha]_{\text{D}}^{22} +9.2$ (c 4.2, CHCl_3).**

8.3.2. Synthesis of allene-ene-allene (*R,R*)-13

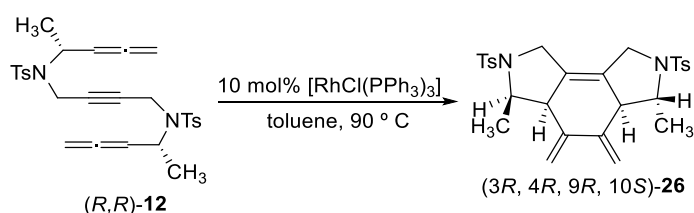
In a 100 mL two-necked round bottom flask, a mixture of (*R*)-**20** (0.90 g, 4.03 mmol) and potassium carbonate (2.79 g, 20.19 mmol) in acetonitrile (40 mL) was stirred and heated at reflux. (*E*)-1,4-dibromo-2-butene (0.43 g, 2.01 mmol) was then slowly added and the reaction was stirred for 3 hours (TLC monitoring). The salts were filtered off and the solvent was evaporated under reduced pressure. The reaction crude was purified by column chromatography using a mixture of hexanes/ethyl acetate (8:2) as the eluent to afford (*R,R*)-**21** (0.98 g, 98% yield) as a colourless solid. **Molecular formula:** $C_{26}H_{30}N_2O_4S_2$; **MW:** 498.66 g/mol; **m.p.:** 130-132°C; **1H -NMR (300 MHz, $CDCl_3$) δ (ppm)** 1.42 (d, $^3J_{H,H} = 7.20$ Hz, 6H, CH_3), 2.13 (d, $^4J_{H,H} = 2.3$ Hz, 2H, $C\equiv CH$), 2.42 (s, 6H, CH_3 -Ts), 3.66-3.74 (m, 2H, NCH_2), 3.85-3.90 (m, 2H, NCH_2), 4.86 (dq, $^3J_{H,H} = 7.2$ Hz, $^4J_{H,H} = 2.3$ Hz, 2H, NCH), 5.76-5.78 (m, 2H, $HC=CH$), 7.29 (d, $^3J_{H,H} = 8.4$ Hz, 4H, CH -Ts), 7.71 (d, $^3J_{H,H} = 8.4$ Hz, 4H, CH -Ts); **^{13}C -NMR (100 MHz, $CDCl_3$) δ (ppm)** 21.6 (CH_3 -Ts), 22.8 (CH_3), 46.2 ($NCH + NCH_2$), 73.5 ($C\equiv CH$), 81.31 ($C\equiv CH$), 127.7 (CH -Ts), 129.6 ($HC=CH$), 130.51 (CH -Ts), 136.2 (C -Ts), 143.6 (C -Ts); **IR (ATR) ν (cm^{-1})** 3256, 1324, 1160; **ESI-MS (m/z):** 499.1 [$M+H$] $^+$; **EA** calculated for $C_{26}H_{30}N_2O_4S_2$: C 62.62, H 6.06, N 5.62, found: C 62.47, H 6.14, N 5.67; Chiral **HPLC** analysis: Chiralpak IC column, 4.6 x 250 mm, 5 μm ; 1 mL/min flow rate of a 2-propanol (50%): heptane (50%) mobile phase; $\lambda = 232$ nm.; $R_t = 23.0$ min. and $R_t = 28.7$ min. for the two enantiomers and $R_t = 26.3$ min. for the *meso* form; $R_t = 28.4$ min for the enantiomerically pure product; $[\alpha]_D^{22} +185.0$ (c 0.57, $CHCl_3$).

In a 100 mL two-necked round bottom flask, a mixture of (*R,R*)-**21** (0.92 g, 1.85 mmol), paraformaldehyde (0.28 g, 9.32 mmol) and copper(I) iodide (0.35 g, 1.84 mmol) in dioxane (30 mL) was stirred and heated at reflux. Dicyclohexylamine (1.33 mL, 6.69 mmol) was then added and the reaction was stirred for 25 hours (TLC monitoring). The reaction crude was purified by column chromatography using a mixture of hexanes/ethyl acetate (9:1) as the eluent to afford (*R,R*)-**13** (0.93 g, 95% yield) as a brown oil. **Molecular formula:** $C_{28}H_{34}N_2O_4S_2$; **MW:** 526.71 g/mol; **1H -NMR (300 MHz, $CDCl_3$) δ (ppm)** 1.19 (d, $^3J_{H,H} = 6.8$ Hz, 6H, CH_3), 2.42 (s, 6H, CH_3 -Ts), 3.62-3.68 (m, 2H, NCH_2), 3.78-3.83 (m, 2H, NCH_2), 4.53-4.62 (m, 2H, $HC=C=CH_2$), 4.72-4.81 (m, 4H, $HC=C=CH_2$), 4.86-4.90 (m, 2H, CHN), 5.66-5.69 (m, 2H, $HC=CH$), 7.29 (d, $^3J_{H,H} = 8.3$ Hz, 4H, CH -Ts), 7.71 (d, $^3J_{H,H} = 8.3$ Hz, 4H, CH -Ts); **^{13}C -NMR (100 MHz, $CDCl_3$) δ (ppm)** 18.7 (CH_3), 21.4 (CH_3 -Ts), 44.8 (NCH_2), 51.7 (NCH), 77.7 ($HC=C=CH_2$), 91.5 ($HC=C=CH_2$), 127.1 (CH -Ts), 129.6 ($HC=CH$), 130.5 (CH -Ts), 137.8 (C -Ts), 143.2 (C -Ts), 208.5 ($HC=C=CH_2$); **IR (ATR) ν (cm^{-1})** 2979, 1954, 1333, 1150; **ESI-MS (m/z):** 527.2 [$M+H$] $^+$, 544.2 [$M+NH_4$] $^+$, 549.2 [$M+Na$] $^+$; **EA** calculated for $C_{28}H_{34}N_2O_4S_2$: C 63.85, H 6.51, N 5.32, found: C 63.87, H 6.53, N 5.39; Chiral **HPLC** analysis: Chiralpak IA column, 4.6 x 250 mm, 5 μm ; 1 mL/min flow rate of a 2-propanol (15%): heptane (85%) mobile phase; $\lambda = 232$ nm.; $R_t = 18.2$ min. and $R_t = 20.6$ min. for the two enantiomers and $R_t = 21.9$ min. for the *meso* form; $R_t = 20.4$ min for the enantiomerically pure product; $[\alpha]_D^{22} +155.6$ (c 3.57, $CHCl_3$).

8.3.3. Synthesis of allene-ene-allene (*S,S*)-14

In a 25 mL two-necked round bottom flask, under nitrogen atmosphere, NaH (0.22 g, 5.50 mmol) was washed with hexanes (3 x 5 mL) and dried under vacuum. A solution of (*S*)-18 (0.3 mL, 3.66 mmol) in THF (10 mL) was then added and cooled at 0°C. After 30 minutes a solution of (*E*)-1,4-dibromo-2-butene (0.37 g, 1.73 mmol) in THF (5 mL) was added and the reaction was stirred at room temperature for 4 hours (TLC monitoring). A saturated aqueous solution of NaHCO₃ was added and the aqueous phase was extracted with ethyl acetate (3 x 15 mL). The organic phase was dried with anhydrous sodium sulfate, filtered and evaporated under reduced pressure. The reaction crude was purified by column chromatography using a mixture of hexanes/ethyl acetate (10:1) as the eluent to afford (*S,S*)-23 (0.20 g, 60% yield) as a yellow oil. **Molecular formula:** C₁₂H₁₆O₂; **MW:** 192.26 g/mol; **¹H-NMR (400 MHz, CDCl₃) δ (ppm)** 1.42 (d, ³J_{H,H} = 6.8 Hz, 6H, CH₃), 2.40 (d, ⁴J_{H,H} = 2.0 Hz, 2H, HC≡C), 3.93-3.98 (m, 2H), 4.17 (qd, ³J_{H,H} = 6.8 Hz, ⁴J_{H,H} = 2.0 Hz, 2H, CHO), 4.21-4.25 (m, 2H), 5.81-5.84 (m, 2H); **¹³C-NMR (75 MHz, CDCl₃) δ (ppm)** 22.1 (CH₃), 64.5, 68.6, 73.1 (C≡CH), 83.7 (C≡CH), 129.5 (HC=CH); **IR (ATR) ν (cm⁻¹)** 3275, 2918, 1093; **ESI-HRMS (m/z):** calculated for [C₁₂H₁₆O₂ + Na]⁺: 215.1043, found 215.1043; [α]_D²² -41.4 (c 2.28, CHCl₃).

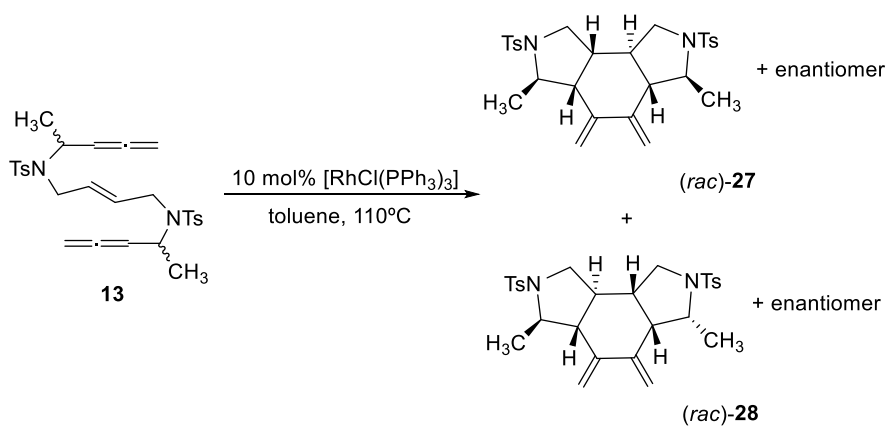
In a 25 mL two-necked round bottom flask, a mixture of (*S,S*)-23 (0.14 g, 0.73 mmol), paraformaldehyde (0.11 g, 3.66 mmol) and copper(I) iodide (0.13 g, 0.68 mmol) in dioxane (15 mL) was stirred and heated at reflux. Dicyclohexylamine (0.49 mL, 2.46 mmol) was then added and the reaction was stirred for 4 hours (TLC monitoring). The reaction crude was purified by column chromatography using a mixture of hexanes/ethyl acetate (50:1) as the eluent to afford (*S,S*)-14 (0.12 g, 75% yield) as a yellow oil. **Molecular formula:** C₁₄H₂₀O₂; **MW:** 220.31 g/mol; **¹H-NMR (400 MHz, CDCl₃) δ (ppm)** 1.29 (d, ³J_{H,H} = 6.5 Hz, 6H, CH₃), 3.88-3.94 (m, 2H, OCH₂), 3.95-4.03 (m, 2H, HC=C=CH₂), 4.05-4.10 (m, 2H, OCH₂), 4.72-4.81 (m, 4H, HC=C=CH₂), 5.03-5.09 (m, 2H, OCH), 5.78-5.80 (m, 2H, HC=CH); **¹³C-NMR (75 MHz, CDCl₃) δ (ppm)** 21.7 (CH₃), 68.2, 73.5, 76.0 (HC=C=CH₂), 92.9 (HC=C=CH₂), 129.6 (HC=CH), 208.3 (HC=C=CH₂); **IR (ATR) ν (cm⁻¹)** 2927, 1951, 1093; **ESI-HRMS (m/z):** calculated for [C₁₄H₂₀O₂ + Na]⁺: 243.1356, found 243.1378; [α]_D²² -28.4 (c 1.83, CHCl₃).

8.3.4. Cycloaddition reaction of (*R,R*)-12

In a 10 mL 2-necked round bottom flask, a mixture of (*R,R*)-12 (0.054 g, 0.10 mmol) and tris(triphenylphosphine)rhodium(I)chloride (0.0096 g, 0.01 mmol) was purged with nitrogen and

dissolved in anhydrous toluene (3 mL). The mixture was stirred at 90°C for 1h (TLC monitoring). The solvent was removed and the crude was purified by column chromatography using a mixture of hexanes/ethyl acetate (90:10) as the eluent to give cycloadduct (3*R*, 4*R*, 9*R*, 10*S*)-**26** (0.022 g, 40% yield) as a colourless solid. **Molecular formula:** C₂₈H₃₂N₂O₄S₂; **MW:** 524.69 g/mol; **m.p.:** 87-89°C; **¹H-NMR (400 MHz, CDCl₃) δ(ppm)** 0.51 (d, ³J_{H,H} = 6.5 Hz, 3H), 1.55 (d, ³J_{H,H} = 6.0 Hz 3H), 2.37 (s, 3H), 2.43 (s, 3H), 2.86 (br s, 1H), 2.95 (br s, 1H), 3.51 (dq, ³J_{H,H} = 7.6 Hz, ³J_{H,H} = 3*6.0 Hz, 1H), 3.62 (m, 1H), 3.71 (m, 1H), 3.88 (m, 1H), 3.96 (m, 1H), 4.04 (dq, ³J_{H,H} = 7.9 Hz, ³J_{H,H} = 3*6.6 Hz, 1H), 4.64 (d, ²J_{H,H} = 2.2 Hz, 1H), 4.79 (m, 1H), 5.11 (d, ²J_{H,H} = 2.2 Hz, 1H), 5.39 (m, 1H), 7.23 (d, ³J_{H,H} = 8.2 Hz, 2H), 7.33 (d, ³J_{H,H} = 8.2 Hz, 2H), 7.66 (d, ³J_{H,H} = 8.2 Hz, 2H), 7.72 (d, ³J_{H,H} = 8.2 Hz, 2H); **¹³C-NMR (100 MHz, CDCl₃) δ (ppm)** 15.9, 21.6, 21.7, 22.8, 47.0, 47.2, 50.1, 51.0, 59.3, 59.8, 108.3, 115.7, 126.1, 127.2, 127.6, 129.5, 129.9, 130.0, 133.8, 136.0, 143.3, 143.7, 144.0, 144.9; **IR (ATR) ν (cm⁻¹)** 3211, 2918, 1386, 1162; **ESI-MS (m/z):** 525.2 [M+H]⁺; **ESI-HRMS (m/z):** calculated for [C₂₈H₃₂N₂O₄S₂ + Na]⁺: 547.1696, found 547.1710; **[α]_D²²** +1.3 (c 1.20, CHCl₃).

8.3.5. Cycloaddition reaction of **13**



In a 10 mL two-necked round bottom flask, a solution of **13** (0.05 g, 0.095 mmol) in anhydrous toluene (1 mL) was purged with nitrogen and heated at reflux. A solution of tris(triphenylphosphine)rhodium(I)chloride (0.009 g, 0.0097 mmol) in anhydrous toluene (2 mL) was then added. The mixture was stirred at reflux for 1.5 h (TLC monitoring). The solvent was evaporated and the crude was purified by column chromatography using mixtures of hexanes/ethyl acetate of increasing polarity (from 10:1 to 8:1) as the eluent to give cycloadduct **27** (0.016 g, 33% yield) and **28** (0.013 g, 27% yield) as colourless solids. **Molecular formula:** C₂₈H₃₄N₂O₄S₂; **MW:** 526.71 g/mol; **IR (ATR) ν (cm⁻¹)** 2895, 1323, 1154; **ESI-HRMS (m/z):** calculated for [C₂₈H₃₄N₂O₄S₂ + Na]⁺: 549.1852, found 549.1840. Chiral **HPLC** analysis: Chiralpak IA column, 4.6 x 250 mm, 5 μm; 1 mL/min flow rate of a 2-propanol (20%): heptane (80%) mobile phase; λ = 232 nm.; Rt = 14.8 min. and Rt = 16.6 min. for the racemic mixture of the major diastereoisomer **27** and Rt = 18.4 min and Rt = 32.7 min. for the racemic mixture of the minor diastereoisomer **28**.

NMR data for (*rac*)-**27**.

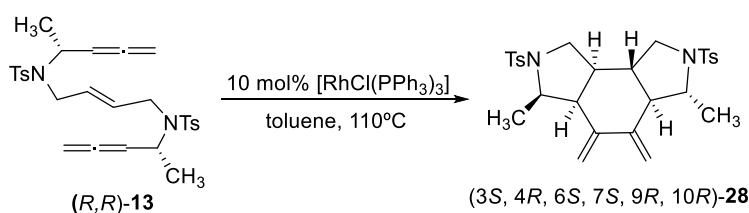
¹H-NMR (300 MHz, CDCl₃) δ (ppm) 0.65 (m, 1H), 1.27 (d, ³J_{H,H} = 6.0 Hz, 3H), 1.29 (d, ³J_{H,H} = 6.0 Hz, 3H), 1.78-1.95 (m, 2H), 2.42 (s, 3H), 2.49 (s, 3H), 2.54 (dd, ³J_{H,H} = 9.8 Hz, ³J_{H,H} = 6.0 Hz, 1H), 2.81 (dd, ²J_{H,H} = 9.9 Hz, ³J_{H,H} = 10.6 Hz, 1H), 3.18 (dq, ³J_{H,H} = 9.8 Hz, ³J_{H,H} = 3*6.0 Hz, 1H), 3.38 (m, 1H),

3.48 (dq, $^3J_{H,H} = 9.4$ Hz, $^3J_{H,H} = 3 \times 6.0$ Hz, 1H), 3.70 (dd, $^2J_{H,H} = 9.9$ Hz, $^3J_{H,H} = 7.0$ Hz, 1H), 3.77 (m, 1H), 4.54 (d, $^2J_{H,H} = 1.4$ Hz, 1H), 4.80 (d, $^2J_{H,H} = 1.7$ Hz, 1H), 5.00 (d, $^2J_{H,H} = 1.4$ Hz, 1H), 5.11 (d, $^2J_{H,H} = 1.7$ Hz, 1H), 7.32 (d, $^3J_{H,H} = 8.4$ Hz, 2H), 7.37 (d, $^3J_{H,H} = 8.4$ Hz, 2H), 7.69 (d, $^3J_{H,H} = 8.4$ Hz, 2H), 7.70 (d, $^3J_{H,H} = 8.4$ Hz, 2H); $^{13}\text{C-NMR}$ (75 MHz, CDCl_3) δ (ppm) 19.7, 20.4, 21.6, 21.7, 41.9, 42.3, 51.8, 52.4, 52.5, 54.9, 55.9, 57.8, 107.8, 114.8, 126.7, 126.9, 129.9, 130.0, 136.1, 137.5, 143.3, 144.1, 144.9, 145.8.

NMR data for (*rac*)-**28**

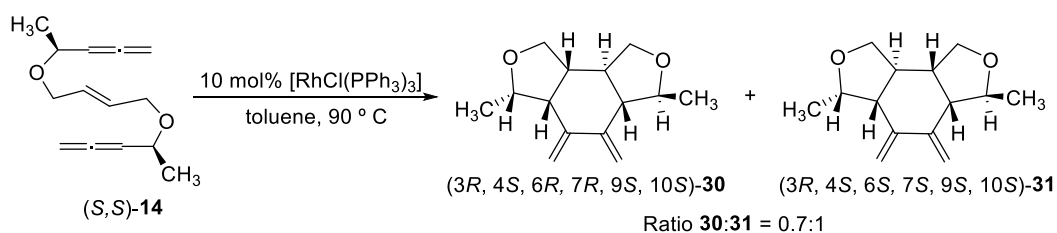
$^1\text{H-NMR}$ (400 MHz, CDCl_3) δ (ppm) 0.79 (d, $^3J_{H,H} = 6.9$ Hz, 3H), 0.97 (m, 1H), 1.48 (d, $^3J_{H,H} = 6.1$ Hz, 3H), 1.80-1.89 (m, 2H), 2.44 (s, 3H), 2.47 (s, 3H), 2.70 (dd, $^3J_{H,H} = 10.0$ Hz, $^3J_{H,H} = 6.8$ Hz, 1H), 2.84 (t, $J_{H,H} = 11.4$ Hz, 1H), 2.90 (dd, $^2J_{H,H} = 9.6$ Hz, $^3J_{H,H} = 6.0$ Hz, 1H), 3.20 (d, $J_{H,H} = 9.6$ Hz, 1H), 3.45 (dq, $^3J_{H,H} = 10.2$ Hz, $^3J_{H,H} = 6.9$ Hz, 1H), 3.66 (dq, $^3J_{H,H} = 9.0$ Hz, $^3J_{H,H} = 6.1$ Hz, 1H), 3.71 (dd, $^2J_{H,H} = 11.6$ Hz, $^3J_{H,H} = 6.2$ Hz, 1H), 4.59 (d, $^2J_{H,H} = 1.7$ Hz, 1H), 4.71 (d, $^2J_{H,H} = 1.7$ Hz, 1H), 5.05 (d, $^2J_{H,H} = 1.7$ Hz, 1H), 5.21 (d, $^2J_{H,H} = 1.7$ Hz, 1H), 7.33 (d, $^3J_{H,H} = 8.1$ Hz, 2H), 7.40 (d, $^3J_{H,H} = 8.1$ Hz, 2H), 7.66 (d, $^3J_{H,H} = 8.1$ Hz, 2H), 7.75 (d, $^3J_{H,H} = 8.1$ Hz, 2H); $^{13}\text{C-NMR}$ (100 MHz, CDCl_3) δ (ppm) 20.0, 21.6, 21.7, 22.1, 40.7, 43.5, 48.6, 51.9, 52.9, 54.6, 58.7, 59.0, 107.1, 116.0, 127.2, 127.8, 129.8, 130.3, 133.1, 134.1, 143.7, 144.4, 145.7, 146.7.

8.3.6. Cycloaddition reaction of (*R,R*)-**13**



In a 10 mL 2-necked round bottom flask, a mixture of (*R,R*)-**13** (0.050 g, 0.095 mmol) and tris(triphenylphosphine)rhodium(I)chloride (0.0088 g, 0.0095 mmol) was purged with nitrogen and dissolved in anhydrous toluene (2 mL). The mixture was stirred at reflux for 2h (TLC monitoring). The solvent was removed and the crude was purified by column chromatography using a mixture of hexanes/ethyl acetate (70:30) as the eluent to give cycloadduct (*3S, 4R, 6S, 7S, 9R, 10R*)-**28** (0.0315 g, 63% yield) as a colourless solid. Chiral HPLC analysis: Chiralpak IA column, 4.6 x 250 mm, 5 μm ; 1 mL/min flow rate of a 2-propanol (20%): heptane (80%) mobile phase; $\lambda = 232$ nm.; Rt = 32.7 min. for a single enantiomer; $[\alpha]_{\text{D}}^{22} -26.1$ (*c* 1.78, CHCl_3).

8.3.7. Cycloaddition reaction of (*S,S*)-**14**



In a 10 mL 2-necked round bottom flask, a mixture of (*S,S*)-**14** (0.052 g, 0.23 mmol) and tris(triphenylphosphine)rhodium(I)chloride (0.022 g, 0.023 mmol) was purged with nitrogen and

dissolved in anhydrous toluene (4 mL). The mixture was stirred at 90°C for 1h (TLC monitoring). The solvent was removed and the crude was purified by column chromatography using a mixture of hexanes/ethyl acetate (80:20) as the eluent to give an inseparable mixture of cycloadducts (3*R*, 4*S*, 6*R*, 7*R*, 9*S*, 10*S*)-**30** and (3*R*, 4*S*, 6*S*, 7*S*, 9*S*, 10*S*)-**31** (0.027 g, 52% combined yield, in a 0.7:1 ratio) as a colourless oil. **Molecular formula:** C₁₄H₂₀O₂. **MW:** 220.31 g/mol; **ESI-HRMS (*m/z*):** calculated for [C₁₄H₂₀O₂ + Na]⁺: 243.1356, found 243.1363.

(3*R*, 4*S*, 6*R*, 7*R*, 9*S*, 10*S*)-**30**

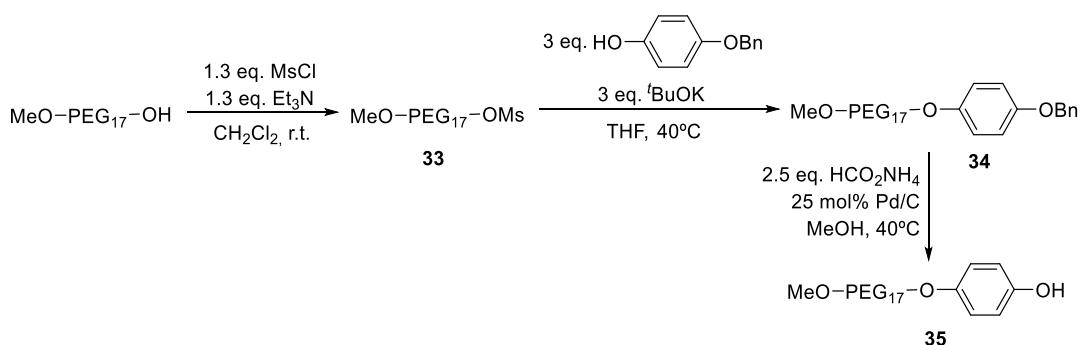
¹H-NMR (400 MHz, CDCl₃) δ (ppm) 1.09 (d, ³J_{H,H} = 6.7 Hz, 3H), 1.33 (d, ³J_{H,H} = 5.9 Hz, 3H), 1.91 (tt, J_{H,H} = 2*9.1 Hz, J_{H,H} = 2*2.0 Hz 1H), 2.16 (m, 1H), 2.19 (m, 1H), 3.25 (dd, ²J_{H,H} = 10.0 Hz, ³J_{H,H} = 6.2 Hz, 1H), 3.43 (dd, ²J_{H,H} = 9.6 Hz, ³J_{H,H} = 7.8 Hz, 1H), 3.67 (dd, ²J_{H,H} = 8.8 Hz, ³J_{H,H} = 4.0 Hz, 1H), 3.72 (d, ²J_{H,H} = 8.8 Hz, 1H), 4.03 (m, 1H), 4.04 (m, 1H), 4.21 (dq, ³J_{H,H} = 10.0 Hz, ³J_{H,H} = 6.7 Hz, 1H), 4.54 (m, 1H), 4.84 (m, 1H), 5.12 (m, 1H), 5.30 (m, 1H); **¹³C-NMR (100 MHz, CDCl₃) δ (ppm)** 19.0, 20.3, 43.9, 46.8, 48.9, 54.2, 71.0, 71.1, 76.5, 78.2, 105.4, 114.6, 147.8, 148.3.

(3*R*, 4*S*, 6*S*, 7*S*, 9*S*, 10*S*)-**31**

¹H-NMR (400 MHz, CDCl₃) δ (ppm) 1.17 (d, J = 6.4 Hz, 3H), 1.27 (d, ³J_{H,H} = 6.0 Hz, 3H), 2.20 (m, 1H), 2.24 (m, 1H), 2.52 (m, 1H), 2.53 (m, 1H), 3.38 (dd, ²J_{H,H} = 9.6 Hz, ³J_{H,H} = 7.8 Hz, 1H), 3.56 (dd, ²J_{H,H} = 8.6 Hz, ³J_{H,H} = 2.5 Hz, 1H), 3.86 (dq, ³J_{H,H} = 12 Hz, ³J_{H,H} = 6.0 Hz, 1H), 3.97 (dd, ²J_{H,H} = 8.6 Hz, ³J_{H,H} = 5.0 Hz, 1H), 4.08 (t, J_{H,H} = 2*7.5 Hz, 1H), 4.45 (quint, ³J_{H,H} = 6.4 Hz, 1H), 4.70 (m, 1H), 4.83 (m, 1H), 5.29 (m, 1H), 5.31 (m, 1H); **¹³C-NMR (100 MHz, CDCl₃) δ (ppm)** 17.9, 19.6, 40.6, 44.4, 50.7, 53.9, 70.8, 71.9, 75.3, 77.3, 109.7, 113.1, 144.6, 146.7.

8.4. Experimental procedure for the products synthesised in Chapter 5

8.4.1. Synthesis of poly(ethylene glycol) derivative **35**



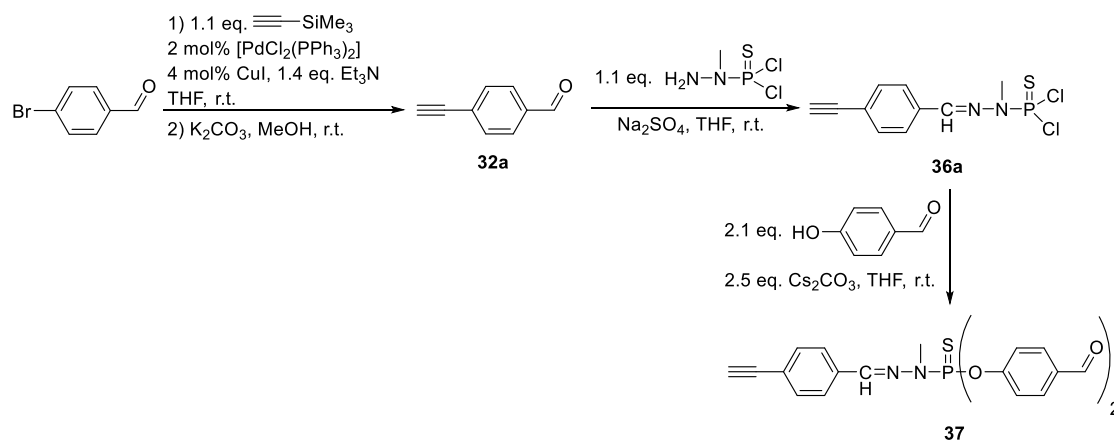
Commercially available poly(ethylene glycol) methyl ether with an average weight of 750 g/mol (36 g, 48 mmol) was dried under vacuum at 80°C for 2 hours and cooled at room temperature. Anhydrous CH₂Cl₂ (100 mL) and freshly distilled triethylamine (8.7 mL, 67.4 mmol) were added and the mixture was cooled to 0°C. Methanesulfonyl chloride (4.9 mL, 67.4 mmol) was added dropwise for 15 minutes and left stirring at 0°C for 15 minutes more, the reaction mixture was then left to stir at room temperature overnight. The reaction was filtered and the solvent removed under reduced pressure. The crude was dissolved in CH₂Cl₂ (200 mL) and extracted with water (2 x 40 mL). The aqueous phase was extracted with CH₂Cl₂ (3 x 100 mL). The combined organic layer was dried over anhydrous Na₂SO₄ and concentrated under reduced pressure to afford **33** (33.98 g, 86% yield) as a yellow oil. $\bar{M}_n = 828$ g/mol; **¹H-NMR (400 MHz, CDCl₃) δ (ppm)**

3.07 (s, 3H, SO_2CH_3), 3.36 (s, 3H, OCH_3), 3.52-3.55 (m, 2H), 3.59-3.68 (m, $\approx 58\text{H}$), 3.74-3.77 (m, 2H), 4.35-4.38 (m, 2H).

A mixture of 4-(benzyloxy)phenol (7.4 g, 36 mmol) and potassium *tert*-butoxide (4.2 g, 36 mmol) in THF (50 mL) was stirred at room temperature for an hour. A solution of **33** (10 g, 12 mmol) in THF (50 mL) was then added and the mixture was heated at 40°C for 48 hours. The solvent was removed under reduced pressure and the crude was dissolved in methanol (180 mL), filtered through celite and the solvent was removed under reduced pressure. The residue was dissolved in CH_2Cl_2 (180 mL), filtered through celite and the solvent was removed under reduced pressure again. The crude was purified by column chromatography on silica gel using, first, diethyl ether, then dichloromethane and finally a mixture of dichloromethane : ethanol (9:1) as the eluent to afford **34** (6.52 g, 58% yield) as an oily brown solid.¹²² $\bar{M}_n = 932$ g/mol; $^1\text{H-NMR}$ (400 MHz, CDCl_3) δ (ppm) 3.35 (s, 3H, OCH_3), 3.51-3.54 (m, 2H), 3.56-3.67 (m, $\approx 60\text{H}$), 3.68-3.71 (m, 2H), 3.79-3.82 (m, 2H), 4.04-4.07 (m, 2H), 4.98 (s, 2H, $\text{CH}_2\text{-Bn}$), 6.81-6.88 (m, 4H, CH-Ar), 7.28-7.41 (m, 5H, CH-Bn).

A mixture of **34** (16.4 g, 17.6 mmol), palladium on carbon (4.7 g, 10 wt. % loading, 4.42 mmol) and ammonium formate (2.8 g, 44.2 mmol) in methanol (280 mL) was heated at 40°C for 48 hours. Upon completion ($^1\text{H-NMR}$ monitoring) the solution was filtered through celite and the solvent removed under reduced pressure. The crude was dissolved in CH_2Cl_2 (400 mL) and washed with water (2 x 200 mL). The organic layer was dried over anhydrous Na_2SO_4 and concentrated under reduced pressure to afford **35** (12.57 g, 85% yield) as a brown oil.¹²² $\bar{M}_n = 842$ g/mol; $^1\text{H-NMR}$ (400 MHz, CDCl_3) δ (ppm) 3.37 (s, 3H, OCH_3), 3.53-3.71 (m, $\approx 74\text{H}$), 3.80-3.83 (m, 2H), 4.05-4.08 (m, 2H), 6.74-6.81 (m, 4H, CH-Ar).

8.4.2. Synthesis of compound 37



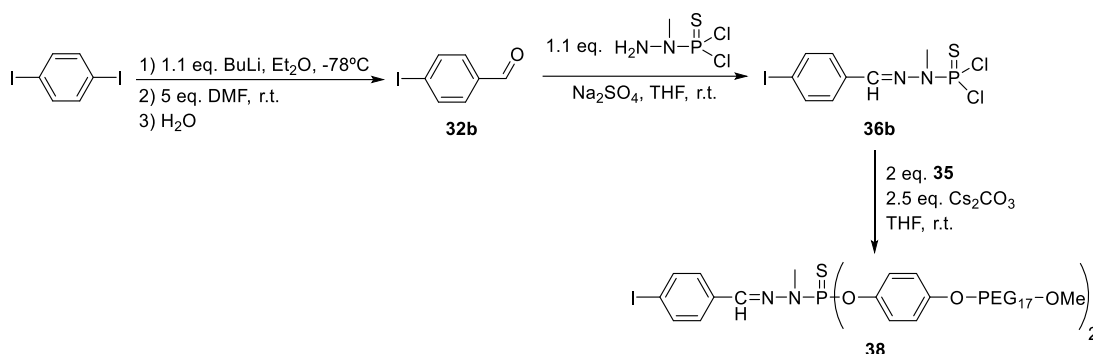
In a 50 mL Schlenk flask, 4-bromobenzaldehyde (3 g, 15.9 mmol), bis(triphenylphosphine) palladium(II) dichloride (228 mg, 0.32 mmol) and copper(I) iodide (121 mg, 0.63 mmol) were degassed under argon atmosphere and dissolved in anhydrous THF (15 mL). A mixture of triethylamine (3.2 mL, 22.9 mmol), ethynyltrimethylsilane (2.4 mL, 16.5 mmol) in THF (2 mL) was added and left to stir at room temperature for 2 hours until completion (TLC monitoring). The solvent was then removed under reduced pressure. The crude was dissolved in pentane, filtered through celite and the solvent was removed. The residue was dissolved in MeOH (19 mL) and potassium carbonate (223 mg, 1.61 mmol) was added. The reaction was left to stir for 1.5 hours

at room temperature until completion (TLC monitoring). The solvent was removed under reduced pressure, the crude was dissolved in diethyl ether (40 mL) and extracted with an aqueous solution of sodium hydrogencarbonate (2 x 30 mL) and water (2 x 10 mL). The organic layer was dried over anhydrous Na_2SO_4 , concentrated under reduced pressure and purified by column chromatography on silica gel using a mixture of hexanes/ethyl acetate (10:1) as the eluent to give 4-ethynylbenzaldehyde, **32a** (1.71 g, 82% yield) as an orange solid.¹²³ **Molecular formula:** $\text{C}_9\text{H}_6\text{O}$; **MW:** 130.14 g/mol; **$^1\text{H-NMR}$ (400 MHz, CDCl_3) δ (ppm)** 3.30 (s, 1H, $\text{C}\equiv\text{CH}$), 7.64 (d, $^3J_{\text{H,H}} = 8.4$ Hz, 2H, CH-Ar), 7.84 (d, $^3J_{\text{H,H}} = 8.4$ Hz, 2H, CH-Ar), 10.0 (s, 1H, CHO).

N-methyl-dichlorophosphorhydrazine (8.7 mL of a 0.243M solution, 2.11 mmol), filtered through a 0.45 μm PTFE filter, was added to a mixture of 4-ethynylbenzaldehyde (250 mg, 1.92 mmol) and anhydrous sodium sulfate (300 mg) in THF (5 mL) at 0°C, and left to stir at room temperature for 1 hour ($^1\text{H-NMR}$ monitoring). Upon completion, the solution was filtered and the solvent was removed under reduced pressure. The crude was dissolved in the minimum amount of THF and **36a** was obtained by precipitation upon addition of pentane (492 mg, 88% yield) as a brown solid. **Molecular formula:** $\text{C}_{10}\text{H}_9\text{N}_2\text{Cl}_2\text{PS}$; **MW:** 291.13 g/mol; **m.p.:** 112-113°C; **$^1\text{H-NMR}$ (300 MHz, CDCl_3) δ (ppm)** 3.19 (s, 1H, $\text{HC}\equiv\text{C}$), 3.51 (dd, $^3J_{\text{H,P}} = 13.8$ Hz, $^5J_{\text{H,H}} = 0.3$ Hz, 3H, NCH_3), 7.53 (d, $^3J_{\text{H,H}} = 8.4$ Hz, 2H, CH-Ar), 7.67-7.71 (m, 3H, $\text{CH-Ar} + \text{CH=N}$); **$^{31}\text{P}\{^1\text{H}\}$ -NMR (121.5 MHz, CDCl_3) δ (ppm)** 63.0.

A mixture of 4-hydroxybenzaldehyde (336 mg, 2.75 mmol) and cesium carbonate (984 mg, 3.02 mmol) in THF (20 mL) under inert atmosphere was left to stir for one hour at room temperature. **36a** (400 mg, 1.37 mmol) was then added and the mixture was left stirring overnight. Upon completion ($^{31}\text{P}\{^1\text{H}\}$ -NMR monitoring), the solids were removed by centrifugation and the solvent was eliminated under reduced pressure. The crude was dissolved in chloroform (10 mL) and extracted with water (3 x 5 mL). The organic layer was dried over anhydrous Na_2SO_4 and concentrated under reduced pressure to afford **37** (471 mg, 74% yield) as an orange gummy solid. **Molecular formula:** $\text{C}_{24}\text{H}_{19}\text{N}_2\text{O}_4\text{PS}$; **MW:** 462.46 g/mol; **$^1\text{H-NMR}$ (400 MHz, CDCl_3) δ (ppm)** 3.18 (s, 1H, $\text{HC}\equiv\text{C}$), 3.41 (d, $^3J_{\text{H,P}} = 10.8$ Hz, 3H, NCH_3), 7.40 (dd, $^3J_{\text{H,H}} = 8.2$ Hz, $^4J_{\text{H,H}} = 1.2$ Hz, 4H, CH-Ar), 7.52 (d, $^3J_{\text{H,H}} = 8.0$ Hz, 2H, Ar), 7.63 (d, $^3J_{\text{H,H}} = 8.0$ Hz, 2H, CH-Ar), 7.63 (m, 1H, HC=N), 7.88 (d, $^3J_{\text{H,H}} = 8.2$ Hz, 4H, Ar), 9.97 (s, 2H, CHO); **$^{13}\text{C-NMR}$ (75 MHz, CDCl_3) δ (ppm)** 33.1 (d, $^2J_{\text{C,P}} = 13.5$ Hz, NCH_3), 79.1 ($\text{HC}\equiv\text{C}$), 83.3 ($\text{HC}\equiv\text{C}$), 122.1 (d, $^3J_{\text{C,P}} = 5.1$ Hz, CH-Ar), 123.5 ($\text{HC}\equiv\text{C-C}$), 126.9 (CH-Ar), 131.6 (d, $^4J_{\text{C,P}} = 8.2$ Hz, CH-Ar), 132.6 (CH-Ar), 133.8 (d, $^4J_{\text{C,P}} = 1.6$ Hz, C-CH=N), 134.7 (C-CHO), 139.8 (d, $^3J_{\text{C,P}} = 13.8$ Hz, HC=N), 155.3 (d, $^2J_{\text{C,P}} = 7.2$ Hz, C-O-P), 190.8 (CHO); **$^{31}\text{P}\{^1\text{H}\}$ -NMR (162 MHz, CDCl_3) δ (ppm)** 60.1.

8.4.2. Synthesis of compound 38

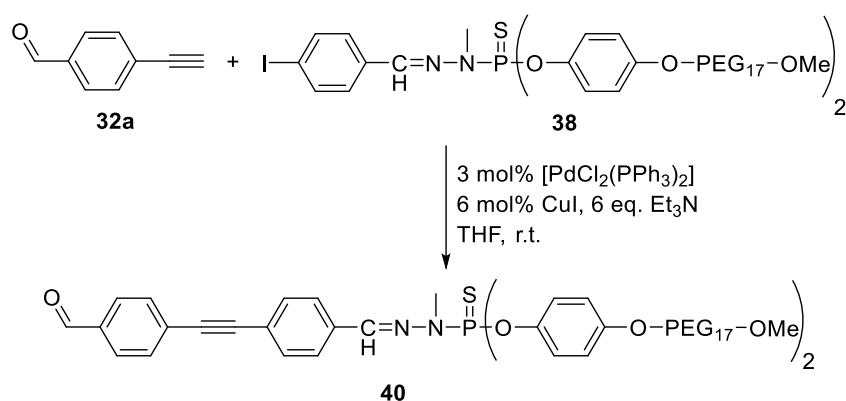


BuLi (6.5 mL of a 2.5 M solution in hexanes, 16 mmol) was slowly added to a solution of 1,4-diiodobenzene (5 g, 15.3 mmol) in anhydrous diethyl ether (80 mL) at -78°C and left to stir for 30 minutes. DMF was then added (6 mL, 76.5 mmol) and the reaction was left to warm to room temperature over the course of 2 hours. The reaction was washed with water (40 mL) and the aqueous phase was extracted with Et₂O (4 x 30 mL). The combined organic layer was extracted with water (60 mL) and brine (60 mL), and then dried over anhydrous Na₂SO₄ and concentrated under reduced pressure. The crude was purified by column chromatography on silica gel using a mixture of hexanes/ethyl acetate (10:1) as the eluent to give 4-iodobenzaldehyde, **32b** (1.74 g, 49% yield) as a colourless solid.¹²⁴ **Molecular formula:** C₇H₅OI; **MW:** 232.02 g/mol; **¹H-NMR (400 MHz, CDCl₃) δ (ppm)** 7.59 (d, ³J_{H,H} = 8.4 Hz, 2H, CH-Ar), 7.91 (d, ³J_{H,H} = 8.4 Hz, 2H, CH-Ar), 9.96 (s, 1H, CHO).

N-methyl-dichlorophosphorhydrazine (19.5 mL of a 0.243M solution, 4.73 mmol), filtered through a 0.45 μm PTFE filter, was added to a mixture of 4-iodobenzaldehyde (1.01 g, 4.3 mmol) and anhydrous sodium sulfate (1.2 g) in THF (20 mL) at 0°C, and left to stir at room temperature for 1 hour (¹H-NMR monitoring). Upon completion the solution was filtered and the solvent was removed under reduced pressure. The crude was dissolved in the minimum amount of THF and **36b** was obtained by precipitation upon addition of pentane (997 mg, 59% yield) as a colourless sticky solid. **Molecular formula:** C₈H₈N₂Cl₂IPS; **MW:** 393.00 g/mol; **¹H-NMR (300 MHz, CDCl₃) δ (ppm)** 3.50 (dd, ³J_{H,P} = 13.8 Hz, ⁵J_{H,H} = 0.3 Hz, 3H, NCH₃), 7.44-7.49 (d, 2H, ³J_{H,H} = 12.9 Hz, CH-Ar), 7.62 (d, ⁴J_{H,P} = 2.7 Hz, 1H, HC=N), 7.74-7.78 (d, 2H, ³J_{H,H} = 12.9 Hz, CH-Ar); **³¹P{¹H}-NMR (121.5 MHz, CDCl₃) δ (ppm)** 62.9.

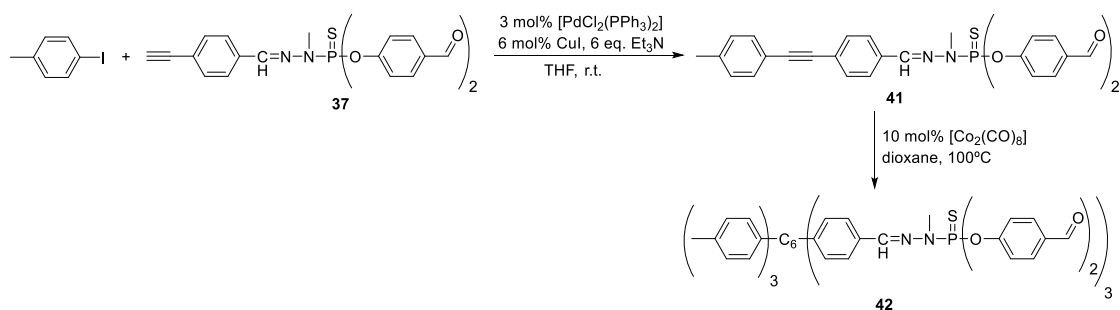
A mixture of **35** (234 mg, 0.59 mmol) and cesium carbonate (427.7 mg, 1.31 mmol) in THF (10 mL) under inert atmosphere was left to stir for one hour at room temperature. **36b** (996.6 mg, 1.18 mmol) was then added and the mixture was left stirring overnight. Upon completion (³¹P{¹H}-NMR monitoring), the solids were removed by centrifugation and the solvent was eliminated under reduced pressure to afford **38** (1.13 g, 95% yield) as a brown oil. **M_n** = 2004 g/mol; **¹H-NMR (300 MHz, CDCl₃) δ (ppm)** 3.29 (d, ³J_{H,P} = 10.2 Hz, 3H, NCH₃), 3.36 (s, 6H, OCH₃), 3.51-3.55 (m, 4H), 3.56-3.76 (m, ≈126H), 3.79-3.83 (m, 4H), 4.03-4.07 (m, 4H), 6.80 (d, ³J_{H,H} = 9.0 Hz, 4H, CH-Ar), 7.10 (dd, ³J_{H,H} = 9.0 Hz, ⁴J_{H,H} = 1.8 Hz, 4H, CH-Ar), 7.45 (d, ³J_{H,H} = 8.4 Hz, 2H, CH-Ar), 7.73 (d, ³J_{H,H} = 8.4 Hz, 2H, CH-Ar); **³¹P{¹H}-NMR (121.5 MHz, CDCl₃)δ (ppm)** 63.9.

8.4.3. Synthesis of compound 40



Compound **38** (2.0 g, 1.00 mmol), bis(triphenylphosphine) palladium(II) dichloride (21.0 mg, 0.03 mmol) and copper(I) iodide (11.4 mg, 0.06 mmol) were degassed in a 25 mL Schlenk flask under nitrogen atmosphere and dissolved in anhydrous THF (10 mL). A mixture of triethylamine (0.83 mL, 6.0 mmol), **32a** (195.2 mg, 1.50 mmol) in THF (5 mL) was added and left to stir at room temperature for 5 hours until completion (TLC monitoring). The solvent was removed under reduced pressure and the crude was purified by column chromatography on silica gel using a mixture of dichloromethane/methanol (10:1) as the eluent to give **40** (1.2 g, 60% yield) as a brown oil. $\bar{M}_n = 2006$ g/mol; $^1\text{H-NMR}$ (400 MHz, CDCl_3) δ (ppm) 3.32 (d, $^3J_{\text{H,P}} = 10.4$ Hz, 3H, NCH_3), 3.35 (s, 6H, OCH_3), 3.51-3.54 (m, 4H), 3.61-3.69 (m, $\approx 128\text{H}$), 3.79-3.82 (m, 4H), 4.03-4.07 (m, 4H), 6.81 (d, $^3J_{\text{H,H}} = 9.2$ Hz, 4H, CH-Ar), 7.09 (dd, $^3J_{\text{H,H}} = 9.2$ Hz, $^4J_{\text{H,H}} = 1.6$ Hz, 4H, CH-Ar), 7.56 (d, $^3J_{\text{H,H}} = 8.4$ Hz, 2H, CH-Ar), 7.61 (br s, 1H, HC=N), 7.67 (d, $^3J_{\text{H,H}} = 8.4$ Hz, 2H, CH-Ar), 7.73 (d, $^3J_{\text{H,H}} = 8.2$ Hz, 2H, CH-Ar), 7.86 (d, $^3J_{\text{H,H}} = 8.2$ Hz, 4H, CH-Ar), 10.0 (s, 1H, CHO); $^{13}\text{C-NMR}$ (100 MHz, CDCl_3) δ (ppm) 33.4 (d, $^2J_{\text{C,P}} = 12.0$ Hz, NCH_3), 59.1 (OCH_3), 67.8, 69.7, 70.4, 70.5, 70.6, 70.8, 71.9, 90.0 ($\text{C}\equiv\text{C}$), 93.3 ($\text{C}\equiv\text{C}$), 115.2 ($\text{C-C}\equiv\text{C}$), 122.3 (d, $^3J_{\text{C,P}} = 4.0$ Hz, CH-Ar), 123.2 ($\text{C-C}\equiv\text{C}$), 127.0 (CH-Ar), 129.4, 129.6 (CH-Ar), 132.21, 132.24, 135.5 (d, $^2J_{\text{C,P}} = 7.0$ Hz, C-O-P), 138.5 (d, $^3J_{\text{C,P}} = 14.0$ Hz, HC=N), 144.3 (d, $^3J_{\text{C,P}} = 7.0$ Hz, CH-Ar), 156.2, 191.4 (CHO); $^{31}\text{P}\{^1\text{H}\}$ -NMR (162 MHz, CDCl_3) δ (ppm) 64.0.

8.4.4. Synthesis of compound 42

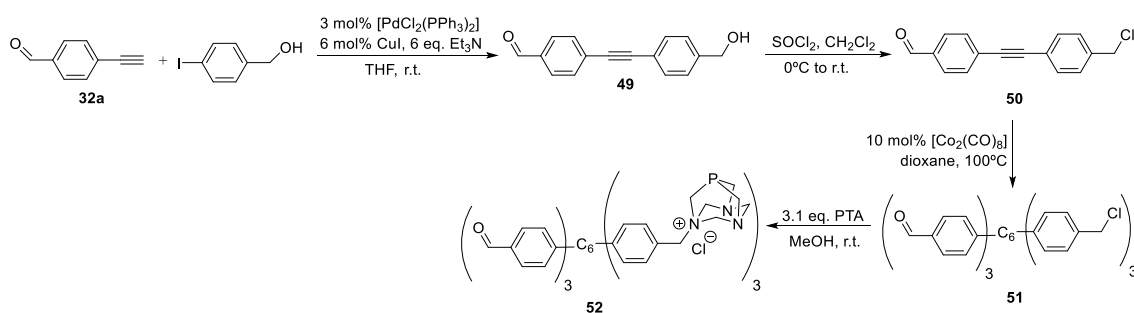


4-iodotoluene (235.5 mg, 1.08 mmol), bis(triphenylphosphine) palladium(II) dichloride (11.4 mg, 0.016 mmol) and copper(I) iodide (6.2 mg, 0.032 mmol) were degassed in a 25 mL Schlenk flask under nitrogen atmosphere and dissolved in anhydrous THF (15 mL). A mixture of triethylamine (0.45 mL, 3.24 mmol), **37** (250.1 mg, 0.54 mmol) in THF (2.5 mL) was added and left to stir at room temperature for 24 hours until completion (TLC monitoring). The solvent was removed

under reduced pressure and the crude was purified by column chromatography on silica gel using a mixture of hexanes/ethyl acetate (8:2) as the eluent to give **41** (158.1 mg, 53% yield) as a brown oil. **Molecular formula:** C₃₁H₂₅N₂O₄P₃; **MW:** 552.58 g/mol; **¹H-NMR (400 MHz, CDCl₃) δ (ppm)** 2.36 (s, 3H, CH₃-Ar), 3.42 (d, ³J_{H,P} = 10.8 Hz, 3H, NCH₃), 7.16 (d, ³J_{H,H} = 7.6 Hz, 2H, CH-Ar), 7.39-7.45 (m, 6H, CH-Ar), 7.54 (d, ³J_{H,H} = 8.4 Hz, 2H, CH-Ar), 7.64 (d, ³J_{H,H} = 8.4 Hz, 2H, CH-Ar), 7.64 (m, 1H, CH=N), 7.88 (d, ³J_{H,H} = 8.4 Hz, 4H, CH-Ar), 9.95 (s, 2H, CHO); **¹³C-NMR (75 MHz, CDCl₃) δ (ppm)** 21.6 (CH₃-Ar), 33.0 (d, ²J_{C,P} = 13.6 Hz, NCH₃), 88.5 (C≡C), 91.7 (C≡C), 119.9 (C-C≡C), 122.1 (d, ³J_{C,P} = 5.5 Hz, CH-Ar), 125.0 (C-C≡C), 127.0 (CH-Ar), 129.3 (CH-Ar), 131.58 (d, ⁴J_{C,P} = 1.6 Hz, CH-Ar), 131.6 (CH-Ar), 132.0 (CH-Ar), 133.7 (d, ⁴J_{C,P} = 1.6 Hz, C-CH=N), 133.9 (C-CHO), 138.8 (C-CH₃), 140.1 (d, ³J_{C,P} = 13.8 Hz, HC=N), 155.3 (d, ²J_{C,P} = 7.3 Hz, C-O-P), 190.9 (CHO); **³¹P{¹H}-NMR (162 MHz, CDCl₃) δ (ppm)** 60.2.

A mixture of compound **41** (90.0 mg, 0.163 mmol) and dicobalt octacarbonyl (6.1 mg, 0.017 mmol) in dioxane (1 mL) in inert atmosphere was heated in a 10 mL Schlenk flask at 100°C. After 24 hours (TLC monitoring) the solvent was removed under reduced pressure and the crude was purified by column chromatography on silica gel using a mixture of hexanes/ethyl acetate (9:1) as the eluent to give **42** (37.8 mg, 42% yield) as a yellow solid. **Molecular formula:** C₉₃H₇₅N₆O₁₂P₃S₃; **MW:** 1657.75 g/mol; **m.p.:** 126-127°C; **¹H-NMR (400 MHz, CDCl₃) δ (ppm)** 2.04-2.08 (m, 9H), 3.26-3.32 (m, 9H), 6.69-6.72 (m, 11H), 6.85-6.90 (m, 5H), 6.94-6.97 (m, 2H), 7.17-7.21 (m, 6H), 7.29-7.46 (m, 15H), 7.76-7.88 (m, 12H), 9.83-9.96 (m, 6H).

8.4.5. Synthesis of compound 52



4-iodobenzyl alcohol (3.33 g, 13.8 mmol), bis(triphenylphosphine) palladium(II) dichloride (242.4 mg, 0.33 mmol) and copper(I) iodide (132.2 mg, 0.69 mmol) were degassed in a 25 mL Schlenk flask under nitrogen atmosphere and dissolved in anhydrous THF (39 mL). A mixture of triethylamine (9.6 mL, 69.0 mmol), 4-ethynylbenzaldehyde **32a** (1.50 g, 11.52 mmol) in THF (6 mL) was added and left to stir at room temperature for 3 hours until completion (TLC monitoring). The solution was filtered and the solvent was removed under reduced pressure. Dichloromethane was added to the crude, forming a precipitate that was collected by filtration and washed with dichloromethane. The colourless solid corresponds to **49** and was used in the next reaction without further purification.

A solution of thionyl chloride (1.25 mL, 17.28 mmol) in dichloromethane (10 mL) was slowly added to a solution of **49** in THF (50 mL) and stirred at room temperature for 2 hours (TLC monitoring). The solvent was then removed under reduced pressure and the crude was dissolved in dichloromethane (50 mL) and washed with a saturated aqueous solution of sodium hydrogencarbonate (3 x 30 mL). The organic layer was dried over anhydrous Na₂SO₄ and

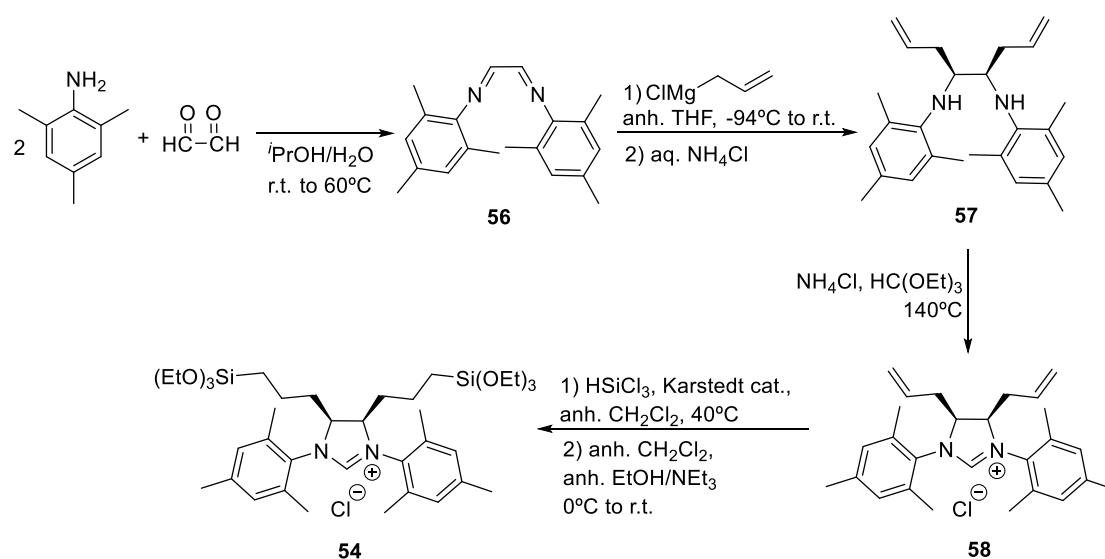
concentrated under reduced pressure to give compound **50** (2.08 g, 71% yield of two steps) as a beige-coloured solid. **Molecular formula:** C₁₆H₁₁OCl; **MW:** 254.71 g/mol; **m.p.:** 135-136°C; **¹H-NMR (400 MHz, CDCl₃) δ (ppm)** 4.60 (s, 2H, CH₂), 7.39 (d, ³J_{H,H} = 8.4 Hz, 2H, CH-Ar), 7.55 (d, ³J_{H,H} = 8.4 Hz, 2H, CH-Ar), 7.67 (d, ³J_{H,H} = 8.6 Hz, 2H, CH-Ar), 7.87 (d, ³J_{H,H} = 8.6 Hz, 2H, CH-Ar), 10.0 (s, 1H, CHO); **¹³C-NMR (100 MHz, CDCl₃) δ (ppm)** 45.8 (CH₂), 89.3 (C-alkyne), 92.9 (C-alkyne), 122.7 (C-Ar), 128.8 (CH-Ar), 129.5 (C-Ar), 129.7 (CH-Ar), 132.2 (CH-Ar), 132.3 (CH-Ar), 135.6 (C-Ar), 138.3 (C-Ar), 191.5 (CHO); **ESI-MS (m/z):** 255.0 [M+H]⁺; **ESI-MS (m/z):** 255.0 [M+H]⁺.

A mixture of compound **50** (100.0 mg, 0.39 mmol) and dicobalt octacarbonyl (13.4 mg, 0.039 mmol) in dioxane (2 mL) in inert atmosphere was heated in a 10 mL Schlenk flask at 100°C for 72 hours (TLC monitoring). The solvent was then removed under reduced pressure and the crude was purified by column chromatography on silica gel using a mixture of hexanes/ethyl acetate (9:1 to 6:4) as the eluent to give **51** (50.6 mg, 51% yield) as a brown solid. **Molecular formula:** C₄₈H₃₃O₃Cl₃; **MW:** 764.14 g/mol; **¹H-NMR (400 MHz, CDCl₃) δ (ppm)** 4.32-4.34 (m, 6H), 6.76-6.79 (m, 6H), 6.87-6.91 (m, 6H), 6.97-6.99 (m, 6H), 7.39-7.42 (m, 6H), 9.75-9.77 (m, 3H); **¹³C-NMR (100 MHz, CDCl₃) δ (ppm)** 45.7, 45.9, 127.4, 127.5, 128.60, 128.65, 131.34, 131.37, 131.8, 131.9, 133.9, 134.0, 135.44, 135.46, 135.63, 135.64, 139.1, 139.24, 139.26, 139.35, 139.38, 139.7, 139.9, 140.0, 140.21, 140.24, 140.6, 146.3, 146.40, 146.45, 146.5, 192.0, 192.1; **ESI-MS (m/z):** 727.2 [M-Cl]⁺, 782.2 [M+NH₄]⁺.

A mixture of **51** (95 mg, 0.125 mmol) and PTA (63 mg, 0.39 mmol) in MeOH (2 mL) under inert atmosphere was stirred at room temperature overnight. The solvents were removed under reduced pressure and the solid was washed with THF to afford **52** as a yellow solid (66 mg, 43% yield). **Molecular formula:** C₆₆H₆₉N₉O₃Cl₃P₃; **MW:** 1235.60 g/mol; **¹H-NMR (400 MHz, CD₃OD) δ (ppm)** 3.96-4.00 (m, 13H), 4.09-4.13 (m, 7H), 4.23-4.27 (m, 6H), 4.37-4.41 (m, 6H), 4.75-4.81 (m, 10H), 7.08-7.30 (m, 18H, CH-Ar), 7.48-7.55 (m, 6H, CH-Ar), 9.72 (s, 3H, CHO); **³¹P{¹H}-NMR (162 MHz, CD₃OD) δ (ppm)** -81.45, -81.43, -81.39; **ESI-MS (m/z):** 1200.4 [M-Cl]⁺, 581.7 [M-2Cl]²⁺.

8.5. Experimental procedure for the products synthesised in Chapter 6

8.5.1. Synthesis of 1,3-dimesityl-4,5-bis[3-(triethoxysilyl)propyl]-4,5-dihydroimidazolium chloride, **54**



A solution of aqueous glyoxal (4.6 mL of a 40% w/v solution, 39.92 mmol) in 2-propanol (10 mL) and H₂O (5 mL) was added to a stirred mixture of mesitylamine (7 mL, 49.9 mmol) in 2-propanol (20 mL). The mixture was stirred at room temperature for 16 hours and then at 60°C for 4 hours. Water (10 mL) was then added and the resulting solid was filtered and recrystallized in hexanes to give compound **56** (4.49 g, 63% yield) as a yellow solid.¹⁶³ **Molecular formula:** C₂₀H₂₄N₂; **MW:** 292.42 g/mol; **¹H-NMR (300 MHz, CDCl₃) δ (ppm)** 2.15 (s, 12H, *o*-CH₃), 2.29 (s, 6H, *p*-CH₃), 6.90 (s, 4H, Ar), 8.09 (s, 2H, N=CHCH=N).

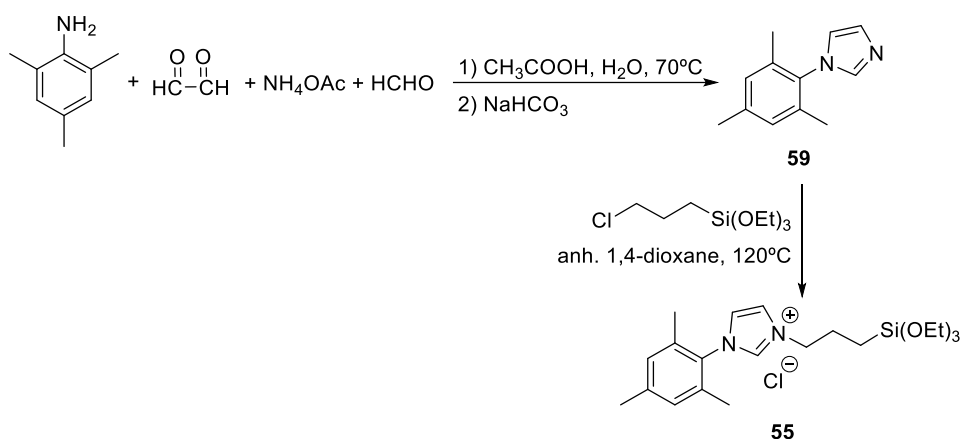
Compound **56** (4.47 g, 15.3 mmol) was transferred into a Schlenk tube, dissolved in anhydrous THF (40 mL), and cooled to -94°C (hexanes/liquid N₂ bath). Allylmagnesium chloride (40 mL of a 2 M solution in anhydrous THF, 80 mmol) was added slowly. The reaction mixture was then warmed up to room temperature and stirred for 16 hours. The crude was then cooled to 0°C and a 1M NH₄Cl_(aq) solution (90 mL) was added with care. The organic phase was separated and the aqueous phase was further extracted with Et₂O (3 x 25 mL). The combined organic phases were dried over anhydrous Na₂SO₄ and concentrated. After 4 days at room temperature a yellow solid precipitated. This was filtered and washed with cold MeOH to give compound **57** (3.08 g, 54% yield) as a colourless solid. **Molecular formula:** C₂₆H₃₆N₂; **MW:** 376.58 g/mol; **m.p.:** 76 – 77°C (lit.^{164b} 76°C). **¹H-NMR (400 MHz, CDCl₃) δ (ppm)** 2.21 (s, 6H, *p*-CH₃), 2.23 (s, 12H, *o*-CH₃), 2.23-2.29 (m, 4H, CH₂CH=CH₂), 3.67 (m, 2H NH + 2H CHNH), 5.00 (dd, ^{3cis}J_{H,H} = 10.2 Hz, ²J_{H,H} = 1.8 Hz, 2H, CH=CH_{cis}H_{trans}), 5.06 (dd, ^{3trans}J_{H,H} = 17.2 Hz, ²J_{H,H} = 1.8 Hz, 2H, CH=CH_{cis}H_{trans}), 5.74 (ddt, ^{3trans}J_{H,H} = 17.2 Hz, ^{3cis}J_{H,H} = 10.2 Hz, ³J_{H,H} = 7.2 Hz, 2H, CH₂CH=CH₂), 6.78 (s, 4H, Ar).

A mixture of compound **57** (2.29 g, 6.08 mmol), ammonium chloride (2.14 g, 40 mmol) and triethylorthoformate (5.1 mL, 28.6 mmol) was stirred under nitrogen atmosphere and heated at 140°C for 15 hours (TLC monitoring). The reaction mixture was cooled down to 40°C and the volatiles evaporated under vacuum until a sticky residue was obtained. Anhydrous hexane was added to this residue and the mixture was triturated in order to facilitate the precipitation of a solid. This solid was then filtered, washed with hexanes and dried under vacuum. The compound was further purified by column chromatography on silica gel (CH₂Cl₂:EtOH, 9:1 → 7:3) to give compound **58** (1.79 g, 70% yield) as a light-brown solid. **Molecular formula:** C₂₇H₃₅N₂Cl; **MW:** 423.04 g/mol; **m.p.:** 257 – 258°C (lit.^{164b} 258°C). **¹H-NMR (300 MHz, CDCl₃) δ (ppm)** 2.29 (s, 6H, CH₃), 2.37 (s, 6H, CH₃), 2.44 (s, 6H, CH₃), 2.42-2.48 (m, 2H, CHHCH=CH₂), 2.65-2.73 (m, 2H, CHHCH=CH₂), 4.95-5.02 (m, 2H CH=CH_{trans}H_{cis} + 2H NCHCHN), 5.05 (dd, ^{3trans}J_{H,H} = 16.8 Hz, ²J_{H,H} = 1.2 Hz, 2H, CH=CH_{cis}H_{trans}), 5.45 (ddt, ^{3trans}J_{H,H} = 16.8 Hz, ^{3cis}J_{H,H} = 10.2 Hz, ³J_{H,H} = 6.6 Hz, 2H, CH₂CH=CH₂), 6.95 (s, 2H, Ar), 6.96 (s, 2H, Ar), 10.07 (s, 1H, NCH=N).

Compound **58** (0.95 g, 2.25 mmol) was transferred into a sealable Schlenk tube under nitrogen atmosphere and dissolved in anhydrous CH₂Cl₂ (22 mL). A mixture of Karstedt's catalyst (1.5 mL, 2% wt Pt solution in xylene, 0.13 mmol Pt) and freshly distilled HSiCl₃ (5.8 mL, 57.38 mmol) was then added. The reaction mixture was stirred under nitrogen at 40°C for 20 hours. Excess of HSiCl₃ was evaporated under vacuum and the residue was redissolved in anhydrous CH₂Cl₂ (11 mL). The mixture was cooled to 0°C and a 1/1 solution of anhydrous EtOH/NEt₃ (6.6 mL) was added slowly. The mixture was stirred at room temperature for 2 hours. The volatiles were removed under vacuum and the residue was treated with anhydrous toluene and then filtered to separate the ammonium salt. The filtrates were concentrated under vacuum and anhydrous hexane was added to precipitate the desired product, which was filtered off and washed with

more hexanes until the filtrates had no colour. The resulting solid was dried under vacuum to give compound **54** (0.95 g, 56% yield) as a grey solid.^{131h} **Molecular formula:** C₃₉H₆₇N₂O₆ClSi₂; **MW:** 751.59 g/mol; **¹H-NMR (300 MHz, CDCl₃) δ (ppm)** 0.48-0.53 (m, 4H, CH₂Si), 1.14 (t, ³J_{H,H} = 6.9 Hz, 18H, OCH₂CH₃), 1.23-1.29 (m, 4H, CH₂CH₂CH₂Si), 1.68-1.88 (m, 4H, CH₂CH₂CH₂Si), 2.25 (s, 6H, CH₃), 2.34 (s, 6H, CH₃), 2.45 (s, 6H, CH₃), 3.68 (q, ³J_{H,H} = 6.9 Hz, 12H, OCH₂CH₃), 4.61 (br s, 2H, NCHCHN), 6.90 (s, 2H, Ar), 6.94 (s, 2H, Ar), 10.64 (s, 1H, NCH=N).

8.5.2. Synthesis of 1-mesityl-3-(3-(triethoxysilyl)propyl)-1H-imidazolium chloride, **59**

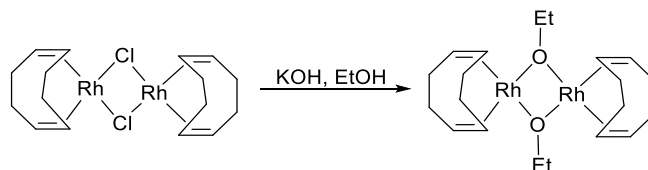


A mixture of mesitylamine (5.6 mL, 38.6 mmol), ammonium acetate (3.08 g, 40.05 mmol) and acetic acid (10 mL) in water (1 mL) was added to a stirred solution of acetic acid (10 mL), formaldehyde_(aq) (3 mL of a 37% w/v solution, 40.3 mmol) and glyoxal_(aq) (5.3 mL of a 40% w/v solution, 46.0 mmol). The reaction mixture was stirred at 70°C overnight. The crude was then, carefully poured over a saturated NaHCO_{3(aq)} solution (300 mL) and the precipitate was filtered, washed with H₂O (5 x 20 mL) and dried under vacuum. The crude was purified by column chromatography on silica gel (hexanes/ethyl acetate, 3:1 to 1:1) to give compound **59** (3.44 g, 48% yield) as a light-brown solid.¹⁷⁹ **Molecular formula:** C₁₂H₁₄N₂; **MW:** 186.25 g/mol; **m.p.:** 113 – 114°C (lit.¹⁸⁰ 112 – 113°C). **¹H-RMN (300 MHz, CDCl₃) δ (ppm)** 1.99 (s, 6H, *o*-CH₃), 2.34 (s, 3H, *p*-CH₃), 6.89 (dd, ³J_{H,H} = 1.1 Hz, ⁴J_{H,H} = 1.1 Hz, 1H, N₁CHCHN₂), 6.97 (br abs, 2H, Ar), 7.23 (dd, ³J_{H,H} = 1.1 Hz, ⁴J_{H,H} = 1.1 Hz, 1H, N₁CHCHN₂), 7.44 (t, ⁴J_{H,H} = 1.1 Hz, 1H, N₁CH=N₂).

1-mesitylimidazole was transferred (5.46 g, 29.3 mmol) into a Schlenk tube fitted with a condenser and a stirring bar and under nitrogen. A solution of 3-(chloropropyl)triethoxysilane (8.5 mL, 33.5 mmol) in anhydrous dioxane (50 mL) was then added. The reaction mixture was refluxed for 18 hours (TLC monitoring). The solvent was evaporated under vacuum and the residue was washed with anhydrous hexanes until the filtrates were colorless. The resulting solid was dried under vacuum to give compound **55** (5.00 g, 40% yield) as a beige solid.¹³¹ⁱ **Molecular formula:** C₂₁H₃₅N₂O₃ClSi; **MW:** 427.05 g/mol; **¹H-NMR (400 MHz, CDCl₃) δ (ppm)** 0.64 (t, ³J_{H,H} = 8.1 Hz, 2H, CH₂-Si), 1.20 (t, ³J_{H,H} = 7.0 Hz, 9H, OCH₂CH₃), 2.06 (s, 6H, *o*-CH₃), 2.03-2.07 (m, 2H, NCH₂CH₂CH₂Si), 2.32 (s, 3H, *p*-CH₃), 3.81 (q, ³J_{H,H} = 7.0 Hz, 6H, OCH₂CH₃), 4.74 (t, ³J_{H,H} = 7.0 Hz, 2H, CH₂N), 6.98 (s, 2H, Ar), 7.14 (s, 1H, N₁CHCHN₂), 7.65 (s, 1H, N₁CHCHN₂), 10.78 (s, 1H, NCH=N).

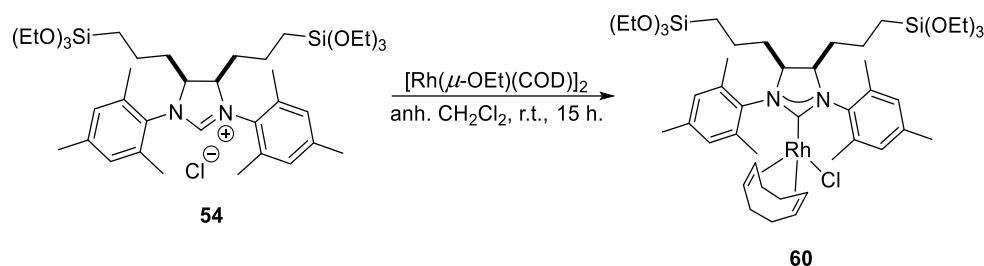
8.5.3. Synthesis of Rh(I)-NHC complexes.

8.5.3.1. Synthesis of ethoxy(1,5-cyclooctadiene)rhodium(I) dimer



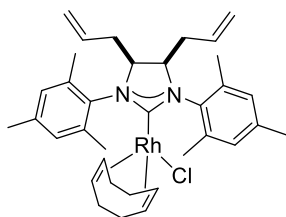
A solution of KOH (265.2 mg, 4.73 mmol) in EtOH (33 mL) was added to a stirred mixture of $[\text{Rh}(\text{COD})(\mu\text{-Cl})]_2$ (1.15 g, 2.33 mmol) in CH_2Cl_2 (100 mL) at room temperature. The solvent was evaporated after 50 minutes of reaction. Ethanol (65 mL) and water (100 mL) were added to the resulting solid. The solid was filtered, washed with H_2O (10 x 10 mL) and dried under vacuum to give $[\text{Rh}(\text{COD})(\mu\text{-OEt})]_2$ (1.06 g, 91% yield) as a yellow powder¹⁸¹. **Molecular formula:** $\text{C}_{20}\text{H}_{34}\text{O}_2\text{Rh}_2$; **MW:** 512.30 g/mol. **¹H-RMN (300 MHz, CDCl_3) δ (ppm)** 1.03 (t, $^3J_{\text{H,H}} = 7.0$ Hz, 6H, OCH_2CH_3), 1.61-1.68 (m, 8H, COD-CH_2), 2.47 (br abs, 8H, COD-CH_2), 2.65 (q, $^3J_{\text{H,H}} = 6.6$ Hz, 4H, OCH_2CH_3), 3.53 (br abs, 8H, COD-CH).

8.5.3.2. Synthesis of **60**, **60**-allyl and **61**



General procedure for **60** and **61**: Imidazolium salt **54** (2.32 mmol) and $[\text{Rh}(\mu\text{-OEt})(\text{COD})]_2$ (1.17 mmol) were transferred into a Schlenk tube under nitrogen atmosphere and dissolved in anhydrous CH_2Cl_2 (50 mL). The reaction mixture was stirred at room temperature for 15 hours (TLC monitoring). The solvent was evaporated under vacuum and the residue was washed with anhydrous hexanes until the filtrate was colorless. The combined filtrates were then concentrated under vacuum to give Rh complex **60** (1.33 g, 60% yield) as an orange gum. **Molecular formula:** $\text{C}_{47}\text{H}_{78}\text{O}_6\text{N}_2\text{ClRhSi}_2$; **MW:** 961.67 g/mol; **¹H-RMN (400 MHz, CDCl_3) δ (ppm)** 0.49 (t, $^3J_{\text{H,H}} = 8.2$ Hz, 4H, major + minor, CH_2Si), 1.142 (t, $^3J_{\text{H,H}} = 7.0$ Hz, 18H, major, OCH_2CH_3), 1.147 (t, $^3J_{\text{H,H}} = 7.0$ Hz, 18H, minor, OCH_2CH_3), 1.37-1.76 (m, 16H, major + minor, $\text{CH}_2\text{CH}_2\text{CH}_2\text{Si}$, $\text{CH}_2\text{CH}_2\text{CH}_2\text{Si}$, COD-CH_2), 2.26 (s, 6H, major, CH_3), 2.30 (s, 6H, minor, CH_3), 2.30 (s, 6H, major, CH_3), 2.36 (s, 6H, minor, CH_3), 2.53 (s, 6H, minor, CH_3), 2.63 (s, 6H, major, CH_3), 3.02 (br abs, 2H, major, COD-CH), 3.32 (br abs, 2H, minor, COD-CH), 3.683 (q, $^3J_{\text{H,H}} = 7.0$ Hz, 12H, major, OCH_2CH_3), 3.687 (q, $^3J_{\text{H,H}} = 7.0$ Hz, 12H, minor, OCH_2CH_3), 4.01-4.09 (m, 2H, major + minor, NCH), 4.43 (br abs, 2H, major + minor, COD-CH), 6.90 (s, 2H, major, Ar), 6.93 (s, 2H, minor, Ar), 6.94 (s, 2H, minor, Ar), 7.00 (s, 2H, major, Ar); **¹³C-NMR (75 MHz, CDCl_3) δ (ppm)** 10.6 (CH_2Si , major), 10.7 (CH_2Si , minor), 18.2 (OCH_2CH_3 , major + minor), 19.1 (CH_3 , major), 19.8 (CH_3 , minor), 20.2 (CH_3 , minor), 20.6 (CH_2 , minor), 20.7 (CH_2 , major), 20.9 (CH_3 , major), 21.0 (CH_3 , minor), 21.7 (CH_3 , major), 27.9 (CH_2 , major), 28.0 (CH_2 , minor), 30.8 (COD-CH_2 , minor), 31.2 (COD-CH_2 , major), 32.5 (COD-CH_2 , major), 32.7 (COD-CH_2 , minor), 58.2 (OCH_2CH_3 , major + minor), 65.3 (NCH , minor),

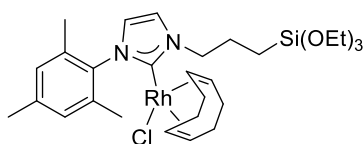
66.1 (NCH, major), 67.1 (d, $^1J_{\text{Rh,C}} = 14.5$ Hz, COD-CH, major), 68.3 (d, $^1J_{\text{Rh,C}} = 14.0$ Hz, COD-CH, minor), 96.5 (d, $^1J_{\text{Rh,C}} = 7.0$ Hz, COD-CH, minor), 96.9 (d, $^1J_{\text{Rh,C}} = 6.9$ Hz, COD-CH, major), 128.3 (CH-Ar, minor), 128.5 (CH-Ar, major), 129.9 (CH-Ar, minor), 130.0 (CH-Ar, major), 134.9 (C-Ar, major), 136.1 (C-Ar, minor), 136.1 (C-Ar, major), 136.5 (C-Ar, minor), 137.2 (C-Ar, major + minor), 138.2 (C-Ar, minor), 139.3 (C-Ar, major), 213.2 (d, $^1J_{\text{Rh,C}} = 48.0$ Hz, Rh-C_{carbene}, minor + major); **ESI-HRMS (*m/z*)** calculated for [C₄₇H₇₈O₆N₂RhSi₂]⁺: 925.4448, found: 925.4470.



60-allyl

Compound **60**-allyl (50% yield), yellow solid. **Molecular formula:**

C₃₅H₄₆N₂ClRh; **MW:** 633.12; **¹H-NMR (500 MHz, DMSO-*d*₆) δ (ppm)** 1.34-1.80 (m, 8H (major) + 8H (minor), COD-CH₂), 2.11-2.20 (m, 2H, (major) + 2H (minor), CHHCH=CH₂), 2.25 (s, 6H, major, CH₃), 2.29 (s, 6H, minor, CH₃), 2.30 (s, 6H, major, CH₃), 2.36 (s, 6H, minor, CH₃), 2.44 (s, 6H, minor, CH₃), 2.49-2.52 (m, 2H (major) + 2H (minor), CHHCH=CH₂), 2.55 (s, 6H, major, CH₃), 3.10 (br abs, 2H, major, COD-CH), 3.39 (br abs, 2H, minor, COD-CH), 4.19-4.35 (m, 4H (major) + 4H (minor), COD-CH + NCHCHN), 4.90 (dd, $^3J_{\text{H,H}} = 10.3$ Hz, $^2J_{\text{H,H}} = 1.5$ Hz, 2H, minor, CH=CH₂), 4.91 (dd, $^3J_{\text{H,H}} = 10.3$ Hz, $^2J_{\text{H,H}} = 1.5$ Hz, 2H, major, CH=CH₂), 4.99 (dd, $^3J_{\text{H,H}} = 16.7$ Hz, $^2J_{\text{H,H}} = 1.5$ Hz, 2H, minor, CH=CH₂), 5.01 (dd, $^3J_{\text{H,H}} = 16.7$ Hz, $^2J_{\text{H,H}} = 1.5$ Hz, 2H, major, CH=CH₂), 5.52 (ddt, $^3J_{\text{H,H}} = 16.7$ Hz, $^3J_{\text{H,H}} = 10.3$ Hz, $^3J_{\text{H,H}} = 6.3$ Hz, 2H, minor, CH₂CH=CH₂), 5.72 (ddt, $^3J_{\text{H,H}} = 16.7$ Hz, $^3J_{\text{H,H}} = 10.3$ Hz, $^3J_{\text{H,H}} = 6.3$ Hz, 2H, major, CH₂CH=CH₂), 6.95 (s, 4H, minor, Ar), 7.00 (s, 4H, major, Ar); **¹³C-NMR (75 MHz, DMSO-*d*₆) δ (ppm)** 18.8 (CH₃, major), 19.6 (CH₃, minor), 19.8 (CH₃, minor), 20.5 (CH₃, major), 20.6 (CH₃, minor), 21.4 (CH₃, major), 27.5 (COD-CH₂, major), 28.0 (COD-CH₂, minor), 31.5 (CH₂CH=CH₂, minor), 31.7 (CH₂CH=CH₂, major), 32.2 (COD-CH₂, major), 32.7 (COD-CH₂, minor), 64.8 (NCH, minor), 64.9 (NCH, major), 66.5 (d, $J_{\text{Rh,C}} = 14.4$ Hz, COD-CH, major), 67.9 (d, $J_{\text{Rh,C}} = 14.4$ Hz, COD-CH, minor), 95.2 (d, $^1J_{\text{Rh,C}} = 6.8$ Hz, COD-CH, major + minor), 116.7 (CH=CH₂, major), 116.9 (CH=CH₂, minor), 128.7 (CH-Ar, major), 129.6 (CH-Ar, minor), 134.9 (CH=CH₂, major), 135.0 (CH=CH₂, minor), 135.4 (C-Ar, major), 135.61 (C-Ar, minor), 135.63 (C-Ar, major), 136.4 (C-Ar, major), 136.8 (C-Ar, minor), 137.0 (C-Ar, major), 137.8 (C-Ar, minor), 138.4 (C-Ar, major), 213.6 (d, $^1J_{\text{Rh,C}} = 48.5$ Hz, Rh-C_{carbene}, minor + major). **ESI-MS (*m/z*):** 597 [M - Cl]⁺.



61

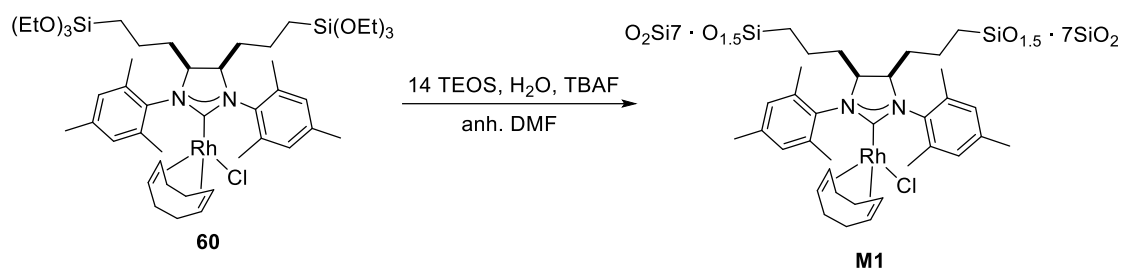
Compound **61** (91% yield), yellow solid. **Molecular formula:**

C₂₉H₄₆O₃N₂ClRhSi; **MW:** 637.13 g/mol; **¹H-NMR (400 MHz, CDCl₃) δ (ppm)** 0.77 (t, $^3J_{\text{H,H}} = 8.4$ Hz, 2H, CH₂Si), 1.25 (t, $^3J_{\text{H,H}} = 7.0$ Hz, 9H, OCH₂CH₃), 1.46-1.70 (m, 2H CH₂CH₂CH₂ + 2H COD-CH₂), 1.82 (s, 3H, CH₃), 1.96-2.20 (m, 4H COD-CH₂ + 2H NCH₂), 2.37 (s, 3H, CH₃), 2.43 (s, 3H, CH₃), 2.96 (m, 1H, COD-CH₂), 3.43 (m, 1H, COD-CH₂), 3.86 (q, $^3J_{\text{H,H}} = 7.0$ Hz, 6H, OCH₂CH₃), 4.19 (m, 1H, COD-CH), 4.76-4.88 (m, 2H, COD-CH), 5.29 (m, 1H, COD-CH), 6.73 (d, $^3J_{\text{H,H}} = 1.8$ Hz, 1H, imidazole), 6.90 (br s, 1H, Ar), 7.03 (d, $^3J_{\text{H,H}} = 1.8$ Hz, 1H, imidazole), 7.09 (br s, 1H, Ar); **¹³C-NMR (75 MHz, CDCl₃) δ (ppm)** 7.83 (CH₂Si), 17.7, 18.3 (OCH₂CH₃), 19.7, 21.0, 24.6, 27.9 (COD-CH₂), 29.1 (COD-

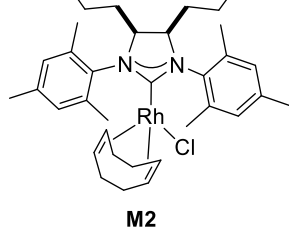
CH₂), 31.5 (COD-CH₂), 34.0 (COD-CH₂), 54.0 (NCH₂), 58.5 (OCH₂CH₃), 67.4 (d, ¹J_{Rh,C} = 14.7 Hz, COD-CH), 68.3 (d, ¹J_{Rh,C} = 14.2 Hz, COD-CH), 96.7 (d, ¹J_{Rh,C} = 7.3 Hz, COD-CH), 96.9 (d, ¹J_{Rh,C} = 7.1 Hz, COD-CH), 120.9 (CH-imidazole), 122.8 (CH-imidazole), 128.0 (CH-Ar), 129.5 (CH-Ar), 134.3 (C-Ar), 136.2 (C-Ar), 137.2 (C-Ar), 138.5 (C-Ar), 181.6 (d, ¹J_{Rh,C} = 51.5 Hz, Rh-C_{carbene}). **ESI-HRMS (m/z)** calculated for [C₂₉H₄₆O₃N₂RhSi]⁺: 601.2327, found: 601.2333.

8.5.4. Preparation of hybrid silica materials.

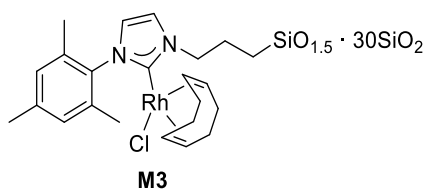
8.5.4.1. Synthesis of **M1-M3**



General procedure for **M1-M3**: A mixture of TBAF (0.16 mL of 1M solution in anhydrous THF, 0.160 mmol) and *milliQ* water (0.745 mL, 41.3 mmol) in anhydrous DMF (3 mL) was added to a stirred solution of complex **60** (0.64 g, 0.6 mmol) and TEOS (1.70 mL, 8.57 mmol) in anhydrous DMF (10 mL) under nitrogen atmosphere. The reaction mixture was stirred at room temperature for 5 minutes. A gel was formed within 1 hour and was left to age at room temperature under nitrogen atmosphere for 6 days. This gel was pulverized, filtered and washed with EtOH (3 x 10 mL), acetone (3 x 10 mL) and anhydrous Et₂O (3 x 10 mL). In order to completely remove residual DMF, the powder obtained was left in a soxhlet apparatus for 48 hours with chloroform. The powder was dried overnight at 40°C under vacuum to afford material **M1** (1.25 g) as an orange powder. ²⁹Si-CP-MAS NMR (79.5 MHz) δ (ppm) -111.4 (Q⁴), -101.9 (Q³), -93.4 (Q²), -66.2 (T³), -56.3 (T²); ¹³C-CP-MAS NMR (100.6 MHz) δ (ppm) 13.3, 20.2, 30.7, 60.0, 67.9, 97.0, 98.6, 130.0, 138.5, 213.3; BET S_{BET}: 453 m²/g; type I sorption isotherm; TGA (air, 30 to 700°C) residual mass 77.06%; EA calculated for C₃₅H₄₈N₂ClRh·2SiO_{1.5}·14SiO₂ (considering complete condensation): 1.77% N, 26.60% C, 3.06% H, 6.51% Rh, found: 1.01% N, 15.45% C, 2.65% H, 4.47% Rh.

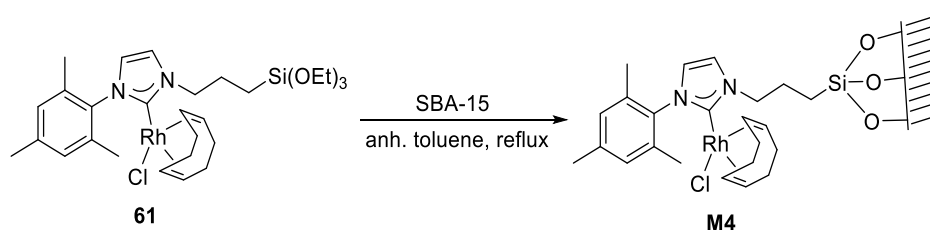


Material **M2** (1.91 g), orange powder. Specific conditions: TBAF (0.215 mL, 0.215 mmol), *milliQ* water (1.5 mL, 83.3 mmol), complex **60** (0.64 g, 0.6 mmol), TEOS (4.6 mL, 20.1 mmol). ²⁹Si-CP-MAS NMR (79.5 MHz) δ (ppm) -110.2 (Q⁴), -101.7 (Q³), -92.5 (Q²), -65.6 (T³), -55.7 (T²); BET S_{BET}: 493 m²/g; type IV sorption isotherm; TGA (air, 30 to 700°C) residual mass 80.66%; EA calculated for C₃₅H₄₈N₂ClRh·2SiO_{1.5}·30SiO₂ (considering complete condensation): 1.10% N, 16.54% C, 1.90% H, 4.05% Rh, found: 0.83% N, 10.65% C, 2.33% H, 2.93% Rh.



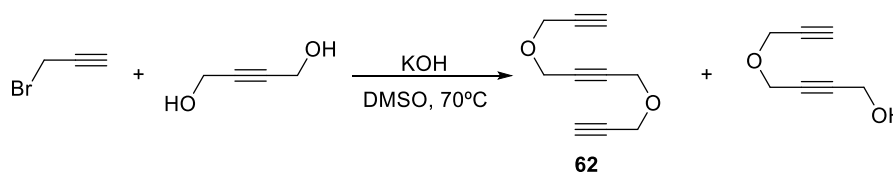
Material **M3** (2.64 g), pale-yellow powder. Specific conditions: TBAF (0.350 mL, 0.350 mmol), *milliQ* water (2.5 mL, 83.3 mmol), EtOH as solvent, complex **61** (0.72 g, 1.13 mmol), TEOS (7.7 mL, 33.9 mmol). **²⁹Si-CP-MAS NMR (79.5 MHz) δ (ppm)** -111.3 (Q⁴), -101.8 (Q³), -91.6 (Q²), -65.1 (T³); **BET** S_{BET} : 325 m²/g; type II sorption isotherm; **TGA** (air, 30 to 700°C) residual mass 75.98%; **EA** calculated for C₂₃H₃₁N₂ClRh·SiO_{1.5}·30SiO₂ (considering complete condensation): 1.20% N, 11.86% C, 1.34% H, 4.42% Rh, found: 1.18% N, 12.19% C, 2.29% H, 3.15% Rh.

8.5.4.2. Synthesis of **M4**



A mixture of complex **61** (0.21 g, 0.34 mmol) and mesostructured silica SBA-15 (1.96 g, 32.70 mmol) was transferred into a Schlenk tube equipped with a Dean-Stark apparatus in anhydrous toluene (40 mL). The reaction mixture was stirred and refluxed for 24 hours. The resulting suspension was filtered and the powder obtained was washed with EtOH (3 x 20 mL), acetone (3 x 20 mL) and anhydrous Et₂O (3 x 20 mL). The powder was dried overnight at 40°C under vacuum. **M4** (1.76 g) was obtained as a colourless powder. **BET** S_{BET} : 512 m²/g; pore diameter (**BJH**): 58.8 Å (desorption); type IV sorption isotherm; pore volume (**BJH**): 0.692 cm³/g (desorption); **TGA** (air, 30 to 700°C) residual mass 84.30%; **EA** found 0.55% N, 5.39% C, 1.00% H, 1.03% Rh.

8.5.5. Synthesis of triyne **62**.

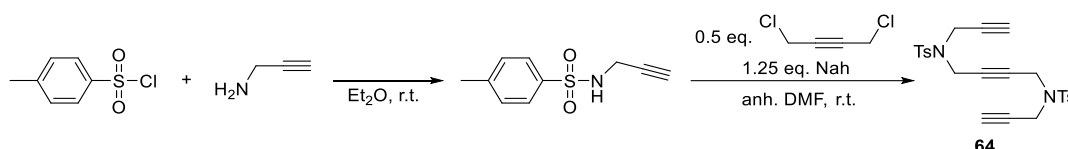


A stirred mixture of 1-bromo-2-propyne (2.01 g, 23.23 mmol) in DMSO (8 mL) and KOH (6.26 g, 58.08 mmol) in 3 mL of water (3 mL) was cooled at 0°C in an ice bath. 2-Butyne-1,4-diol (5.18 mL, 58.08 mmol) in DMSO (3 mL) was then added dropwise. The reaction was stirred at 0°C for 30 minutes and heating at 70°C for 5.5 hours (TLC monitoring). The salts were filtered off, water (10 mL) was added to the filtrate and it was extracted with ethyl acetate (3 x 15 mL). The solvent was evaporated and the residue was purified by column chromatography on silica gel with hexanes/dichloromethane (9:1) to afford 4,9-dioxa-dodeca-1,6,11-triyne **62** (2.65 g, 70% yield) as a yellow oil.^{43b} **Molecular formula**: C₁₀H₁₀O₂; **MW**: 162.07 g/mol; **¹H-NMR (400 MHz, CDCl₃) δ**

(ppm) 2.45 (t, $^4J_{H,H} = 2.4$ Hz, 2H, $C\equiv CH$), 4.24 (d, $^4J_{H,H} = 2.4$ Hz, 4H, $CH_2C\equiv CH$), 4.30 (s, 4H, $CH_2C\equiv CCH_2$).

Further elution with hexanes/dichloromethane (7:3) afforded the monoalkylation product 5-oxa-2,7-octadiyne-1-ol¹⁸² (0.46 g, 16% yield) as a yellow oil. **Molecular formula:** $C_7H_8O_2$; **MW:** 124.14 g/mol; **1H -NMR (400 MHz, $CDCl_3$) δ (ppm):** 2.35 (s, 1H, OH), 2.48 (t, $^4J_{H,H} = 2.4$ Hz, 1H, $C\equiv CH$), 4.25 (d, $^4J_{H,H} = 2.4$ Hz, 2H, $CH_2C\equiv CH$), 4.30 (s, 4H, $CH_2C\equiv CCH_2$).

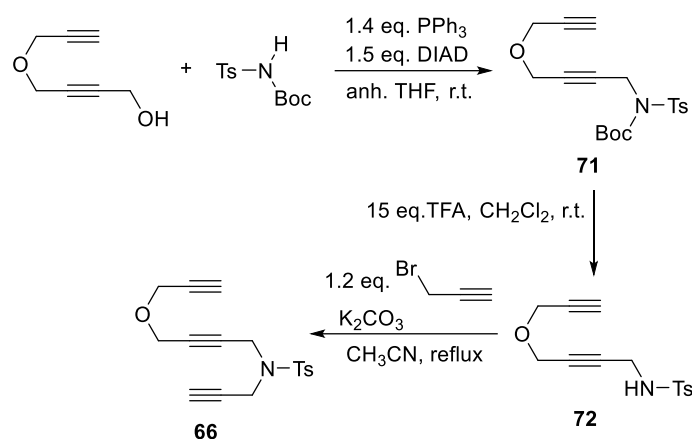
8.5.6. Synthesis of triyne 64.



A stirred mixture of *p*-toluenesulfonyl chloride (4.09 g, 20.98 mmol) in diethyl ether (20 mL) was cooled at 0°C in an ice bath. Propargylamine (2.94 mL, 41.96 mmol) was then added dropwise. The reaction mixture was stirred at room temperature for 2.5 h (TLC monitoring). The solvent was evaporated and the residue was purified by column chromatography on silica gel with hexanes/ethyl acetate (7:3) to afford *N*-tosyl-prop-2-yn-1-amine (3.60 g, 82% yield) as a colourless solid.¹⁸³ **Molecular formula:** $C_{10}H_{11}O_2NS$; **MW:** 209.20 g/mol; **1H -NMR (400 MHz, $CDCl_3$) δ (ppm)** 2.10 (t, $^4J_{H,H} = 2.6$ Hz, 1H, $C\equiv CH$), 2.43 (s, 3H, CH_3 -Ts), 3.80-3.85 (m, 2H, NCH_2), 4.56 (s, 1H, NH), 7.31 (d, $^3J_{H,H} = 8.4$ Hz, 2H, CH -Ts), 7.77 (d, $^3J_{H,H} = 8.4$ Hz, 2H, CH -Ts).

A stirred mixture of sodium hydride in 60% oil dispersion (0.30 g, 5.93 mmol of pure NaH) was washed with hexanes (3 x 10 mL) under nitrogen atmosphere. The solvent was removed and the residue was suspended in anhydrous DMF (8 mL) and it was cooled at 0°C in an ice bath. Propargyl(*p*-toluenesulfonyl)amine (0.99 g, 4.75 mmol) in anhydrous DMF (8 mL) was added slowly at 0°C. The mixture was stirred for 1 hour while warming to room temperature under nitrogen atmosphere. 1,4-dichloro-2-butyne (0.29 g, 2.37 mmol) in DMF (2 mL) was then added dropwise via an addition funnel and the reaction was stirred for additional 2 hours at room temperature (TLC monitoring). NH_4Cl was added to quench the reaction and the mixture was extracted with ethyl acetate (3 x 10 mL). The organic phase was washed with brine (2 x 20 mL), dried over sodium sulfate, filtered and concentrated. The crude was purified by recrystallization in ethyl acetate to afford 4,9-bis(*p*-toluenesulfonyl)-4,9-diazadodeca-1,6,11-triyne **64** (0.41 g, 37%) as a colourless solid.¹⁸⁴ **Molecular formula:** $C_{24}H_{24}O_4N_2S_2$; **MW:** 468.15 g/mol; **m.p.** 161-163 °C; **1H -NMR (400 MHz, $CDCl_3$) δ (ppm)** 2.12 (t, $^4J_{H,H} = 2.8$ Hz, 2H, $C\equiv CH$), 2.44 (s, 6H, CH_3 -Ts), 3.99 (d, $^4J_{H,H} = 2.8$ Hz, 4H, $CH_2C\equiv CH$), 4.02 (s, 4H, $CH_2C\equiv CCH_2$), 7.30 (d, $^3J_{H,H} = 8.4$ Hz, 4H, CH -Ts), 7.67 (d, $^3J_{H,H} = 8.4$ Hz, 4H, CH -Ts); **ESI-MS (m/z):** 469 $[M+H]^+$, 486 $[M+NH_4]^+$, 491 $[M+Na]^+$.

8.5.7. Synthesis of triyne 66.



A mixture of 5-oxa-2,7-octadiyne-1-ol (0.56 g, 4.51 mmol), *N*-(*tert*-butyloxycarbonyl)-*p*-toluenesulfonamide (1.36 g, 5.01 mmol) and triphenylphosphine (1.71 g, 6.52 mmol) were dissolved in anhydrous THF (40 mL) and cooled to 0°C. Diisopropyl azodicarboxylate (1.3 mL, 6.6 mmol) was then added slowly. The reaction mixture was warmed up to room temperature and stirred for 3 hours until completion (TLC monitoring). The solvent was then evaporated and the residue was purified by column chromatography on silica gel with hexanes/ethyl acetate (10:1) to give **71** (1.39 g, 81% yield) as a pale yellow oil. **Molecular formula:** C₁₉H₂₃NO₅S; **MW:** 377.45 g/mol; **¹H-NMR (300 MHz, CDCl₃) δ (ppm)** 1.33 (s, 9H, CH₃-Boc), 2.42 (s, 3H, CH₃-Ts), 2.44 (t, ⁴J_{H,H} = 2.4 Hz, 1H, terminal alkyne), 4.20 (d, ⁴J_{H,H} = 2.4 Hz, 2H, CH₂-O), 4.27 (t, ⁵J_{H,H} = 1.8 Hz, 2H, CH₂-N), 4.65 (t, ⁵J_{H,H} = 1.8 Hz, 2H, CH₂-O), 7.31 (d, ³J_{H,H} = 8.2 Hz, 2H, CH-Ts), 7.89 (d, ³J_{H,H} = 8.2 Hz, 2H, CH-Ts); **¹³C-NMR (75 MHz, CDCl₃) δ (ppm)** 21.9 (CH₃-Ts), 28.1 (CH₃-Boc), 36.2 (CH₂-N), 56.5 (CH₂-O), 56.9 (CH₂-O), 75.32 (C alkyne), 79.1 (C_q-Boc), 79.2 (C alkyne), 82.6 (C alkyne), 85.2 (C alkyne), 128.5 (CH-Ts), 129.5 (CH-Ts), 136.9 (C-Ts), 144.7 (C-Ts), 150.4 (CO-Boc); **IR (ATR) ν (cm⁻¹)** 3276, 1727, 1351, 1144; **ESI-MS (m/z):** 395 [M + NH₄]⁺, 400 [M + Na]⁺, 416 [M + K]⁺; **EA** calculated for C₁₉H₂₃O₅NS: 60.46% C, 6.14% H, 3.71% N, found: 60.06% C, 6.18% H, 3.81% N.

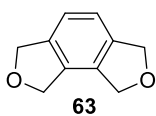
Trifluoroacetic acid (3.8 mL, 40.11 mmol) was added slowly to a solution of **71** (1.00 g, 2.65 mmol) in CH₂Cl₂ (9 mL). The reaction mixture was stirred at room temperature for 2 hours until completion (TLC monitoring). The crude was then treated with a saturated sodium bicarbonate solution (3 x 10 mL) and water (3 x 10 mL). The organic phase was dried over anhydrous Na₂SO₄ and concentrated under vacuum to give **72** (0.57 g, 78% yield) as brown oil. **Molecular formula:** C₁₄H₁₅NO₃S; **MW:** 277.33 g/mol; **¹H-NMR (300 MHz, CDCl₃) δ (ppm)** 2.42 (s, 3H, CH₃-Ts), 2.43, (t, ⁴J_{H,H} = 2.4 Hz, terminal alkyne), 3.87 (dt, ³J_{H,H} = 6.0 Hz, ⁵J_{H,H} = 1.9 Hz, 2H, CH₂-N), 4.02 (t, ⁵J_{H,H} = 1.9 Hz, 2H, CH₂-O), 4.04 (d, ⁴J_{H,H} = 2.4 Hz, CH₂-O), 4.84 (t, ³J_{H,H} = 6.0 Hz, 1H, NH), 7.31 (d, ³J_{H,H} = 8.1 Hz, 2H, CH-Ts), 7.77 (d, ³J_{H,H} = 8.1 Hz, 2H, CH-Ts); **¹³C-NMR (75 MHz, CDCl₃) δ (ppm)** 21.8 (CH₃-Ts), 33.3 (CH₂-N), 56.6 (CH₂-O), 75.3 (C alkyne), 78.9 (C alkyne), 80.0 (C alkyne), 81.4 (C alkyne), 127.6 (CH-Ts), 129.9 (CH-Ts), 136.9 (C-Ts), 144.0 (C-Ts); **IR (ATR) ν (cm⁻¹)** 3272, 1323, 1154; **ESI-MS (m/z):** 278 [M + H]⁺, 300 [M + Na]⁺; **EA** calculated for C₁₄H₁₅O₃NS: 60.63% C, 5.45% H, 5.05% N, found: 60.29% C, 4.62% H, 5.08% N.

A mixture of **72** (0.5 g, 1.80 mmol) and potassium carbonate (1.30 g, 9.4 mmol) was suspended in CH₃CN (70 mL) and heated to reflux. Propargyl bromide (0.23 mL, 2.06 mmol) was then added

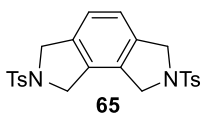
to the reaction mixture. The reaction was refluxed for 1 hour until completion (TLC monitoring). The reaction mixture was then cooled down to room temperature, the salts were filtered off, and the crude was concentrated under vacuum. The residue was purified by column chromatography on silica gel with hexanes/ethyl acetate (8:2) to give **66** (0.54 g, 96% yield) as a yellow oil. **Molecular formula:** $C_{17}H_{17}NO_3S$; **MW:** 315.38 g/mol; **1H -NMR (300 MHz, $CDCl_3$) δ (ppm)** 2.15 (t, $^4J_{H,H} = 2.5$ Hz, 1H, *CH*-terminal alkyne-NTs), 2.42 (s, 3H, CH_3 -Ts), 2.44 (t, $^4J_{H,H} = 2.4$ Hz, 1H, *CH*-terminal alkyne-O), 4.08-4.10 (m, 4H), 4.14 (d, $^5J_{H,H} = 2.4$ Hz, 2H, CH_2 -N), 4.21 (t, $^5J_{H,H} = 1.6$ Hz, 2H, CH_2 -O), 7.30 (d, $^3J_{H,H} = 8.2$ Hz, 2H, *CH*-Ts), 7.71 (d, $^3J_{H,H} = 8.2$ Hz, 2H, *CH*-Ts); **^{13}C -NMR (75 MHz, $CDCl_3$) δ (ppm)** 21.9 (CH_3 -Ts), 36.7 (CH_2 -N), 36.8 (CH_2 -N), 56.7 (CH_2 -O), 56.8 (CH_2 -O), 74.3 (C alkyne), 75.4 (C alkyne), 76.58 (C alkyne), 79.0 (C alkyne), 79.7 (C alkyne), 81.2 (C alkyne), 128.2 (*CH*-Ts), 129.9 (*CH*-Ts), 135.5 (C-Ts), 144.3 (C-Ts); **IR (ATR) ν (cm^{-1})** 3285, 1346, 1158; **ESI-MS (*m/z*):** 316 [*M* + *H*]⁺, 338 [*M* + *Na*]⁺; **EA** calculated for $C_{17}H_{17}O_3NS$: 64.74% C, 5.43% H, 4.44% N, found: 64.76% C, 4.99% H, 4.50% N.

8.5.6. [2+2+2] Cycloaddition of alkynes using materials M.

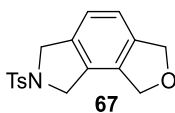
General procedure: The reactions were carried out in a Carousel multireactor. The alkynes (0.1 mmol), the material (0.01 mmol Rh) and EtOH (3 mL) were transferred into the reaction tubes of the reactor and the reaction mixtures were stirred at 80°C (external temperature). When there was no presence of starting material (TLC or GC monitoring), the stirring was stopped and the reaction mixture was allowed to cool down. The solution was then filtered. The recovered catalyst was washed with CH_2Cl_2 (3 x 3 mL) and Et_2O (2 x 3 mL), dried under vacuum and directly used in the next cycle. The filtrates were concentrated under reduced pressure to afford the corresponding cycloadduct.



63 **1,3,6,8-Tetrahydro-2,7-dioxa-as-indacene**,^{43b} colourless solid. **Molecular formula:** $C_{10}H_{10}O_2$; **MW:** 162.18 g/mol; **1H -NMR (300 MHz, $CDCl_3$) δ (ppm)** 5.02-5.04 (m, 4H, CH_2O), 5.12-5.13 (m, 4H, CH_2O), 7.14 (s, 2H, *CH*-Ar).

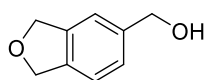


65 **2,7-Bis(p-toluenesulfonyl)-1,3,6,8-tetrahydro-2,7-diaza-as-indacene**,¹⁸⁴ colourless solid. **Molecular formula:** $C_{24}H_{24}N_2O_4S_2$; **MW:** 468.58 g/mol; **1H -NMR (300 MHz, $CDCl_3$) δ (ppm)** 2.40 (s, 6H, CH_3), 4.45 (s, 4H, CH_2), 4.57 (s, 4H, CH_2), 7.04 (s, 2H, *CH*-Ar), 7.31 (d, $^3J_{H,H} = 8.0$ Hz, 4H, *CH*-Ts), 7.74 (d, $^3J_{H,H} = 8.0$ Hz, 4H, *CH*-Ts).



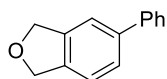
67 **7-(p-toluenesulfonyl)-2-oxa-7-aza-1,3,6,8-tetrahydro-as-indacene**, colourless solid. **Molecular formula:** $C_{17}H_{17}NO_3S$; **MW:** 315.38 g/mol; **m.p.** decomposition; **1H -NMR (300 MHz, $CDCl_3$) δ (ppm)** 2.40 (s, 3H, CH_3), 4.50 (br s, 2H, CH_2 -NTs), 4.62 (br s, 2H, CH_2 -NTs), 4.97 (br s, 2H, CH_2 -O), 5.06 (br s, 2H, CH_2 -O), 7.05-7.12 (m, 2H, *CH*-Ar), 7.31 (d, $^3J_{H,H} = 8.1$ Hz, 2H, *CH*-Ts), 7.76 (d, $^3J_{H,H} = 8.1$ Hz, 2H, *CH*-Ts); **^{13}C -NMR (75 MHz, $CDCl_3$) δ (ppm)** 21.8 (CH_3 -Ts), 52.6 (CH_2 -NTs), 53.7 (CH_2 -NTs), 72.3 (CH_2 -O), 73.7 (CH_2 -O), 120.7 (*CH*-Ar), 121.9 (*CH*-Ar), 127.9 (*CH*-Ts),

129.7 (C-Ar), 130.2 (CH-Ts), 133.9 (C-Ar), 134.0 (C-Ar), 135.9 (C-Ts), 139.5 (C-Ar), 144.1 (C-Ts); IR (ATR) ν (cm^{-1}) 2857, 1340, 1156; ESI-MS (m/z): 316 [M + H]⁺, 338 [M + Na]⁺, 653 [2M + H]⁺; ESI-HRMS (m/z): calculated for [C₁₇H₁₇O₃NS + Na]⁺: 338.0809, found: 338.0821.



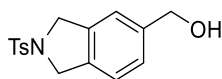
70aa

5-hydroxymethylphthalan,⁵⁰ colourless solid. **Molecular formula:** C₉H₁₀O₂; **MW:** 150.17 g/mol; **¹H-NMR (300 MHz, CDCl₃) δ (ppm)** 4.69 (s, 2H, CH₂OH), 5.09 (s, 5H, CH₂O + OH), 7.19-7.27 (m, 3H, CH-Ar).



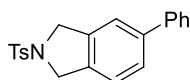
70ab

5-phenylphthalan,⁵⁰ colourless solid. **Molecular formula:** C₁₄H₁₂O; **MW:** 196.24 g/mol; **¹H-NMR (300 MHz, CDCl₃) δ (ppm)** 5.17 (s, 4H, CH₂O), 7.29-7.60 (m, 8H, CH-Ar).



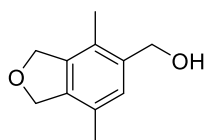
70ba

5-hydroxymethyl-2-(p-toluenesulfonyl)-1,3-dihydroisindole,¹⁸⁵ colourless solid. **Molecular formula:** C₁₆H₁₇NO₃S; **MW:** 303.37 g/mol; **¹H-NMR (300 MHz, CDCl₃) δ (ppm)** 2.39 (s, 3H, CH₃), 4.56 (s, 4H, CH₂-NTs), 4.64 (s, 2H, CH₂OH), 7.11-7.23 (m, 3H, CH-Ar), 7.30 (d, ³J_{H,H} = 8.1 Hz, 2H, CH-Ts), 7.74 (d, ³J_{H,H} = 8.1 Hz, 2H, CH-Ts).



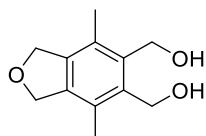
70bb

5-phenyl-2-(p-toluenesulfonyl)-1,3-dihydroisindole,⁵⁰ colourless solid. **Molecular formula:** C₂₁H₁₉NO₂S; **MW:** 349.44 g/mol; **¹H-NMR (300 MHz, CDCl₃) δ (ppm)** 2.43 (s, 3H, CH₃), 4.69 (br abs, 4H, CH₂-NTs), 7.25 (d, ³J_{H,H} = 8.1 Hz, 1H, CH-Ar), 7.30-7.56 (m, 9H, CH-Ar + CH-Ph + CH-Ts), 7.80 (d, ³J_{H,H} = 8.3 Hz, 2H, CH-Ts).



70ia

5-hydroxymethyl-4,7-dimethylphthalan,^{43b} colourless solid. **Molecular formula:** C₁₁H₁₄O₂; **MW:** 178.23 g/mol; **¹H-NMR (300 MHz, CDCl₃) δ (ppm)** 2.21 (s, 6H, CH₃), 4.69 (s, 3H, CH₂OH), 5.11 (s, 4H, CH₂O), 7.07 (s, 1H, CH-Ar).



70ic

5,6-dihydroxymethyl-4,7-dimethylphthalan,^{43b} colourless solid. **Molecular formula:** C₁₂H₁₆O₃; **MW:** 208.25 g/mol; **¹H-NMR (400 MHz, DMSO-d₆) δ (ppm)** 2.18 (s, 6H, CH₃), 4.56 (d, ³J_{H,H} = 5.2 Hz, 4H, CH₂OH), 4.71 (t, ³J_{H,H} = 5.2 Hz, 2H, OH), 5.01 (s, 4H, CH₂O).

Bibliography

- ¹ Reppe, W.; Schweckendiek, W.J. *Justus Liebigs Ann. Chem.* **1948**, 560,104.
- ² For a monograph on [2+2+2] cycloaddition reactions, see: Tanaka, K. *Transition-Metal-Mediated Aromatic Ring Construction*, Wiley, John & Sons, Inc., **2013**. For selected reviews, see: a) Lledó, A.; Pla-Quintana, A.; Roglans, A. *Chem. Soc. Rev.* **2016**, 45, 2010; b) Neuhaus, J.; Willis, M. *Org. Biomol. Chem.* **2016**, 14, 4986; c) Domínguez, G.; Pérez-Castells, J. *Chem. Eur. J.* **2016**, 22, 6720; d) Shibata, Y.; Tanaka, K. *Synthesis* **2012**, 323; e) Marinetti, A.; Jullien, H.; Voituriez, A. *Chem. Soc. Rev.*, **2012**, 41, 4884; f) Broere, D. L. J.; Ruijter, E. *Synthesis* **2012**, 2639; g) Tanaka, K. *Heterocycles* **2012**, 85, 1017; h) Okamoto, S. *Heterocycles* **2012**, 85, 1579; i) Hua, R.; Abrenica, M. V. A.; Wang, P. *Curr. Org. Chem.* **2011**, 15, 712; j) Wedling, N.; Hapke, M. *Chem. Soc. Rev.* **2011**, 40, 4525; k) Domínguez, G.; Pérez-Castells, J. *Chem. Soc. Rev.* **2011**, 40, 3430; l) Inglesby, P. A.; Evans, P. A. *Chem. Soc. Rev.* **2010**, 39, 2791; m) Tanaka, K. *Chem. Asian J.* **2009**, 4, 508; n) Galan, B. R.; Rovis, T. *Angew. Chem. Int. Ed.* **2009**, 48, 2830; o) Shibata, T.; Tsuchikama, K. *Org. Biomol. Chem.* **2008**, 6, 1317; p) Tanaka, K. *Synlett* **2007**, 1977; q) Chopade, P. R.; Louie, J. *Adv. Synth. Catal.* **2006**, 348, 2307; r) Gandon, V.; Aubert, C.; Malacria, M. *Chem. Commun.* **2006**, 2209; s) Yamamoto, Y. *Curr. Org. Chem.* **2005**, 9, 503; t) Kotha, S.; Brahmachary, E.; Lahiri, K. *Eur. J. Org. Chem.* **2005**, 4741; t) Tanaka, K.; Shirasaka, K. *Org. Lett.* **2003**, 5, 4697.
- ³ For selected recent references, see: a) Orian, L.; Swart, M.; Bickelhaupt, F. M. *ChemPhysChem* **2014**, 15, 219; b) Orian, L.; Wolters, L. P.; Bickelhaupt, F. M. *Chem. Eur. J.* **2013**, 19, 13337; c) Calhorda, M. J.; Costa, P. J.; Kirchner, K. *Inorg. Chim. Acta* **2011**, 374, 24; d) Li, X.; Xu, J. *Org. Biomol. Chem.* **2011**, 9, 5997; e) Orian, L.; van Stralen, J. N. P.; Bickelhaupt, F. M. *Organometallics* **2007**, 26, 3816; f) Agenet, N.; Gandon, V.; Vollhardt, K. P. C.; Malacria, M.; Aubert, C. *J. Am. Chem. Soc.* **2007**, 129, 8860; g) Yamamoto, Y.; Kinpara, K.; Ogawa, R.; Itoh, K. *Chem. Eur. J.* **2006**, 12, 5618. For contributions of our group on mechanistic DFT calculations on Rh-catalysed [2+2+2] cycloadditions, see: h) Haraburda, E.; Torres, Ò.; Parella, T.; Solà, M.; Pla-Quintana, A. *Chem. Eur. J.* **2014**, 20, 5034; i) Torres, Ò.; Roglans, A.; Pla-Quintana, A.; Luis, J.M.; Solà, M. *J. Organomet Chem.* **2014**, 768, 15; j) Dachs, A.; Pla-Quintana, A.; Parella, T.; Solà, M.; Roglans, A. *Chem. Eur. J.* **2011**, 17, 14493; k) Dachs, A.; Roglans, A.; Solà, M. *Organometallics* **2011**, 30, 3151; l) Dachs, A.; Osuna, S.; Roglans, A.; Solà, M. *Organometallics* **2010**, 29, 562; m) Dachs, A.; Torrent, A.; Roglans, A.; Parella, T.; Osuna, S.; Solà, M. *Chem. Eur. J.* **2009**, 15, 5289.
- ⁴ For selected references, see: a) Varela, J. A.; Rubin, S. G.; Castedo, L.; Saá, C. *J. Org. Chem.* **2008**, 73, 1320; b) Dazinger, G.; Torres-Rodrigues, M.; Kirchner, K.; Calhorda, M. J.; Costa, P. J. *J. Organomet. Chem.* **2006**, 691, 4434. c) Yamamoto, Y.; Kinpara, K.; Saigoku, T.; Takagishi, H.; Okuda, S.; Nishiyama, H.; Itoh, K. *J. Am. Chem. Soc.* **2005**, 127, 605; d) Kirchner, K.; Calhorda, M.J.; Schmid, R.; Veiros, L.F. *J. Am. Chem. Soc.* **2003**, 125, 11721.
- ⁵ For selected references, see: a) Garcia, P.; Evanno, Y.; George, P.; Sevrin, M.; Ricci, G.; Malacria, M.; Aubert, C.; Gandon, V. *Chem. Eur. J.* **2012**, 18, 4337; b) Dahy, A.A.; Koga, N. *J. Organomet. Chem.* **2010**, 695, 2240; c) Dahy, A.A.; Yamada, K.; Koga, N. *Organometallics* **2009**, 28, 3636; d) Hardesty, J.H.; Koerner, J.B.; Albright, T.A.; Lee, G.-Y. *J. Am. Chem. Soc.* **1999**, 121, 6055. For a revision article comparing Ru and Co, see: e) Varela, J. A.; Saá, C. *J. Organomet Chem.* **2009**, 694, 143.
- ⁶ For selected references of DFT studies catalysed by iridium, see: a) Dahy, A.A.; Koga, N. *Organometallics* **2015**, 34, 4965; b) Guo, C.-H.; Wu, H.-S.; Hapke, M.; Jiao, H. *J. Organomet. Chem.* **2013**, 748, 29; for a selected reference of DFT a study catalysed by chromium, see: c) Liu, Z.; Cheng, R.; He, X.; Liu, B. *ACS Catal.* **2013**, 3, 1172.
- ⁷ Selected references: a) Bottari, G.; Santos, L.; Posadas, C.; Campos, J.; Mereiter, K.; Paneque, M. *Chem. Eur. J.* **2016**, 22, 13715; b) Parera, M.; Dachs, A.; Solà, M.; Pla-Quintana, A.; Roglans, A. *Chem. Eur. J.* **2012**, 18, 13097; c) Dutta, B.; Curchod, B.F.E.; Campomanes, P.; Solari, E.; Scopelliti, R.; Rothlisberger, U.; Severin, K. *Chem. Eur. J.* **2010**, 16, 8400; d) Dachs, A.; Torrent, A.; Pla-Quintana, A.; Roglans, A.; Jutand, A. *Organometallics* **2009**, 28, 6036; e) Uchimura, H.; Ito, J. I.; Iwasa, S.; Nishiyama, H. *J. Organomet Chem.* **2007**, 692, 481; f) Xue, P.; Sung, H. S. Y.; Williams, I. D.; Jia, G. *J. Organomet Chem.* **2006**, 691, 1945; g) Nishiyama, H.; Niwa, E.; Inoue, T.; Ishima, Y.; Aoki, K. *Organometallics* **2002**, 21, 2572; h) Rourke, J. P.; Batsanov, A. S.; Howard, J. A. K.; Marder, T. B. *Chem. Commun.* **2001**, 2626; i) Bianchini, C.; Meli, A.; Peruzzini, M.; Vacca, A.; Vizza, F. *Organometallics* **1991**, 10, 645; j) Bianchini, C.; Caulton, K. G.; Chardon, C.; Eisenstein, O.; Folting, K.; Johnson, T. J.; Meli, A.; Peruzzini, M.; Tauscher, D. J.; Streib, W. E.; Vizza, F. *J. Am. Chem. Soc.* **1991**, 113, 5127; k) Iglesias, M.; del Pino, C.; Ros, J.; García Blanco, S.; Carrera, S. M. *J. Organomet Chem.* **1988**, 338, 38; l) Gastinger, R. G.; Rausch, M. D.; Sullivan, D. A.; Palenik, G. J. J.

Organomet Chem. **1976**, *117*, 355; m) Müller, E. *Synthesis* **1974**, 761; n) Mague, J. T. *Inorg. Chem.* **1973**, *12*, 2649; o) Mague, J. T. *Inorg. Chem.* **1970**, *9*, 1610.

⁸ For a review, see: a) Schmid, R.; Kirchner, K. *Eur. J. Inorg. Chem.* **2004**, 2609. For selected references, see: b) Dutta, B.; Curchod, B. F. E.; Campomanes, P.; Solari, E.; Scopelliti, R.; Rothlisberger, U.; Severin, K. *Chem. Eur. J.* **2010**, *16*, 8400; c) Yamamoto, Y.; Arakawa, T.; Ogawa, R.; Itoh, K. *J. Am. Chem. Soc.* **2003**, *125*, 12143. d) Ernst, C.; Walter, O.; Dinjus, E. *J. Prakt. Chem.* **1999**, *341*, 801; e) Gemel, C.; LaPensée, A.; Mauthner, K.; Mereiter, K.; Schmid, R.; Kirchner, K. *Monatsh. Chem.* **1997**, *128*, 1189; f) Albers, M. O.; de Waal, D. J. A.; Liles, D. C.; Robinson, D. J.; Singleton, E.; Wiege, M. B. *J. Chem. Soc., Chem. Commun.* **1986**, 1680.

⁹ Schore, N. E. *Chem. Rev.* **1988**, *88*, 1081.

¹⁰ Yamamoto, K.; Tsurugi, H.; Mashima, K. *Chem. Eur. J.* **2015**, *21*, 11369.

¹¹ a) Santos, J. C.; Polo, V.; Andrés, J. *Chem. Phys. Lett.* **2005**, *406*, 393; b) Ioffe, A.; Shaik, S. *J. Chem. Soc., Perkin Trans. 2*, **1992**, 2101.

¹² a) Spahn, N. A.; Nguyen, M. H.; Renner, J.; Lane, T. K.; Louie, J. J. *Org. Chem.* **2017**, *82*, 234; b) Murayama, K.; Shibata, Y.; Sugiyama, H.; Uekusa, H.; Tanaka, K. *J. Org. Chem.* **2017**, *82*, 1136; c) Ref. 2e; d) Ref. 2g; e) Ref. 2h; f) Ref. 2i; g) Ref. 2j; h) Shaaban, M. R.; El-Sayed, R.; Elwahy, A. H. M. *Tetrahedron* **2011**, *67*, 6095; i) Varela, J. A.; Saá, C. *Synlett* **2008**, 2571; j) Heller, B.; Hapke, M. *Chem. Soc. Rev.* **2007**, *36*, 1085; k) Ref. 2p; l) Henry, G. D. *Tetrahedron* **2004**, *60*, 6043; m) Varela, J. A.; Saá, C. *Chem. Rev.* **2003**, *103*, 3787.

¹³ Abdulla, K.; Booth, B. L.; Stacey, C. J. *Organomet. Chem.* **1985**, *293*, 103.

¹⁴ Rerek, M. E.; Ji, L. N.; Basolo, F. J. *Chem. Soc. Chem. Commun.* **1983**, 1208.

¹⁵ Pla-Quintana, A.; Roglans, A. *Molecules* **2010**, *15*, 9230.

¹⁶ a) Nakajima, K.; Liang, W.; Nishibayashi, Y. *Org. Lett.* **2016**, *18*, 5006; b) Nakajima, K.; Takata, S.; Sakata, K.; Nishibayashi, Y. *Angew. Chem. Int. Ed.* **2015**, *54*, 7597.

¹⁷ a) Oonishi, Y.; Hato, Y.; Sato, Y. *Adv. Synth. Catal.* **2015**, *357*, 3033; b) Zhang, W.; Zhang, Q.-R.; Dong, L. *Tetrahedron Lett.* **2015**, *56*, 546; c) Hoshimoto, Y.; Ohata, T.; Ohashi, M.; Ogoshi, S. *Chem. Eur. J.* **2014**, *20*, 4105; d) Amatore, M.; Leboeuf, D.; Malacria, M.; Gandon, V.; Aubert, C. *J. Am. Chem. Soc.* **2013**, *135*, 4576.

¹⁸ Paquette, L.A.; Barrett, J.H. *Org. Synth.* **1969**, *49*, 62.

¹⁹ Snyder, H.R.; Brooks, L.A. *Org. Synth.* **1932**, *12*, 26.

²⁰ Roberts, S. *Comprehensive Organic Functional Group Transformations: Synthesis: Carbon with No Attached Heteroatoms* (1995) Cambridge; UK: Elsevier Science, p.419.

²¹ a) Brun, S.; García, L.; González, I.; Torrent, A.; Dachs, A.; Pla-Quintana, A.; Parella, T.; Roglans, A. *Chem. Commun.* **2008**, 4339; b) Torrent, A.; Gonzalez, I.; Pla-Quintana, A.; Roglans, A.; Moreno-Mañas, M.; Parella, T.; Benet-Buchholz, J. *J. Org. Chem.* **2005**, *70*, 2033. c) Pla-Quintana, A.; Torrent, A.; Benet-Buchholz, J.; Moreno-Mañas, M.; Roglans, A. *Organometallics* **2004**, *23*, 2762.

²² Shibata, T.; Kurokawa, H.; Kanda, K. *J. Org. Chem.* **2007**, *72*, 6521.

²³ Tanaka, K.; Nishida, G.; Sagae, H.; Hirano, M. *Synlett* **2007**, 1426.

²⁴ a) Varela, J. A.; Saá, C. *J. Organomet. Chem.* **2009**, *694*, 143; b) Varela, J. A.; García-Rubén, S.; Castedo, L.; Saá, C. *J. Org. Chem.* **2008**, *73*, 1320; c) García-Rubén, S.; Varela, J. A.; Castedo, L.; Saá, C. *Chem. Eur. J.* **2008**, *14*, 9772; d) Varela, J. A.; García-Rubén, S.; González-Rodríguez, C.; Castedo, L.; Saá, C. *J. Am. Chem. Soc.* **2006**, *128*, 9262

²⁵ Shibata, T.; Arai, Y.; Tahara, Y. *Org. Lett.* **2005**, *7*, 4955.

²⁶ Lai, K. W.; Sawyer, J. R.; Evans, P. A. *J. Am. Chem. Soc.* **2005**, *127*, 12466.

²⁷ Masutomi, K.; Sugiyama, H.; Uekusa, H.; Shibata, Y.; Tanaka, K. *Angew. Chem. Int. Ed.* **2016**, *55*, 15373, and references cited therein.

²⁸ For a pioneering work, see: Singleton, D. M. *Tetrahedron Lett.* **1973**, *14*, 1245.

²⁹ Tsuchikama, K.; Kuwata, Y.; Shibata, T. *J. Am. Chem. Soc.* **2006**, *128*, 13686.

³⁰ Shibata, T.; Kawachi, A.; Ogawa, M.; Kuwata, Y.; Tsuchikama, K.; Endo, K. *Tetrahedron* **2007**, *63*, 12853.

³¹ Tanaka, K.; Takahashi, M.; Imase, H.; Osaka, T.; Noguchi, K.; Hirano, M. *Tetrahedron* **2008**, *64*, 6289.

³² Kobayashi, M.; Suda, T.; Noguchi, K.; Tanaka, K. *Angew. Chem. Int. Ed.* **2011**, *50*, 1664.

³³ a) Benson, R. E.; Lindsey, R. V. *J. Am. Chem. Soc.* **1959**, *81*, 4247; b) Benson, R. E.; Lindsey, R. V. *J. Am. Chem. Soc.* **1959**, *81*, 4250.

³⁴ a) Aubert, C.; Llerena, D.; Malacria, M. *Tetrahedron Lett.* **1994**, *35*, 2341; b) Llerena, D.; Buisine, O.; Aubert, C.; Malacria, M. *Tetrahedron* **1998**, *54*, 9373.

³⁵ Buisine, O.; Aubert, C.; Malacria, M. *Synthesis* **2000**, 985.

³⁶ a) Petit, M.; Aubert, C.; Malacria, M. *Org. Lett.* **2004**, *6*, 3937; b) Petit, M.; Aubert, C.; Malacria, M. *Tetrahedron* **2006**, *62*, 10582.

³⁷ Saito, N.; Ichimaru, T.; Sato, Y. *Chem. Asian. J.* **2012**, *7*, 1521.

- ³⁸ Ohta, Y.; Yasuda, S.; Yokogawa, Y.; Kurokawa, K.; Mukai, C. *Angew. Chem. Int. Ed.* **2015**, *54*, 1240.
- ³⁹ Haraburda, E.; Lledó, A.; Roglans, A.; Pla-Quintana, A. *Org. Lett.* **2015**, *17*, 2882.
- ⁴⁰ a) Egbertson, M. S.; Wai, J. S.; Cameron, M.; Hoerrner, R. S. *Discovery of MK-0536: A Potential Second-Generation HIV-1 Integrase Strand Transfer Inhibitor with a High Genetic Barrier to Mutation. In Antiviral Drugs: From Basic Discovery through Clinical Trials*, John Wiley & Sons, Inc., Hoboken, **2011**; b) Metifiot, M.; Johnson, B.; Smith, S.; Zhao, X. Z.; Marchand, C.; Burke, T.; Hughes, S.; Pommier, Y. *Antimicrob. Agents Chemother.* **2011**, *55*, 5127.
- ⁴¹ a) Pierre, F.; Chua, P. C.; O'Brien, S. E.; Siddiqui-Jain, A.; Bourbon, P.; Haddach, M.; Michaux, J.; Nagasawa, J.; Schwaebe, M. K.; Stefan, E.; Vialettes, A.; Whitten, J. P.; Chen, T. K.; Darjania, L.; Stansfield, R.; Anderes, K.; Bliesath, J.; Drygin, D.; Ho, C.; Omori, M.; Proffitt, C.; Streiner, N.; Trent, K.; Rice, W. G.; Ryckman, D. M. *J. Med. Chem.* **2011**, *54*, 635; b) van Eis, M. J.; Evenou, J.-P.; Floersheim, P.; Gaul, C.; Cowan-Jacob, S. W.; Monovich, L.; Rummel, G.; Schuler, W.; Stark, W.; Strauss, A.; von Matt, A.; Vangrevelinghe, E.; Wagner, J.; Soldermann, N. *Bioorg. Med. Chem. Lett.* **2011**, *21*, 7367.
- ⁴² Oonishi, Y.; Hato, Y.; Sato, Y. *Adv. Synth. Catal.* **2015**, *357*, 3033.
- ⁴³ a) Grigg, R.; Scott, R.; Stevenson, P. *Tetrahedron Lett.* **1982**, *23*, 2691; b) Grigg, R.; Scott, R.; Stevenson, P. *J. Chem. Soc. Perkin Trans.* **1988**, 1357.
- ⁴⁴ Minnaard, A. J.; Feringa, B. L.; Lefort, L.; de Vries, J. G. *Acc. Chem. Res.* **2007**, *40*, 1267.
- ⁴⁵ van den Berg, M.; Minnaard, A. J.; Schudde, E. P.; van Esch, J.; de Vries, A. H. M.; de Vries, J. G.; Feringa, B. L. *J. Am. Chem. Soc.* **2000**, *122*, 11539.
- ⁴⁶ a) Perreault, S.; Rovis, T. *Synthesis* **2013**, *45*, 719; b) Martin, T. J.; Rovis, T. *Angew. Chem. Int. Ed.* **2013**, *52*, 5368; c) Dalton, D. M.; Rappé A. K.; Rovis, T. *Chem. Science* **2013**, *4*, 2062; d) Friedman, R. K.; Oberg, K.M.; Dalton, F. M.; Rovis, T. *Pure Appl. Chem.* **2010**, *82*, 1353; e) Dalton, D. M.; Oberg, K. M.; Yu, R. T.; Lee, E. E.; Perreault, S.; Oinen, M. E.; Pease, M. L.; Malik, G.; Rovis, T. *J. Am. Chem. Soc.* **2009**, *131*, 15717; f) Oinen, M. E.; Yu, R. T.; Rovis, T. *Org. Lett.* **2009**, *11*, 4934; g) Friedman, R. K.; Rovis, T. *J. Am. Chem. Soc.* **2009**, *131*, 10775; h) Yu, R. T.; Lee, E. E.; Malik, G.; Rovis, T. *Angew. Chem. Int. Ed.* **2009**, *48*, 2379; i) Oberg, K. M.; Lee, E. E.; Rovis, T. *Tetrahedron* **2009**, *65*, 5056; j) Yu, R. T.; Rovis, T. *J. Am. Chem. Soc.* **2008**, *130*, 3262; k) Lee, E. E.; Rovis, T. *Org. Lett.* **2008**, *10*, 1231; l) Yu, R. T.; Rovis, T. *J. Am. Chem. Soc.* **2006**, *128*, 12370. m) Yu, R. T.; Rovis, T. *J. Am. Chem. Soc.* **2006**, *128*, 2782.
- ⁴⁷ García, L.; Roglans, A.; Laurent, R.; Majoral, J.-P.; Pla-Quintana, A.; Caminade, A.-M. *Chem. Commun.* **2012**, *48*, 9248.
- ⁴⁸ Solà, J.; Revés, M.; Riera, A.; Verdaguer, X. *Angew. Chem. Int. Ed.* **2007**, *46*, 5020.
- ⁴⁹ Achard, T.; Benet-Buchholz, J.; Riera, A.; Verdaguer, X. *Organometallics* **2009**, *28*, 480.
- ⁵⁰ Brun, S.; Parera, M.; Pla-Quintana, A.; Roglans, A.; León, T.; Achard, T.; Solà, J.; Verdaguer, X.; Riera, A. *Tetrahedron* **2010**, *66*, 9032.
- ⁵¹ León, T.; Parera, M.; Roglans, A.; Riera, A.; Verdaguer, X. *Angew. Chem. Int. Ed.* **2012**, *51*, 6951.
- ⁵² Arduengo, A.; Harlow, R. L.; Kline, M. *J. Am. Chem. Soc.* **1991**, *113*, 361.
- ⁵³ For selected reviews, see: a) Kaufhold, S.; Petermann, L.; Staehle, R.; Rau, S. *Coord. Chem. Rev.* **2015**, *304-305*, 73; b) Hopkinson, M. N.; Richter, C.; Schedler, M.; Glorius, F. *Nature*, **2014**, *510*, 485; c) Han, Y.-F.; Jin, G.-X. *Chem. Soc. Rev.* **2014**, *43*, 2799.
- ⁵⁴ a) Tekavec, T. N.; Arif, A. M.; Louie, J. *Tetrahedron* **2004**, *60*, 7431; b) Louie, J.; Gibby, J. E.; Farnworth, M. V.; Tekavec, T. N. *J. Am. Chem. Soc.* **2002**, *124*, 15188.
- ⁵⁵ Duong, H. A.; Cross, M. J.; Louie, J. *J. Am. Chem. Soc.* **2004**, *126*, 11438.
- ⁵⁶ a) Stolley, R. M.; Duong, H. A.; Louie, J. *Organometallics* **2013**, *32*, 4952; b) McCormick, M. M.; Duong, H. A.; Zuo, G.; Louie, J. *J. Am. Chem. Soc.* **2005**, *127*, 5030.
- ⁵⁷ Alvarez, S.; Medina, S.; Domínguez, G.; Pérez-Castells, J. *J. Org. Chem.* **2013**, *78*, 9995.
- ⁵⁸ Medina, S.; Domínguez, G.; Pérez-Castells, J. *Org. Lett.* **2012**, *14*, 4982.
- ⁵⁹ Alvarez, S.; Medina, S.; Domínguez, G.; Pérez-Castells, J. *J. Org. Chem.* **2015**, *80*, 2436.
- ⁶⁰ González, I.; Pla-Quintana, A.; Roglans, A. *Synlett* **2009**, *17*, 2844.
- ⁶¹ a) Seayad, A. M.; Selvakumar, K.; Ahmed, M.; Beller, M. *Tetrahedron Lett.* **2003**, *44*, 1679. b) Frey, G. D.; Rentzsch, C. F.; Preysing, D.; Scherg, T.; Mühlhofer, M.; Herdtwech, E.; Herrmann, W. A. *J. Organomet. Chem.* **2006**, *691*, 5725.
- ⁶² Geny, A.; Gaudrel, S.; Slowinski, F.; Amatore, M.; Chouraqui, G.; Malacria, M.; Aubert, C.; Gandon, V. *Adv. Synth. Catal.* **2009**, *351*, 271
- ⁶³ a) Saino, N.; Kogure, D.; Kase, K.; Okamoto, S. *J. Organomet. Chem.* **2006**, *691*, 3129; b) Saino, N.; Kogure, D.; Okamoto, S. *Org. Lett.* **2005**, *7*, 3065.
- ⁶⁴ For selected references related to the mechanistic aspects of this reaction, see: a) Amarante, G. W.; Benassi, M.; Milagre, H. M. S.; Braga, A. A. C.; Maseras, F.; Eberlin, M. N.; Coelho, F. *Chem. Eur. J.* **2009**,

- 15, 12460; b) Amarante, G. W.; Milagre, H. M. S.; Vaz, B. G.; Ferreira, B. R. V.; Eberlin, M. N.; Coelho, F. *J. Org. Chem.* **2009**, *74*, 3031; c) Roy, D.; Sunoj, R. B. *Org. Lett.* **2007**, *9*, 4873; d) Robiette, R.; Aggarwal, V. K.; Harvey, J. N. *J. Am. Chem. Soc.* **2007**, *129*, 15513; e) Santos, L. S.; da Silveira Neto, B. A.; Consorti, C. S.; Pavam, C. H.; Almeida, W. P.; Coelho, F.; Dupont, J.; Eberlin, M. N. *J. Phys. Org. Chem.* **2006**, *19*, 731; f) Aggarwal, V. K.; Fulford, S. Y.; Lloyd-Jones, G. C. *Angew. Chem. Int. Ed.* **2005**, *44*, 1706; g) Price, K. E.; Broadwater, S. J.; Walker, B. J.; McQuade, D. T. *J. Org. Chem.* **2005**, *70*, 3980; h) Price, K. E.; Broadwater, S. J.; Jung, H. M.; McQuade, D. T. *Org. Lett.* **2005**, *7*, 147; i) Santos, L. S.; Pavam, C. H.; Almeida, W. P.; Coelho, F.; Eberlin, M. N. *Angew. Chem. Int. Ed.* **2004**, *43*, 4330.
- ⁶⁵ Morita, K.; Suzuki, Z.; Hirose, H. *Bull. Chem. Soc. Jpn.* **1968**, *41*, 2815.
- ⁶⁶ Baylis, A. B.; Hillman, M.E.D. *German Patent* 2155113, **1972**; *Chem. Abstr.* **1972**, *77*, 34174.
- ⁶⁷ a) Drewes, S.E.; Roos, G.H.P. *Tetrahedron* **1988**, *44*, 4653; b) Drewes, S.E.; Emslie, N.D. *J. Chem. Soc. Perkin Trans. 1* **1982**, 2079.
- ⁶⁸ a) Hoffmann, H.M.R.; Rabe, J. *J. Org. Chem.* **1985**, *50*, 3849; b) Hoffmann, H.M.R.; Rabe, J. *Helv. Chim. Acta* **1984**, *67*, 413; c) Hoffmann, H.M.R.; Rabe, J. *Angew. Chem. Int. Ed.* **1983**, *22*, 795.
- ⁶⁹ a) Basavaiah, D.; Bharathi, T. K.; Gowriswari, V.V.L. *Tetrahedron Lett.* **1987**, *28*, 4351; b) Basavaiah, D.; Gowriswari, V.V.L.; Bharathi, T. K. *Tetrahedron Lett.* **1987**, *28*, 4591; c) Basavaiah, D.; Bharathi, T. K.; Gowriswari, V.V.L. *Synthetic Commun.* **1987**, *17*, 1893; d) Basavaiah, D.; Gowriswari, V.V.L. *Tetrahedron Lett.* **1986**, *27*, 2031.
- ⁷⁰ Basavaiah, D.; Reddy, B. S.; Badsara, S. S. *Chem. Rev.* **2010**, *110*, 5447.
- ⁷¹ a) Langer, P. *Angew. Chem. Int. Ed.* **2000**, *39*, 3049; b) Ciganek, E. *Organic Reactions*: Paquette, L.A., Ed.; Wiley: New York, **1997**; Vol. 51, p 201; c) Basavaiah, D.; Dharma Rao, P.; Suguna Hyma, R. *Tetrahedron* **1996**, *52*, 8001; d) Fort, Y.; Berthe, M.C.; Caubere, P. *Tetrahedron* **1992**, *48*, 6371; e) Bode, M.L.; Kaye, P.T. *Tetrahedron Lett.* **1991**, *32*, 5611; f) Hill, J.S.; Isaacs, N.S. *J. Phys. Org. Chem.* **1990**, *3*, 285.
- ⁷² For reviews of MBH adducts applications, see: Basavaiah, D.; Veeraghavaiah, G. *Chem. Soc. Rev.* **2012**, *41*, 68; b) Declerck, V.; Martinez, J.; Lamaty, F. *Chem. Rev.* **2009**, *109*, 1; c) Singh, V.; Batra, S. *Tetrahedron* **2008**, *64*, 4511; d) Basavaiah, D.; Rao, K.V.; Reddy, R.J. *Chem. Soc. Rev.* **2007**, *36*, 1581; e) Basavaiah, D.; Rao, A. J.; Satyanarayana, T. *Chem. Rev.* **2003**, *103*, 811; f) Ref 71c.
- ⁷³ Teng, H.-L.; Huang, H.; Tao, H.-Y.; Wang, C.-J. *Chem. Commun.* **2011**, 5494.
- ⁷⁴ Chandrasekhar, S.; Narsihmulu, Ch.; Saritha, B.; Sultana, S. S. *Tetrahedron Lett.* **2004**, *45*, 5865.
- ⁷⁵ Junior, C. G. L.; de Assis, P. A. C.; Silva, F. P. L.; Sousa, S. C. O.; de Andrade, N. G.; Barbosa, T. P.; Neris, P. L. N.; Segundo, L. V. G.; Anjos, I. C.; Carvalho, G. A. U.; Rocha, G. B.; Oliveira, M. R.; Vasconcellos, M. L. A. *Bioorg. Chem.* **2010**, *38*, 279.
- ⁷⁶ Ren, K.; Zhang, L.; Hu, B.; Zhao, M.; Tu, Y.; Xie, X.; Zhang, T. Y.; Zhang, Z. *ChemCatChem* **2013**, *5*, 1317.
- ⁷⁷ Kagan, H. B.; Fiaud, J. C. *Topics in Stereochemistry*, vol. 18, Kinetic Resolution, 249. Wiley, John & Sons, Inc. **1988**.
- ⁷⁸ Fukuyama, T.; Jow, C.-K.; Cheung, M. *Tetrahedron Lett.* **1995**, *36*, 6373.
- ⁷⁹ a) Shibuya, M.; Sudoh, T.; Kawamura, T.; Yamamoto, Y. *Org. Biomol. Chem.* **2015**, *13*, 5862; b) Jones, A. L.; Snyder, J. K. *Org. Lett.* **2010**, *12*, 1592.
- ⁸⁰ For monographs and general reviews of asymmetric organometallic catalysis, see: a) Aubert, C.; Amatore, M. *Eur. J. Org. Chem.* **2015**, 265; b) Christmann, M.; Bräse, S. *Asymmetric Synthesis: The Essentials*, Shibasaki, M.; Matsunaga, S. "Part II, Metal Catalysed Asymmetric Synthesis", **2007**, Wiley-VCH, Weinheim; c) Ma, J.-A.; Cahard, D. *Angew. Chem. Int. Ed.* **2004**, *43*, 4566; d) Beller, M.; Bolm, C. *Transition Metals for Organic Synthesis*, **2004**, 2nd edition, Wiley-VCH, Weinheim; e) Ojima, I. *Catalytic Asymmetric Synthesis*, **2000**, 2nd edition, Wiley-VCH, New York; f) Special number "Catalytic Asymmetric Synthesis", *Acc. Chem. Res.* **2000**, *33*, 323; g) Jacobsen, E. N.; Pfaltz, A.; Yamamoto, H. *Comprehensive Asymmetric Catalysis*, **1999**, Springer, (vol. I-III), Berlin; h) Noyori, R. *Asymmetric Catalysis in Organic Synthesis*, **1994**, Wiley, New York.
- ⁸¹ Campolo, D.; Gastaldi, S.; Roussel, C.; Bertrand, M. P.; Nechab, M. *Chem. Soc. Rev.* **2013**, *42*, 8434.
- ⁸² Fischer, F.; Jungk, P.; Weding, N.; Spannenberg, A.; Ott, H.; Hapke, M. *Eur. J. Org. Chem.* **2012**, *29*, 5828.
- ⁸³ Mori, A.; Araki, T.; Miyauchi, Y.; Noguchi, K.; Tanaka, K. *Eur. J. Org. Chem.* **2013**, 6774.
- ⁸⁴ a) Žádný, J.; Jančařík, A.; Andronova, A.; Šámal, M.; Chocholoušová, J.; Vacek, J.; Pohl, R.; Šaman, D.; Císařová, I.; Stará, I. G.; Starý, I. *Angew. Chem. Int. Ed.* **2012**, *51*, 5857; b) Sehnal, P.; Stará, I. G.; Šaman, D.; Tychý, M.; Mísek, J.; Cvacka, J.; Rulíšek, L.; Chocholoušová, J.; Vacek, J.; Goryl, G.; Szymonski, M.; Císařová, I.; Starý, I. *Proc. Natl. Acad. Sci.* **2009**, *106*, 13169; c) Sehnal, P.; Stará, I. G.; Starý, I.; Rulíšek, L.; Šaman, D.; Císařová, I. *J. Org. Chem.* **2008**, *73*, 2074; d) Starý, I.; Stará, I. G.; Alexandrová, Z.; Sehnal, P.;

- Teplý, F.; Šaman, D.; Rulíšek, L. *Pure Appl. Chem.* **2006**, *78*, 495; e) Stará, I. G.; Alexandrová, Z.; Teplý, F.; Sehnal, P.; Starý, I.; Šaman, D.; Budešínský, M.; Cvacka, J. *Org. Lett.* **2005**, *13*, 2547
- ⁸⁵ Crittall, M. R.; Fairhurst, N. W. G.; Carbery, D. R. *Chem. Comm.* **2012**, *48*, 11181.
- ⁸⁶ Haraburda, E. *PhD Dissertation*. University of Girona, **2015**.
- ⁸⁷ a) Crabbé, P.; André, D.; Fillion, H. *Tetrahedron Lett.* **1979**, *10*, 893; b) Crabbé, P.; Fillion, H.; André, D.; Luche, J.-L. *J. Chem. Soc. Chem. Commun.* **1979**, 859; c) Rona, P.; Crabbé, P. *J. Am. Chem. Soc.* **1969**, *91*, 3289.
- ⁸⁸ González, M.; Rodríguez, R.A.; Cid, M.M.; López, C.S. *J. Comput. Chem.* **2012**, *33*, 1236.
- ⁸⁹ a) Caminade, A.-M.; Turrin, C.-O.; Laurent, R.; Ouali, A.; Delavaux-Nicot, B. *Dendrimers: Towards catalytic, material and biomedical uses*, **2011**, Wiley; b) Astruc, D.; Boisselier, E.; Ornelas, C. *Chem. Rev.* **2010**, *110*, 1857.
- ⁹⁰ a) Fréchet, J. M. J.; Tomalia, D. A. *Dendrimers and other dendritic polymers*; John Wiley and Sons: Chichester, **2001**; b) Newkome, G. R.; Moorefield, C. N.; Vögtle, F. *Dendrimers and dendrons. Concepts, syntheses, applications*, **2001**, Wiley-VCH, Weinheim; c) Majoral, J.-P.; Caminade, A.-M.; *Chem. Rev.* **1999**, *99*, 845.
- ⁹¹ Buhleier, E.; Wehner, F.; Vögtle, F. *Synthesis* **1978**, *78*, 155.
- ⁹² Denkwalter, R. G.; Kolc, J.; Lukasage, W. J. *United States Patent* 4289872, **1981**.
- ⁹³ Newkome, G. R.; Yao, Z. Q.; Baker, G. R.; Gupta, V. K. *J. Org. Chem.* **1985**, *50*, 2003.
- ⁹⁴ Tomalia, D. A.; Baker, H.; Dewald, J.; Hall, M.; Kallos, G.; Martin, S.; Roeck, J.; Ryder, J.; Smith, P. *Polym. J.* **1985**, *17*, 117.
- ⁹⁵ Hawker, C. J.; Fréchet, J. M. J. *J. Am. Chem. Soc.* **1990**, *112*, 7638.
- ⁹⁶ Worner, C.; Mülhaupt, R. *Angew. Chem. Int. Ed.* **1993**, *32*, 1306.
- ⁹⁷ de Brabander-van den Berg, E. M. M.; Meijer, E. W. *Angew. Chem. Int. Ed.* **1993**, *32*, 1308.
- ⁹⁸ Rebrov, E. A.; Muzafarov, A.; Papkov, V. S.; Zhdanov, A. A. *Dokl. Akad. Nauk SSSR* **1989**, *309*, 376.
- ⁹⁹ Rengan, K.; Engel, R. *J. Chem. Soc. Perkin Trans. 1: Organic and Bio-Organic Chemistry* **1991**, 987.
- ¹⁰⁰ Launay, N.; Caminade, A.-M.; Lahana, R.; Majoral, J.-P. *Angew. Chem. Int. Ed.* **1994**, *33*, 1589.
- ¹⁰¹ a) Hawker, C. J.; Fréchet, J. M. J. *J. Am. Chem. Soc.* **1990**, *112*, 7638; b) Hawker, C. J.; Fréchet, J. M. J. *Chem. Commun.* **1990**, 1010.
- ¹⁰² Moore, J. S. *Acc. Chem. Res.* **1997**, *30*, 402.
- ¹⁰³ Tomalia, D. A.; Baker, H.; Dewald, J.; Hall, M.; Kallos, G.; Martin, S.; Roeck, J.; Ryder, J.; Smith, P. *Macromolecules* **1986**, *19*, 2466.
- ¹⁰⁴ Rebrov, E. A.; Muzafarov, A.; Papkov, V. S.; Zhdanov, A. A. *Dokl. Akad. Nauk SSSR* **1989**, *309*, 376.
- ¹⁰⁵ a) Caminade, A.-M.; Laurent, R.; Turin, C. O.; Rebout, C.; Delavaux-Nicot, B.; Ouali, A.; Zablocka, M.; Majoral, J.-P. *C. R. Chimie* **2010**, *13*, 1006; b) Caminade, A.-M.; Maraval, V.; Laurent, R.; Turrin, C. O.; Sutra, P.; Leclaire, J.; Giffre, L.; Marchand, P.; Baudoin-Dehoux, C.; Rebout, C.; Majoral, J.-P. *C. R. Chimie* **2003**, *6*, 791.
- ¹⁰⁶ Caminade, A.-M.; Laurent, R.; Zablocka, M.; Majoral, J.-P. *Molecules* **2012**, *17*, 13605.
- ¹⁰⁷ Launay, N.; Caminade, A.-M.; Majoral, J.-P. *J. Organomet. Chem.* **1997**, *529*, 51.
- ¹⁰⁸ Hecht, S.; Fréchet, J. M. J. *J. Am. Chem. Soc.* **1999**, *121*, 4084.
- ¹⁰⁹ Hahn, U.; Maisonhaute, E.; Amatore, C.; Nierengarten, J.-F. *Angew. Chem. Int. Ed.* **2007**, *46*, 951.
- ¹¹⁰ Hawker, C. J.; Wooley, K. L.; Fréchet, J. M. J. *Macromol. Symp.* **1994**, *77*, 11.
- ¹¹¹ Hawker, C. J.; Fréchet, J. M. J. *J. Am. Chem. Soc.* **1992**, *114*, 8405.
- ¹¹² Mak, C. C.; Chow, H.-F. *Chem. Commun.* **1996**, 1185.
- ¹¹³ Hadad, C.; García-Martínez, J. C.; Rodríguez-López, J. *J. Org. Chem.* **2012**, *77*, 6223.
- ¹¹⁴ Wooley, K. L.; Hawker, C. J.; Fréchet, J. M. J. *Chem. Soc. Perkin Trans. I* **1991**, 1059.
- ¹¹⁵ Luman, N. R.; Grinstaff, M. W. *Org. Lett.* **2005**, *7*, 4863.
- ¹¹⁶ Maraval, V.; Maraval, A.; Spataro, G.; Caminade, A.-M.; Majoral, J.-P.; Kim, D. H.; Knoll, W. *New J. Chem.* **2006**, *30*, 1731.
- ¹¹⁷ Kimoto, A.; Cho, J.; Higuchi, M.; Yamamoto, K. *Macromolecules* **2004**, *37*, 5531.
- ¹¹⁸ Gottis, S.; Rodríguez, L.-I.; Laurent, R.; Angurell, I.; Seco, M.; Rossell, O.; Majoral, J.-P.; Caminade, A.-M. *Tetrahedron Lett.* **2013**, *54*, 6864.
- ¹¹⁹ Lee, J. W.; Kim, B.-K.; Kim, J. H.; Shin, W. S.; Jin, S.-H. *J. Org. Chem.* **2006**, *71*, 4988.
- ¹²⁰ Kose, M. M.; Yesilbag, G.; Sanyal, A. *Org. Lett.* **2008**, *10*, 2353.
- ¹²¹ a) Hameau, A.; Fruchon, S.; Bijani, C.; Barducci, A.; Blanzat, M.; Poupot, R.; Pavan, G. M.; Caminade, A.-M.; Turrin, C.-O. *J. Polym. Sci. A Polym. Chem.* **2015**, *53*, 761; b) Barrière, C.; Latour, V.; Fau, P.;

- Caminade, A.-M.; Turrin, C.-O. *Tetrahedron Lett.* **2012**, *53*, 1908; c) Fuchs, S.; Pla-Quintana, A.; Mazères, S.; Caminade, A.-M.; Majoral, J.-P. *Org. Lett.* **2008**, *10*, 4751; d) Caminade, A.-M.; Majoral, J.-P. *Prog. Polym. Sci.* **2005**, *30*, 491.
- ¹²² Wei, Y. *PhD Dissertation*. Paul Sabatier University, **2009**.
- ¹²³ Kulhánek, J.; Burès, F.; Pytela, O.; Mikysek, T.; Ludvík, J. *Chem. Asian J.* **2011**, *6*, 1604.
- ¹²⁴ Tietze, L. F.; Behrendt, F.; Major, F.; Krewer, B.; Marian von Hof, J. *Eur. J. Org. Chem.* **2010**, 6909.
- ¹²⁵ Mitsudo, K.; Harada, J.; Tanaka, Y.; Mandai, H.; Nishioka, C.; Tanaka, H.; Wakamiya, A.; Murata, Y. Suga, S. *J. Org. Chem.* **2013**, *78*, 2763.
- ¹²⁶ Muller, J.-L.; Klankermayer, J.; Leitner, W. *Chem. Commun.* **2007**, 1939.
- ¹²⁷ a) Servin, P.; Laurent, R.; Dib, H.; Gonsalvi, L.; Peruzzini, M.; Majoral, J.-P.; Caminade, A.-M. *Tetrahedron Lett.* **2012**, *53*, 3876; b) Servin, P.; Laurent, R.; Gonsalvi, L.; Tristany, M.; Peruzzini, M.; Majoral, J.-P.; Caminade, A.-M. *Dalton Trans.* **2009**, 4432.
- ¹²⁸ For recent selected references, see: a) Berndsen, R.H.; Weiss, A.; Badul, U.K.; Wong, T.J.; Meraldi, P.; Griffioen, A.W.; Dyson, P.J.; Nowak-Sliwinska, P. *Sci. Rep.* **2017**, *7*, 43005; b) Pettinari, R.; Marchetti, F.; Petrini, A.; Pettinari, C.; Lupidi, G.; Fernández, B.; Diéguez, A.R.; Santoni, G.; Nabissi, M. *Inorg. Chim. Acta* **217**, 454, 139; c) Pettinari, R.; Marchetti, F.; Petrini, A.; Pettinari, C.; Lupidi, G.; Smoleński, P.; Scopelliti, R.; Riedel, T.; Dyson, P.J. *Organometallics* **2016**, *35*, 3734; d) Tabrizi, L.; Chiniforoshan, H. *J. Organomet. Chem.* **2016**, *822*, 211.
- ¹²⁹ Judeinstein, P.; Sanchez, C. *J. Mater. Chem.* **1996**, *6*, 511.
- ¹³⁰ Special issues on hybrid materials: a) Mehdi, A.; Reye, C.; Corriu, R. *Chem. Soc. Rev.* **2011**, *40*, 563; b) Sanchez, C.; Shea, K. J.; Kitagawa, S. Guest Ed. *Chem. Soc. Rev.* **2011**, *40*, 471.
- ¹³¹ For a recent review, see: a) Zhong, R.; Lindhorst, A. C.; Groche, F. J.; Kühn, F. E. *Chem. Rev.* **2017**, *117*, 1970. For selected references, see: b) Ferré, M.; Cattoën, X.; Wong Chi Man, M.; Pleixats, R. *ChemCatChem* **2016**, *8*, 2824; c) Garcés, K.; Fernández-Alvarez, F.; García-Orduña, P.; Lahoz, F.; Pérez-Torrente, J.; Oro, L. *ChemCatChem* **2015**, *7*, 2501; d) Lázaro, G.; Fernández-Alvarez, F.; Munárriz, J.; Polo, V.; Iglesias, M.; Pérez-Torrente, J.; Oro, L. *Catal. Sci. Technol.* **2015**, *5*, 1878; e) Lázaro, G.; Fernández-Alvarez, F.; Iglesias, M.; Horna, C.; Vispe, E.; Sancho, R.; Lahoz, F.; Iglesias, M.; Pérez-Torrente, J.; Oro, L. *Catal. Sci. Technol.* **2014**, *4*, 62; f) Blum, J.; Nairoukh, Z. *J. Org. Chem.* **2014**, *79*, 2397; g) Li, P.; Herrmann, W.; Kühn, F. *ChemCatChem* **2013**, *5*, 3324; h) Monge-Marcet, A.; Pleixats, R.; Cattoën, X.; Wong Chi Man, M. *J. Molec. Catal. A. Chem.* **2012**, *357*, 59; i) Borja, G.; Monge-Marcet, A.; Pleixats, R.; Parella, T.; Cattoën, X.; Wong Chi Man, M. *Eur. J. Org. Chem.* **2012**, 3625; j) Ciriminna, R.; Carà, P. D.; Sciortino, M.; Pagliaro, M. *Adv. Synth. Catal.* **2011**, *353*, 677; k) Monge-Marcet, A.; Pleixats, R.; Cattoën, X.; Wong Chi Man, M. *Catal. Sci. Technol.* **2011**, *1*, 1544; l) Yin, L.; Liebscher, J. *Chem. Rev.* **2007**, *107*, 133; m) Corma, A.; García, H. *Adv. Synth. Catal.* **2006**, *348*, 1391; n) Hoffmann, F.; Cornelius, M.; Morell, J.; Fröba, M. *Angew. Chem. Int. Ed.* **2006**, *45*, 3216; o) Wight, A. P.; Davis, M. E. *Chem. Rev.* **2002**, *102*, 3589; p) De Vos, D. E.; Dams, M.; Sels, B. F.; Jacobs, P. A. *Chem. Rev.* **2002**, *102*, 3615; q) Lindner, E.; Schneller, T.; Auer, F.; Mayer, H. A. *Angew. Chem. Int. Ed.* **1999**, *38*, 2155; r) Ying, J. Y.; Mehnert, C. P.; Wong, M. S. *Angew. Chem. Int. Ed.* **1999**, *38*, 56; s) Moreau, J. J. E.; Wong Chi Man, M. *Coord. Chem. Rev.* **1998**, *178-180*, 1073.
- ¹³² Zamboulis, A.; Moitra, N.; Moreau, J. J. E.; Cattoën, X.; Wong Chi Man, M. *J. Mater. Chem.* **2010**, *20*, 9338.
- ¹³³ Sanchez, C.; Ribot, F. *New J. Chem.* **1994**, *18*, 1007.
- ¹³⁴ For a monograph, see: *The Physics and Chemistry of Sol-Gel Processing*: ed. Brinker, C. J.; Scherer, G. W. Academic press: Boston, MA, 1990. For a review, see: Ciriminna, R.; Fidalgo, A.; Pandarus, V.; Béliand, F.; Ilharco, L. M.; Pagliaro, M. *Chem. Rev.* **2013**, *113*, 6592.
- ¹³⁵ Corriu, R. J. P.; Leclercq, D. *Angew. Chem. Int. Ed. Engl.* **1996**, *35*, 1421.
- ¹³⁶ Sanchez, C.; Belleville, P.; Popall, M.; Nicole, L. *Chem. Soc. Rev.* **2011**, *40*, 696.
- ¹³⁷ Baney, R. H.; Itoh, M.; Sakakibara, A.; Suzuki, T. *Chem. Rev.* **1995**, *95*, 1409.
- ¹³⁸ Dieudonné, P.; Wong Chi Man, M.; Pichon, B. P.; Vellutini, L.; Bantignies, J.-L.; Blanc, C.; Creff, G.; Finet, S.; Sauvajol, J.-L.; Bied, C.; Moreau, J. J. E. *Small* **2009**, *5*, 503.
- ¹³⁹ a) Corriu, R. J. P. *Eur. J. Inorg. Chem.* **2001**, 1109; b) Loy, D. A.; Shea, K. J. *Chem. Mater.* **2001**, *13*, 3306; c) Corriu, R. J. P. *Angew. Chem. Int. Ed.* **2000**, *39*, 1376; d) Loy, D. A.; Shea, K. J. *Chem. Rev.* **1995**, *95*, 1431.
- ¹⁴⁰ a) Inagaki, S.; Fukushima, Y.; Kuroda, K. *J. Chem. Soc., Chem. Commun.* **1993**, 680; b) Kresge, C. T.; Leonowicz, M. E.; Roth, W. J.; Vartuli, J. C.; Beck, J. S. *Nature* **1992**, *359*, 710; c) Beck, J. S.; Vartuli, J. C.; Roth, W. J.; Leonowicz, M. E.; Kresge, C. T.; Schmitt, K. D.; Chu, C. T.-W.; Olson, D. H.; Sheppard, E. W.; McCullen, S. B.; Higgins, J. B.; Schlenker, J. L. *J. Am. Chem. Soc.* **1992**, *114*, 10834.
- ¹⁴¹ Ying, J. Y.; Mehnert, C. P.; Wong, M. S. *Angew. Chem. Int. Ed.* **1999**, *38*, 56.

- ¹⁴² Monnier, A.; Schüth, F.; Huo, Q.; Kumar, D.; Margolese, D.; Maxwell, R. S.; Stucky, G. D.; Krishnamurty, M.; Petroff, P.; Firouzi, A.; Janicke, M.; Chmelka, B. F. *Science* **1993**, *216*, 1299.
- ¹⁴³ Corma, A. *Chem. Rev.* **1997**, *97*, 2373.
- ¹⁴⁴ a) Schmidt-Winkel, P.; Yang, P.; Margolese, D. I.; Chmelka, B. F.; Stucky, G. D. *Adv. Mater.* **1999**, *11*, 303; b) Zhao, D.; Huo, Q.; Melosh, N.; Fredrickson, G. H.; Chmelka, B. F.; Stucky, G. D. *Science* **1998**, *179*, 548.
- ¹⁴⁵ Yanagisawa, T.; Shimzu, T.; Kuroda, K.; Kato, C. *Bull. Chem. Soc. Jpn.* **1990**, *63*, 988.
- ¹⁴⁶ a) Jung, J. H.; Kobayashi, S.; Van Bommel, K. J. C.; Shinkai, S.; Shimizu, T. *Chem. Mater.* **2002**, *14*, 1445; b) Kobayashi, S.; Hamasaki, N.; Suzuki, M.; Kimura, M.; Shirai, H.; Hanabusa, K. *J. Am. Chem. Soc.* **2002**, *124*, 6550; c) Clavier, G. M.; Pozzo, J. L.; Bouas-Laurent, H.; Liere, C.; Roux, C.; Sanchez, C.; *J. Mat. Chem.* **2000**, *10*, 1725. d) Jung, J. H.; Onoi, Y.; Hanabusa, K.; Shinkai, S. *J. Am. Chem. Soc.* **2000**, *122*, 5008.
- ¹⁴⁷ Corma, A. *Chem. Rev.* **1995**, *95*, 559.
- ¹⁴⁸ Mansfield, E.; Kar, A.; Quinn, T. P.; Hooker, A. *Anal. Chem.* **2010**, *82*, 9977.
- ¹⁴⁹ Jaroniec, C. P.; Gilpin, R. K.; Jaroniec, M. *J. Phys. Chem. B* **1997**, *101*, 6861.
- ¹⁵⁰ Stradella, L.; Argentero, M. *Thermochimica Acta* **1993**, *219*, 315.
- ¹⁵¹ Brinker, C. J.; Lu, Y.; Fan, H. Y. (Sandia Corporation Patent) United States US RE41, 612 E, 2010.
- ¹⁵² Lelli, M.; Gajan, D.; Lesage, A.; Caporini, M. A.; Vitzthum, V.; Miéville, P.; Héroguel, F.; Rascón, F.; Roussey, A.; Thieleux, C.; Boualleg, M.; Veyre, L.; Bodenhouse, G.; Copéret, C.; Emsley, L. *J. Am. Chem. Soc.* **2011**, *133*, 2104.
- ¹⁵³ *Gas adsorption equilibria. Experimental methods and adsorptive isotherms.* Ed. Keller, J. U. Springer: Boston, 2005.
- ¹⁵⁴ Sing, K. S. W.; Everett, D. H.; Haul, R. A. W.; Moscou, L.; Pierotti, R. A.; Rouquérol, J.; Siemieniowska, T. *Pure Appl. Chem.* **1985**, *4*, 603.
- ¹⁵⁵ Brunauer, S.; Emmett, P. H.; Teller, E. *J. Am. Chem. Soc.* **1938**, *60*, 309.
- ¹⁵⁶ Barrett, E. P.; Joyner, L. G.; Halenda, P. P. *J. Am. Chem. Soc.* **1951**, *73*, 373.
- ¹⁵⁷ a) Conte, V.; Elakkari, E.; Floris, B.; Mirruzzo, V.; Tagliatesta, P. *Chem. Commun.* **2005**, 1587; b) González, I.; Bouquillon, S.; Roglans, A.; Muzart, J. *Tetrahedron Lett.* **2007**, *48*, 6425; c) Lin, Y.Y.; Tsai, S.C.; Yu, S. J. *J. Org. Chem.* **2008**, *73*, 4920.
- ¹⁵⁸ Wang, Y.-H.; Huang, S.-H.; Lin, T.-C.; Tsai, F.-Y. *Tetrahedron* **2010**, *66*, 7136.
- ¹⁵⁹ a) Geny, A.; Agenet, N.; Iannazzo, L.; Malacria, M.; Aubert, C.; Gandon, V. *Angew. Chem. Int. Ed.* **2009**, *48*, 1810; b) Thiel, I.; Spannenberg, A.; Hapke, M. *ChemCatChem* **2013**, *5*, 2865.
- ¹⁶⁰ For a review, see: Cole-Hamilton, D. J. *Science* **2003**, *299*, 1702.
- ¹⁶¹ a) Diversi, P.; Ingrosso, G.; Lucherini, A.; Minutillo, A. *J. Mol. Catal.* **1987**, *40*, 359; b) Perkins, P.; Vollhardt, K. P. C. *J. Am. Chem. Soc.* **1979**, *101*, 3985.
- ¹⁶² a) Thiel, I.; Hapke, M. *J. Molec. Catal. A* **2014**, *383-384*, 153. b) S. Reinhard, P. Soba, F. Rominger, J. Blümel, *Adv. Synth. Catal.* **2003**, *345*, 589; c) Fu, Y. S.; Yu, S. J. *Angew. Chem. Int. Ed.* **2001**, *40*, 437.
- ¹⁶³ Arduengo III, A. J.; Krafczyk, R.; Schmutzler, R. *Tetrahedron* **1999**, *55*, 14523.
- ¹⁶⁴ a) Weigl, K.; Köhler, K. Dechert, S., Meyer, F. *Organometallics* **2005**, *16*, 4049; b) Weigl, K. *PhD Dissertation.* University of Kaiserslautern, **2006**.
- ¹⁶⁵ Dastgir, S.; Coleman, K.; Green, M. *Dalton Trans.* **2011**, *40*, 661.
- ¹⁶⁶ Peñafiel, I.; Pastor, I.; Yus, M.; Esteruelas, M.; Oliván, M. *Organometallics* **2012**, *31*, 6154.
- ¹⁶⁷ a) Green, L. M.; Meek, D. W. *Organometallics* **1989**, *8*, 659; b) Uson, R.; Oro, L.A.; Cabeza, J.A. *Inorg. Synth.* **1985**, *23*, 126.
- ¹⁶⁸ Weigl, K.; Köhler, K.; Dechert, S.; Meyer, F. *Organometallics* **2005**, *24*, 4049.
- ¹⁶⁹ a) Polshettiwar, V.; Varma, R. S. *Acc. Chem. Res.* **2008**, *41*, 629; b) Singh, B. K.; Kaval, N.; Tomar, S.; Van der Eycken, E.; Parma, V. S. *Org. Process Res. Dev.* **2008**, *12*, 468; c) Kappe, C. O. *Angew. Chem. Int. Ed.* **2004**, *43*, 6250; d) Larhed, M.; Möberg, C.; Hallberg, A. *Acc. Chem. Res.* **2002**, *35*, 717.
- ¹⁷⁰ Coelho, F.; Almeida, W.P.; Veronese, D.; Mateus, C.R.; Silva Lopes, E.C.; Rossi, R.C.; Silveira, G.P.C.; Pavam, C.H. *Tetrahedron* **2002**, *58*, 7437.
- ¹⁷¹ Zhu, B.; Yan, L.; Pan, Y.; Lee, R.; Liu, H.; Han, Z.; Huang, K.-W.; Tan, C.-H.; Jiang, Z. *J. Org. Chem.* **2011**, *76*, 6894.
- ¹⁷² Ramachandran, P. V.; Helppi, M. A.; Lehmkuhler, A. L.; Marchi, J. M.; Schmidt, C. M.; Yip-Schneider, M. T. *Bioorg. Med. Chem. Lett.* **2015**, *25*, 4270.
- ¹⁷³ Li, L.; Chen, B.; Ke, Y.; Li, Q.; Zhuang, Y.; Duan, K.; Huang, Y.; Pang, J.; Qiu, L. *Chem. Asian J.* **2013**, *8*, 2167.
- ¹⁷⁴ Nishida, M.; Shiga, H.; Mori, M. *J. Org. Chem.* **1998**, *63*, 8606.
- ¹⁷⁵ Xu, F.; Wang, C.; Wang, H.; Li, X.; Wan, B. *Green Chem.* **2015**, *17*, 799.

Bibliography

- ¹⁷⁶ Tanaka, K.; Takeishi, K.; Noguchi, K. *J. Am. Chem. Soc.* **2006**, *128*, 4586.
- ¹⁷⁷ Pagekopf, B.L.; Belanger, D.B.; O'Mahony, D.J.R.; Livinghouse, T. *Synthesis* **2000**, 1009.
- ¹⁷⁸ Kitamura, T.; Sato, Y.; Mori, M. *Adv. Synth. Catal.* **2002**, *344*, 678.
- ¹⁷⁹ E.I. Du Pont De Nemours and company. "Process for the manufacture of imidazoles". Arduengo III, A. J.; Gentry Jr, F. P.; Taverkere, P. K.; Simmons III, H. E. US Patent 6177575 B1. **2001**.
- ¹⁸⁰ Gardiner, M.G.; Herrmann, W.A.; Reisinger, C.-P.; Schwarz, J.; Spiegler, M. *J. Organomet. Chem.* **1999**, *572*, 239.
- ¹⁸¹ Green, L.; Meek, D. *Organometallics* **1989**, *3*, 659.
- ¹⁸² Banti, D.; Groaz, E.; North, M. *Tetrahedron* **2004**, *60*, 8043.
- ¹⁸³ Deng, J. Tabei, J.; Shiotsuki, M.; Sanda, F.; Masuda, T. *Macromolecules* **2004**, *37*, 5538.
- ¹⁸⁴ Ojima, I.; Vu, A. T.; McCullagh, J. V.; Kinoshita, A. *J. Am. Chem. Soc.* **1999**, *121*, 3230.
- ¹⁸⁵ Kinoshita, H.; Shinokubo, H.; Oshima, K. *J. Am. Chem. Soc.* **2003**, *125*, 7784.

